Regulation of Keratin 8 During Cancer Cell Division

by

Ceyda Seren Ceyhan

A Dissertation Submitted to the
Graduate School of Sciences and Engineering
in Partial Fulfillment of the Requirements for
the Degree of

Doctor of Philosophy

in

Molecular Biology and Genetics

KOÇ ÜNİVERSİTESİ

February, 2025

Regulation of Keratin 8 During Cancer Cell Division

Koç University

Graduate School of Sciences and Engineering

This is to certify that I have examined this copy of a doctoral dissertation by

Ceyda Seren Ceyhan

and have found that it is complete and satisfactory in all respects,
and that any and all revisions required by the final
examining committee have been made.

Committee Members:

Prof. Dr. Nurhan Özlü Sıcakkan (Advisor)

Assoc. Prof. Dr. Nurcan Tunçbağ

Dr. Onur Çizmecioğlu

Dr. Ayşe Koca Çaydaşı

Dr. Anne-Lore Schlaitz

Date: February 6, 2025

To my mom, Hayriye Gürsoy, who has been my guiding light...

ABSTRACT

Regulation of Keratin 8 During Cancer Cell Division

Ceyda Seren Ceyhan

Doctor of Philosophy in Molecular Biology and Genetics

February, 2025

Keratins are cytoskeletal proteins classified as Type I and Type II intermediate filaments. These filamentous structures provide mechanical strength and stability to the cells, but it is not known well how these robust structures are regulated and function during dynamic processes, such as cell division. To better understand the biochemistry of cell division and the regulation of keratins, I focused on keratin 8 in cancer cell division. Keratin 8 is a good candidate with a maintained expression during tumorigenesis and has diverse expression patterns in different cell types. During cell division, these filamentous structures split into non-filamentous clusters with mechanisms that are not well understood. To uncover the phosphorylation-dependent disassembly, I analyzed the cell cycle-dependent phosphoproteome of keratin 8 in different cell lines and investigated its commonly regulated phosphorylation sites. I took label-free and dimethyl labeling-based quantitative approaches combined with TiO_2 phosphopeptide enrichment methodology. I applied DDA, DIA, and PRM-based mass spectrometry methods and identified and quantified commonly regulated or cell-type specific phosphorylation sites of keratin 8 during cell division. To understand the functional role of keratins, interaction partners of keratin 8 were investigated by immunoprecipitation. I focused on the relation of keratin 8 with other cytoskeletal elements and further searched for its role in mitosis by analyzing its relation with microtubules. I performed microtubule pelleting assays to determine keratin 8-dependent microtubule interactors. I focused on the NDC80 complex during metaphase and further investigated the role of keratin 8 at the kinetochore-microtubule attachment by super-resolution imaging. Our study brought a better understanding of the regulation and functioning of keratins during cell division.

ÖZETÇE

Kanser Hücre Bölünmesinde Keratin 8'in Düzenlenmesi

Ceyda Seren Ceyhan

Moleküler Biyoloji ve Genetik, Doktora

Şubat, 2025

Keratinler, Tip I ve Tip II ara filamentler olarak sınıflandırılan hücre iskeleti proteinlerdir. Bu yapılar hücreye mekanik dayanıklılık ve stabilite sağlar. Ancak bu sağlam yapıların, hücre bölünmesi gibi dinamik süreçlerde nasıl düzenlendiği ve işlev gördüğü hakkında yeterli bilgi bulunmamaktadır. Hücre bölünmesinin biyokimyasını ve keratinlerin düzenlenmesini daha iyi anlamak amacıyla kanser hücre bölünmesinde keratin 8'e odaklanıldı. Keratin 8, ifade seviyesinin tümör oluşumu sırasında korunması ve farklı hücre tiplerinde gösterdiği çeşitlilik nedeniyle dikkat çeken bir adaydır. Bu filament yapılar, hücre bölünmesi sırasında, tam olarak bilinmeyen mekanizmalar yardımıyla filament olmayan kümelere ayrılmaktadır. Keratin 8'in fosforilasyona bağlı çözünürlüğünü anlamak amacıyla farklı hücre hatlarında hücre döngüsüne bağlı fosfoproteom analizi gerçekleştirildi ve hücreler arası düzenlenen fosforilasyon bölgeleri incelendi. Bu amaç doğrultusunda TiO_2 fosfopeptit zenginleştirme yöntemi ile hem etiketsiz hem de dimetil etiketleme bazlı kantitatif yaklaşımlar kullanıldı. DDA, DIA ve PRM temelli kütle spektrometresi yöntemleri uygulanarak keratin 8'in hücre bölünmesi sırasında hücre tipine özgü veya hücreler arası ortak olarak düzenlenen fosforilasyon bölgeleri belirlendi ve kantitatif olarak analiz edildi. Keratinlerin işlevsel rollerini daha iyi anlamak için keratin 8 ile etkileşen proteinler immünopresipitasyon yöntemiyle araştırıldı. Keratin 8'in diğer hücre iskeleti proteinleriyle ilişkisini incelenerek mikrotübüllerle olan etkileşimine odaklanıldı ve mitozdaki rolü detaylandırıldı. Keratin 8'e bağlı mikrotübül etkileşimcilerini belirlemek için mikrotübül çöktürme metotları uygulandı. Metafaz sırasında keratin 8'in NDC80 kompleksi ile olan ilişkisi analiz edilerek kinetokor-mikrotübül bağlantısındaki rolü süper-çözünürlüklü görüntüleme ile araştırıldı. Bu çalışma, hücre bölünmesi sırasında keratinlerin düzenlenmesi ve işlevi ile ilgili kapsamlı bir bilgi sunmuştur.

ACKNOWLEDGEMENTS

First and foremost, I would like to express my sincere gratitude to my advisor, Prof. Dr. Nurhan Özlü Sıcakkan, who supervised me throughout this journey. She has taught me invaluable lessons, both academically and personally. I am deeply thankful for the freedom she gave me to wonder and discover, which allowed me to grow as a researcher. Carrying her trust and encouragement with me, I feel prepared to confidently move forward.

I would like to thank my thesis monitoring committee members, Assoc. Prof. Dr. Nurcan Tunçbağ and Dr. Onur Çizmecioğlu, for their guidance and discussions throughout my Ph.D. studies. I would also like to extend my special thanks to Dr. Ayşe Koca Çaydaşı and Dr. Anne-Lore Schlaitz for accepting to participate in my Ph.D. thesis defense jury and giving their valuable time and critical reading on my thesis.

I would like to express my gratitude for the financial support provided by the Scientific and Technological Research Council of Turkey (TÜBİTAK) and the BİDEB 2214-A International Research Fellowship Program. I am also deeply thankful to EPIC-XS for supporting my work and to the Functional Genomics Center Zurich (FGCZ) for the valuable contributions of Dr. Antje Dittmann and Dr. Jonas Grossmann. Additionally, I extend my thanks to the Proteomics Facility of Koç University, the Molecular Imaging Core Facility of Koç University Research Center for Translational Medicine (KUTTAM-CMIC), the ZMBH Imaging Facility and Flow Cytometry & FACS Core Facility (FFCF) for their essential technical assistance.

A heartfelt thank you to Dr. Anne-Lore Schlaitz for welcoming me into her lab and providing invaluable support during the final year of this journey. She did not only teach me the core principles of scientific research but also dedicated her valuable time and insightful feedback. Thanks to Simone, Martijn, Suzan, Hannah, Hatice, and Anika I discovered how joyful and fulfilling academia can be. I will always strive to seek and create the peaceful and inspiring environment they fostered.

I would like to thank Dr. Nazan Saner for always sharing my excitement for academia and teaching me how to think scientifically. From her, I learned the importance of focusing on the details while knowing when to step back to see the bigger picture before getting lost in them. It was an honor to work with her. I would like to thank Büşra Akarlar for warmly introducing me to proteomics with her open door and ever-welcoming "therapy couch" from the very beginning. As I finish my Ph.D., I have come to understand how she manages mass spectrometers, though Meriç remains a mystery...

I would like to thank the remarkable educators who have guided me along the way. First and foremost, I am deeply grateful to Zeynep Uzbilek, who made me fall in love with biology. I would like to express my heartfelt gratitude to Prof. Dr. Erkay Savaş for showing me that the pursuit of knowledge can be enriched not only through dedication and hard work but also by finding joy along the way. I look forward to our next stop with excitement. I am deeply grateful to Prof. Dr. Meltem Müftüoğlu, who taught me to trust myself instead of seeking approval. I would like to express my deepest gratitude to Prof. Dr. Aykut Üren. No words could ever truly capture the depth of my admiration for him, not only for the incredible work he does but for the amazing person he is. It was his support that kept me going. Thank you for giving me a chance, believing in me, and making such a profound impact on my life. I look forward to the days when our paths cross again…

I would like to express my deep gratitude to my friends who became family. To my best friend, Berk Işıldak: I could never have imagined that being completely myself with someone could be so much fun. He has supported me through life as it is. Thank you for growing with me, standing by me with trust, and being my family. I dedicate the kinetochores in this thesis to him. To Gizem Çuvalcı: The beautiful moments we've shared have taught me so much. I've learned how a friendship can push me to grow when I truly care. I'm so grateful she's been there, and I know she always will be. To Büşra Yılmaz: Thank you for making me laugh in every circumstance and showing me the strength of a woman. I'm so thankful that you're a part of my life. To Barış Korcan Tekin, Furkan Gültekin, Melis Umay Tekbaş, and Elif Yılmaz: You are my youth and my first chosen family. Thank you for always being there for me.

I would like to express my heartfelt gratitude to Burcu Bilginer for handing me a magic wand. I know, in a parallel universe, we're raising an ethically approved toast right now. With heartfelt gratitude, I extend my thanks to Dr. Hakan Bilgen and Dr. Alper Keskin, who have taken care of not only my physical health but also my mental and emotional well-being. I would like to thank Mehmet Eroldu for proving to me that I can pursue my beliefs, no matter who stands in my way. Another heartfelt thanks go to the KU Orkestra family, who gave me a place to forget everything and truly be in the moment.

I would like to thank my second mother, Arzu Şahin. Thank you for raising me with all your love and for keeping my childhood safe and calm. I love you and Grandpa Gazi so much. I would like to thank my sister, Çağla Ceren Ceyhan, my chestnut candy, the smartest person, and the craziest sister I know. Thank you for always having my back and for giving me just the right amount of worry. I'm grateful for all the colors she brought into my life. And to my dad, Ali Ceyhan, for everything he's taught me. It's all been a part of shaping who I am today.

Words cannot fully express the depth of my gratitude or the emotions I feel for the one person who made this past year unforgettable, Valentin Lukas Kiechle. He has transformed my life into something beyond anything I could have ever imagined. Through every beautiful moment we shared, he helped me discover my happiness, kept us grounded, and showed me that a healthy, loving relationship is not just possible but effortless. Thank you, Valentin, for wholeheartedly supporting me, being proud of me, and sharing my laughter.

There is one person I must acknowledge with the deepest joy: Dr. Berfu Nur Yiğit. From the very first moment I saw her, I knew we were destined to share moments. With her, we didn't just go through an academic process, we shared life itself. We laughed, we cried, and we felt emotions we couldn't even name. But we always grew deeper, discovering ourselves together. She taught me how to have fun when facing challenges, how to love without hesitation, and how to protect myself. Though, with her, I never needed to. This thesis wouldn't have been possible without you, my sister, who stood beside me, behind me, and above me through the years…

Finally, my most profound gratitude goes to my dear mom, Hayriye Gürsoy, who, above all, taught me how to be happy. Thank you for always being there, for being open to growth, and for teaching me the value of love. As you feel proud of me, I am proud of the woman you have become. Thank you for being who you are. This thesis and all my achievements are dedicated to you. I love you with all my heart…

TABLE OF CONTENTS

LIST OF TABLES

LIST OF FIGURES

ABBREVIATIONS

ABC	Ammonium Bicarbonate
ACN	Acetonitrile
AF	Actin Filament
AGC	Automatic Gain Control
APC/C	Anaphase-Promoting Complex/Cyclosome
APS	Ammonium Persulfate
BCA	Bicinchoninic Acid
BR	Biological Replicate
BSA	Bovine Serum Albumin
CAKI-2	Human Renal Cancer Cell Line
CCAN	Constitutive Centromere-Associated Network
CDK	Cyclin Dependent Kinase
CRISPR	Clustered Regularly Interspaced Short Palindromic Repeats
Cys, C	Cysteine
DAPI	4’6-Diamidino-2-Phenylindole
DDA	Data-Dependent Acquisition
DIA	Data-Independent Acquisition
DMEM	Dulbecco's Modified Eagle Medium
DMSO	Dimethyl Sulfoxide
DTT	Dithiothreitol
ECL	Enhanced Chemiluminescence
EDTA	Ethylenediaminetetraacetic Acid
EGTA	Ethylene Glycol Tetraacetic Acid
EMT	Epithelial-Mesenchymal Transition
FA	Formic Acid
FACS	Fluorescence-Activated Cell Sorting

FBS	Fetal Bovine Serum
FDR	False Discovery Rate
GFP	Green Fluorescence Protein
GO	Gene Ontology
G0	Gap Zero
G1	Gap One
G2	Gap Two
G418	Geneticin
HCD	Higher-Energy Collision Dissociation
HEK 293	Human Embryonic Kidney Cell Line
HeLa S3	Subclone of HeLa, Human Cervical Cancer Cell Line
HEPES	4-(2-Hydroxyethyl)-1-Piperazineethanesulfonic Acid
HRP	Horseradish Peroxidase
IAA	Iodoacetamide
IF	Intermediate Filament
kDa	Kilodalton
KT	Kinetochore
K18	Keratin 18
K19	Keratin 19
K8	Keratin 8
K8/18	Keratin 8 and 18
LB	Lysogeny Broth
Lys, K	Lysine
MCC	Mitotic Checkpoint Complex
MCF7	Human Breast Cancer Cell line
MDA-MB-231	Human Breast Cancer Cell Line
Met, M	Methionine
MQ	MaxQuant
MT	Microtubule
NCE	Normalized Collision Energy
NLS	Nuclear Localization Signal

nTPM	Normalized Transcripts Per Million
PBS	Phosphate-Buffered Saline
PBS-T	Phosphate Buffered Saline-Tween 20
PCR	Polymerase Chain Reaction
PD	Proteome Discoverer
PEI	Polyethylenimine
PFA	Paraformaldehyde
PMSF	Phenylmethylsulfonyl Fluoride
PRM	Parallel Reaction Monitoring
PTM	Post-Translational Modification
p-H3	Phospho-Histone H3
p-K8 (S34)	Phospho-Keratin 8 Serine 34
P/S	Penicillin/Streptomycin
ROI	Region of Interest
S	Synthesis
SAC	Spindle Assembly Checkpoint
SAINT	Significance Analysis of Interactome
SDS-PAGE	Sodium Dodecyl Sulfate Polyacrylamide Gel Electrophoresis
Ser, S	Serine
STLC	S-Trityl-L-Cysteine
TBS-T	Tris Buffered Saline-Tween 20
TEMED	Tetramethylethylenediamine
TFA	Trifluoroacetic Acid
Thr, T	Threonine
Tyr, Y	Tyrosine
ULF	Unit-Length Filament
WCL	Whole-Cell Lysate

Chapter 1

INTRODUCTION

The cell cycle is a sequential series of events for a cell to grow and divide. It consists of two major phases: the interphase (gap one (G_1), synthesis (S), and gap two (G_2) phases) and the M phase (mitosis and cytokinesis), ending with cell division. When the environmental and cellular conditions are compatible, the cell grows and replicates its DNA during interphase. At the M phase, cell division occurs in two main stages consisting of mitosis (prophase, prometaphase, metaphase, anaphase, and telophase) and cytokinesis. The division starts with the separation of chromosomes during mitosis and ends with the physical cleavage of cells during cytokinesis, forming two new daughter cells.

In higher eukaryotes, the cell cycle is regulated by multiple checkpoints that monitor and regulate the key stages to prevent possible errors. The checkpoints occur near the end of the G_1 phase, at the G_2/M transition, and during metaphase. The G_1 checkpoint determines whether the conditions are favorable to proceed to the cell division. At the G_2 checkpoint, the cell ensures that the DNA has been replicated correctly. The M checkpoint, also known as the spindle assembly checkpoint (SAC), ensures accurate chromosome segregation by monitoring the proper attachment of chromosomes to spindle microtubules and delaying mitotic progression if connections are erroneous or absent [1]. Aberrant attachments are corrected by a tension-sensing mechanism where Aurora B kinase, localized in the inner centromere, creates a phosphorylation gradient for kinetochore proteins, such as the NDC80 complex residing at the outer kinetochore, destabilizing improper attachments and activating SAC signals [2]. The intricate regulation of the SAC signaling heavily relies on the dynamic interactions between microtubules and their associated proteins.

Microtubules, actin filaments, and intermediate filaments (IFs) are three major components of the cytoskeleton. During dynamic processes, such as cell division, the

cytoskeleton undergoes structural changes and regulations that cause a difference in the cellular phenotype, which ability is called cell plasticity. While the roles of microtubules and actin filaments in regulating cell plasticity during cell division are well-studied, the regulation and functioning of intermediate filaments remain less well-understood.

Intermediate filaments are fibrous structures with a diameter of around 10 nm and built from soluble monomers in a stepwise process. They have five different classes and are abundant in cells under heavy mechanical stress, such as neuronal axons, muscle cells, and epithelial cells. Type I (acidic) and Type II (basic/neutral) intermediate filaments consist of keratin proteins. They are a big family of proteins synthesized from 54 functional keratin genes in the human genome located on chromosomes 12 and 17 [3]. They are mainly distributed in epithelial cells, expressed in a cell type-specific manner, and function to give strength, stability, and integrity to the cells. To function properly, acidic and basic keratins form heterodimers that build into filaments. In simple epithelia, the most common Type I keratins are keratin 18 (K18) and keratin 19 (K19), and the most common Type II is keratin 8 (K8) [4].

Keratin 8 and 18 (K8/18) are expressed as the primary keratin pair in simple epithelial cells. In cancer, epithelial tumors maintain keratin expression respective to the origin of the cell type. Given the heterogeneous expression pattern of keratins and the availability of keratin-specific antibodies, they are studied as immunohistochemical markers in diagnostic tumor pathology [3]. Additionally, they are regulators of cancer cell signaling. In certain cases, continuous phosphorylation of keratin filaments leads to their disassembly and eventual loss, which is a hallmark feature of EMT [5]. In such situations, the phosphorylated forms, or phosphoproteoforms, of keratins can serve as biomarkers to assess the EMT state [6]. These findings underscore the importance of phosphorylation in regulating keratin dynamics and its implications for EMT monitoring.

In Chapter 2, a brief literature review relevant to this research is presented. Chapter 3 describes the materials and methods, ensuring methodological transparency and reproducibility. Chapter 4 presents the results with comprehensive analyses and interpretations. Finally, Chapter 5 concludes the thesis with a discussion of the findings, their implications, and potential directions for future research.

Chapter 2

LITERATURE REVIEW

2.1 The Cell Cycle

The cell cycle is a sequential series of events for a cell to grow and divide. It consists of two major phases: the interphase (G_1, S, and G_2 phases) and the M phase (mitosis and cytokinesis), ending with cell division. For a cell to divide successfully, environmental and cellular conditions should be compatible. When conditions are unfavorable, cells can delay their progression through the G_1 phase and may enter a resting phase called the G_0 (G zero). Before starting to proliferate again, the cell may stay in this stage for days, weeks, or even years while carrying out maintenance and other tasks. Indeed, many cells remain permanently in G_0 until they or the organism dies. When the conditions are optimal at the interphase, the cell duplicates its contents at the G_1 phase, replicates its DNA at the S phase, and grows and prepares for mitosis at the G_2 phase. At the M phase, two copies of the genetic material are divided into the two daughter cells, and the cell cycle can restart (Figure 2.1).

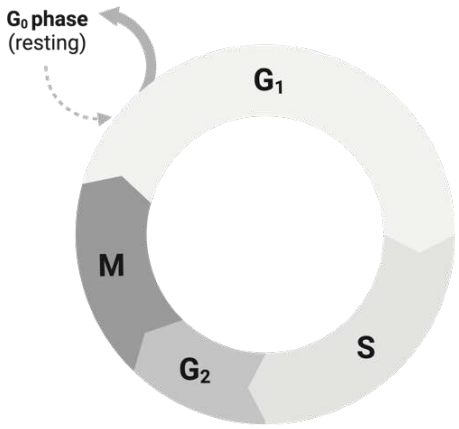

Figure 2.1: The stages of the eukaryotic cell cycle.

At the M phase, cell division occurs in two main stages consisting of mitosis (prophase, prometaphase, metaphase, anaphase, and telophase) and cytokinesis. Mitosis occurs in a strict sequential order of five stages, while cytokinesis begins in anaphase and continues through telophase (Figure 2.2). The division of the cell starts with the separation of chromosomes during mitosis and ends with the physical cleavage of cells during cytokinesis.

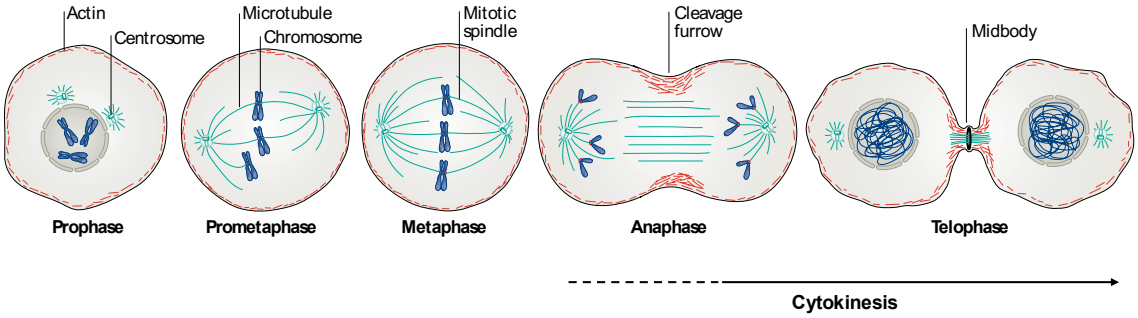

Figure 2.2: The stages of the M phase. Adapted from [7].

Chromosomes and the cytoskeleton define the stages of the M phase. Prophase is the first step of mitosis when DNA condenses into chromosomes and microtubules (MTs) polymerize to form a bipolar spindle. In prometaphase, the nuclear envelope breaks down, and the mitotic spindle begins to capture and organize the chromosomes. In metaphase, chromosome arms are attached to kinetochores (KTs), which are connected to opposite spindle poles via microtubules, and the chromosomes align at the metaphase plate. After all the chromosomes at the metaphase plate are correctly attached to microtubules, anaphase is triggered to start the separation of the sister chromatids. In telophase, the cell starts to re-establish its normal structures; the mitotic spindle breaks down, two new nuclei form, and chromosomes begin to decondense. As cells begin to exit division during telophase, the spindle rearranges to an array dominated by interzonal microtubules and condenses into an intercellular bridge, or midbody, where separation of the daughter cells takes place. The midbody forms by the rearrangement of the actin and microtubule cytoskeleton, and the final stage of separation, called abscission, occurs in the intercellular bridge after the actin and microtubule cytoskeletons have been cleared. Cytokinesis ends up with two new cells, each with a complete set of chromosomes identical to those of the mother cell.

2.1.1 Cell Cycle Control

In higher eukaryotes, the cell cycle is regulated by multiple checkpoints at which the cell ensures the completion of events in one phase before progressing to the next phase. Three checkpoints occur near the end of the G_1 phase, at the G_2/M transition, and during metaphase. The G_1 checkpoint determines whether the conditions are favorable to proceed to the cell division. The cell checks for cellular reserves, cell size, and external influences, such as growth factors, before carrying the cell past the checkpoint. At the G_2 checkpoint, the cell ensures that the DNA has been replicated correctly. At the M checkpoint, also known as the spindle assembly checkpoint (SAC), the attachment of the sister chromatids to the spindle microtubules is checked [1]. The cell cycle proceeds when the kinetochores of each pair of sister chromatids are attached to spindle fibers arising from opposite poles of the cell.

At each checkpoint, transitions are regulated by cyclin-dependent kinases (CDKs) and their activating cyclin subunits (Figure 2.3a). The cyclins are required for the activation of the kinases. Once activated, the serine (Ser, S)/threonine (Thr, T) kinases phosphorylate key substrates to promote DNA synthesis and mitotic progression. In most cases, the kinase levels remain relatively constant during the cell cycle, whereas the concentration of the cyclin subunits oscillates (Figure 2.3b).

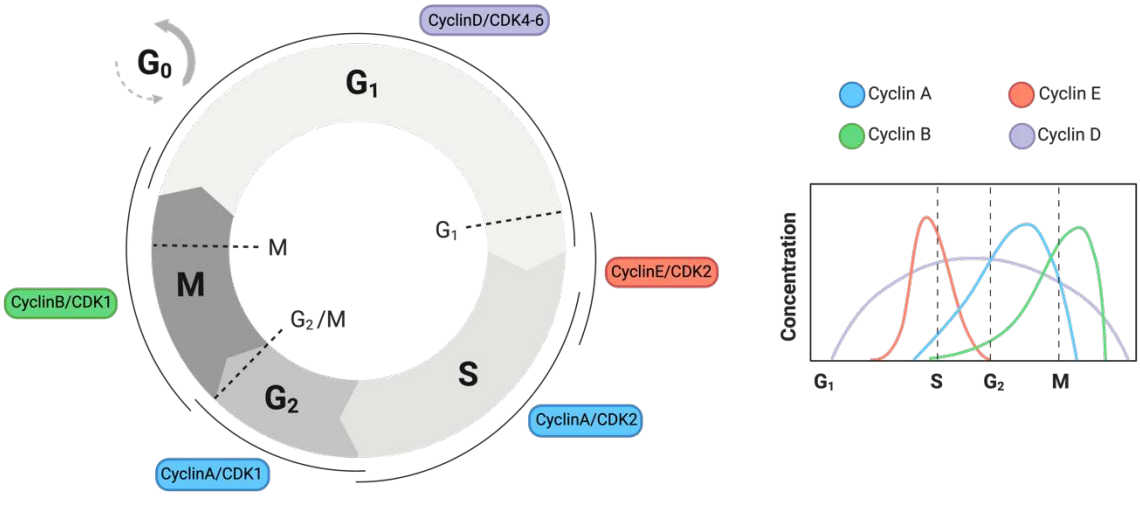

(a) (b)

Figure 2.3: Regulation of the cell cycle: (a) the cyclin/CDK pairs and checkpoints in their respective stages, (b) the oscillatory patterns of cyclin levels throughout the cell cycle.

2.1.2 Spindle Assembly Checkpoint

SAC is a surveillance mechanism ensuring accurate segregation of replicated chromosomes by monitoring the tension status of kinetochore-microtubule attachments. It halts the metaphase to anaphase transition when there is an unattached and/or untensed kinetochore. SAC acts at the final stage of mitosis, and if it fails, errors cannot be corrected in subsequent cell cycles. Unlike other checkpoints that focus on preparing the cell for division, SAC directly prevents aneuploidy, which can lead to severe consequences, such as cancer.

To segregate replicated chromosomes equally to the daughter cells, kinetochores must attach to microtubules from opposite poles of the mitotic spindle (biorientation). In other cases, an error correction mechanism destabilizes erroneous kinetochore-microtubule attachments [8]. These erroneous attachments can be syntelic (kinetochore attached to microtubules from the same pole), monotelic (only one kinetochore is attached to spindle), or amphitelic (kinetochores attached to microtubules from opposite poles without centromeres under tension). When there is an amphitelic attachment with centromeres under tension, biorientation is achieved (Figure 2.4).

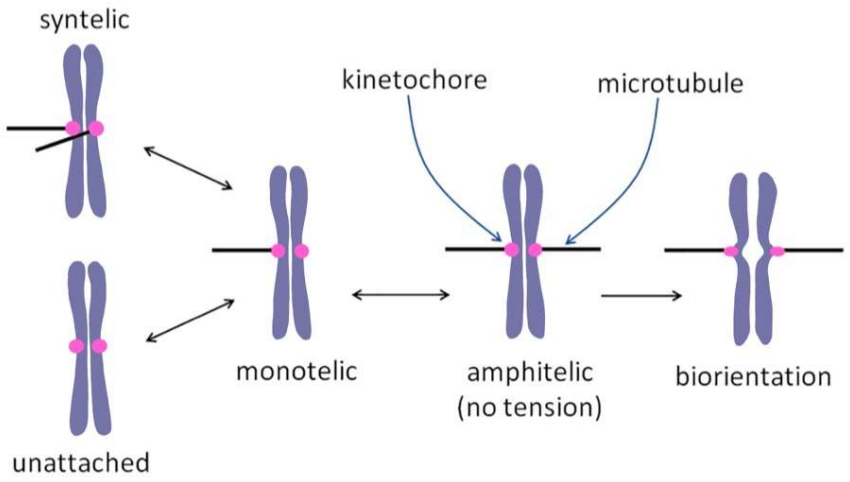

Figure 2.4: Model for the transitions of different KT-MT attachment states. Double-headed arrows denote reversible transitions. Adapted from [8].

To achieve the biorientation state, aberrant attachments are corrected by Aurora B kinase localized in the inner centromere. It is a key component of the chromosomal passenger complex (CPC), ensuring SAC activation and fidelity of chromosome segregation [3, 4]. For the transitions of sister chromatids between different kinetochore-microtubule attachment states, Aurora B kinase disrupts attachments selectively at the microtubule plus end while leaving lateral attachments unaffected. This mechanism allows the continuous formation and correction of attachments until tension stabilizes biorientation [11]. In more detail, Aurora B kinase creates a phosphorylation gradient for kinetochore proteins, such as NDC80 residing at the outer kinetochore, destabilizing improper attachments and activating SAC signals. Correct bipolar attachments remove NDC80 from this gradient (Figure 2.5), and dephosphorylation by PP1 and PP2A stabilizes these connections, stabilizing and silencing the SAC signals [6, 7].

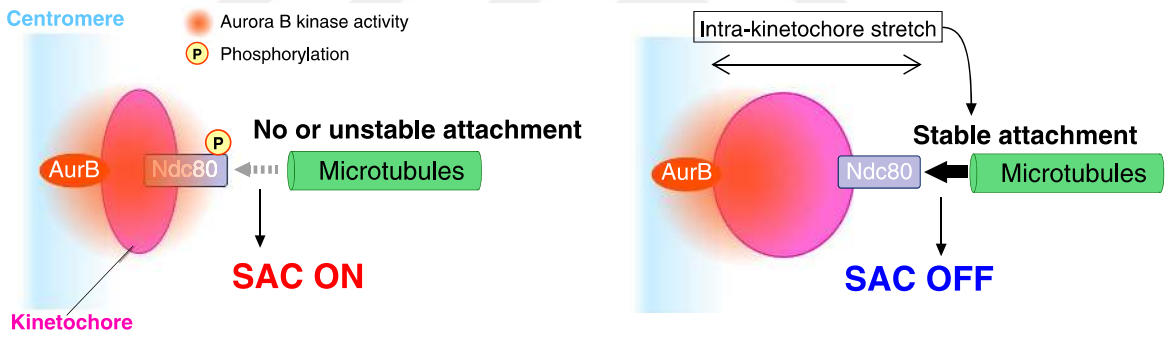

Figure 2.5: Kinetochore-microtubule attachment and spindle assembly checkpoint: (a) the aberrant microtubule attachment where NDC80 remains in the Aurora B activity gradient activating SAC, (b) the correct and stable microtubule attachment with intra-kinetochore stretch deactivating SAC. Adapted from [2].

While the stretch within the kinetochore aids in stabilizing these attachments, it is not essential for SAC silencing [2]. Several kinases have major roles in the regulation of SAC to ensure proper chromosome segregation. While the proper biorientation is not achieved, SAC remains active, and anaphase-promoting machinery is inhibited by mitotic checkpoint complex (MCC) formation comprised of MAD2, CDC20, BUBR1/MAD3, and BUB3 [14]. When the biorientation is achieved, anaphase-promoting complex/cyclosome (APC/C) binds

to CDC20, and by the degradation of securin, separase gets activated to dissolve the cohesion between sister chromatids, allowing the chromosomes to be separated.

2.1.3 Kinetochores

Kinetochores are large protein complexes assembled on centromeric DNA acting as signaling hubs for the regulation of SAC. Their primary function is to connect the chromosomes to the spindle microtubules to facilitate proper chromosome segregation [15]. They assemble on inner centromere components: the constitutive centromere-associated network (CCAN) and the outer kinetochore, which includes the KMN network (KNL1 complex, Mis12 complex, NDC80 complex) (Figure 2.6).

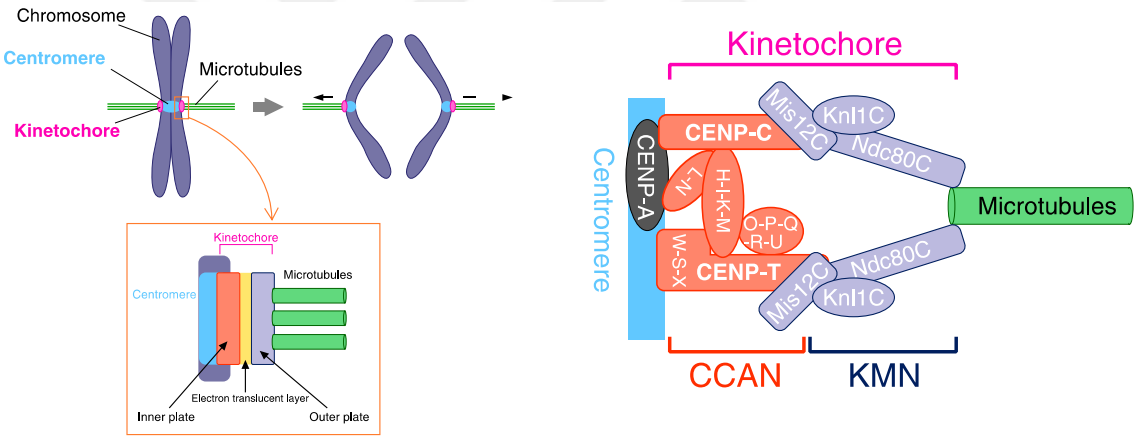

(a) (b)

Figure 2.6: The kinetochore in M-phase: (a) the trilaminar structural model for kinetochore, (b) the model of kinetochore structure. Adapted from [2].

KMN network is responsible for microtubule attachment with its key component NDC80 complex directly mediating the interactions. NDC80 complex is composed of four subunits; NDC80/Hec1 and Nuf2 interact with microtubules, and Spc24 and Spc25 are responsible for NDC80 attachment to inner kinetochore proteins (Figure 2.7). The flexible loop of the Hec1 subunit allows the Ndc80 complex to show conformational flexibility by adopting straight and bent forms. When the complex is not bound to the centromere, it remains in an auto-inhibited, tightly bent confirmation, reducing its microtubule binding affinity. Upon

kinetochore assembly, interactions with kinetochore components promote a straightened conformation, enhancing microtubule binding [16].

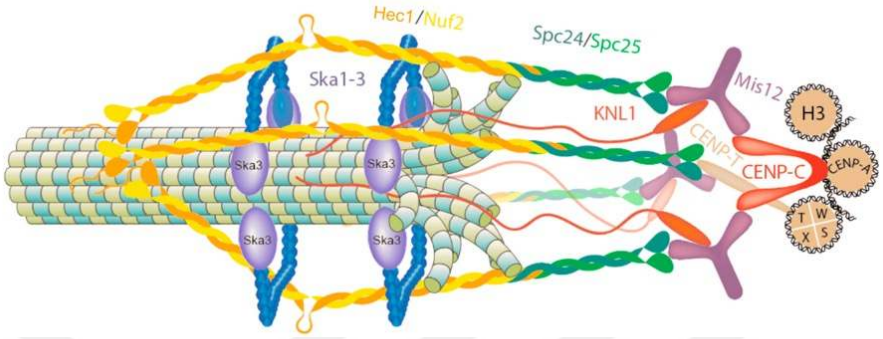

Figure 2.7: Interaction of the NDC80 complex with microtubules and kinetochore proteins in higher eukaryotes. Adapted from [17].

2.2 The Cytoskeleton

The cytoskeleton is a dynamic network of filament proteins that shapes the cell structure, enables motility, and facilitates intracellular transport. It has three major components: microtubules, intermediate filaments (IFs), and actin filaments (AFs, microfilaments). The major component of the cytoskeleton is the microtubules. They are conserved in all eukaryotic cells involved in mitosis, intracellular transport, and maintenance of the cell shape. They are composed of alpha- and beta-tubulin subunits assembled into linear protofilaments with a diameter of around 25 nm. The least studied component of the cytoskeleton is the intermediate filaments. They are found mostly in animal cells, providing mechanical strength and stability. Intermediate filaments are built from monomers in a stepwise fashion with a diameter of around 10 nm. Another major component, actin filaments, are also present in all eukaryotic cells. They are thin and flexible filaments driving migration and shape changes. The globular proteins called G-actin polymerize noncovalently into actin filaments called F-actin with a diameter of around 7 nm. These three components work together to ensure cellular integrity, adaptability, and functionality in both normal and pathological conditions.

There are many linker proteins of cytoskeletal elements that regulate their functions (Figure 2.8). Mainly, IFs and MTs interact in the cell interior, MTs and AFs in the cell

periphery, and IFs and AFs at the periphery of the IF network. While there are cross-linkers and motor proteins for MTs and for AFs, IFs are only connected by cross-linkers. Crosstalk between AFs-IFs and MTs-IFs is facilitated by cross-linkers and motors. There are also special cases, such as actin-vimentin and MTs-neurofilament binding, that occur directly. Crosstalk between AFs-MTs is facilitated by numerous cross-linkers as well as AF-based and MT-based motors [18]. This three-way cytoskeletal crosstalk enables specific functions.

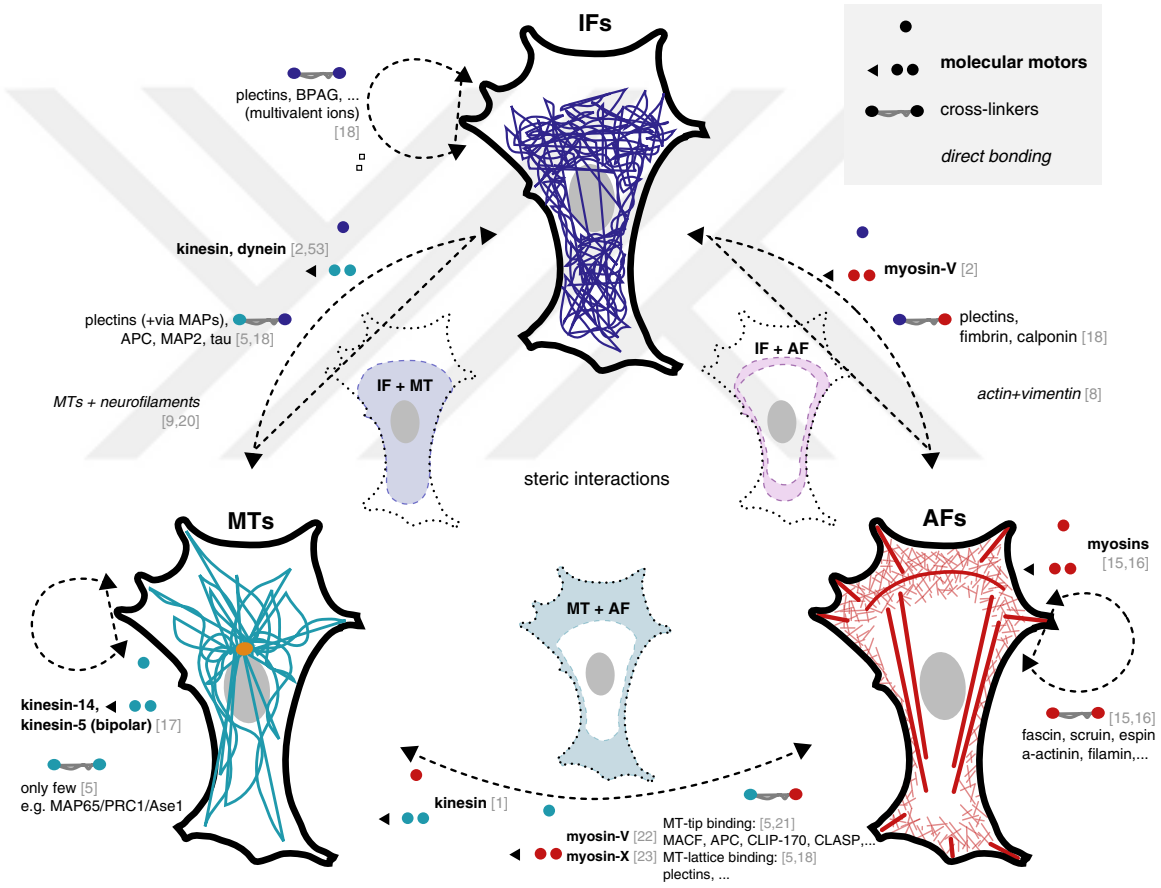

Figure 2.8: Physical interaction between cytoskeletal systems. Adapted from [18].

2.2.1 Intermediate Filaments

Intermediate filaments are fibrous structures with a large and heterogeneous family of proteins. Their main function is to give mechanical strength to the cells. In epithelial tissues, they spread through the cytoplasm and cellular junctions, thereby strengthening the epithelium.

Intermediate filaments are built from soluble monomers in a stepwise fashion. The assembly occurs by the formation of contacts between α-helical coiled coils. First, the soluble monomers form dimers via the interaction of their central domains to form parallel helical coils. The parallel dimer then associates with another parallel dimer in an anti-parallel manner to form tetramers. Since the tetrameric subunit is made up of two anti-parallel dimers, its two ends are the same, and this causes a lack of overall structural polarity, which is critical for actin filaments and microtubules. With the lateral association of eight tetramers (32 monomers), Unit-Length Filaments (ULFs) form, and the end-to-end annealing of ULFs results in the formation of a thick filament with a diameter of 16 nm. Further annealing of ULFs results in filament elongation and final intermediate filaments (Figure 2.9).

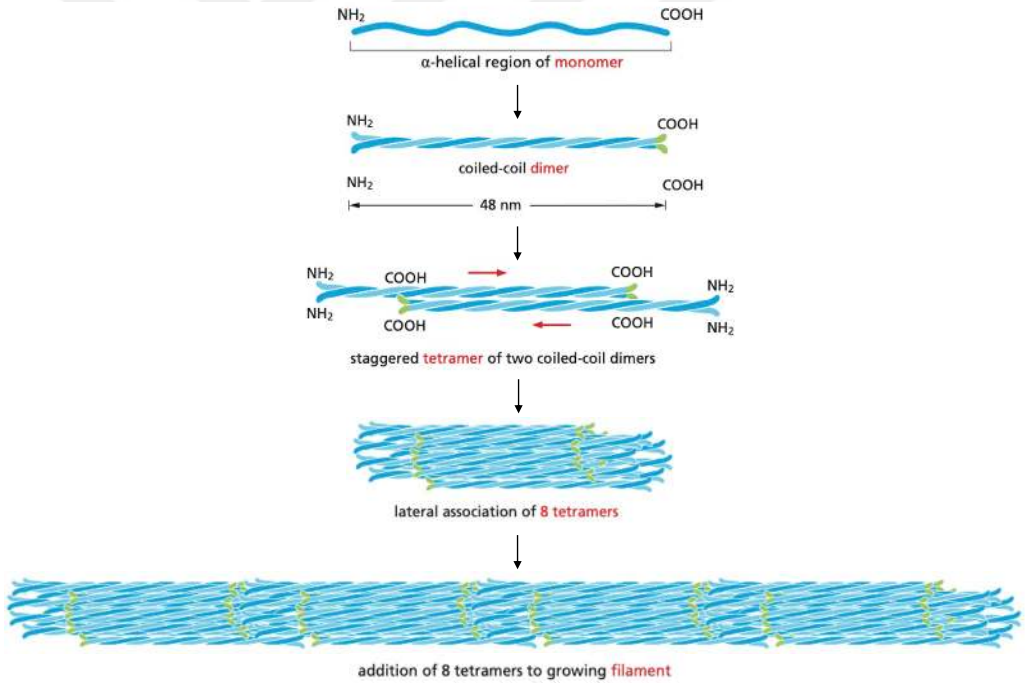

Figure 2.9: A model of intermediate filament construction. Adapted from [1].

Intermediate filaments are subdivided into five different classes. Type I (acidic) and Type II (basic/neutral) are keratins, Type III consists of desmin, vimentin, and GFAP, Type IV is neurofilaments, and Type V is Lamins (Figure 2.10). They are distributed in different cell types, and their functions vary.

Class	Protein	Distribution	Function	
I	Acidic Keratins	Epithelial Cells	Tissue Strength	 Epithelial cell
II	Basic Keratins	Epithelial Cells	Tissue Strength	
III	Desmin, Vimentin, GFAP	Muscle, Mesenchymal cells, Glial cells	Sarcomere Organization	 Smooth muscle
IV	Neurofilaments	Neurons	Axon Organization	 Axon
V	Lamins	Nucleus	Nuclear Organization	 Nuclei

Figure 2.10: Classes of intermediate filaments. Adapted from [19].

Cytoskeletal elements are essential for maintaining the integrity of intermediate filaments. Research has demonstrated that the stability of microtubules is required for preserving the intermediate filament network [20]. While studies have predominantly focused on vimentins, there have also been investigations centered on other classes of intermediate filaments, such as keratins. Studies indicate that microtubule depolymerization disrupts keratin filaments, and keratin particles co-localize with microtubules, suggesting their transport with the help of motor proteins [21], [22]. Furthermore, keratin particles have been observed to grow and move toward the cell center through an actin-dependent process [23]. Together, these findings highlight the regulation of intermediate filaments through interactions with other cytoskeletal elements.

2.2.2 Regulation of Intermediate Filaments

The dynamics and functions of the cytoskeleton are mainly regulated by post-translational modifications and binding partners. The regulation of microfilaments and actin filaments is primarily done via their associated proteins or other post-translational modifications. However, intermediate filaments are unique in that phosphorylation has the main role in their regulation.

Phosphorylation of intermediate filament proteins regulates the filament organization, solubility, and cell-protective functions (Figure 2.11). Various cellular properties are affected by the IF phosphorylation, leading to their reorganization, disassembly, and aggregation [24].

Well-known IF protein phosphorylation sites are “head” and “tail” domain regions that consist of mostly serine amino acids. In general, the head domains of IFs, which are composed of many basic residues, are positively charged and play a key role in IF assembly. Subsequent phosphorylation at serine/threonine residues in the head domains can change the charge, resulting in the disassembly of IFs by promoting IF solubility. However, in some cases, the phosphorylation of IFs can promote their formation and increase their stability [25]. In general, the phosphorylation of intermediate filament proteins is a crucial factor in maintaining the structural dynamics of the filaments.

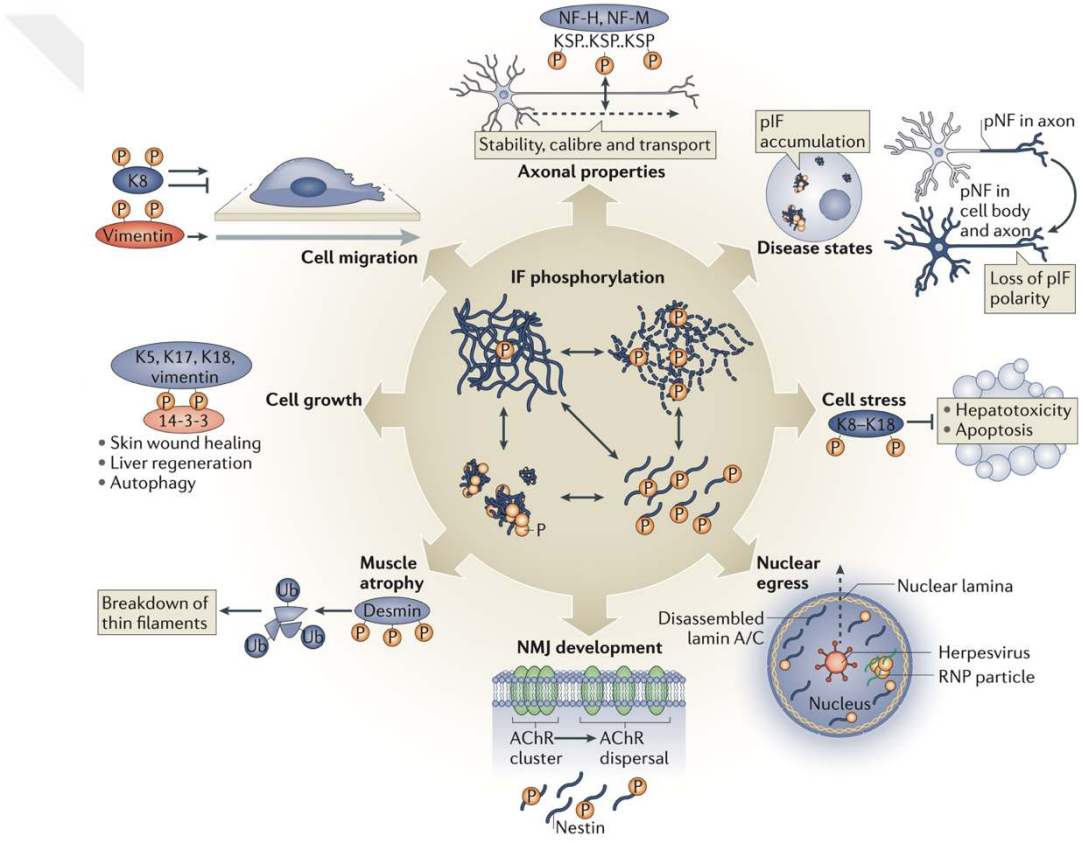

Figure 2.11: Multifunctional roles of IF protein phosphorylation [24].

2.3 Keratins

One major family of intermediate filaments is the keratin family of fibrous structural proteins. The Type I and Type II intermediate filaments are categorized as acidic and neutral/basic keratins, respectively, and they form heterodimers to function properly. There are 54 functional keratin genes in the human genome located on chromosomes 12 and 17 [3].

They are found in epithelial cells, expressed in a cell type-specific manner, and function to give strength, stability, and integrity to the cells.

2.3.1 Keratins in Cancer

Carcinoma, a cancer of epithelial origin, is the majority of human cancers. Keratins are mainly distributed in epithelial cells with diverse expression patterns, and their expressions are maintained in several types of cancer [26]. Given the fact that epithelial tumors maintain keratin expression respective to the origin of the cell type, the heterogeneous expression pattern of keratins, and the availability of keratin-specific antibodies, they are studied as immunohistochemical markers in diagnostic tumor pathology [3] (Table 2.1).

Table 2.1: Keratins as diagnostic markers in tumor pathology [26].

Cancer site and subtype	**Keratin expression**
Biliary duct	K7, K8, K18–20
Bladder, transitional cell	K5[a], K7, K8, K18, K19, K20[a]
Breast	K5[a,b], K6[a,b], K7, K8, K14[a,b], K17[a,b], K18, K19
Cervix	K4–8, K10, K13–19
Colon	K7[a], K8, K18–20
Kidney, clear cell	K8, K18, K19[a]
Papillary	K7, K8, K18, K19
Chromophobe	K7, K8, K18, K19[a]
Liver	K7[a], K8, K18, K19[a], K20[a]
Lung, adenocarcinoma	K7, K8, K18, K19
Small cell	K8, K18, K19[a]
Ovary, adenocarcinoma[c]	K7, K8, K18, K19
Pancreas	K5[a], K7, K8, K18, K19, K20[a]
Pleura (mesothelioma)	K5, K7[a], K8, K18, K19
Prostate	K8, K18, K19
Skin, squamous	K1, K4–6, K8[d], K10, K13–17, K18[d], K19[d]
Merkel cell	K8, K18, K20
Stomach	K7[a], K8, K18, K19, K20[a]
Uterus	K5[a], K7, K8, K18, K19

[a] Focal/heterogeneous staining in some, but not all, cases.

[b] Focal or extended staining in basal-like tumors.

[c] Non-mucinous.

[d] In poorly differentiated cases.

Keratins are not considered only as markers but also as regulators of cancer cell signaling. In simple epithelial cells, Keratin 8 and 18 (K8/18) are expressed as the primary keratin pair, and the loss of K8/18 expression is associated with metastasis [3]. During malignant transformation, their expression is maintained until the tumor becomes invasive. At the early steps of metastasis, carcinoma cells undergoing epithelial-mesenchymal transition (EMT) may retain epithelial characteristics, such as keratin expression, while acquiring mesenchymal traits (Figure 2.12). In such cases, keratins can serve as diagnostic markers in determining the tumor origin. Conversely, the loss of keratin expression during EMT facilitates the cytoskeletal reorganization into a mesenchymal morphology, accompanied by the upregulation of vimentins and other mesenchymal markers [27].

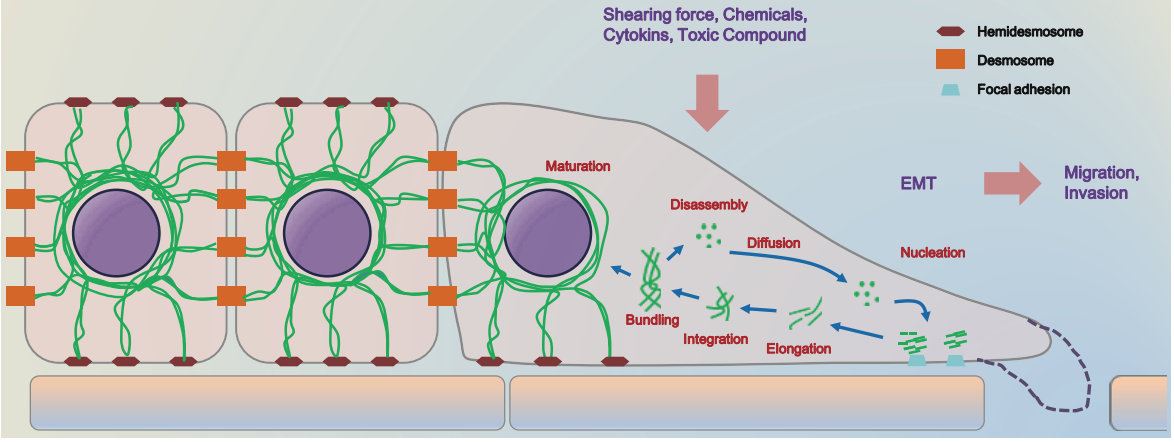

Figure 2.12: The keratin cycle illustrating its role in EMT [6].

Reorganization of the keratin network and its dynamicity leads to increased migration in cancer cells, which is necessary for metastasis. Many proteins, including kinases, bind to keratin filaments and induce their regulation by phosphorylation. Keratin 8 (K8) is a Type II intermediate filament that is generally hyperphosphorylated, and such as in liver disease, its site-specific phosphorylation is being used as a progression marker [28].

2.3.2 Regulation of Keratin 8

Keratin 8 is an intermediate filament protein encoded by the *KRT8* gene. It contains a common α-helical rod domain sided by non-helical head and tail domains of diverse lengths and sequences having several phosphorylation sites (Figure 2.13). To function properly,

keratin 8 heterodimerizes with keratin 18. The alignment of the rod domains of K8 and K18 leads to the formation of a stable heterodimer. The resulting heterodimers further assemble into higher-order structures, contributing to the structural integrity of the epithelial cells.

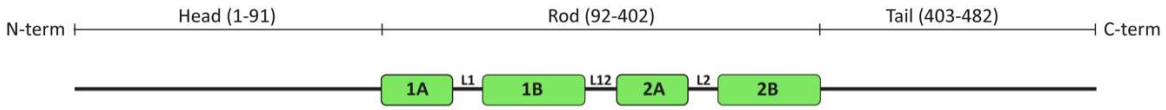

Figure 2.13: Domain structure of keratin 8. Adapted from [6].

For the regulatory events of keratin 8, phosphorylation is a key modification. Phosphorylation of keratin 8 plays an essential and site-specific role in regulating keratin filament formation by affecting its solubility. It is a very dynamic concept depending on the dimers and physiologic state of the cell. Simple epithelial keratins are the most soluble ones, and about 5% of the K8/K18 pair is soluble under basal cell conditions [29]. Additionally, it is known that the solubility of keratin 8 increases in mitosis or under heat stress [30]. However, there are studies show that a highly conserved tyrosine (Tyr, Y) residue in the rod domain of keratin 8 (Tyr267) promotes insolubility and filament formation [25].

In certain cases, the continuous phosphorylation of keratin filaments leads to their disassembly and eventual loss, a hallmark feature of EMT [5]. In such situations, keratins can no longer serve as biomarkers; however, their phosphorylated forms, or phosphoproteoforms, alongside mesenchymal markers, can be used to assess the EMT state [6]. These findings underscore the importance of phosphorylation in regulating keratin dynamics and its implications for EMT monitoring.

Chapter 3

MATERIALS AND METHODS

3.1 Cell Culture

MCF7 (human breast cancer cell line), HeLa S3 (subclone of HeLa, human cervical cancer cell line), MDA-MB-231 (human breast cancer cell line), CAKI-2 (human renal cancer cell line), and HEK 293 (human embryonic kidney cell line) cells were cultured on 10 cm Petri dishes in 10 ml culture media at 37°C in 5% CO2. For MCF7, HeLa S3, MDA-MB-231, and HEK 293 cells, DMEM-based media (Gibco, 41966029); for CAKI-2 cells, McCoy's 5A media (Wisent, 317-010) were supplemented with 10% FBS, 1% non-essential amino acid solution (PAN-Biotech, P08-32100) and P/S. At around 80% confluency, cells were passaged, frozen, or pelleted according to further experiments. Cells were washed with 1X PBS and incubated with 1 ml 0.05% trypsin-EDTA at 37°C for 5 minutes. Trypsin-EDTA was deactivated with cell media at a 1:3 (trypsin-EDTA/media) ratio. For passaging, cells were collected and seeded into new Petri dishes. To collect the cell pellet, the cell suspension was transferred in a 15 ml falcon tube and centrifuged at 400 g for 2 minutes. The pellet was washed with 1X PBS, and centrifugation was repeated. The cell pellet was flash-frozen in liquid nitrogen and stored at -80°C for further experiments. To freeze the cells for storage in liquid nitrogen, a freezing media with 70% culture media, 20% FBS, and 10% DMSO was used.

Genetically modified HeLa cells were prepared with CRISPR/Cas9-mediated keratin 8 knockout (K8 KO) by Dr. Büşra Harmanda. HeLa cells transfected with non-targeting guides were used in the control, and HeLa K8 KO cells transduced with a vector containing green fluorescence protein (GFP) fused to the N-terminus of keratin 8 (K8-GFP) were used in the rescue experiments. HeLa cells transfected with GFP (HeLa GFP) or with K8-GFP (HeLa

K8-GFP) were grown in 400 µg/ml G418 (Santa Cruz, sc-29065A) containing DMEM-based media. Culturing and harvesting of cells were performed as described above.

3.2 Cell Synchronization

Cell cycle synchronization was started when the cells reached around 50% confluency. A single thymidine block was applied to arrest the cells at interphase. Cells were incubated with 2 mM thymidine (Calbiochem, 50-89-5) given in culture media for 24 hours, and interphase cells were harvested or fixed at the end of the treatment. To progress through the cell cycle, cells were washed with 1X PBS and incubated with fresh culture media for 4 hours. To arrest the cells at mitosis, cells were treated with STLC (alfaAesar, L14384). 10 µM STLC was added to the culture media and incubated for 16 hours. The incubation time differs only in the MCF7 cell line, requiring 20 hours to achieve similar synchronization efficiency. Mitotic cells were harvested by mitotic shake-off or fixed at the end of STLC treatment. To arrest the cells at cytokinesis, cells were treated with purvalanol A. 100 µM purvalanol A (Tocris Bioscience, 1580) was added to the culture media without STLC release and incubated for 15 minutes. Cytokinesis cells were harvested by shake-off or fixed at the end of purvalanol A treatment.

3.3 FACS Analysis

To verify synchronization, the proportion of cells in the G1, S, and G2/M phases was quantified through fluorescence-activated cell sorting (FACS) analysis based on DNA content. Cells were seeded in five 10 cm Petri dishes for the negative control (asynchronous cells for the secondary antibody background control), asynchronous, interphase, mitosis, and cytokinesis synchronization groups. At around 90% confluency, untreated or synchronized cells were collected, centrifuged at 400 g and 4°C for 2 minutes, and washed once with 5 ml ice-cold 1X PBS. Pellets were resuspended in 400 µl ice-cold 1X PBS and transferred into round-bottom tubes. To fix the cells, 1 ml 70% ethanol was added dropwise. The tubes were gently inverted to mix and incubated at -20°C for at least an hour. Fixed cells were centrifuged at 1400 g for 7 minutes and washed with 1 ml 1X PBS. Cells were resuspended in 200 µl permeabilization buffer (0.25% Triton X-100 in 1X PBS) and rotated for 15 minutes at 4°C. For blocking, cells were resuspended in 1 ml blocking buffer (1% BSA in 1X PBS)

and rotated for 25 minutes at 4°C. The primary antibody, anti-phospho-histone H3 (Cell Signaling Technology, 3377T) (Table 3.2), was diluted at the required amount with 1% BSA in 1X PBS, and the cells, except those in the negative control group, were rotated with 100 µl at 4°C overnight. After primary antibody incubation, cells were centrifuged at 1400 g for 7 minutes and washed with 1 ml 1X PBS. The secondary antibody, anti-rabbit Alexa Fluor 647 (Invitrogen, A31573) (Table 3.3), was diluted at the required amount with 1% BSA in 1X PBS, and the cells, including those in the negative control group, were rotated for 30 minutes at room temperature. After secondary antibody incubation, cells were centrifuged at 1400 g for 7 minutes and washed with 1 ml 1X PBS. Pellet of the negative control group was resuspended in 500 µl 0.1% Triton X-100 in 1X PBS, while the remaining pellets were resuspended in 500 µl staining solution (10 µg/ml Hoechst (Thermo Fischer Scientific, 33342), 200 µg/ml RNase A (New England Biolabs, T3018), 0.1% Triton X-100 in 1X PBS). Pellets were rotated for 30 minutes at room temperature and analyzed within 6 hours. The analysis was performed by Dr. Monika Langlotz with a BD FACSymphony A1 flow cytometry equipped with four lasers (405/488/561/637 nm) (Appendix A). Files were processed using BD FACSDiva (version 9.0.2) software (Appendix B).

3.4 Cloning

Keratin 18 (pcDNA3) was obtained from Addgene (Plasmid #18064) and used to construct a keratin 18-RFP (K18-RFP) vector. For this purpose, a pLVX-puro backbone containing ezrin-RFP (Appendix C) was used. Throughout the experimental process, plasmids and primers were designed in silico using SnapGene (version 8) software. DNA gel electrophoresis was performed with 1% agarose gel, and HyperLadder 1 kb (Bioline, BIO-33053) was used to determine the size of the DNA fragments. Gel and PCR products were purified using NucleoSpin Gel and PCR Clean-up kit (MACHEREY-NAGEL) following the manufacturer's instructions.

Ezrin-RFP vector was cut from NotHI_HF and XhoI restriction sites to remove ezrin from the vector. Digestion was performed at 37°C overnight in a total reaction volume of 50 µl with 1 µg DNA, 1 µl NotHI_HF, 1 µl XhoI, and 5 µl CutSmart Buffer. Enzymes were heat-inactivated at 65°C for 20 minutes and stored at 4°C. DNA gel electrophoresis was performed, and the cut vector was purified for subsequent cloning.

To amplify the keratin 18 for the Gibson assembly, a polymerase chain reaction (PCR) was performed. 50 µl reaction mixture was prepared with 10 µL 5X Q5 Reaction Buffer, 1 µL 10 mM dNTPs, 2.5 µL 10 µM primer mix (forward 5' AGCGCTACCGGACTCAGATCCACCATGAGCTTCACCACTCGCT 3', reverse 5' TCCTCGGAGGAGGCCATGGCATGCCTCAGAACTTTGGTGT 3'), 0.5 µL 2 U/µl Q5 High Fidelity DNA Polymerase (NEB, M0491L), and 5 ng DNA. PCR was performed as initial denaturation at 98°C for 30 seconds, 35 cycles of denaturation at 98°C for 10 seconds, annealing at 63°C for 30 seconds, extension at 72°C for 25 seconds, and final extension at 72°C for 2 minutes. DNA gel electrophoresis was performed, and the PCR product was purified for subsequent cloning.

Cloning was performed using the Gibson technique [31]. Purified products are ligated using the Gibson assembly mixture. For the reaction, a 1:2 ratio of vector to DNA sequence with 8.1 ng insert and 25 ng vector was used. The insert and the vector were mixed with 3.75 µl Gibson assembly mixture and incubated at 50°C for 30 minutes. The Gibson product was transformed into Stbl3 chemically competent *E. coli* cells. 2 µL Gibson product was mixed with 50 µl Stbl3 and incubated for 30 minutes on ice, followed by 2 minutes of heat shock at 42°C and 2 minutes of incubation on ice. 1 mL LB was added to the cells and incubated at 300 rpm and 37°C for 1 hour. Concentrated cells were seeded onto ampicillin LB agar plates and incubated at 37°C overnight. Colonies grown on ampicillin LB agar plates were verified the next day by colony PCR.

For the colony PCR, each colony was picked up with a 200 µL tip, smeared to PCR tubes, spread onto an agar plate, and dipped into a liquid culture. The agar plate and the liquid cultures were grown at 37°C overnight. For PCR, 20 µl reaction mixture was prepared with 0.4 µl 10 µM primer mix, the same as used for cloning, using 10 µL EmeraldAmp MAX HS PCR Master Mix (Takara Bio, RR330A). As a positive control, 3 ng insert was used. PCR was performed as initial denaturation at 98°C for 5 minutes, 40 cycles of denaturation at 98°C for 10 seconds, annealing at 63°C for 30 seconds, extension at 72°C for 2 minutes, and final extension at 72°C for 5 minutes. DNA gel electrophoresis was performed, and the plasmid DNA of the positive colony was purified. The purified product was sent for Sanger sequencing (Appendix D).

GFP, K8-GFP, and K8(S34-35D)-GFP vectors were obtained from Dr. Büşra Harmanda.

3.5 CRISPR/Cas12a-Assisted PCR Tagging and dTAG System

For the rapid and target-specific degradation of keratin 8 in HeLa S3 cells, the CRISPR-Cas12a-assisted PCR tagging method was combined with the dTAG system [32], [33]. A knock-in was performed to integrate the desired sequence into the target gene locus, enabling target-specific degradation upon chemical treatment. Throughout the experimental process, DNA gel electrophoresis was performed with 1% agarose gel, and GeneRuler 1 kb Plus DNA Ladder (Thermo Fischer Scientific, SM1331) was used to determine the size of the DNA fragments. Gel and PCR products were purified using NucleoSpin Gel and PCR Clean-up kit (MACHEREY-NAGEL) following the manufacturer's instructions.

For the CRISPR-mediated locus-specific knock-in, M1 (M1_KRT8 5' CGCACCAGCTCCTCCAGGGCCGTGGTTGTGAAGAAGATCGAGACACGTGATGG GAAGCTGGTGTCTGAGTCCTCTGACGTCCTGCCCAAGT 3') and M2 oligos (M2_KRT8_enAsCas12a 5' ACAGCTGCGGCAGCCCCTCCCAGCCTACCCCTCCTGCGCTGCCCCAGAGCCTGG G 3') were designed as described in [32] to match with the target gene *KRT8*. A template plasmid (pMacTag-2A-AS02N) containing a mutant version of the FKBP12 protein ($FKBP12^{F36V}$), an HA tag, a T2A region, and a G418 resistance gene, also known as neomycin resistance gene, was constructed by Dr. Anne-Lore Schlaitz (Appendix E). Together with the oligos, the template plasmid was used to prepare the PCR cassette for the knock-in at the 3'UTR of the *KRT8* gene. For tagging PCR, 100 µl reaction mixture was prepared with 10 µl 5X HiFi Reaction Buffer, 5 µl 10 mM dNTPs, 2.5 µl 10 µM M1 tagging oligo, 2.5 µl 10 µM M2 tagging oligo, 5 µl 5 M betaine, 1 µl 50 mM $MgCl_2$, 0.5 µl 2 U/µl PRECISOR HiFi DNA Polymerase PLUS (BioCat, 1706), and 100 ng template DNA. The tagging PCR was performed as initial denaturation at 95°C for 3 minutes, 35 cycles of denaturation at 95°C for 20 seconds, annealing at 54°C for 30 seconds, extension at 72°C for 2:20 minutes, and final extension at 72°C for 5 minutes. DNA gel electrophoresis was performed, and the PCR cassette was purified for subsequent transfection.

Plasmid transfection was performed with Lipofectamine 2000 as in the following procedure. Cells were seeded into a 24-well plate. At around 90% confluency, culture media was changed to 400 µl P/S-free culture media. 250 ng PCR cassette and 250 ng helper plasmid (enAsCas12a) were diluted in 50 µl Opti-MEM and incubated at room temperature for 5 minutes. In parallel, 1 µl Lipofectamine 2000 was diluted in 50 µl Opti-MEM and incubated at room temperature for 5 minutes. The PCR cassette and Lipofectamine 2000 mixtures were combined in a 1:1 ratio and incubated at room temperature for 20 minutes. The transfection mixture was added drop by drop to one well of the 24-well plate. As a control, only the helper plasmid was used for transfection. After 6 hours, cells were transferred into 6-well plates. For the selection of the transfected cells, a G418 kill curve was established using concentrations ranging from 200 to 1200 µg/ml. After 48 hours of transfection, cells were selected with 700 µg/ml G418 for two weeks, and the selection efficiency was assessed using immunofluorescence imaging of HA staining.

The transfected pool of HeLa S3 cells was sorted with flow cytometry-based single-cell sorting into four 96-well plates. Colonies grown from single cells were selected and screened for homozygous insertion. For screening, selected clones were split into additional 96-well plates, and the genomic DNAs were isolated with a QuickExtract DNA Extraction Solution (Biosearch Technologies, QE09050). Cells in 96-well plates were washed with 1X PBS and incubated at 650 rpm and 65°C for 15 minutes with 20 µl Quick DNA extraction solution. Cells were resuspended and transferred into a 96-well PCR plate. The plate was sealed for the run in a PCR machine with the following program: 65°C for 15 minutes, 68°C for 15 minutes, and 98°C for 10 minutes. The DNA was ready to be used for PCR. 50 µl reaction mixture was prepared for the PCR with 5 µl 10X PCR Reaction Buffer (Sigma-Aldrich, P2192-1VL), 1 µl 10 mM dNTPs, 1 µl 5 µM forward primer (for: 5’ TGGTCTGAGCTCGGCCTAT 3’), 1 µl 5 µM reverse primer (rev: 5’ TGGCAGAGCTAGCTGAGGTT 3’ or dTAG_rev: 5’ GGCGATGCGCTGCGAATC 3’), 0.25 µl 5 U/µl Taq DNA Polymerase (Sigma-Aldrich, D1806), and 5 µl of extracted DNA. As a positive control, 625 ng genomic DNA from the transfected pool of cells was used. The PCR was performed as initial denaturation at 94°C for 1 minute, 40 cycles of denaturation at 94°C for 20 seconds, annealing at 62°C for 20 seconds, extension at 68°C for 1:30 minutes, and final extension at 68°C for 10 minutes. DNA gel electrophoresis was performed, and the

positive single-cell clones were determined. The PCR products of the positive clones were purified and sent for Sanger sequencing.

3.6 Transfection

Plasmid transfection was performed with Lipofectamine 2000 as in the following procedure. Cells were seeded into a 12-well plate. At around 30-50% confluency, culture media was changed to 600 µl P/S-free culture media. 500 ng DNA was diluted in 50 µl Opti-MEM (Thermo Fisher Scientific, 31985047) and incubated at room temperature for 5 minutes. In parallel, 1 µl Lipofectamine 2000 (Invitrogen, 11668019) was diluted in 50 µl Opti-MEM and incubated at room temperature for 5 minutes. The DNA and Lipofectamine 2000 mixtures were combined in a 1:1 ratio and incubated at room temperature for 15 minutes. The transfection mixture was added dropwise to one well of the 12-well plate. After 6 hours, transfection media was changed to cell culture media.

3.7 Lentiviral Packaging and Transduction

For lentiviral packaging, cells were seeded into a 10 cm petri dish. At around 70% confluency, culture media was refreshed with 8 ml culture media. 30 µl PEI (Polysciences, 23966) was diluted in 1 ml Opti-MEM (Thermo Fisher Scientific, 31985047) and incubated at room temperature for 5 minutes. Subsequently, 3.5 µg packaging vector psPAX2 (Addgene, 12260), 1.5 µg envelope protein pCMV-VSG-G (Addgene, 8454), and 5 µg transfer vector were added to the PEI mixture and incubated at room temperature for 15 minutes. The transfection mixture was added dropwise to a 10 cm petri dish and incubated overnight. On the second day, transfection media was changed to cell culture media. The following day, media was collected into a falcon, stored at 4°C, and 7.5 ml culture media was added to the 10 cm petri dish. On the next day, media was collected into the previous falcon. The viral supernatant was filtered through a 0.45 µm sterile filter, aliquoted in 1 ml, and stored at -20°C.

For transduction, cells were seeded into a 6-well plate. At around 50% confluency, culture media was changed with 500 µl culture media including 24 µg protamine sulfate (Sigma-Aldrich, P4505). Subsequently, 1 ml viral aliquot was added dropwise. On the second

day, cells were checked under a microscope, and on the following day, the transduction was repeated. The transfected cells were selected for a week using an established kill curve.

3.8 Microscopy and Quantification

For the microscopy imaging, Leica DMi8/SP8 TCS-DLS confocal laser scanning microscope equipped with HC PL APO 63x/1.40 oil CS2 objective and LAS X software, ZEISS LSM800 confocal laser scanning microscope equipped with 63x/1.40 Plan-Apochromat oil objective, argon (488 nm), DPSS (561 nm), and HeNe (633 nm) lasers and ZEN software, Leica SD DMi8 spinning disk confocal microscope equipped with Yokogawa CSU-X1 scanner unit, Hamamatsu ORCA-Flash4.0 LT+ camera, HC PL APO 63x/1.40-0.60 oil objective and MetaMorph software, and Leica TCS SP8 STED 3X microscope equipped with HC PL APO 100x/1.40 STED White oil objective and LAS X software were used. For Leica TCS SP8 STED 3X microscopy imaging, deconvolution was performed using the Huygens software to enhance the image clarity.

Immunofluorescence intensities were quantified using Fiji software. Briefly, RGB values of regions of interest (ROIs) at the metaphase plate were measured, and the mean intensity values were taken. The same process was applied to random spots on the chromosomal background to normalize the fluorescence intensities. Graphs were plotted by GraphPad Prism 10.

To quantify the multinucleation rate, cells were stained to visualize the cell boundaries and the nuclei. Quantification was performed by Halenur Ayaydın.

3.8.1 Immunofluorescence Staining

For the immunofluorescence experiments, cells were seeded on coverslips at 12-well plates or on µ-Slide 18-well chamber slides (ibidi, 81817). Cells were washed with 1X PBS and fixed according to the purpose of the subsequent experiment. For PFA fixation, cells were incubated in 4% PFA at room temperature for 15 minutes. For methanol fixation, cells were incubated in 100% methanol at -20°C for 15 minutes. Fixed cells were washed with 1X PBS three times for 5 minutes. The cells were permeabilized with 0.1% Triton X-100 in PBS for 10 minutes and washed with 1X PBS three times for 5 minutes. For blocking, cells were

incubated with 5% donkey serum and PBS-T (0.1% Tween 20 in PBS) for 1 hour at room temperature. Primary antibodies were diluted at the required amount with PBS-T, and cells were incubated for 3 hours at room temperature or 4°C overnight. Cells were washed with 1X PBS three times for 5 minutes. Secondary antibodies were diluted at the required amount with PBS-T, and cells were incubated at room temperature for 1 hour. Cells were washed with 1X PBS three times for 5 minutes, and DNA was stained with 5 µg/ml Hoechst or 1 µg/ml DAPI (Sigma-Aldrich, D8417) in PBS for 5 minutes at room temperature. Cells were washed with 1X PBS three times for 5 minutes. Cells on coverslips were mounted and stored at -20°C for later imaging, while cells on chamber slides were imaged directly in 1X PBS. Antibodies used for immunofluorescence are listed in Table 3.1 and Table 3.3.

3.8.2 Live Cell Imaging

For live cell imaging, cells were seeded on µ-Slide 8-well chamber slides (ibidi, 80826). During imaging, time-lapse images were collected with a Leica DMi8/SP8 TCS-DLS confocal laser scanning or Leica SD DMi8 spinning disk confocal microscope at 37°C and 5% CO_2 in a humidified chamber.

3.9 SDS-PAGE and Western Blotting

For SDS-PAGE, 10% separating (5 ml 30% Acrylamide-Bisacrylamide (29:1), 3.75 ml 4X Tris-Cl/SDS pH 8.8, 50 µl 10% APS, 10 µl TEMED) and 5% stacking (650 µl 30% acrylamide-bisacrylamide (29:1), 1.25 ml 4X Tris-Cl/SDS pH 6.8, 25 µl 10% APS, 5 µl TEMED) gels were poured sequentially. Protein samples were mixed with 5X SDS sample buffer (50% glycerol, 0.02% (w/v) bromophenol blue, 10% (w/v) SDS, 250 mM Tris-Cl pH 6.8) containing 500 mM DTT, and heated for 5 minutes at 95°C before loading into the wells. Colorplus Protein Marker (NEB, 7712S), GangNam-Stain Prestained Protein Ladder (iNtRON Biotechnology, 24052), or PageRuler Plus Prestained Protein Ladder (Thermo Fischer Scientific, 69619) was used to determine the molecular weight of the samples. Samples were run at 70 V for 30 minutes and at 120 V for 2 hours in 1 L of 1X SDS running buffer pH 8.3 (10X SDS running buffer: 144.1 g glycine, 30.34 g tris base, 10 g SDS (1%) in 1 L total volume). Proteins were transferred to a nitrocellulose membrane (GVS, 1215471) with a wet-transfer method using 1X transfer buffer (10X transfer buffer: 144.1 glycine,

30.34 g tris base in 1 L total volume) containing 20% methanol at 35 mA and 4°C overnight. To confirm the transfer, the membrane was incubated in Ponceau S for 1 minute, and the transferred proteins were visualized. The membrane was washed with distilled water and blocked with 5% non-fat dried milk powder in 1X TBS-T (0.05% Tween 20, 10 mM Tris-HCl, 150 mM NaCl) for 1 hour at room temperature. Primary antibodies were diluted at the required amount with 2% BSA in 1X TBS-T, and the membrane was incubated for 3 hours at room temperature or 4°C overnight. The membrane was washed with 1X TBS-T three times for 5 minutes. Secondary antibodies were diluted at the required amount with the blocking buffer, and the membrane was incubated for 1 hour at room temperature. The membrane was washed with 1X TBS-T three times for 5 minutes. Proteins were visualized either using the Pierce ECL Western Blotting Substrate (Thermo Fisher Scientific, 32106) with the ChemiDoc MP Imaging System (Bio-Rad, 12003154) or in the darkroom with HRP-conjugated secondary antibodies, or using LI-COR Odyssey DLx Imaging System with IRDye-conjugated secondary antibodies. Antibodies used for immunoblotting are listed in Table 3.2 and Table 3.3.

3.10 GFP-Trap for Immunoprecipitation

GFP-expressing cells were synchronized to interphase, mitosis, and cytokinesis. The synchronized cells were pelleted and flash-froze. The pellets were lysed in ice-cold lysis buffer (40 mM HEPES pH 7.5, 120 mM NaCl, 1 mM EDTA, 1% Triton X-100, 2% Empigen BB, EDTA-free protease inhibitor tablet (Thermo Fisher Scientific, 32955) and PhosSTOP (Roche, 4906837001), 1 mM sodium orthovanadate, 1 mM PMSF) by pipetting and passing through a 25-gauge needle. Lysates were incubated on ice for 30 minutes and centrifuged at 17,000 g and 4°C for 10 minutes. Dilution buffer (40 mM HEPES pH 7.5, 120 mM NaCl, 1 mM EDTA) was added to the supernatant in a 2:3 ratio. The concentration of the diluted lysate was measured with the Pierce Coomassie (Bradford) Protein Assay Kit (Pierce, PI-23200). GFP-Trap_A (Chromotek, gta-20) beads were mixed with the diluted lysate and rotated for 2 hours at 4°C. After incubation, beads were washed with the dilution buffer, and the bound proteins were eluted. For western blot analysis, proteins were eluted with 1X SDS sample buffer for 10 minutes at 95°C and collected by centrifugation at 2.500 g and 4°C for 2 minutes. For mass spectrometry analysis, proteins were eluted with glycine elution buffer

(200 mM glycine pH 2.5) for 30 seconds under constant mixing and collected by centrifugation at 2.500 g and 4°C for 2 minutes. 1 M tris base (pH 10.4) was used to neutralize the sample.

3.11 Microtubule Pelleting Assay

Cells were grown in 15 cm Petri dishes and synchronized to mitosis. The synchronized cells were pelleted and flash-froze. The pellets were lysed in ice-cold lysis buffer (100 mM K-Pipes pH 6.8, 2 mM EGTA, 1 mM $MgCl_2$, 1% NP-40, 20 µM cytochalasin D, 20 µM latrunculin B, EDTA-free protease inhibitor (Pierce, 88266)) by pipetting and passing through a 25-gauge needle. Lysates were incubated on ice for 20 minutes and centrifuged at 2.800 g and 4°C for 10 minutes. The lysate concentration was measured with the Pierce BCA Protein Assay Kit (Pierce, PI-23227). Lysate was cleared with ultracentrifugation at 100,000 g and 4°C for 30 minutes. The supernatant was incubated with 25 µM Taxol and 0.5 mM GTP for 20 minutes at room temperature to stabilize the microtubules. A 40% glycerol cushion buffer with 1 mM DTT, 25 µM Taxol, 1 mM GTP, EDTA-free protease inhibitor (Pierce, 88266) in final containing 1X BRB80 buffer (5X BRB80 buffer pH 6.8: 317 mM K-Pipes, 5 mM $MgCl_2$, 5 mM EGTA) was used to pellet the stabilized microtubules with ultracentrifugation at 100,000 g and 25°C for 30 minutes. The pellet was resuspended in CM buffer (100 mM K-Pipes pH 7, 2 mM EGTA, 1 mM $MgCl_2$, 20 µM cytochalasin D, 20 µM latrunculin B) and the 40% glycerol cushion buffer was added on top again. Microtubules were pelleted again with ultracentrifugation at 100,000 g and 25°C for 30 minutes. The pellet was resuspended with 3X SDS Blue Loading Dye (NEB, B77035) for gel electrophoresis. SDS-PAGE was performed, and the gel was fractionated into five for further in-gel digestion and mass spectrometry analysis.

3.12 Cell Lysis and Protein Digestion

The cell pellets were lysed according to the lysis buffer of the subsequent protocol. For immunoblotting, RIPA buffer (1 M Tris-HCl pH 7.5, 5 M NaCl, 10% SDS, 5% sodium deoxycholate, 10% Triton X-100) was supplemented with EDTA-free protease inhibitor tablet (Thermo Fisher Scientific, 32955) and PhosSTOP (Roche, 4906837001). The pellets were incubated with the lysis buffer on ice for 30 minutes and centrifuged at 2.500 g and 4°C

for 10 minutes. For proteomics analysis, 8 M urea in 50 mM ABC was supplemented with an EDTA-free protease inhibitor tablet (Thermo Fisher Scientific, 32955), PhosSTOP (Roche, 4906837001), and 1 mM sodium orthovanadate. The pellets were sonicated for 2 minutes and incubated with the lysis buffer on ice for 1 hour. Lysis efficiency was enhanced by pipetting the lysate and passing it through a 25-gauge needle. The lysates were centrifuged at 17,000 g and 4°C for 15 minutes. Protein concentrations were measured with the Pierce BCA Protein Assay Kit (Pierce, PI-23227).

3.12.1 In-Solution Digestion

To ensure complete protein denaturation, cell lysates were incubated with DTT and IAA. Briefly, the lysates were incubated first with 10 mM DTT at 1,000 rpm and 4°C for 45 minutes and then with 20 mM IAA at dark and room temperature for 30 minutes. After the reduction of disulfide bonds and alkylation of cysteine (Cys, C) residues, the lysate was diluted from 8 M to 1 M urea with 50 mM ABC solution. Trypsin was added at a 1:50 ratio of enzyme (ug) to protein (ug) and incubated at 37°C overnight. Tryptic digestion was repeated once again for 1 hour to increase the digestion efficiency. Digestion was ended by adding 10% FA until the pH reached 2. The peptides were desalted using Sep-Pak Vac 1 cc columns (Waters, WAT023590).

3.12.2 In-Gel Digestion

To ensure complete protein denaturation, cell lysates were incubated first with 100 mM DTT at 90°C for 5 minutes and then with 100 mM IAA and 100 mM ABC at dark and room temperature for 20 minutes. Samples were loaded to a 4-15% Mini-PROTEAN TGX Precast Protein Gel (Bio-Rad, 4561085) and stained with PageBlue Protein Staining Solution (Thermo Fisher Scientific, PI-24620) for 2 hours. The gel was rinsed with distilled water overnight, and the desired bands were fractionated. The gel fractions were incubated with a 1:1 ratio of ACN to ABC solution (ACN/ABC: 100% ACN and 100 mM ABC) at room temperature and 800 rpm for 1 hour. The gels were repeatedly washed with 100 mM ABC and 100% ACN at room temperature and 800 rpm for 15 minutes until the gels were cleared. When the gels were clear enough, they were incubated with the ACN/ABC solution at room temperature and 800 rpm for 15 minutes, followed by incubation with 100% ACN until the

gels fully shrank. The gels were dried in SpeedVac and each fraction was incubated with 150 ng trypsin in 100 mM ABC at 37°C overnight. The peptides were collected, and the gels were incubated sequentially with 100 mM ABC, ACN/ABC, and 100% ACN at room temperature and 800 rpm for 15 minutes to extract the remaining peptides. The peptides were desalted using Sep-Pak Vac 1 cc columns (Waters, WAT023590).

3.13 Stable Isotope Dimethyl Labeling

On-column dimethyl labeling was performed as described in [34] for 1 mg of in-solution digests. The combinations of several isotopomers of formaldehyde and cyanoborohydride were used to label the N-terminus and ε-amino group of lysine (Lys, K) residues. Briefly, the combination of regular formaldehyde and cyanoborohydride generated a mass increase of 28 Da per primary amine on a peptide (light label). Using deuterated formaldehyde, a mass increase of 32 Da per primary amine (intermediate label) was generated. The third label with a mass increase of 36 Da was achieved by combining deuterated and ^{13}C-labeled formaldehyde with cyanoborodeuteride (heavy label). Before sample loading for dimethyl labeling, Sep-Pak Vac 1 cc columns (Waters, WAT023590) were washed with 100% ACN and Solvent A (0.1% FA in H_2O). Dried samples were reconstituted in Solvent A, and peptides were loaded onto columns. Labeling reagents consisting of 4% (v/v) proper formaldehyde solution (CH_2O, CD_2O, or $^{13}CD_2O$), 0.6 M proper sodium cyanoborohydride solution ($NaBH_3CN$, or $NABD_3CN$) (Sigma-Aldrich), and 50 mM sodium phosphate buffer pH 7.5 (NaH_2PO_4 and Na_2HPO_4) (Thermo Fisher Scientific) were freshly prepared for each sample and passed through the columns. Columns were washed with Solvent A, and labeled peptides were eluted with Solvent B (80% ACN and 0.1% FA in H_2O). Peptides were dried in SpeedVac and resuspended in 5% FA and 5% ACN in H_2O for mass spectrometry analysis.

Peptide digests of interphase-, mitosis-, and cytokinesis-synchronized cells were labeled with light, intermediate, and heavy dimethyl mass tags, respectively. To ensure accurate quantification across different cell cycle stages, labeled samples were combined at a 1:1:1 ratio based on their average peptide intensities obtained by mass spectrometry analysis.

3.14 Peptide Fractionation

HyperSep™ SCX Strong Cation Exchanger SPE Columns (Thermo Fischer Scientific, HYPE60108-420) were used for the fractionation of 1 mg digests. Dried samples were resuspended in loading buffer pH 2.65 (7 mM KH_2PO_4, 30% ACN). The columns were washed with 100% methanol, elution buffer 5 (loading buffer with 500 mM KCl), H_2O, equilibration buffer pH 7.5 (50 mM K_2HPO_4, 500 mM NaCl), H_2O, and loading buffer sequentially. Samples were loaded onto the columns, and flow-through was collected as fraction FT. Fractions were collected using elution buffers with increasing KCl concentrations (elution buffer 1: loading buffer with 30 mM KCl, elution buffer 2: loading buffer with 60 mM KCl, elution buffer 3: loading buffer with 90 mM KCl, elution buffer 4: loading buffer with 120 mM KCl, elution buffer 5: loading buffer with 500 mM KCl). Eluted samples were dried in SpeedVac, desalted using Sep-Pak Vac 1 cc columns (Waters, WAT023590), and stored at -20°C.

3.15 Phosphopeptide Enrichment

The SCX fractions (100-200 µg) were enriched with TiO_2 beads [35]. C8 plugs were placed into GELoader Tips (Eppendorf, 30001222) and washed with 100% methanol by centrifugation at 100 g for 10 minutes. 10 mg TiO_2 beads were resuspended in 1 ml loading buffer (80% (v/v) ACN, 6% (v/v) TFA). 50 µL bead solution was loaded onto the tips, packed by gravity, and centrifuged at 100 g for 1 hour. Beads were equilibrated with 30 µl loading buffer and centrifuged at 100 g for 30 minutes. In the meantime, dried samples were resuspended in the loading buffer at the final concentration of 1 µg/µl. Samples were loaded onto the tips by centrifugation at 50 g. Samples were washed with 50 µl washing buffer (50% (v/v) ACN, 0.1% (v/v) TFA) and centrifuged at 100 g for 1 hour. Bound peptides were eluted first with 25 µl elution buffer 1 pH 11 (10% NH_3H_2O) and then with 3 µl elution buffer 2 (80% (v/v) ACN, 2% (v/v) FA) into 35 µl of 10% FA by centrifugation at 100 g. 3 µl 100% FA was added to the elute, and the samples were directly run at the mass spectrometer. It is important to note that the centrifugation forces were adjusted during the experiment based on the observed flow rate. This real-time adjustment ensured optimal peptide retention while preventing sample loss or inefficient binding, thereby enhancing the efficiency and reproducibility of the enrichment process.

3.16 Data Acquisition

Data acquisition was performed using three different methods: Data-Dependent Acquisition (DDA), Data-Independent Acquisition (DIA), and Parallel Reaction Monitoring (PRM). DIA analysis was conducted in collaboration with the FGCZ by Dr. Antje Dittmann.

3.16.1 Data-Dependent Acquisition

Samples were subjected to a reversed-phase Nano LC-MS/MS (UltiMate 3000 RSLCnano System, Thermo Fischer Scientific) connected to a Q Exactive quadrupole Orbitrap mass spectrometer (Thermo Fisher Scientific). The peptides were directly loaded onto an in-house packed C18 column (365 µM x 75 µM, 40 cm, 1.9 µm pur, Dr. Maisch) and separated at 300 nL/min, a total gradient duration of 90 minutes. Parameters were set as 2 default charges in the positive mode with 70,000 resolution, 3e6 automatic gain control (AGC) target, 60 ms maximum injection time, and 400-1500 m/z scan range. The top 15 most intense ions were selected and fragmented for the Orbitrap analysis. MS2 analysis, using higher-energy collision dissociation (HCD), was performed with 17,500 resolution, 5e4 AGC target, 100 ms maximum injection time, 2 m/z isolation window, 120 m/z fixed first mass, 26% normalized collision energy (NCE), centroided, unassigned, 1, 6, -8, >8 charge exclusion, and 50 s dynamic exclusion.

The phosphopeptides were directly loaded onto an in-house packed C18 column (365 µM x 75 µM, 40 cm, 1.9 µm pur, Dr. Maisch) and separated at 200 nL/min, a total gradient duration of 120 minutes. Parameters were set as 2 default charges in the positive mode with 70,000 resolution, 3e6 AGC target, 120 ms maximum injection time, and 300-1600 m/z scan range. The top 10 most intense ions were selected and fragmented for the Orbitrap analysis. MS2 analysis, HCD, was performed with 17,500 resolution, 1e6 AGC target, 100 ms maximum injection time, 1.6 m/z isolation window, 100 m/z fixed first mass, 27% NCE, centroided, unassigned, 1, 6, -8, >8 charge exclusion, and 30 s dynamic exclusion.

3.16.2 Data-Independent Acquisition

Samples were pooled (Table 3.4, Table 3.5), dried, and resuspended in 10-20 µl loading buffer (3% ACN and 0.1% FA in H_2O). Subsequently, 20-40% of the samples were subjected

to a reversed-phase Nano LC-MS/MS (Waters) connected to an Orbitrap Exploris 480 mass spectrometer (Thermo Fisher Scientific). The peptides were directly loaded onto a nanoEase M/Z HSS C18 T3 (100Å, 1.8 µm, 1 P/K, 75 µm x 250 mm) column and separated with a total gradient duration of 110 minutes. To build a DIA library, DDA was performed with the parameters of 3-second cycle time, 15,000 resolution, 1.2 isolation window, and 30% NCE. For the phosphopeptides, parameters were set as 3-second cycle time, 60,000 resolution, 200 ms max injection time, 1.2 m/z isolation window, and 30% CE. MS1 of DIA was performed with the same parameters as DDA, and for tMS, parameters were set as 2 default charge, 30% NCE, 15,000 resolution, 1,000% AGC target, 22 ms injection time, centroided, and with windows of 8 m/z, 4 m/z overlap, staggered; 350-1,000 (for interphase samples); 400-1,050 (for cytokinesis samples).

3.16.3 Parallel Reaction Monitoring

Samples were subjected to a reversed-phase Nano LC-MS/MS (UltiMate 3000 RSLCnano System, Thermo Fischer Scientific) connected to a Q Exactive HF Orbitrap mass spectrometer (Thermo Fisher Scientific). The peptides were directly loaded onto an in-house packed C18 column (365 µM x 75 µM, 40 cm, 1.9 µm pur, Dr. Maisch) column and separated with a total gradient duration of 90 minutes. General parameters were set as 2 default charges in positive mode, and for MS2, 30,000 resolution, 2e5 AGC target, 100 ms max injection time, 1.2 m/z isolation window, 28% NCE, and 100 m/z fixed first mass were set.

3.17 Data Processing

Raw data was processed using Proteome Discoverer (PD) (version 2.3), MaxQuant (MQ), and Perseus software for DDA files. The search was subjected against the UniProt *Homo sapiens* database with a fixed modification of carbamidomethyl (C) and variable modifications of oxidation (methionine (Met, M)) and phospho (S, T, Y). Dimethyl (K) was included in the list of variable modifications for dimethyl-labeled samples. Trypsin/P was selected as the proteolytic enzyme with two missed cleavages allowed, and the minimum length required for a peptide was six amino acids. The initial precursor mass tolerance was set to 10 ppm, and the fragment mass tolerance was set to 0.6 Da. The peptide and protein false discovery rate (FDR) was set to 0.01. A threshold of at least 0.75 probabilities was used

for the phospho residue localization. In PD, the phosphopeptide site localization was identified using the phosphoRS algorithm, which was implemented with the node IMP-ptmRS. DIA files were processed in collaboration with the FGCZ by Dr. Antje Dittmann using PD (version 2.5) and by Dr. Jonas Grossmann using Spectronaut (version 17) software. PRM files were processed and visualized using Skyline software.

SAINTexpress, an upgraded implementation of Significance Analysis of INTeractome (SAINT) for filtering high-confidence interaction data, and Perseus were used to analyze the PD results obtained by immunoprecipitation and microtubule pelleting assays. Identified protein lists were filtered with at least two values from three replicates of the data sets. Normalization was performed within the experimental groups. Data distribution and correlation were visualized using InfernoRDN, and statistical significance analysis was conducted using Perseus software. Proteins with a SAINT probability score of ≥ 0.6 were analyzed using the STRING database and g:Profiler annotation server. Dysregulated proteins and protein interactions were visualized using GraphPad Prism 10, Cytoscape (version 3.10.3), and Python scripts.

Table 3.1: Primary antibodies used for immunofluorescence staining.

Antibody	**Host**	**Dilution**	**Company**	**Catalog No**
Anti-Keratin 8	Mouse	1:100	Santa Cruz	sc-8020
Anti-Keratin 8	Rabbit	1:100	Abcam	ab53280
Anti-Phospho-Keratin 8 S34	Rabbit	1:10	Davids Biotech	HAM-SB2
Anti-NDC80	Mouse	1:100	Novus Biologicals	NB100-338
Anti-CREST	Mouse	1:100	Calbiotech	HCT-0100
Anti-CENP-C	Guinea Pig	1:2000	MBL	PD030
Anti-BUB1	Mouse	1:200	Santa Cruz	sc-47723
Anti-HURP	Rabbit	1:250	Proteintech	12038-1-AP
Anti-Alpha-Tubulin	Mouse	1:500	Sigma-Aldrich	T6199
Anti-Alpha-Tubulin	Rabbit	1:200	Proteintech	11224-1-AP
Anti-N-Cadherin	Rabbit	1:100	Santa Cruz	sc-7939
Anti-HA	Mouse	1:150	Cell Signaling Technology	2367

Table 3.2: Primary antibodies used for immunoblotting and FACS.

Antibody	**Host**	**Dilution**	**Company**	**Catalog No**
Anti-Keratin 8	Mouse	1:1000	Santa Cruz	sc-8020
Anti-Keratin 8	Rabbit	1:2000	Abcam	ab53280
Anti-NDC80	Mouse	1:1000	Novus Biologicals	NB100-338
Anti-Alpha-Tubulin	Rabbit	1:2500	Proteintech	11224-1-AP
Anti-Beta-Actin	Mouse	1:1000	Abcam	ab8224
Anti-Beta-Actin	Mouse	1:5000	Abcam	ab6276
Anti-Beta-Actin	Mouse	1:1000	Abcam	ab8224
Anti-GAPDH	Rabbit	1:1000	Cell Signaling Technology	2118S
Anti-Phospho-Histone H3	Mouse	1:1000	Cell Signaling Technology	9706
Anti-Phospho-Histone H3	Rabbit	1:1600	Cell Signaling Technology	3377T
Anti-GFP	Mouse	1:2000	Roche	11814460001

Table 3.3: Secondary antibodies used for immunofluorescence staining, immunoblotting, and FACS.

Antibody	**Host**	**Dilution**	**Company**	**Catalog No**
Anti-Mouse Alexa Fluor 488	Donkey	1:1000	Invitrogen	A-21202
Anti-Rabbit Alexa Fluor 488	Donkey	1:1000	Invitrogen	A-21206
Anti-Guinea Pig Alexa Fluor 555	Goat	1:500	Invitrogen	A-21435
Anti-Rabbit Alexa Fluor 568	Goat	1:500	Invitrogen	A-11011
Anti-Mouse Alexa Fluor 633	Goat	1:1000	Invitrogen	A-21052
Anti-Rabbit Alexa Fluor 633	Goat	1:500	Invitrogen	A-21071
Anti-Rabbit Alexa Fluor 647	Goat	1:10000	Invitrogen	A-31573
Anti-Mouse Atto 594	Goat	1:200	Sigma-Aldrich	76085
Anti-Rabbit STAR 635P	Goat	A:200	Abberior	ST635P-1002
Anti-Mouse HRP	Horse	1:1000	Cell Signaling Technology	7076S
Anti-Rabbit HRP	Goat	1:1000	Cell Signaling Technology	7074S
Anti-Mouse IRDye 680	Goat	1:10000	LI-COR Biosciences	926-68070
Anti-Rabbit IRDye 800	Donkey	1:10000	LI-COR Biosciences	926-32213

Table 3.4: Sample sets for DIA library generation.

(a) Proteome samples

MCF7	Interphase	HeLa	Interphase	MDA-MB-231	Interphase	CAKI-2	Interphase
	Mitosis		Mitosis		Mitosis		Mitosis
	Cytokinesis		Cytokinesis		Cytokinesis		Cytokinesis

(b) Phosphoproteome samples

MCF7	Interphase	SCX Fraction 1 (Flow Through)	HeLa	Interphase	SCX Fraction 1 (Flow Through)	MDA-MB-231	Interphase	SCX Fraction 1 (Flow Through)	CAKI-2	Interphase	SCX Fraction 1 (Flow Through)
		SCX Fraction 2			SCX Fraction 2			SCX Fraction 2			SCX Fraction 2
		SCX Fraction 3			SCX Fraction 3			SCX Fraction 3			SCX Fraction 3
		SCX Fraction 4			SCX Fraction 4			SCX Fraction 4			SCX Fraction 4
		SCX Fraction 5			SCX Fraction 5			SCX Fraction 5			SCX Fraction 5
		SCX Fraction 6			SCX Fraction 6			SCX Fraction 6			SCX Fraction 6
	Mitosis	SCX Fraction 1 (Flow Through)		Mitosis	SCX Fraction 1 (Flow Through)		Mitosis	SCX Fraction 1 (Flow Through)		Mitosis	SCX Fraction 1 (Flow Through)
		SCX Fraction 2			SCX Fraction 2			SCX Fraction 2			SCX Fraction 2
		SCX Fraction 3			SCX Fraction 3			SCX Fraction 3			SCX Fraction 3
		SCX Fraction 4			SCX Fraction 4			SCX Fraction 4			SCX Fraction 4
		SCX Fraction 5			SCX Fraction 5			SCX Fraction 5			SCX Fraction 5
		SCX Fraction 6			SCX Fraction 6			SCX Fraction 6			SCX Fraction 6
	Cytokinesis	SCX Fraction 1 (Flow Through)		Cytokinesis	SCX Fraction 1 (Flow Through)		Cytokinesis	SCX Fraction 1 (Flow Through)		Cytokinesis	SCX Fraction 1 (Flow Through)
		SCX Fraction 2			SCX Fraction 2			SCX Fraction 2			SCX Fraction 2
		SCX Fraction 3			SCX Fraction 3			SCX Fraction 3			SCX Fraction 3
		SCX Fraction 4			SCX Fraction 4			SCX Fraction 4			SCX Fraction 4
		SCX Fraction 5			SCX Fraction 5			SCX Fraction 5			SCX Fraction 5
		SCX Fraction 6			SCX Fraction 6			SCX Fraction 6			SCX Fraction 6

Table 3.5: Sample pooling for DIA library generation.

(a) DDA proteome analysis

Pool 1	Pool 2	Pool 3
Interphase	Mitosis	Cytokinesis
4 cell lines	4 cell lines	4 cell lines

(b) DDA phosphoproteome analysis

Pool 1	Pool 2	Pool 3	Pool 4	Pool 5	Pool 6	Pool 7	Pool 8	Pool 9	Pool 10	Pool 11	Pool 12	Pool 13	Pool 14	Pool 15	Pool 16	Pool 17	Pool 18
Interphase						Mitosis						Cytokinesis					
F1	F2	F3	F4	F5	F6	F1	F2	F3	F4	F5	F6	F1	F2	F3	F4	F5	F6
4 cell lines	4 cell lines	4 cell lines	4 cell lines	4 cell lines	4 cell lines	4 cell lines	4 cell lines	4 cell lines	4 cell lines	4 cell lines	4 cell lines	4 cell lines	4 cell lines	4 cell lines	4 cell lines	4 cell lines	4 cell lines

(c) DIA proteome analysis

Pool 1	Pool 2	Pool 3	Pool 4	Pool 5	Pool 6	Pool 7	Pool 8	Pool 9	Pool 10	Pool 11	Pool 12
MCF7			HeLa			MDA-MB-231			CAKI-2		
Interphase	Mitosis	Cytokinesis	Interphase	Mitosis	Cytokinesis	Interphase	Mitosis	Cytokinesis	Interphase	Mitosis	Cytokinesis
All fractions	All fractions	All fractions	All fractions	All fractions	All fractions	All fractions	All fractions	All fractions	All fractions	All fractions	All fractions

(d) DIA phosphoproteome analysis

Pool 1	Pool 2	Pool 3	Pool 4	Pool 5	Pool 6	Pool 7	Pool 8	Pool 9
				MCF7				
Interphase			Mitosis			Cytokinesis		
F1-4	F2-5	F3-6	F1-4	F2-5	F3-6	F1-4	F2-5	F3-6

Pool 10	Pool 11	Pool 12	Pool 13	Pool 14	Pool 15	Pool 16	Pool 17	Pool 18
				HeLa				
Interphase			Mitosis			Cytokinesis		
F1-4	F2-5	F3-6	F1-4	F2-5	F3-6	F1-4	F2-5	F3-6

Pool 19	Pool 20	Pool 21	Pool 22	Pool 23	Pool 24	Pool 25	Pool 26	Pool 27
				MDA-MB-231				
Interphase			Mitosis			Cytokinesis		
F1-4	F2-5	F3-6	F1-4	F2-5	F3-6	F1-4	F2-5	F3-6

Pool 28	Pool 29	Pool 30	Pool 31	Pool 32	Pool 33	Pool 34	Pool 35	Pool 36
				CAKI-2				
Interphase			Mitosis			Cytokinesis		
F1-4	F2-5	F3-6	F1-4	F2-5	F3-6	F1-4	F2-5	F3-6

Chapter 4

RESULTS

4.1 Functional Role of Keratin 8

Successful cell division requires the coordinated activities of cellular proteins. Given the diverse expression patterns and morphology of keratins, the functional role of keratin 8 was investigated by examining its interaction partners and the regulation of cytoskeletal elements during cancer cell division. Cell biology studies supported proteomic findings to explore how keratin 8 interacts with other proteins and functions throughout the cell cycle.

4.1.1 Interactors of Keratin 8 During Cancer Cell Division

A comprehensive interactome analysis was performed in HeLa cells to uncover the functional role of keratin 8 and its molecular regulation during cancer cell division. For this purpose, HeLa K8-GFP and HeLa GFP cells were arrested at interphase, mitosis, and cytokinesis, and immunoprecipitation was performed with GFP-Trap. Bound proteins were prepared for proteomic analysis and subjected to LC-MS/MS (Figure 4.1). Raw data files from at least two biological replicates, each with three technical replicates, were processed using PD, Perseus, and SAINTexpress.

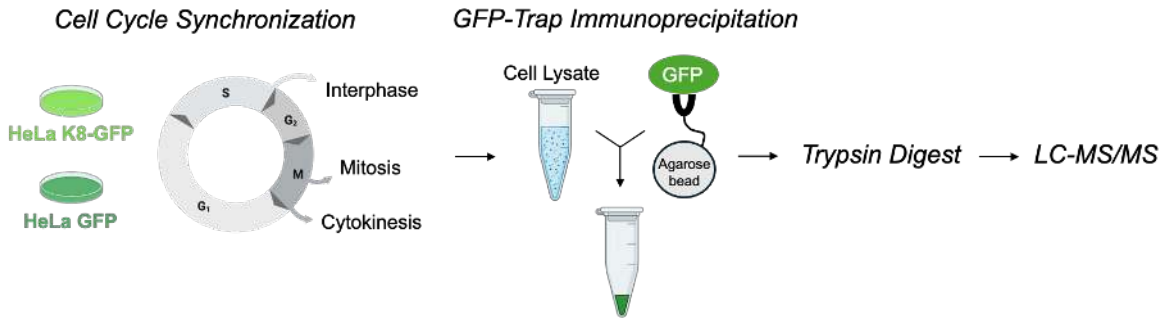

Figure 4.1: Experimental workflow of cell cycle-dependent interactome analysis.

To verify the synchronization of HeLa K8-GFP and HeLa GFP cells, FACS analysis was performed based on DNA content (Figure 4.2, Appendix B). Histogram results revealed the distribution of cells across the cell cycle. In asynchronous cells, the majority of the cells were in the G_1 phase, as indicated by the peak corresponding to the 1X DNA content. A fraction was in the S phase, represented by the region between G_1 and G_2/M peaks, indicating active DNA synthesis. The remaining cells were in the G_2/M phase, reflected by the second peak at 2X DNA content, indicating the cells were ready for mitosis. In interphase, cells in G_1 were the largest population, and in mitosis, the G_2/M peak was prominent. As the cells progressed through cytokinesis, the peaks in histograms indicated subpopulations of cells with varying DNA content. The cells in mitosis and cytokinesis were distinguished by the phospho-histone H3 analysis (Appendix B). The results highlighted an efficient synchronization of the HeLa K8-GFP and HeLa GFP cells for further analysis.

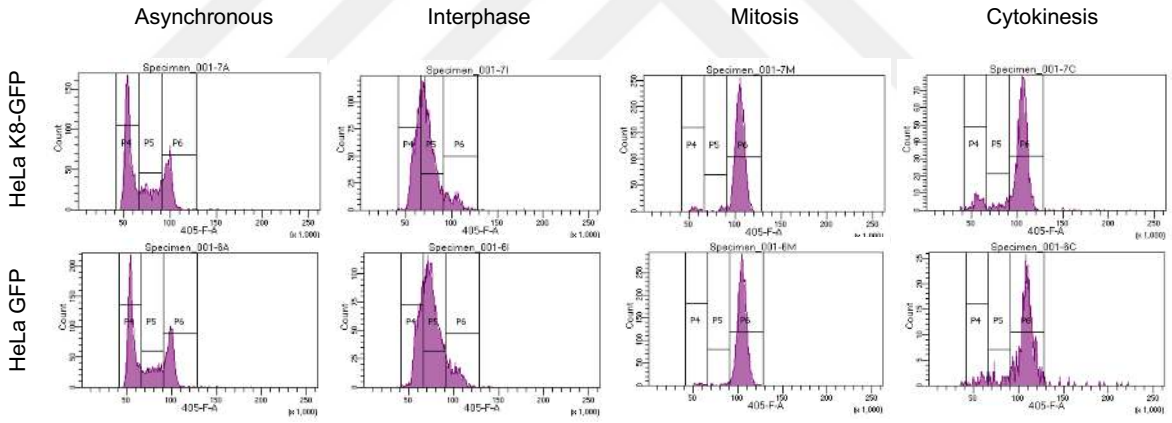

Figure 4.2: FACS histograms of asynchronous and synchronized HeLa K8-GFP and HeLa GFP cells.

Synchronized cell lysates were immunoprecipitated, and the efficiency was validated by western blot analysis using one-third of the samples (Figure 4.3). 40 µg whole-cell lysate (WCL) was loaded into the gel, and the corresponding volume relative to the total lysate was calculated. For unbound fractions, the volumes were adjusted proportionally based on the percentage of WCL, and 10% of the bound fraction was directly loaded. Results showed successful enrichment of keratin 8 in the bound fraction compared to the other fractions. Additionally, the appearance of a higher molecular weight band of keratin 8 in mitosis

samples indicated a potential hyperphosphorylation of the protein. The mitotic phase was confirmed by phospho-histone H3 (p-H3) detection, and actin was used as the loading control.

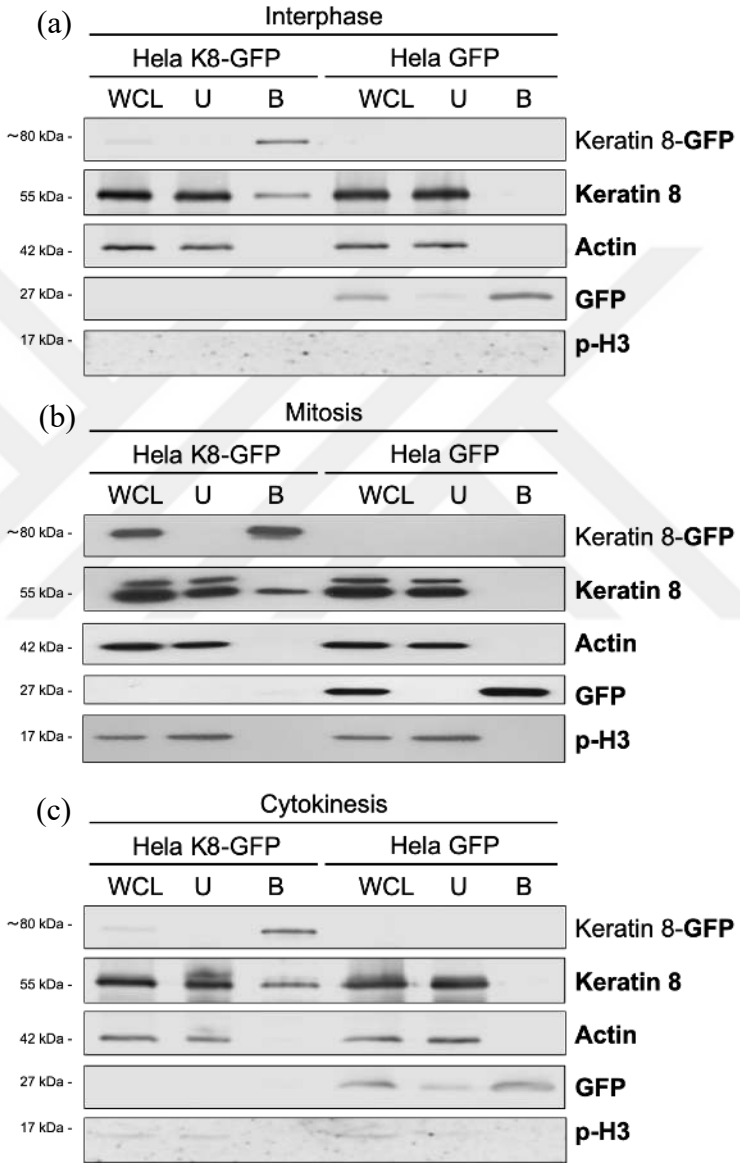

Figure 4.3: Western blot confirmation of GFP-Trap immunoprecipitation in (a) interphase, (b) mitosis, and (c) cytokinesis samples. Antibodies used are indicated in bold. WCL: Whole-Cell Lysate, U: Unbound, B: Bound.

Following the immunoprecipitation and proteomic analysis of the synchronized cells, raw data files of three biological replicates for mitosis and two biological replicates each for interphase and cytokinesis samples were processed using PD. The protein lists of each biological replicate were exported, and using InfernoRDN, the correlation of each biological replicate was analyzed (Figure 4.4). To overcome the level of variability in the data sets, identified proteins were filtered with at least two values from three biological replicates.

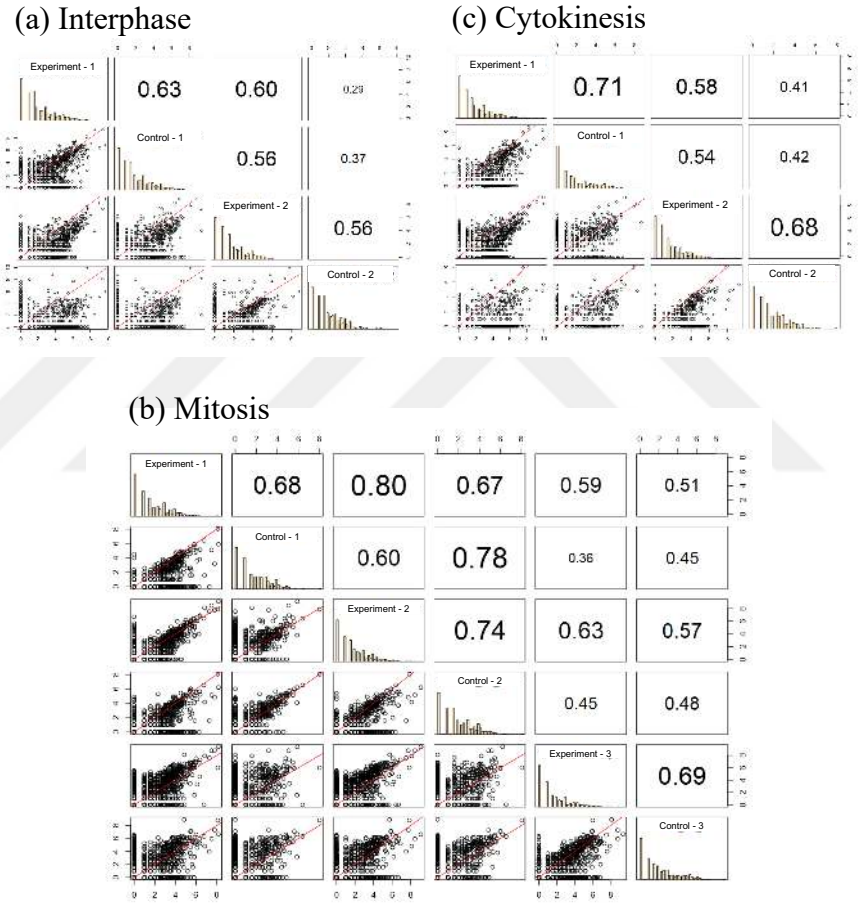

Figure 4.4: Pearson correlation plots of protein PSM values across biological replicates in (a) interphase, (b) mitosis, and (c) cytokinesis samples. HeLa K8-GFP and HeLa GFP cells were indicated as "Experiment" and "Control" respectively.

Using SAINTexpress, GFP interacting proteins were filtered out, allowing the identification of keratin 8-interacting proteins. Proteins with a SAINT probability score of ≥ 0.6 were analyzed and clustered using Cytoscape (Figure 4.5). Singletons also indicated some

important interaction partners of keratin 8, such as its dimerization partner keratin 18, other intermediate filaments, cytoskeletal elements, and motor proteins (Appendix F).

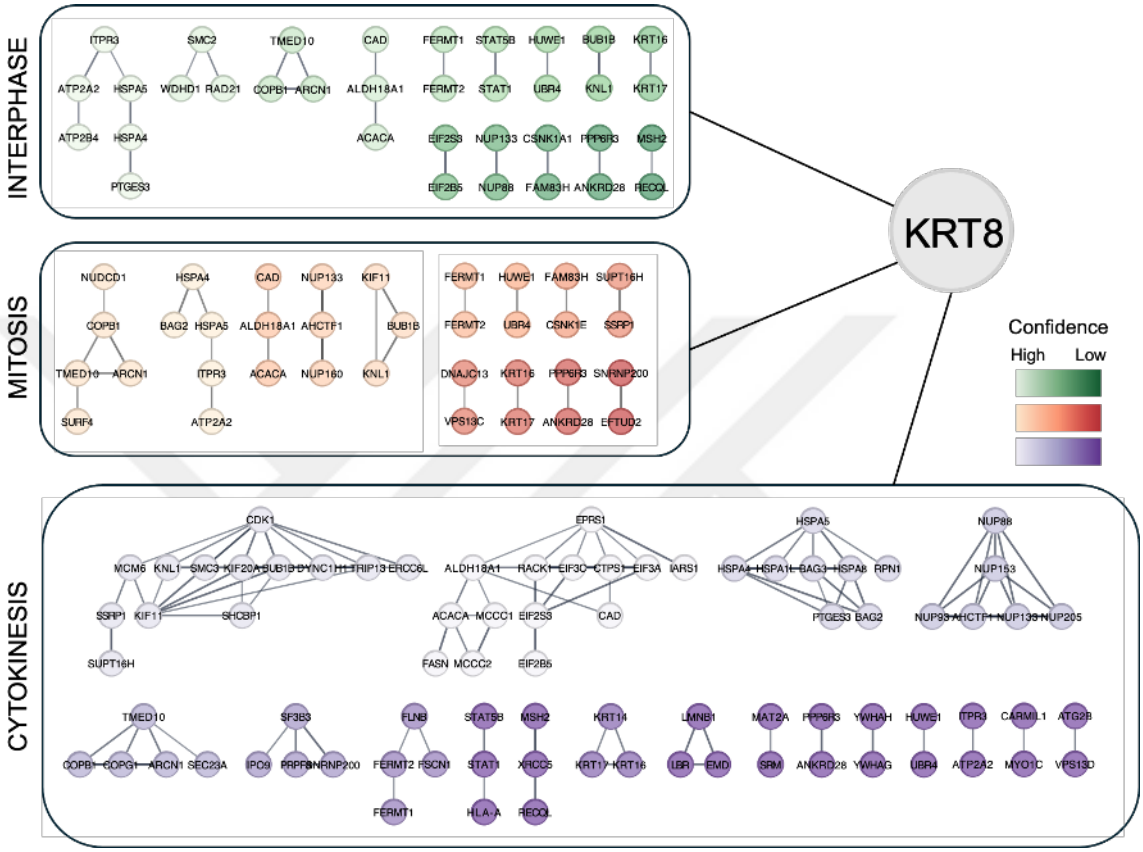

Figure 4.5: Clustered interaction partners of keratin 8 in interphase, mitosis, and cytokinesis. Nodes and edges were colored separately for cell cycle stages and based on confidence scores determined by the STRING database.

In total, 153 proteins were detected as keratin 8 interactors during cell division. The interactome analysis was consistent with the data retrieved from the BioGRID database of interactions (accessed January 2025). Based on previously reported findings in the literature, 27 proteins were confirmed as keratin 8 interactors. Additionally, the known interacting partners of keratin 8 were further characterized by identifying their interactions across different stages of the cell cycle. Besides, 126 proteins were identified as novel interacting partners of keratin 8 (Figure 4.6). In total, 61 proteins for interphase, 60 proteins for mitosis, and 130 proteins for cytokinesis were detected as cell cycle-dependent keratin 8 interactors

(Appendix F). Within those, 13 were specific to interphase, 9 to mitosis, and 69 to cytokinesis.

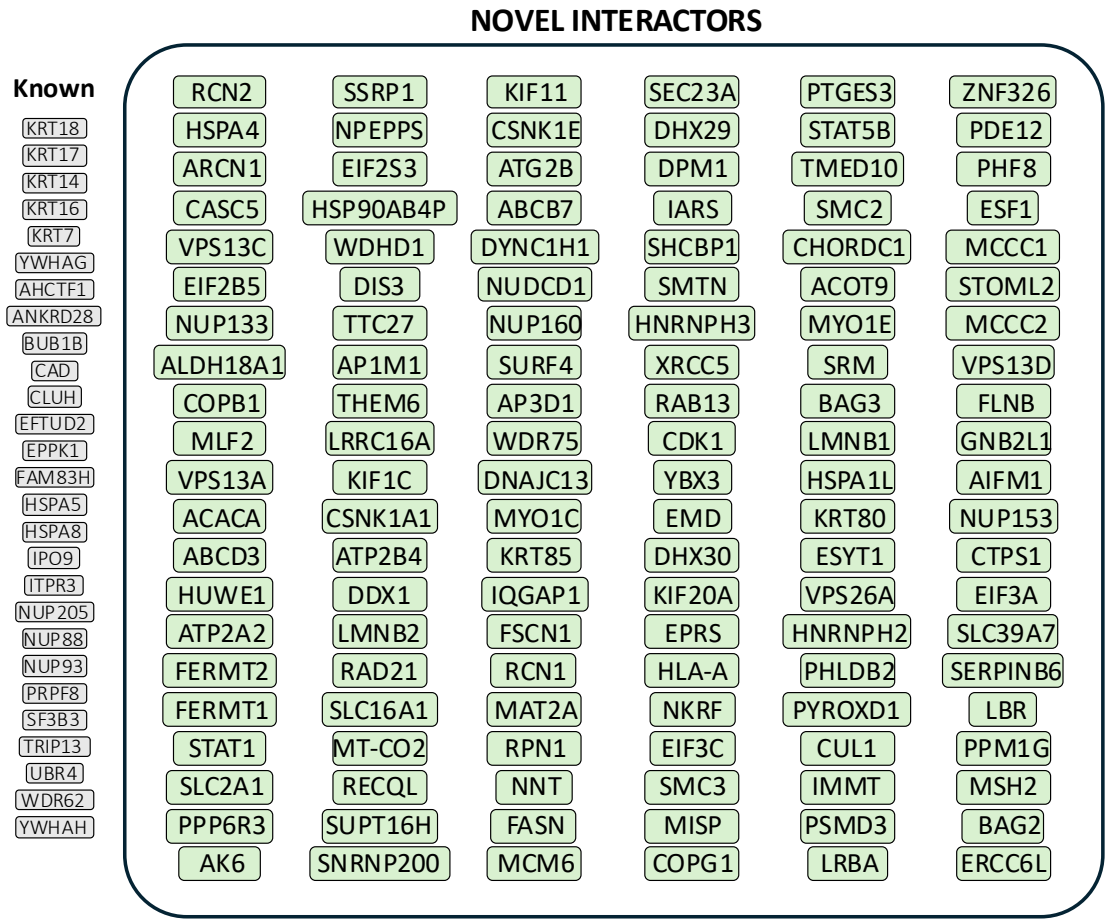

Figure 4.6: Known and novel interaction partners of keratin 8 identified with this study.

With this study, many interactors with established associations with microtubules were identified. Specifically in mitosis, keratin 8 interaction with a plus-end directed motor protein KIF11, a subunit of cytoplasmic dynein complex DYNC1H1, a mitotic spindle positioning protein MISP, a kinetochore scaffolding protein KNL1 (CASC5), and BUBR1 (BUB1B, BUB1 mitotic checkpoint serine/threonine kinase B), suggested a possible regulatory role of keratin 8 in bipolar spindle formation, positioning and kinetochore-microtubule attachment. This hypothesis was further supported by previous studies showing chromosome alignment and segregation defects in the absence of keratin 8 [36].

At each stage, gene ontology (GO) analysis was performed using g:Profiler for proteins with a SAINT probability score of ≥ 0.6. The changes in the top 10 highest-scoring annotations identified for interphase were mapped for mitosis and cytokinesis (
Figure 4.7). The results suggested a more specialized and dynamic involvement of keratin 8 interactors through the end of the cell division.

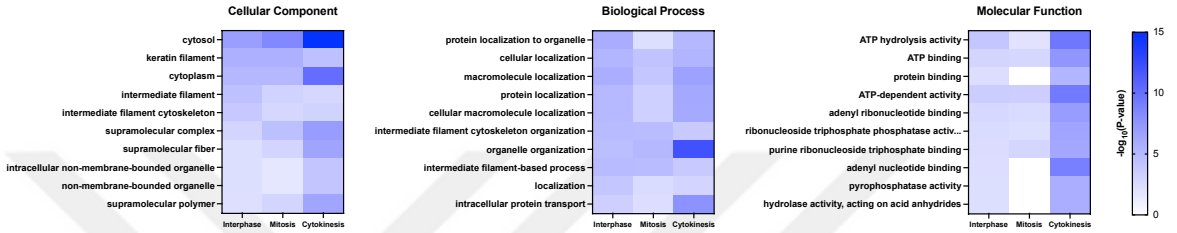

Figure 4.7: GO annotation grouped into cellular component, biological process, and molecular function of keratin 8 interactors at interphase, mitosis, and cytokinesis.

To compare the interactors from each stage, a heatmap was built based on the SAINT probability scores. From each stage, interactors with a SAINT probability score of ≥ 0.6 were mapped, and the change between interaction probabilities throughout the cell cycle was visualized (Figure 4.8). Hierarchical clustering was performed with Ward's method, minimizing cluster variance.

The interaction of keratin 8 with keratin 18 showed the lowest probability at mitosis, aligning with the increased solubility of the filaments at this stage. Based on the comparisons, interactors of keratin 8 were showing an increased involvement in chromosome dynamics, spindle assembly checkpoint regulation, cytoskeletal network and nuclear envelope integrity, cellular trafficking, and DNA damage and stress response at mitosis and cytokinesis as also highlighted by the gene ontology analysis. Strong interactors of keratin 8 were mostly gained after mitosis and were more abundant in cytokinesis. The moderate interactors at cytokinesis were mostly lost afterward. A group of proteins, including KNL1, were found to interact with keratin 8 at all cell cycle stages with a strong interaction probability. This also supported the interactions found between these proteins and keratin 8.

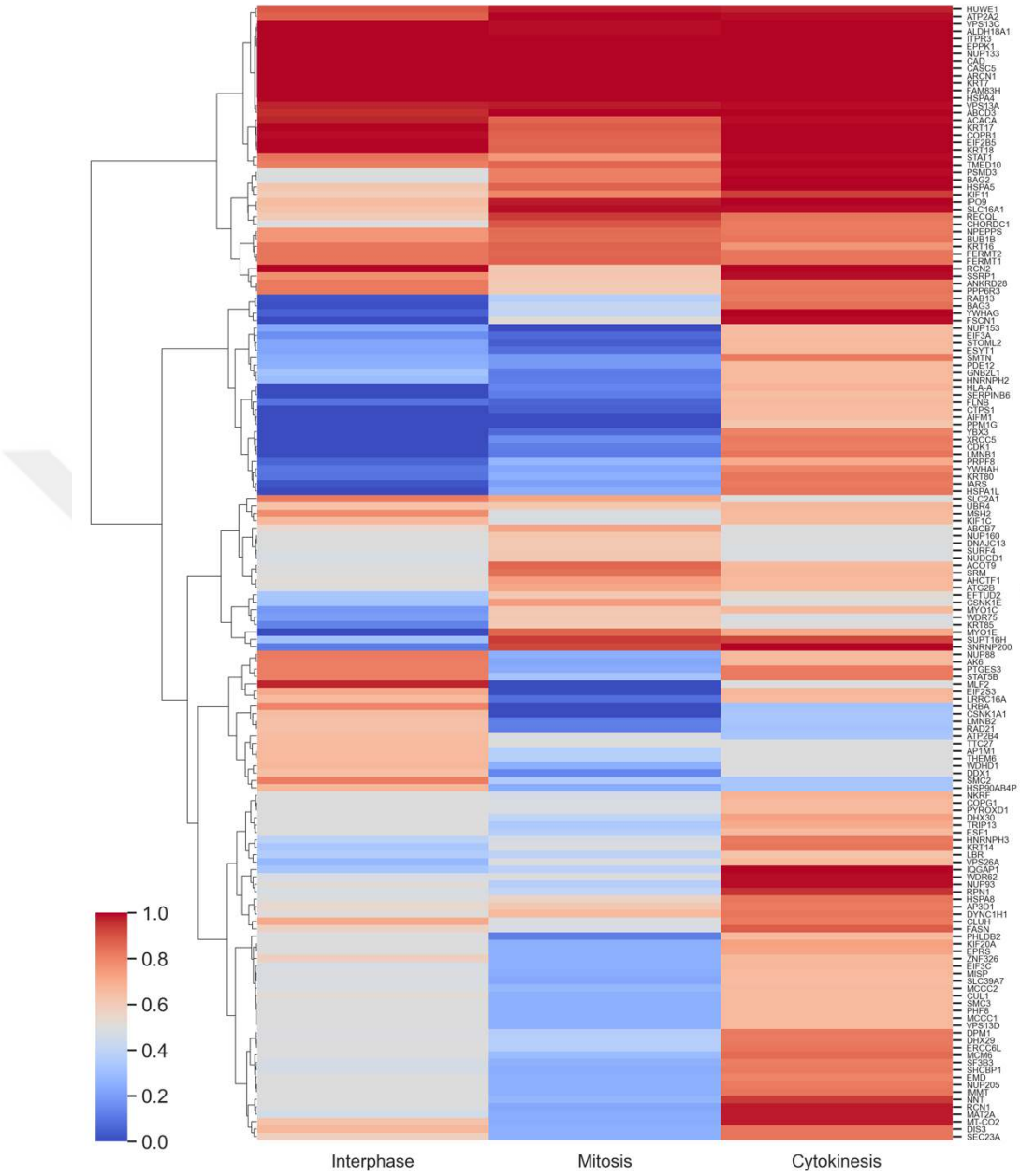

Figure 4.8: Clustered heatmap of keratin 8 interactors based on SAINT probability scores across cell cycle stages. The dendrogram represents the hierarchical relationships between genes based on their SAINT scores across different cell cycle stages.

4.1.2 Keratin 8-Dependent Microtubule-Binding Proteins in Mitosis

Considering the interaction partners of keratin 8, the effect of keratin 8 on the microtubule network was investigated. For this purpose, microtubules were stabilized with Taxol in mitotic control and K8 KO HeLa cells and pelleted with ultracentrifugation.

Samples were separated using gel electrophoresis, fractionated for proteomic analysis, and subjected to LC-MS/MS (Figure 4.9). Raw data files from three biological replicates, each with three technical replicates, were processed using PD, Perseus, InfernoRDN, and GraphPad Prism 10.

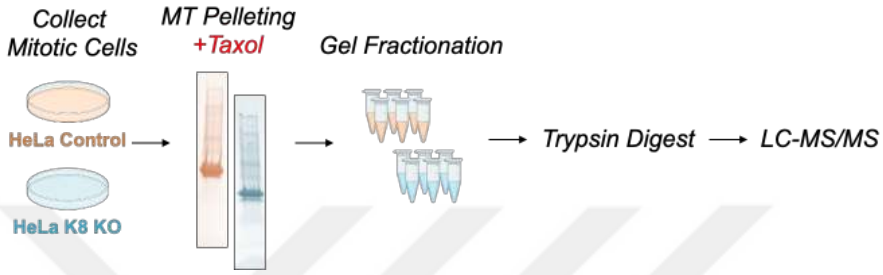

Figure 4.9: Experimental workflow of keratin 8-dependent microtubule interactome analysis in mitosis.

Control, K8 KO, and K8 KO +K8-GFP HeLa cells were synchronized for microtubule pelleting assays and further experiments. The synchronization was verified by FACS analysis based on DNA content and phospho-histone H3 analysis (Figure 4.10, Appendix B). The multinucleation rate reported in [36] was insufficient for detection by FACS analysis.

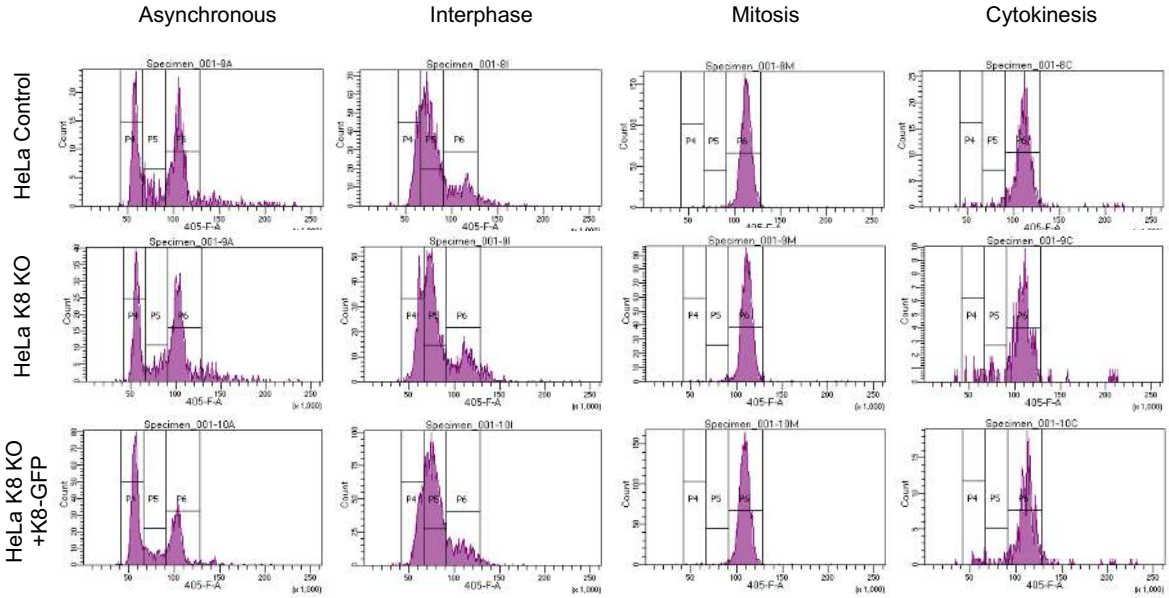

Figure 4.10: FACS histograms of asynchronous and synchronized control, K8 KO, and K8 KO +K8-GFP HeLa cells.

Synchronized cell lysates were treated with Taxol, and microtubules were precipitated. Samples were loaded into the gel and fractioned into five from approximately 150, 100, 60, and 50 kilodaltons (kDa) based on staining intensities (Figure 4.11).

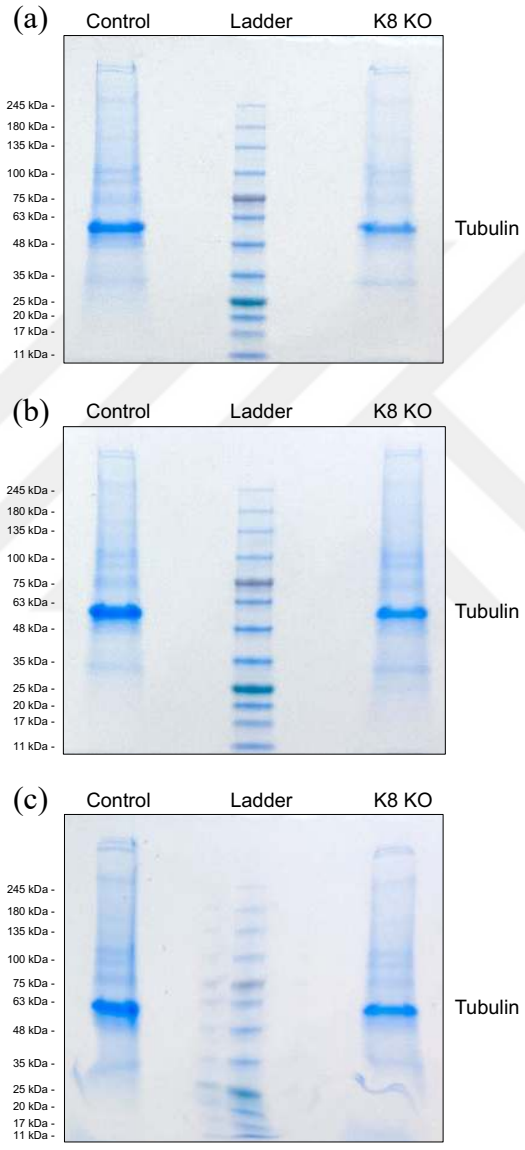

Figure 4.11: Protein gel staining of microtubule pelleting assays in three biological replicates (a, b, c).

Following the gel fractionation and proteomic analysis, raw data files of three biological replicates were processed using PD. The protein lists of each biological replicate were exported, and using Perseus, identified proteins were filtered with at least two values from

three biological replicates. The correlation of each biological replicate was analyzed using InfernoRDN and reported with minimal biological variability (Figure 4.12).

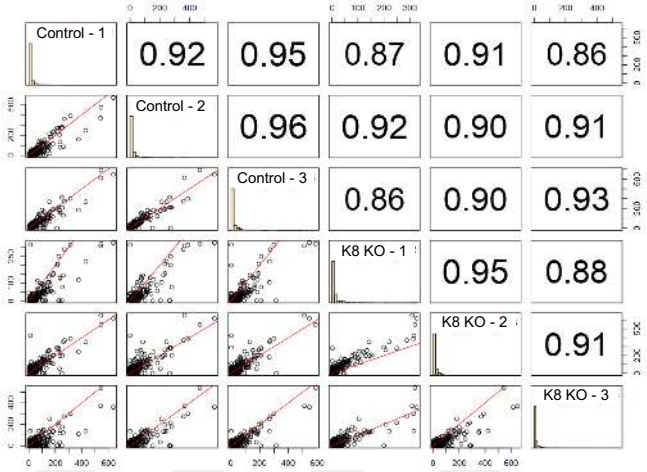

Figure 4.12: Pearson correlation plot of protein PSM values across biological replicates in mitosis samples. Control and K8 KO HeLa cells were indicated as “Control” and “K8 KO”, respectively.

To compare the microtubule-binding proteins between control and K8 KO samples, PSM values were normalized to TUBB as the most abundant tubulin in the data sets. InfernoRDN was used to visualize and assess the data distribution across biological replicates (Figure 4.13).

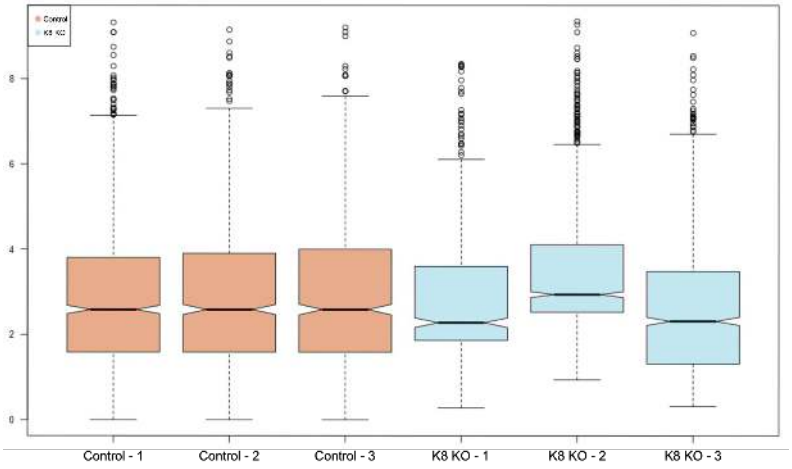

Figure 4.13: TUBB normalized data distribution of biological replicates from control and K8 KO HeLa cells indicated as “Control” and “K8 KO”, respectively.

To identify statistically significant differences between the experimental groups, a Student's *t*-test was conducted with a P-value of 0.05 and a $\log_2$(Fold Change) threshold of ±1 using Perseus. Subsequently, GO analysis was performed using g:Profiler, and the top 3 highest-scoring annotations were mapped (Figure 4.14). The results showed that down-regulated proteins losing their interactions with microtubules in the absence of keratin 8 were mostly cytoskeletal and cell cycle-related proteins. On the other hand, the upregulated proteins with increased microtubule interactions in the absence of keratin 8 were mostly cytoplasmic proteins with regulatory roles in translation. To investigate these in more detail, dysregulated proteins were plotted with fold change and statistical significance values using GraphPad Prism 10 (Figure 4.15).

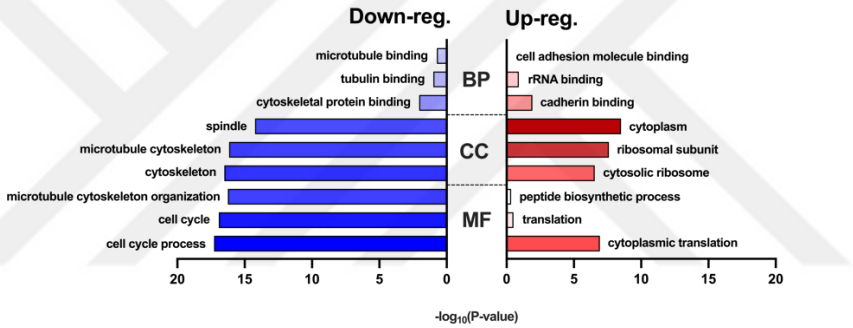

Figure 4.14: GO annotation grouped into biological process, cellular component, and molecular function of significantly up- or down-regulated keratin 8-dependent microtubule interactors at mitosis.

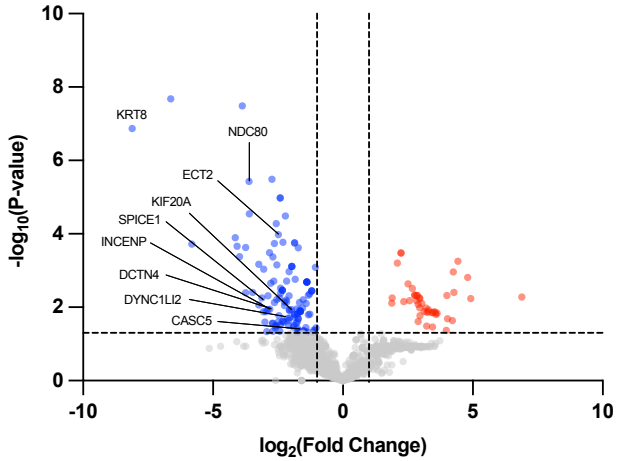

Figure 4.15: Volcano plot showing keratin 8-dependent microtubule interactors in mitosis. Data represents P-value = 0.05, $\log_2$(Fold Change) = ±1. Student's *t*-test.

With this study, 173 proteins are detected as significant keratin 8-dependent MT interactors at mitosis. In the up-regulated proteins, other keratins and IF linkers were abundant. This showed that keratins and linker proteins interact more with microtubules in the absence of keratin 8, which was very likely to compensate for the deficiency in the cytoskeletal network. In the down-regulated proteins, the interaction with microtubules was less in the absence of keratin 8. Many important key regulatory proteins in mitotic progression were detected, such as NDC80, KNL1, and INCENP for kinetochore-microtubule attachment, SPICE1 for spindle formation, DCTN4 and DYNC1L12 for spindle positioning, and ECT2 and KIF20A for cleavage furrow formation. Keratin 8 was detected with the highest fold change as a significantly down-regulated protein due to its absence in the K8 KO data set.

4.1.3 Role of Keratin 8 in Kinetochore-Microtubule Attachment

To investigate the interaction between keratin filaments and microtubules in more detail, the kinetochore-microtubule interactions were examined by focusing on NDC80, which shows significantly reduced interaction with microtubules in the absence of keratin 8. Initially, the expression levels of NDC80 in asynchronous control, K8 KO, and K8 KO +K8-GFP HeLa cells were analyzed with western blotting. GAPDH was used as the loading control. Statistical significance was evaluated using one-way ANOVA (Figure 4.16).

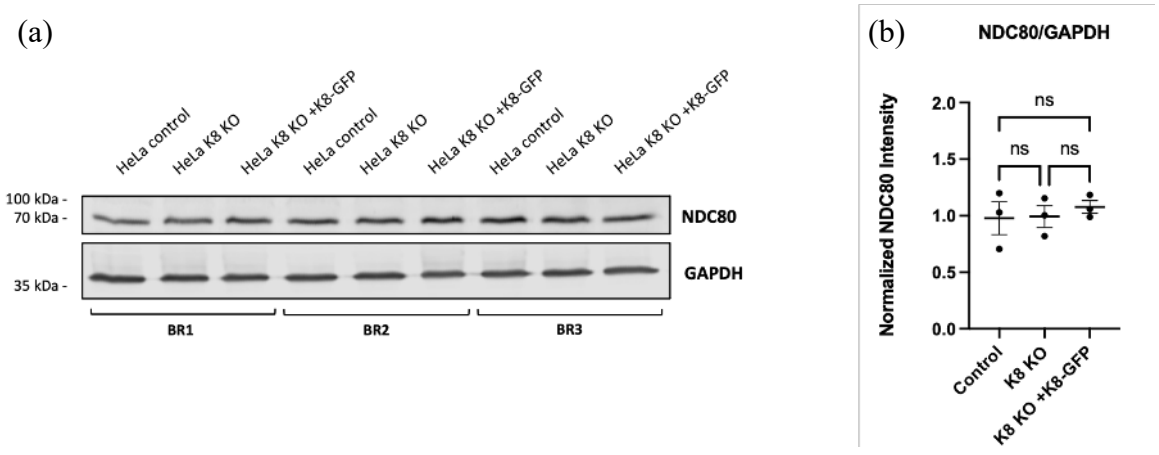

Figure 4.16: Western blot (a) analysis in three biological replicates (BR) and (b) quantification of NDC80 levels in asynchronous control, K8 KO, and K8 KO +K8-GFP HeLa cells. Data represents mean ± SEM. ns: not significant. One-way ANOVA.

The results confirmed that no significant change in NDC80 levels in asynchronous cells was detected between cell lines. To check the levels in mitotic cells and to validate the proteomics findings of the microtubule pelleting assays, western blot analysis was performed with two biological replicates. Using one-third of the WCL, supernatant, and pellet samples, tubulin and NDC80 levels were examined. After Taxol treatment of the cleared lysate, samples were subjected to ultracentrifugation. The supernatant, including soluble microtubules, was collected as the first supernatant fraction. After resuspending the pellet with insoluble microtubules, samples were subjected to ultracentrifugation, and the second supernatant fraction was collected. The pellet was resuspended and used in further steps. 40 µg WCL was loaded into the gel, and the corresponding volume relative to the total lysate was calculated. For supernatant fractions, the volumes were adjusted proportionally based on the percentage of WCL, and one-third of the pellet was directly loaded. Results showed successful enrichment of the tubulin in both samples (Figure 4.17a, b). The mitotic phase was confirmed by p-H3 detection, and GAPDH was used as the loading control.

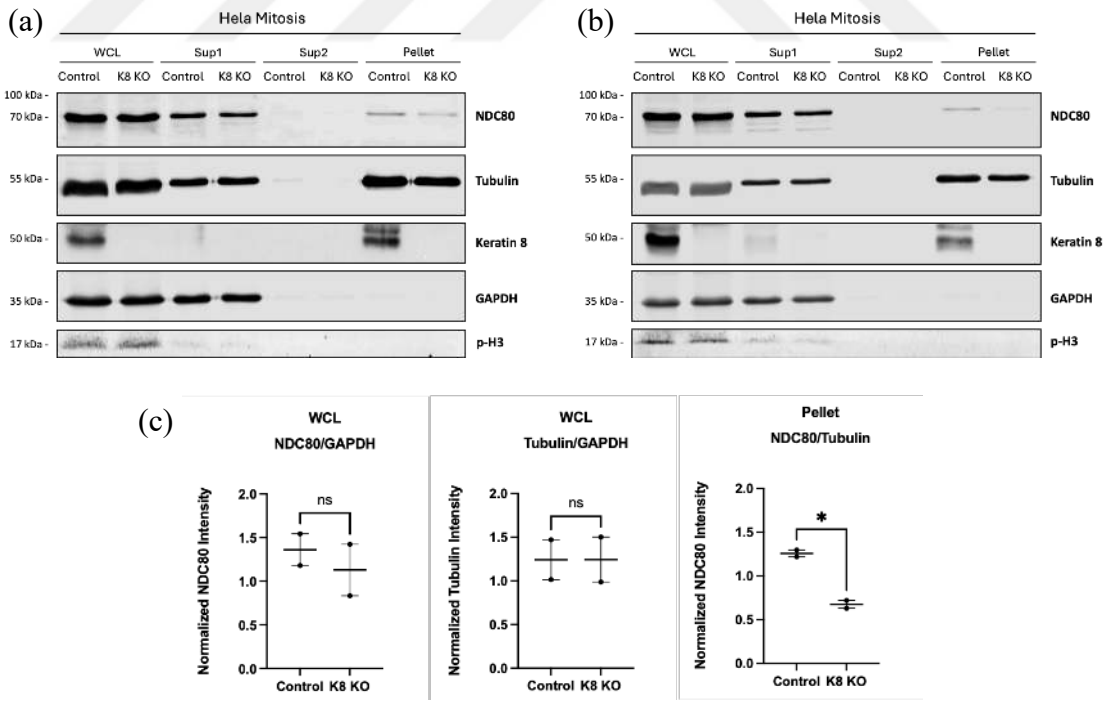

Figure 4.17: Western blot (a, b) analysis in two biological replicates, and (c) quantification of NDC80 and tubulin levels in mitotic control and K8 KO HeLa cells. WCL: Whole-Cell Lysate, Sup1: Supernatant with soluble microtubules, Sup2: Supernatant without soluble microtubules. Data represents mean ± SEM. *p < 0.05. ns: not significant. Student's *t*-test.

In WCLs, NDC80 and tubulin levels were normalized to GAPDH to check their expression levels in mitotic cells. Statistical significance was evaluated using one-way ANOVA, and the results confirmed that no significant change was detected between cell lines (Figure 4.17c). In pellets, NDC80 levels were normalized to tubulin to check the difference in the tubulin-binding of the protein in the presence or absence of keratin 8. The results showed a significant difference between control and K8 KO HeLa cells and supported the proteomics findings (Figure 4.17c).

To further investigate the keratin 8-dependent interaction between NDC80 and microtubules, NDC80 was imaged with confocal microscopy in control, K8 KO, and K8 KO +K8-GFP HeLa cells at metaphase. Observations indicated a defective localization of NDC80 on the metaphase plate, which was rescued with the addition of K8-GFP (Figure 4.18a).

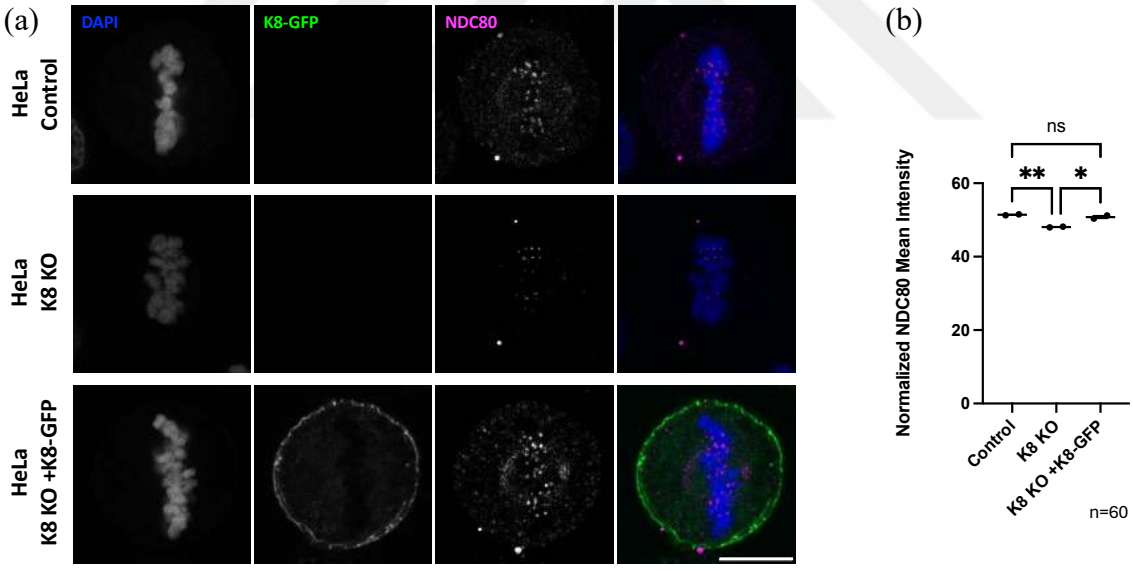

Figure 4.18: Effect of K8 KO on NDC80 localization at the metaphase plate: (a) Representative confocal microscopy image of DAPI (blue), K8-GFP (green), and NDC80 (magenta) in control, K8 KO, and K8 KO +K8-GFP HeLa cells. Scale bar = 10 μm. (b) Quantification of normalized mean fluorescence intensity of NDC80 on chromosomes in control (n = 60), K8 KO (n = 60), and K8 KO +K8-GFP (n = 60) Hela cells. Data represents mean ± SEM. **p < 0.01, *p < 0.05. ns: not significant. One-way ANOVA.

To validate the observations, 30 cells from each biological replicate of control, K8 KO, and K8 KO +K8-GFP HeLa cells were quantified. Centering the metaphase cell, five z-slices were used for the quantification. Chromosomal ROIs for NDC80 in each z-slice were determined, and the mean intensity was measured from the maximum projected image. NDC80 intensities of two random spots on the chromosome were measured and used for the chromosomal background normalization. Statistical significance was evaluated using one-way ANOVA, and normalized NDC80 mean intensities on the metaphase plate showed a significant decrease in K8 KO cells, which were rescued with the addition of K8-GFP (Figure 4.18b).

Although the microscopy data was consistent with the proteomics findings, the results were not fully aligned due to the inability to visualize keratin 8 on the metaphase plate. To overcome this, high-resolution confocal microscopy was performed. Control, K8 KO, and K8 KO +K8-GFP HeLa cells were prepared for imaging without mounting to prevent the shrinkage of the cells. After imaging, deconvolution was performed, and the results confirmed that keratin 8 was present at the metaphase plate in close proximity to NDC80 (Figure 4.19).

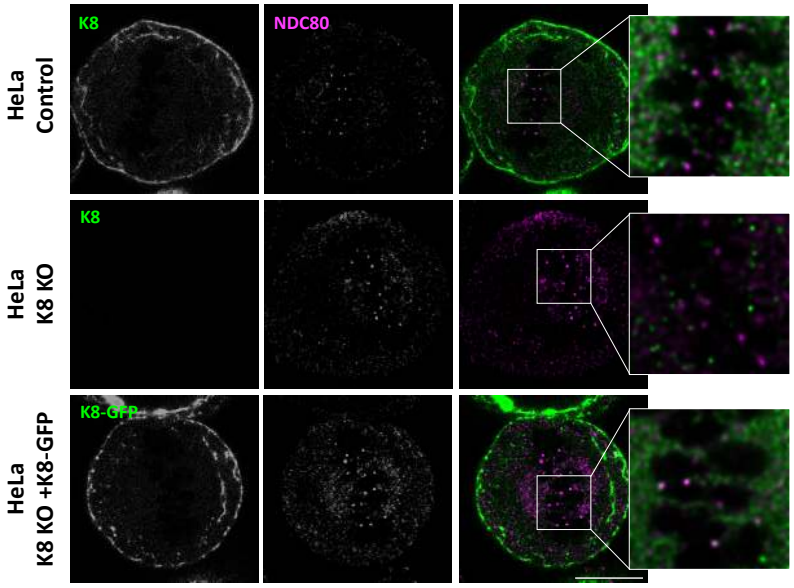

Figure 4.19: High-resolution imaging of keratin 8 and NDC80 localization at the metaphase plate. Representative image of K8/K8-GFP (green) and NDC80 (magenta) in control, K8 KO, and K8 KO +K8-GFP HeLa cells. Scale bar = 10 µm.

By applying an alternative fixation method suggested by Dr. Pierre Coulombe, HeLa cells were fixed with 100% methanol for 15 minutes at -20°C to remove the soluble pool of keratin 8. As a control, HeLa cells were fixed with 4% PFA for 15 minutes at room temperature. Fixed cells were prepared for high-resolution microscopy imaging without mounting, and deconvolution was performed after imaging. The results showed a decreased keratin 8 intensity at the metaphase plate with methanol fixation, suggesting a possible localization of the soluble form of the protein (Figure 4.20).

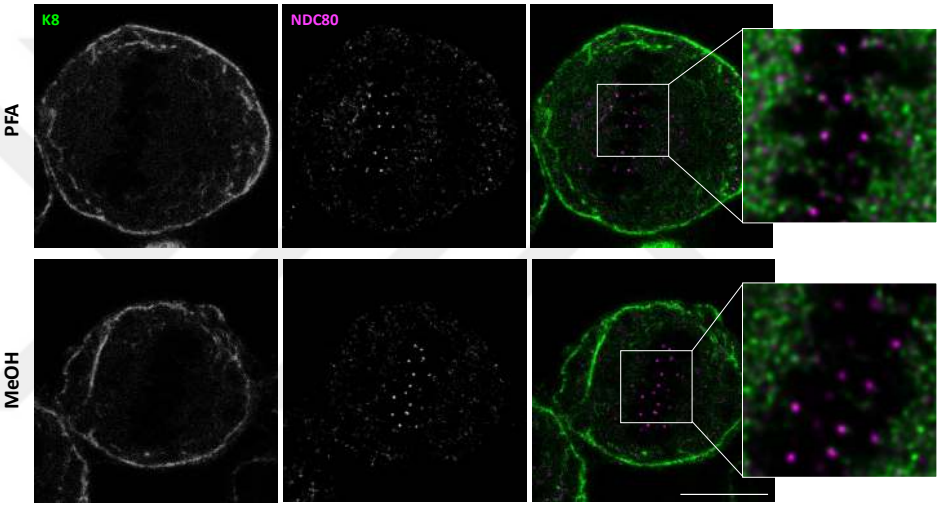

Figure 4.20: High-resolution imaging of keratin 8 NDC80 with 4% PFA and 100% methanol fixation in HeLa cells. Scale bar = 10 µm.

To increase the resolution of imaging at the metaphase plate, super-resolution imaging was performed in K8 KO +K8-GFP HeLa cells using STED microscopy. Due to the experimental setup, high-resolution confocal microscopy imaging of K8-GFP was combined with super-resolution STED microscopy imaging of NDC80 at the metaphase plate. After imaging, deconvolution was performed, and the results showed an increased resolution of the NDC80 protein (Figure 4.21). The results supported that keratin 8 was present at the metaphase plate in close proximity to NDC80, but the distance between the proteins was higher compared to the confocal imaging. Imaging results aligned with the interactome data where NDC80 was not found as an interactor of keratin 8 in mitosis.

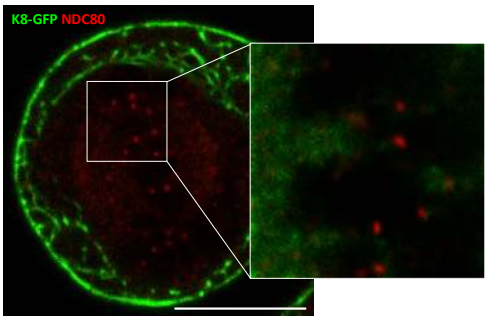

Figure 4.21: Super-resolution imaging of keratin 8 and NDC80 localization at the metaphase plate. Representative image of K8-GFP (green) and NDC80 (red) in K8 KO +K8-GFP HeLa cells. Scale bar = 10 µm.

To search if the absence of keratin 8 has further defects through the centromere, CENP-A/B/C localization was imaged in control, K8 KO, and K8 KO +K8-GFP HeLa cells. CREST antibody was used to stain the CENP-A/B/C proteins [37]. Observations indicated no change in proteins' localization at the metaphase plate (Figure 4.22a).

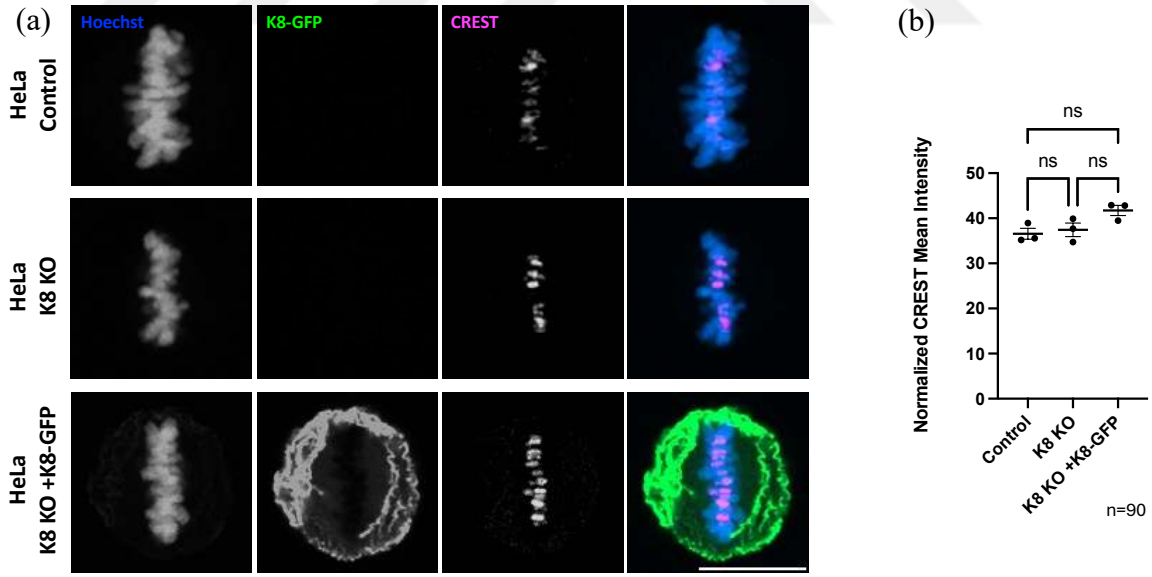

Figure 4.22: Effect of K8 KO on CENP-A/B/C localization at the metaphase plate: (a) Representative confocal microscopy image of Hoechst (blue), K8-GFP (green), and CREST (magenta) in control, K8 KO, and K8 KO +K8-GFP HeLa cells. Scale bar = 10 µm. (b) Quantification of normalized mean fluorescence intensity of CREST on chromosomes in control (n = 90), K8 KO (n = 90), and K8 KO +K8-GFP (n = 90) Hela cells. Data represents mean ± SEM. ns: not significant. One-way ANOVA.

To validate the observations, 30 cells from each biological replicate of control, K8 KO, and K8 KO +K8-GFP HeLa cells were quantified. Centering the metaphase cell, three z-slices were used for the quantification. Chromosomal ROIs for CREST in each z-slice were determined, and the mean intensity was measured from the maximum projected image. CREST intensities of two random spots on the chromosome were measured and used for the chromosomal background normalization. Statistical significance was evaluated using one-way ANOVA, and normalized CREST mean intensities on the metaphase plate showed no significant change between control, K8 KO, and K8 KO +K8-GFP HeLa cells (Figure 4.22b).

To assess whether the absence of detectable change in the CREST localization was attributable to a cumulative effect, CENP-C was imaged in control, K8 KO, and K8 KO +K8-GFP HeLa cells. Observations indicated no change in CENP-C localization at the metaphase plate (Figure 4.23).

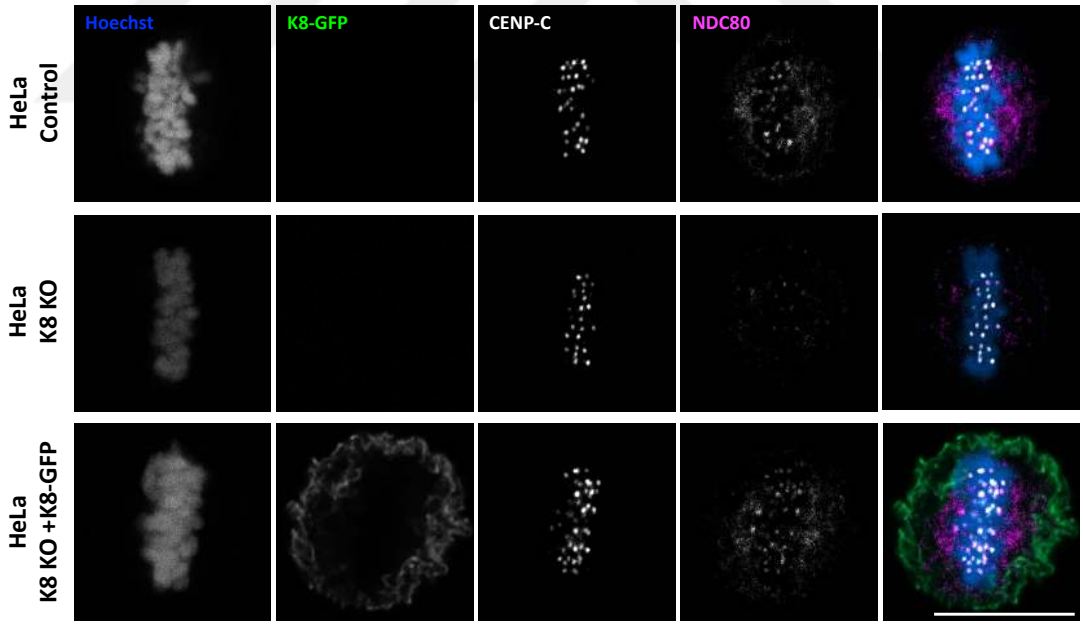

Figure 4.23: Confocal microscopy imaging of Hoechst (blue), K8-GFP (green), CENP-C (white), and NDC80 (magenta) in control, K8 KO, and K8 KO +K8-GFP HeLa cells. Scale bar = 10 µm.

Following the investigation of NDC80 with keratin 8 at the kinetochore-microtubule attachment, kinetochore microtubules were investigated to search for any defects. In control,

K8 KO, and K8 KO +K8-GFP HeLa cells, a microtubule-associated protein HURP that stabilizes kinetochore MTs and regulates chromosome congression was stained with keratin 8. Cells were prepared for high-resolution microscopy imaging without mounting, and deconvolution was performed after imaging (Figure 4.24).

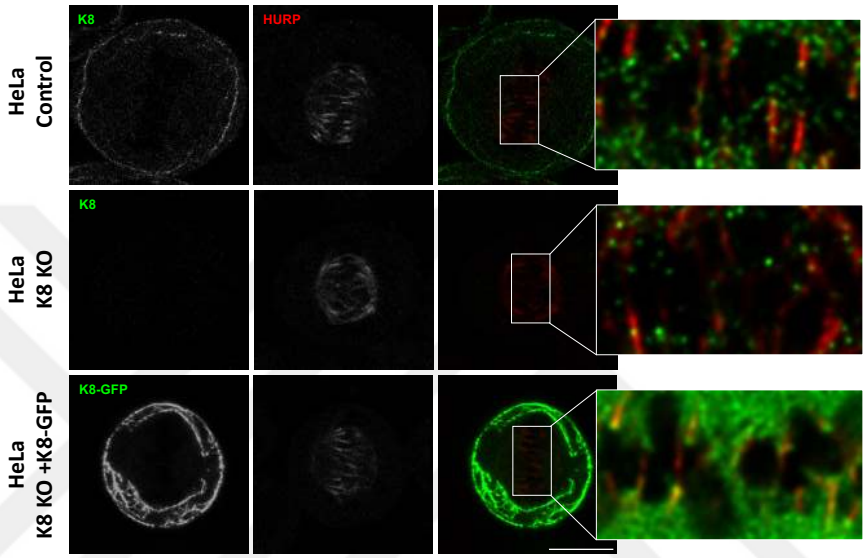

Figure 4.24: High-resolution imaging of keratin 8 and HURP localization at metaphase. Representative image of K8/K8-GFP (green) and HURP (red) in control, K8 KO, and K8 KO +K8-GFP HeLa cells. Scale bar = 10 µm.

In K8 KO HeLa cells, the kinetochore fibers were further apart compared to the control. Results suggested that the absence of keratin 8 would affect the kinetochore fibers due to the lack of structural support at the metaphase plate. The phenotype was rescued with the addition of K8-GFP, where the over-expression of keratin 8 showed a dense web-like structure. This highlighted the scaffolding role of the protein. As the scaffolding increased with the addition of K8-GFP, kinetochore fibers showed an increased intensity of HURP staining at the tip of the fibers, which possibly affected the microtubule attachment.

To further investigate the kinetochore fibers, microtubule depolymerization was performed in control and K8 KO HeLa cells. Cells were treated with ice-cold DMEM-based media for 5 or 15 minutes on ice and fixed immediately aiming to depolymerize microtubules but the kinetochore fibers. In the untreated group, microtubules showed a defective phenotype in the absence of keratin 8 compared to the control. However, no difference was

observed in the kinetochore fibers of control and K8 KO HeLa cells with the cold treatment (Figure 4.25).

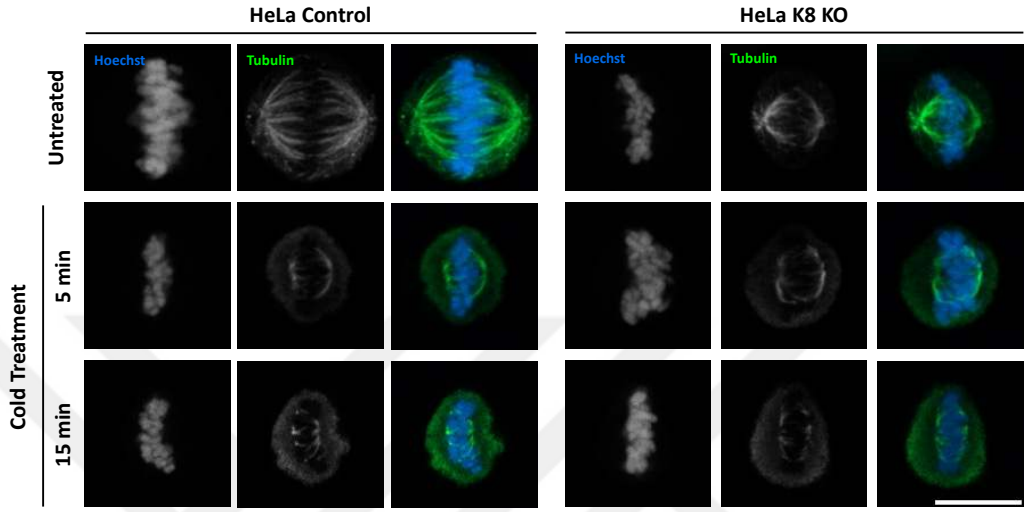

Figure 4.25: Confocal microscopy imaging of Hoechst (blue) and tubulin (green) in control and K8 KO HeLa cells at metaphase. Cells were untreated or cold-treated for 5 or 15 minutes. Scale bar = 10 µm.

To investigate spindle assembly checkpoint activation in the absence of keratin 8, control and K8 KO HeLa cells were stained with BUB1 (Figure 4.26). The results showed that the checkpoint activation was observable in K8 KO HeLa cells with a decreased intensity compared to the control.

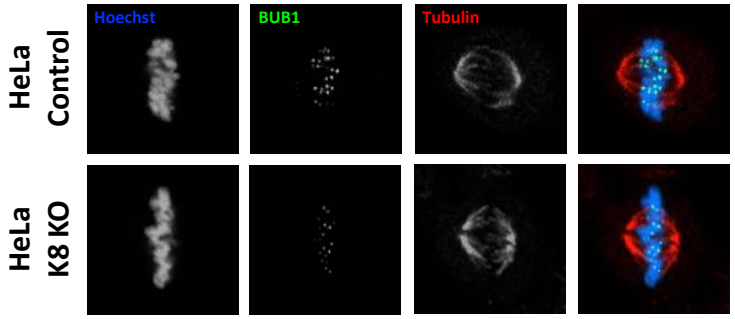

Figure 4.26: Confocal microscopy imaging of Hoechst (blue), BUB1 (green), and tubulin (red) in control and K8 KO HeLa cells at metaphase. Scale bar = 10 µm.

To further investigate the spindle assembly checkpoint activation, microtubules were depolymerized in control and K8 KO HeLa cells with the cold treatment, followed by BUB1 staining (Figure 4.27). As previously reported, kinetochore fibers showed similar phenotypes in both groups in response to cold. In the untreated K8 KO HeLa cells, BUB1 intensity was not observable, possibly due to imaging settings. With the cold treatment, an increase in the BUB1 intensity was observed. However, it was suggested that the phenotype was due to the microtubule depolymerization and chromosomal defects in the absence of keratin 8.

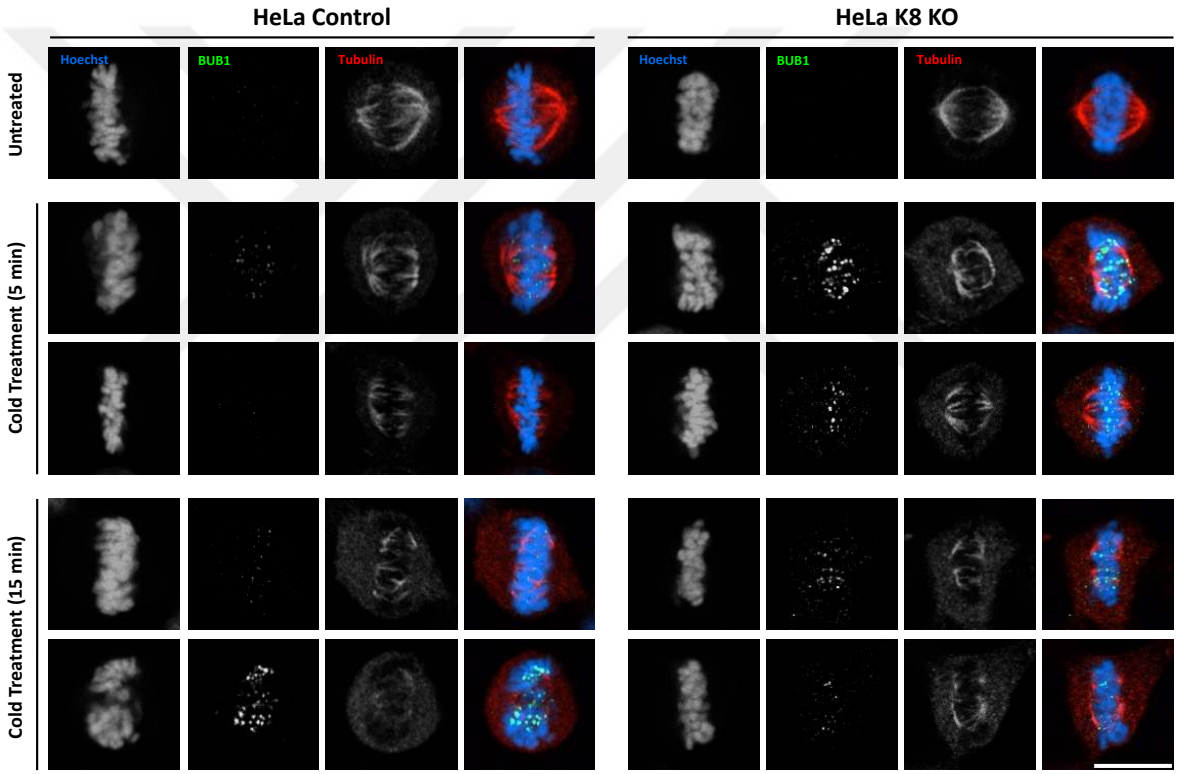

Figure 4.27: Confocal microscopy imaging of Hoechst (blue), BUB1 (green), and tubulin (red) in control and K8 KO HeLa cells at metaphase. Cells were untreated or cold-treated for 5 or 15 minutes. Scale bar = 10 µm.

4.1.4 Characterization of Cytoskeletal Network in the Absence of Keratin 8

Regulatory dynamics of cytoskeletal elements were observed with live imaging in the absence of keratin 8. For this purpose, microtubules were labeled with 100 nM SiR-tubulin (Spirochrome, SC002) 6 hours before, and chromosomes were stained with 200 ng/ml Hoechst 30 minutes before imaging in control and K8 KO HeLa cells. Time-lapse imaging

was performed with 5-minute intervals for an hour (Figure 4.28). Observations showed a spindle positioning defect where one of the poles was shifting downward in K8 KO HeLa cells.

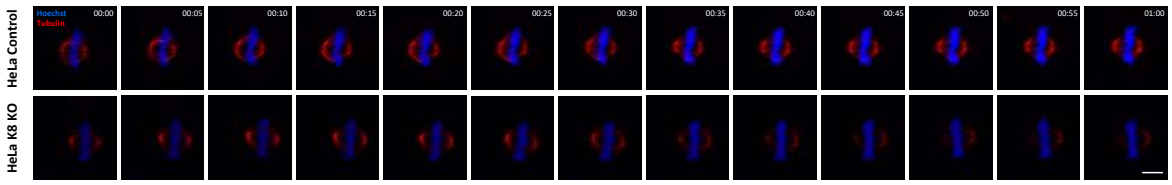

Figure 4.28: Live cell imaging of Hoechst (blue), and SiR-tubulin (red) in control and K8 KO HeLa cells at metaphase. Scale bar = 100 µm.

During live cell imaging, cells couldn't divide due to stress conditions. To overcome this, the DMEM-based media was replaced with a CO2-independent Leibovitz's L-15 medium (Thermo Fisher Scientific, 21083027) including 20% FBS a day before imaging. Cells divided successfully with the optimized imaging conditions (Figure 4.29). The spindle positioning defect was supported by the new observations in healthy dividing cells, and the defective spindle positioning was rescued with the addition of K8-GFP.

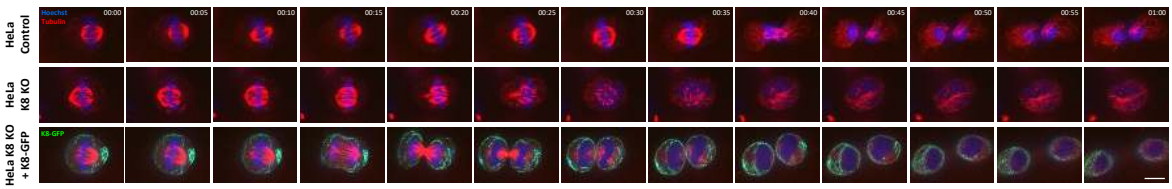

Figure 4.29: Live cell imaging of Hoechst (blue), SiR-tubulin (red), and K8-GFP (green) in control, K8 KO, and K8 KO +K8-GFP HeLa cells at metaphase. Scale bar = 100 µm.

To investigate the actin dynamics in the absence of keratin 8, filamentous actin was labeled with 100 nM SiR-actin (Spirochrome, SC001) 6 hours before, and chromosomes were stained with 200 ng/ml Hoechst 30 minutes before imaging in control and K8 KO HeLa cells. Time-lapse imaging was performed with 5-minute intervals for an hour (Figure 4.30). Imaging conditions were not yet optimized for SiR-actin. During imaging, cells couldn't divide, and possibly, SiR-actin labeling had more toxic effects on the cells compared to SiR-

tubulin. However, an interesting phenotype of actin localization to spindle poles was observed in the absence of keratin 8.

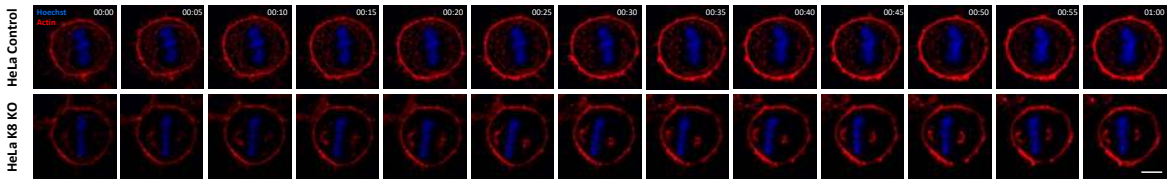

Figure 4.30: Live cell imaging of Hoechst (blue), and SiR-actin (red) in control and K8 KO HeLa cells at metaphase. Scale bar = 100 µm.

To further investigate the phenotype, control, K8 KO, and K8 KO +K8-GFP HeLa cells were labeled with SiR-actin, and the actin localization on the spindle poles was examined (Figure 4.31). Observations showed a decreased actin intensity at the spindle poles in the presence of keratin 8.

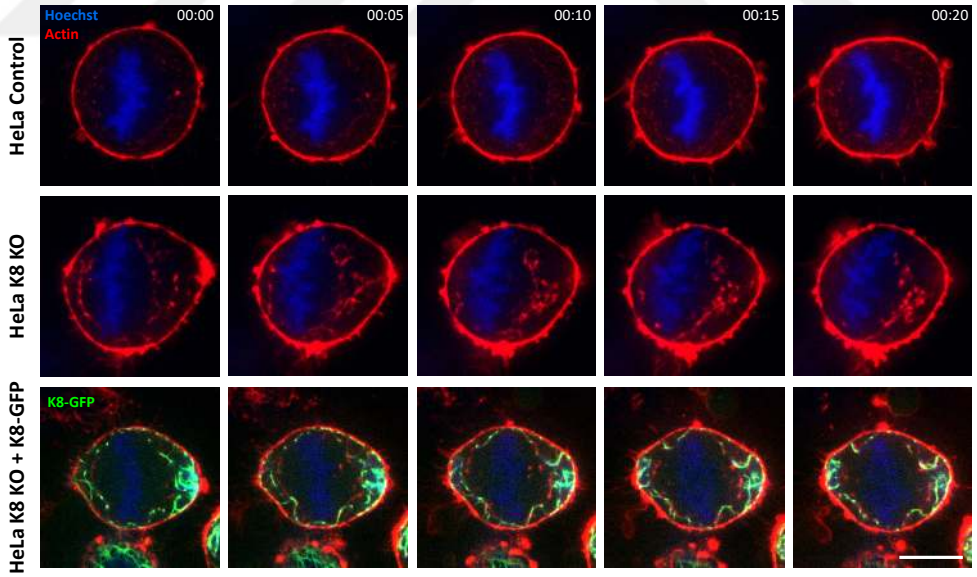

Figure 4.31: Live cell imaging of Hoechst (blue), SiR-actin (red), and K8-GFP (green) in control, K8 KO, and K8 KO +K8-GFP HeLa cells at metaphase. Scale bar = 10 µm.

To support the previous findings, K8 KO +K8-GFP HeLa cells were labeled with SiR-tubulin or Sir-actin, and the localization of keratin 8 with the cytoskeletal elements was investigated (Figure 4.32).

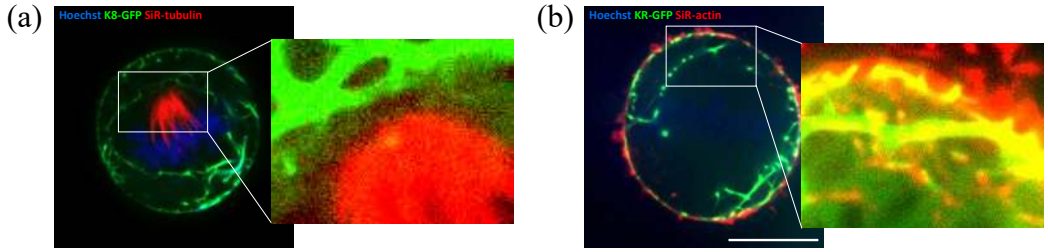

Figure 4.32: Live cell imaging of Hoechst (blue), K8-GFP (green), (a) SiR-tubulin, or (b) SiR-actin (red) in K8 KO +K8-GFP HeLa cells at metaphase. Scale bar = 10 µm.

Focusing on the spindle poles, co-localization of keratin 8 with tubulin was observed at the centrosome. In addition to that, keratin 8 was co-localizing with filamentous actin on the cell periphery. Findings supported that keratin 8 may stabilize spindle poles and maintain the structural integrity of the spindle apparatus.

4.1.5 Generation of HeLa S3 dTAG Cell Line

To have an orthogonal approach for the degradation of keratin 8 in HeLa S3 cells, the CRISPR-Cas12a-assisted PCR tagging method was combined with the dTAG system. Initially, a PCR cassette was prepared using the template plasmid with M1- and M2-tagging oligos targeting the *KRT8* gene. DNA gel electrophoresis was performed with the PCR product, and the gel fraction was cut for purification (Figure 4.33). PCR reaction without the template was used as the negative control.

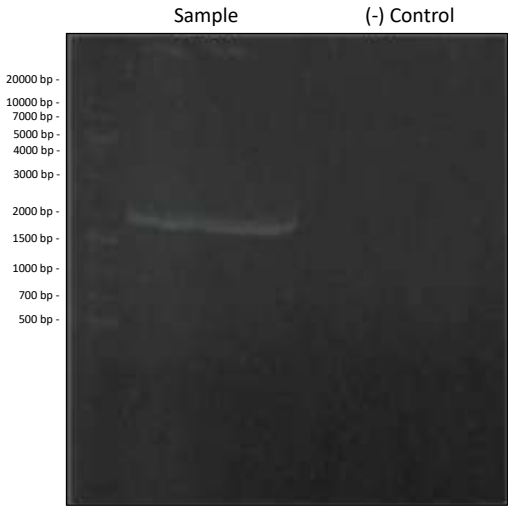

Figure 4.33: Agarose gel electrophoresis image of PCR cassette with the negative control.

Before the transfection of the PCR cassette with the helper plasmid, a kill curve for G418 selection was established. HeLa S3 cells were treated with G418 at concentrations ranging from 200 µg/mL to 1200 µg/mL for 9 days. Cell viability was assessed using microscopy and was expressed as a percentage of untreated control cells. The optimal concentration was determined as 700 µg/mL (Figure 4.34).

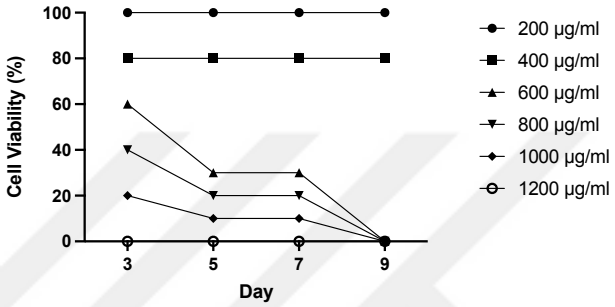

Figure 4.34: G418 kill curve for HeLa S3 cells. Data represents the percentage of cell survival as a function of increasing G418 concentration for 9 days.

HeLa S3 cells were transfected with the purified PCR cassette and the helper plasmid. After transfection, cells were selected with 700 µg/mL G418 treatment for two weeks. To check for the transfection efficiency, cells were seeded onto coverslips and stained with HA (Figure 4.35). HeLa REEP4-HA cells were used as the positive control.

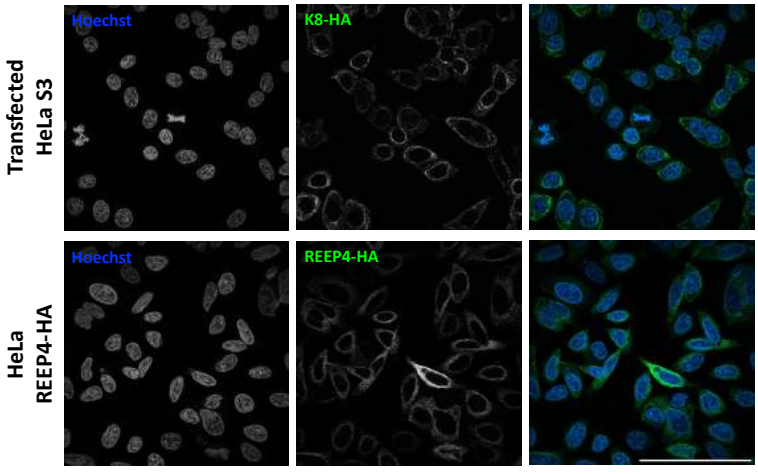

Figure 4.35: Confocal microscopy imaging of Hoechst (blue) and HA (green) in transfected HeLa S3 and untransfected HeLa REEP4-HA cells. Scale bar = 100 µm.

The results showed that the transfected pool of HeLa S3 cells was positive for the insertion. Hereafter, these cells will be referred to as HeLa S3 dTAG. To confirm the insertion, three primers were designed for the genomic screening. Forward primer (for) was designed to bind before the 3'UTR of the *KRT8* gene, the first reverse primer (rev) was designed to bind after the 3'UTR of the *KRT8* gene, and the second reverse primer (dTAG_rev) was designed to bind at the 3' end of the inserted PCR cassette. Using the forward primer with the first reverse primer (for + rev) or forward primer with the second reverse primer (for + dTAG_rev), it was aimed to detect the insertion in the genome. PCR was performed with the primer combinations and genomic DNA of HeLa S3 or HeLa S3 dTAG cells (Figure 4.36). The results of the HeLa S3 cells showed no insertion with the PCR product at the length of the genomic DNA between the two primers (for + rev). However, HeLa S3 dTAG cells showed a heterozygous insertion profile in the genome. Based on the high chance of non-specific binding of the primers in the genomic DNA, it was decided to validate the insertion with different primer pairs.

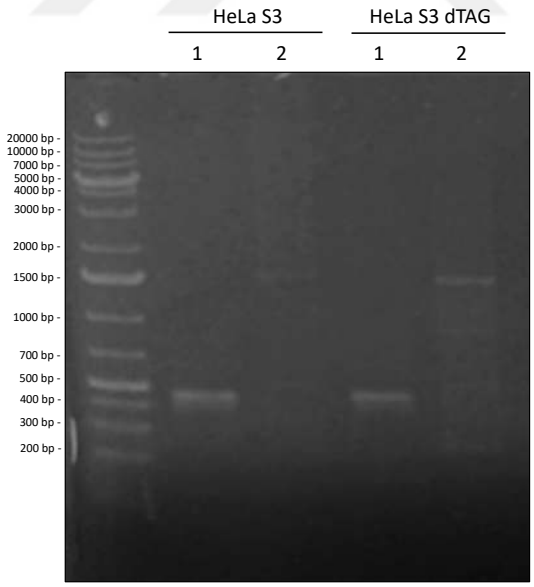

Figure 4.36: Agarose gel electrophoresis image of HeLa S3 and HeLa S3 dTAG cells' PCR products. Primer pairs are shown as 1: (for + rev) and 2: (for + dTAG_rev).

In the meantime, the transfected pool of HeLa S3 cells was sorted with flow cytometry-based single-cell sorting, and the colonies grown from single cells were screened for

insertion. The genomic DNA of the selected clones was isolated, and PCR was performed with the previously designed primer pairs (Figure 4.37). Genomic DNA of the HeLa S3 dTAG cells was used as the positive control.

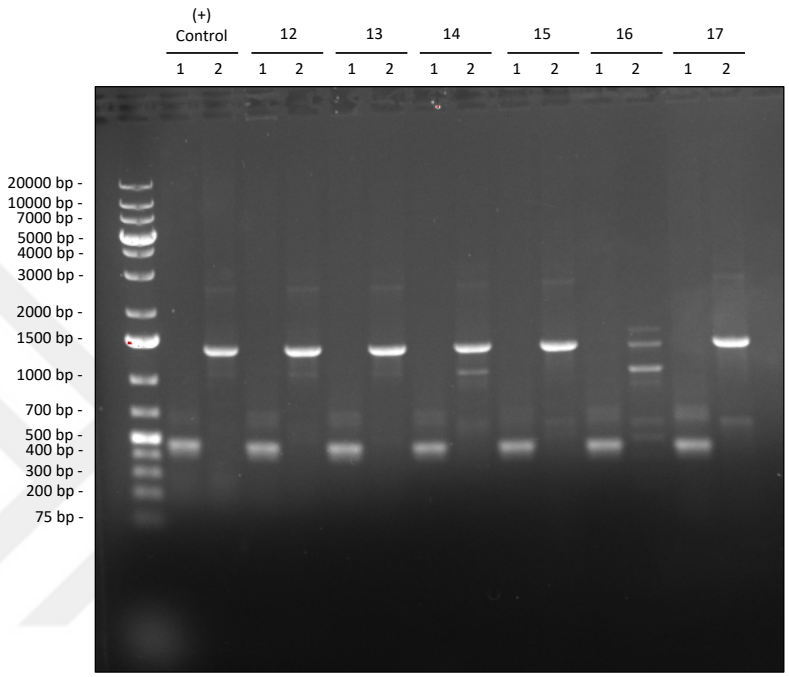

Figure 4.37: Agarose gel electrophoresis image of HeLa S3 dTAG single-cell clones' PCR products. Primer pairs are shown as 1: (for + rev) and 2: (for + dTAG_rev).

To investigate the insertion, single-cell clones #14, #15, and #16 were chosen with different patterns of DNA bands. The PCR products were sent for Sanger sequencing, and the cells were cultured for dTAG-13 treatment to observe the effects of the instant degradation of keratin 8.

4.2 Regulation of Keratin 8 Phosphorylation

Successful cell division requires the dynamic regulation of keratin filaments. Given that the solubility of keratin filaments increases by phosphorylation and the phosphoproteoforms of keratin 8 serve as cancer progression markers, the regulation of keratin 8 phosphorylation was investigated by examining its phosphorylation profile in different cancer cell lines during the dynamic process of cell division.

To investigate the phosphorylation pattern of keratin 8, different cancer cell lines were selected with varying levels of the protein. Based on the nTPM (normalized Transcripts Per Million) levels of keratin 8 retrieved from the Human Protein Atlas (accessed January 2025), MCF7 cells were detected to have the highest level of keratin 8. Along with it, HeLa, MDA-MB-231, and CAKI-2 were selected with decreasing levels. As a non-cancerous cell line and with undetectable keratin 8 expression, HEK 293 cells were included as the control. Western blot analysis was performed to show the levels of keratin 8 in selected cell lines (Figure 4.38).

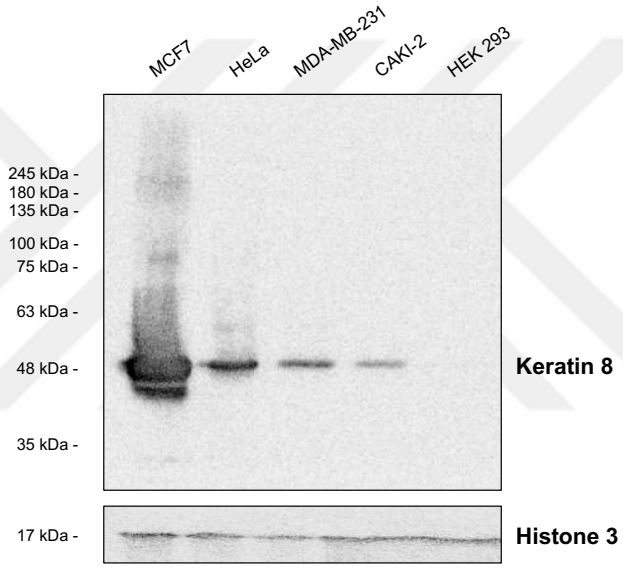

Figure 4.38: Western blot analysis of keratin 8 levels in MCF7, HeLa, MDA-MB-231, CAKI-2, and HEK 293 cells.

4.2.1 Ectopic Expression of K8/18 in HEK 293 Cells

To investigate the filament formation, solubility, and phosphorylation profile of keratin 8 in HEK 293 cells, ectopic expression of the keratin 8/18 pair was aimed. For this purpose, a K18-RFP vector was constructed to be used with K8-GFP.

To construct a keratin 18-RFP vector, an ezrin-RFP vector was digested, removing ezrin from the vector. DNA gel electrophoresis was performed with the digestion product, and the gel fraction of the cut vector was purified (Figure 4.39a). To amplify K18 for further Gibson cloning, PCR was performed with the designed primers and 1.5 and 5 ng of template DNA. DNA gel electrophoresis was performed with the PCR product, and the gel fraction of the

PCR product from 5 ng template DNA was purified (Figure 4.39b). PCR reaction without the template was used as the negative control.

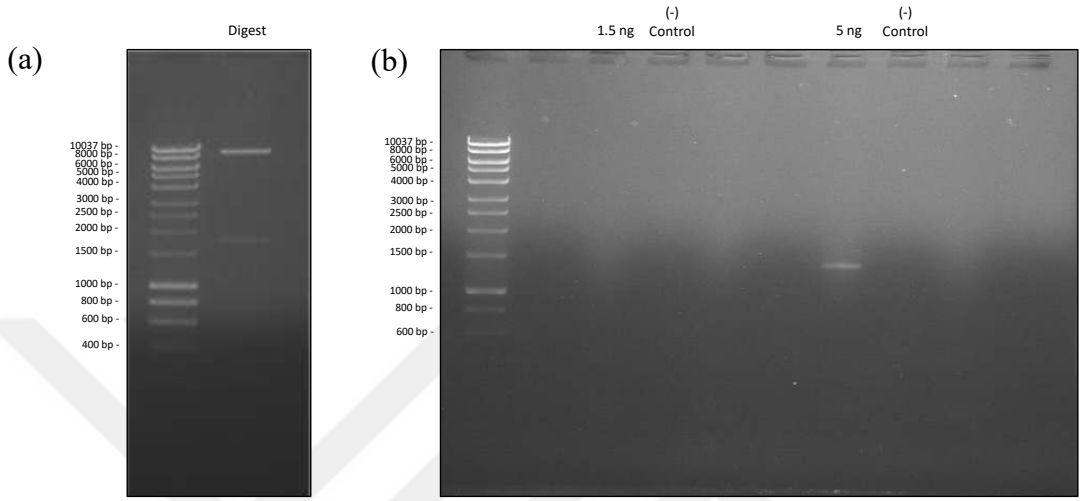

Figure 4.39: Agarose gel electrophoresis images of (a) ezrin-RFP vector digest and (b) K18 PCR product with negative controls.

DNA gel electrophoresis was performed with the insert and digested vector to calculate the ratios for the Gibson cloning (Figure 4.40). A 1:2 ratio of insert to vector was used for further calculations.

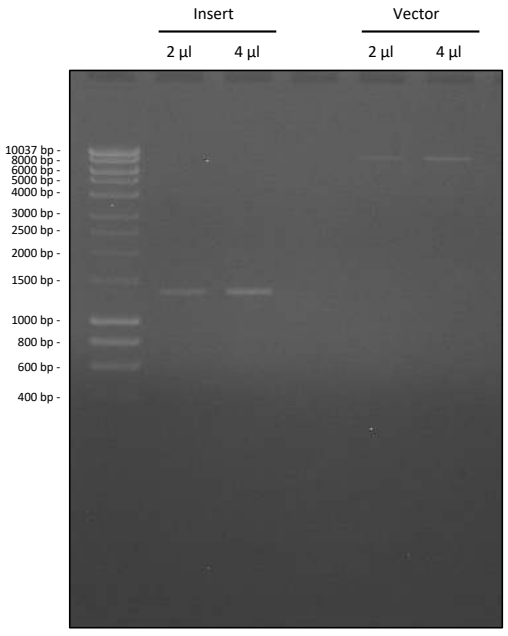

Figure 4.40: Agarose gel electrophoresis image of K18 insert and digested vector.

After Gibson cloning and transformation, colonies were grown on LB agar plates. Subsequently, a colony PCR and DNA gel electrophoresis were performed (Figure 4.41). A Gibson cloning sample without an insert and a colony PCR sample with an insert were used as negative and positive controls, respectively.

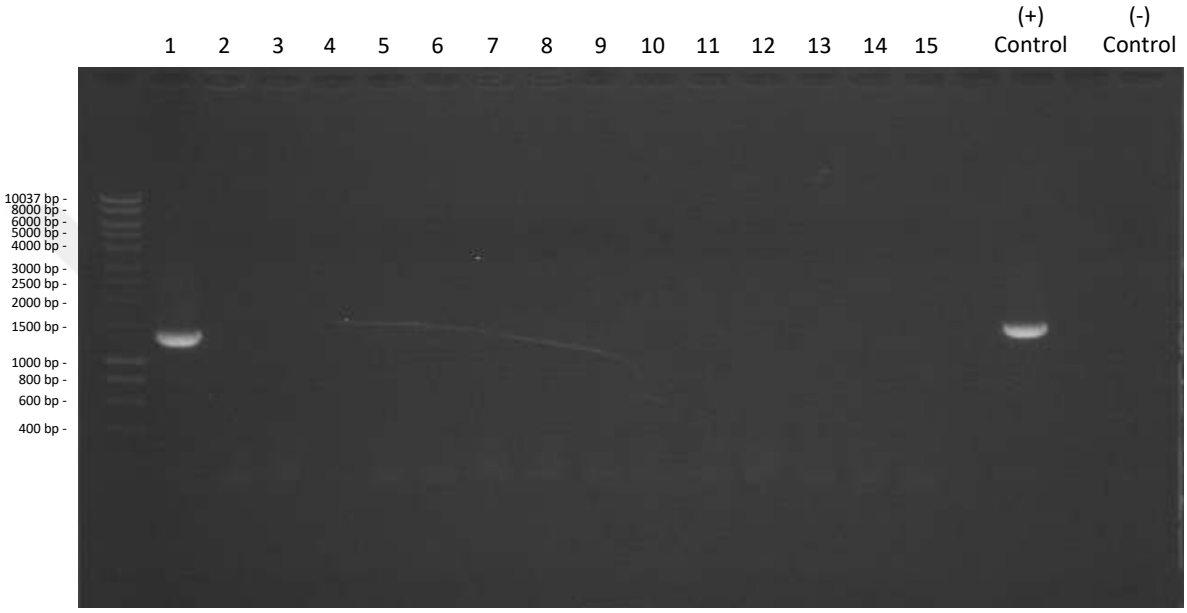

Figure 4.41: Agarose gel electrophoresis image of colony PCR products with positive and negative controls.

The plasmid DNA of colony #1 was purified and sent for Sanger sequencing (Appendix D). After validating the vector sequence was validated, the K18-RFP vector was used in further experiments.

K8-GFP and K18-RFP vectors were transfected in HEK 293 cells to observe the effects of ectopic keratin expression. Upon individual transfection of K8-GFP or K18-RFP into cells, protein aggregation was observed following expression. Conversely, co-transfection of both vectors resulted in the formation of keratin 8/18 filaments (Figure 4.42). HeLa cells were used as the control, and there was no protein aggregation upon single transfection. In each case, keratin 8/18 filaments were formed due to the expression of the other heterodimerization partner in the HeLa cells.

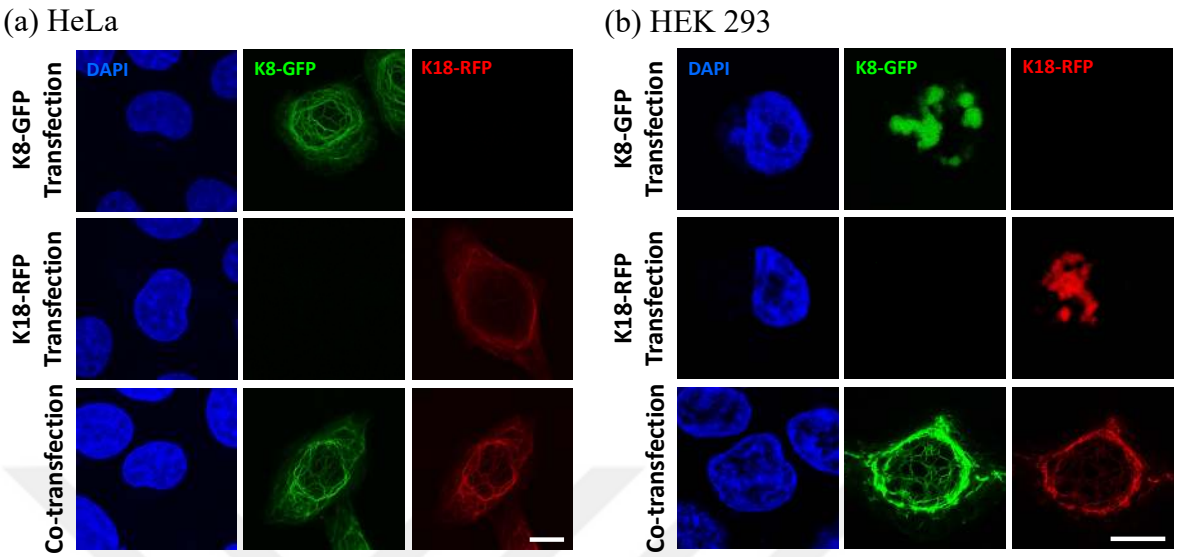

Figure 4.42: Confocal microscopy imaging of DAPI (blue), K8-GFP (green), and K18-RFP (red) in transfected HeLa or HEK 293 cells. Scale bar = 10 µm.

To generate a stable cell line, lentiviral packaging and transduction were performed in HEK 293 cells. For the selection of the transduced cells, a puromycin (STEMCELL Technologies, 73342) kill curve was established using concentrations ranging from 1 to 5 µg/ml (Figure 4.43). After 48 hours of transfection, cells were selected with 3 µg/ml puromycin for a week. Hereafter, HEK 293 cells transduced with keratin 8-GFP and keratin 18-RFP will be referred to as HEK 293 +K8/18.

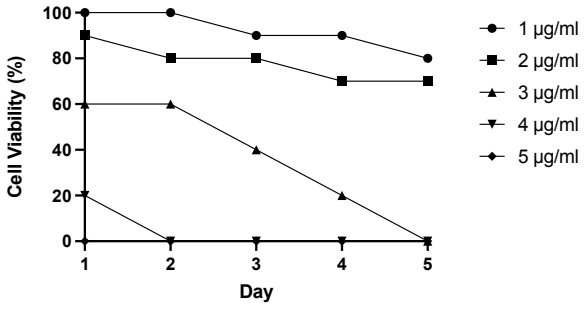

Figure 4.43: Puromycin kill curve for HEK 293 cells. Data represents the percentage of cell survival as a function of increasing puromycin concentration for 5 days.

Including the stable HEK 293 +K8/18 cell line, western blot analysis was repeated to show the levels of keratin 8 in all cell lines (Figure 4.44).

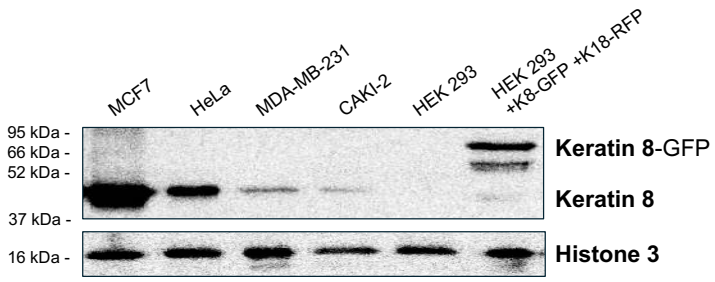

Figure 4.44: Western blot analysis of endogenous and ectopic keratin 8 levels in MCF7, HeLa, MDA-MB-231, CAKI-2, HEK 293, and HEK 293 +K8/K18 cells.

The results showed a high expression level of keratin 8 in HEK 293 +K8/K18 cells. The levels were close to the expression level of keratin 8 in HeLa cells. The generated stable cell line was used in further experiments to search for the phosphorylation profile of keratin 8.

4.2.2 Quantitative DDA Analysis of Cell Cycle-Dependent Keratin 8 Phosphorylation

A comprehensive phosphoproteome analysis was performed in MCF7, HeLa, MDA-MB-231, CAKI-2, and HEK 293 +K8/K18 cells to uncover the cell cycle-dependent phosphorylation profile of keratin 8. For this purpose, cells were arrested at interphase, mitosis, and cytokinesis, and isolated proteins were digested into peptides. Peptides from interphase, mitosis, and cytokinesis were labeled with light, medium, and heavy dimethyl mass tags, respectively, and mixed at a 1:1:1 ratio. 5 µg of the peptide mix was separated and subjected to LC-MS/MS for the global proteome analysis. The remaining mix was fractionated into six for further phosphopeptide enrichment and enriched fractions were subjected to LC-MS/MS for the global phosphoproteome analysis (Figure 4.45). DDA was performed by selecting the most intense precursor ions for fragmentation, using a top 10 approach in each scan cycle. Raw data files from two biological replicates, each with three technical replicates, were processed using PD, MaxQuant, Perseus, and InfernoRDN.

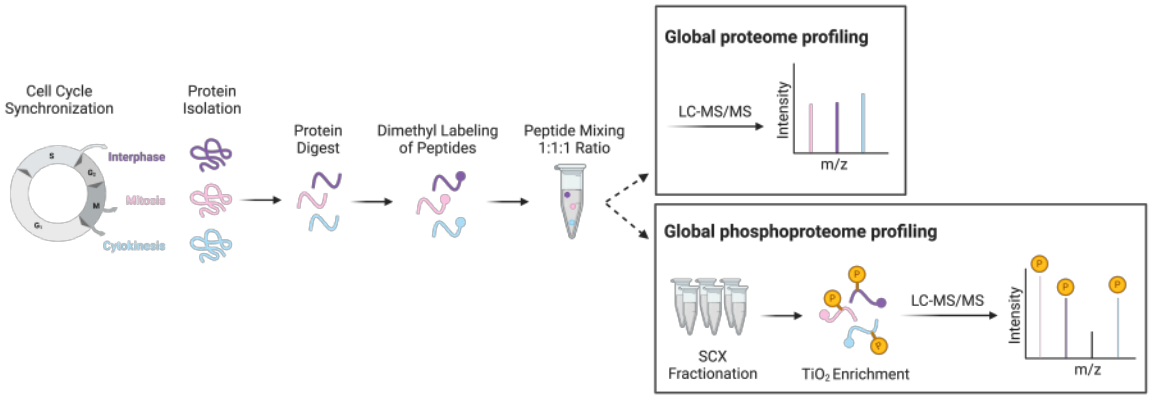

Figure 4.45: Experimental workflow of cell cycle-dependent and quantitative proteome and phosphoproteome profiling.

Synchronization steps were optimized for MCF7, HeLa, MDA-MB-231, CAKI-2, and HEK 293 +K8/K18 cells, and the synchronization was verified by FACS analysis based on DNA content and phospho-histone H3 analysis (Figure 4.46, Appendix B). The heterogeneity in the cell lines led to slight differences in the histograms. For MCF7 cells, histograms were fragmented and exhibited a striped pattern due to the low number of cells analyzed. However, the synchronization efficiency was supported by the phospho-histone H3 analysis (Appendix B). In HEK 293 +K8/18 cells, the histogram of the interphase was wider, possibly due to the multinucleation in the cells.

Following synchronization, proteins were isolated by urea lysis and digested into peptides by tryptic cleavage. Peptides from interphase, mitosis, and cytokinesis were labeled with light, medium, and heavy dimethyl mass tags, respectively, and mixed at a 1:1:1 ratio. With the samples, global proteome analysis was performed. For the global phosphoproteome analysis, peptides were fractionated into six to decrease the complexity, and the low-abundant phosphopeptides were enriched using TiO_2 beads. Following the mass spectrometry analysis, raw data files of two biological replicates were processed using Maxquant. The normalized protein ratios from the peptide list of the proteome and the phosphorylation site list of the phosphoproteome analysis were used for further analysis. The correlation of biological replicates was visualized using InfernoRDN (Figure 4.47). Overall, the global proteome and phosphoproteome analysis identified approximately 3,000 proteins and 7,000 phosphopeptides for each cell line.

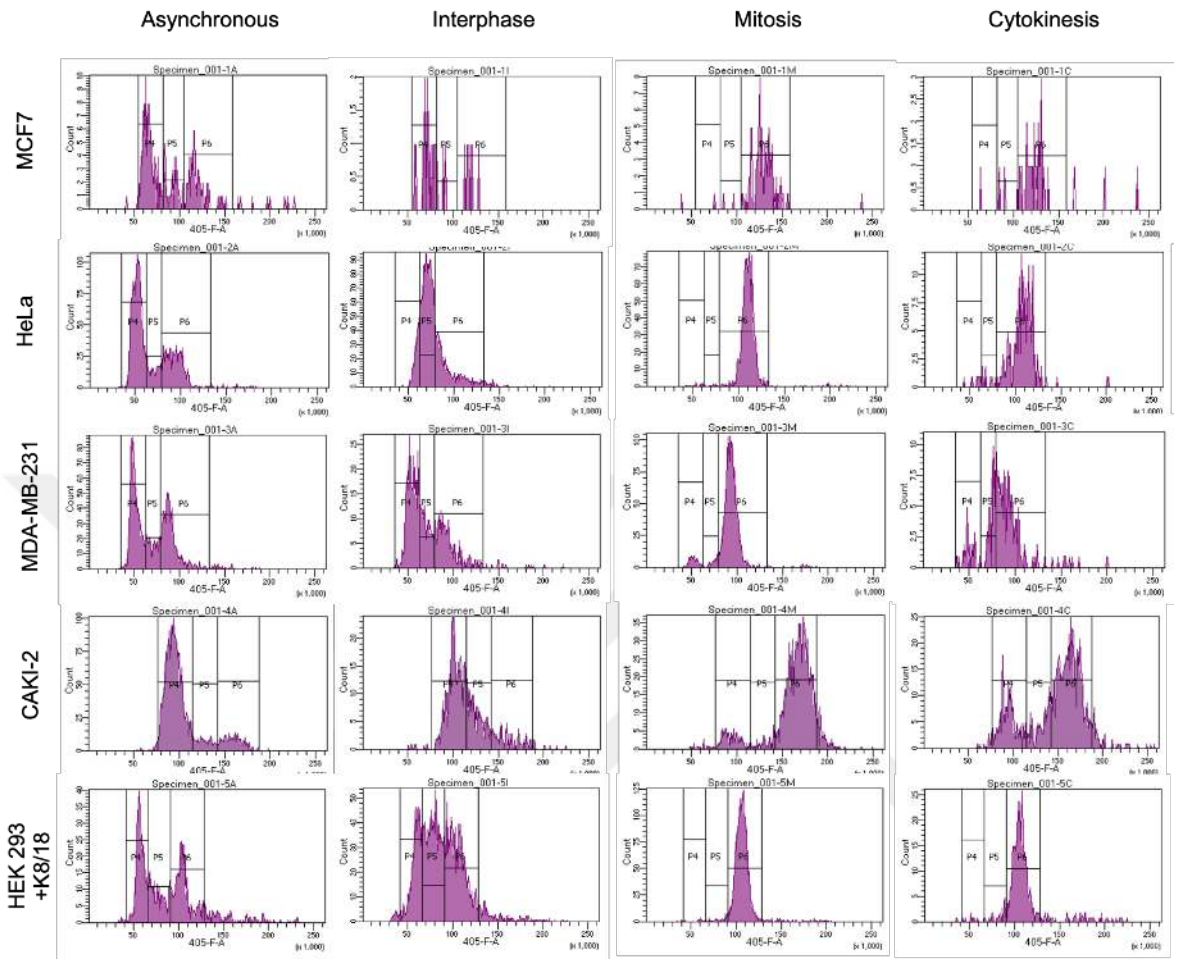

Figure 4.46: FACS histograms of asynchronous and synchronized MCF7, HeLa, MDA-MB-231, CAKI-2, and HEK 293 +K8/K18 cells.

To check the phosphopeptide enrichment efficiencies in MCF7, HeLa, MDA-MB-231, CAKI-2, and HEK 293 +K8/K18 cells, the number of phosphopeptides was compared with the non-phosphopeptides for each cell line (Figure 4.48). MCF7 cells showed the highest phosphopeptide enrichment efficiency with 58.1% phosphopeptides in the sample. This was followed by HeLa, CAKI-2, MDA-MB-231, and HEK 293 +K8/18 cells in decreasing order. HEK 293 +K8/18 cells showed the lowest phosphopeptide enrichment efficiency with 50.4% phosphopeptides in the sample. The results were correlating the endogenous expression levels of keratin 8 in the cells. MCF7 cells with the highest level of keratin 8 expression showed the highest enrichment of phosphopeptides.

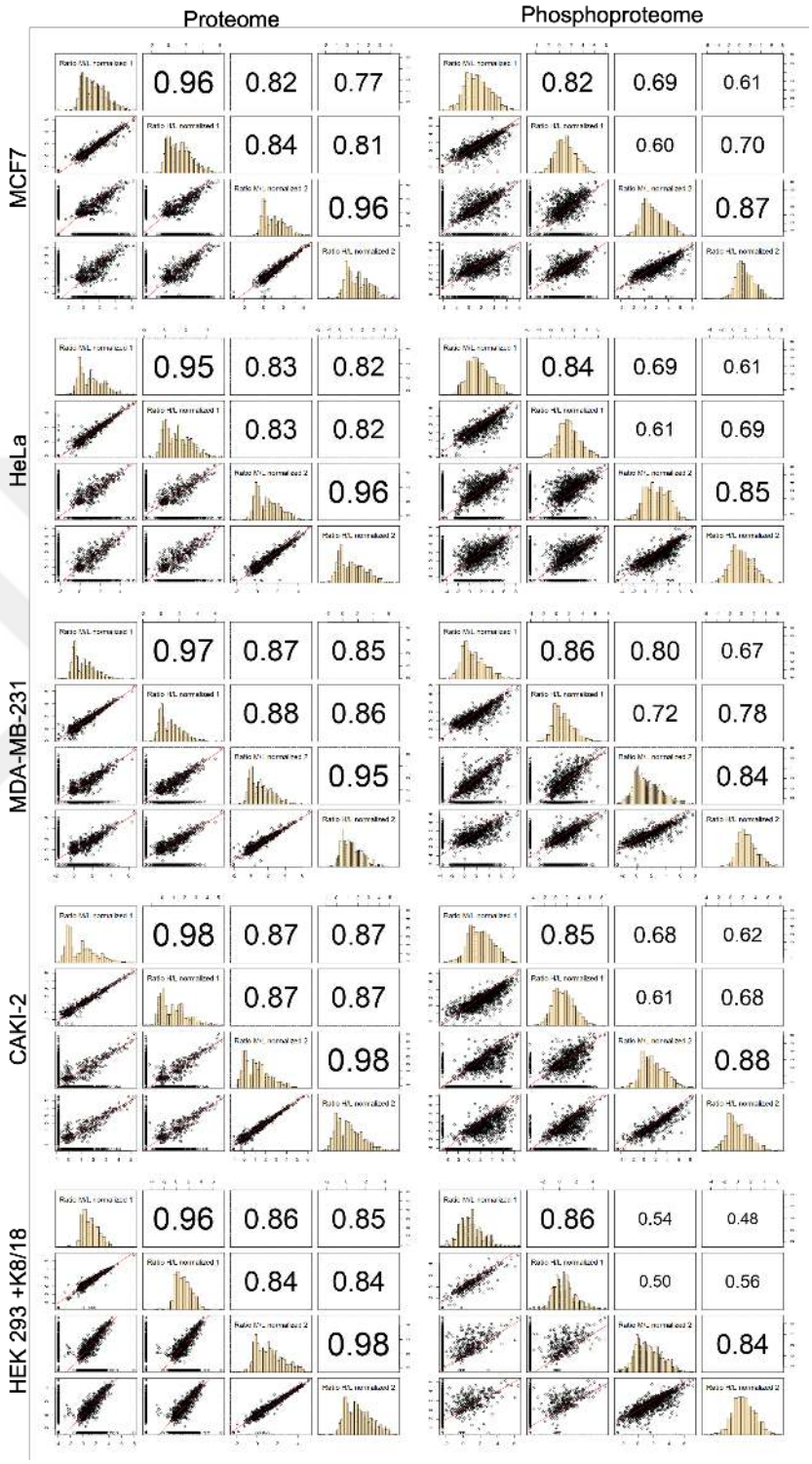

Figure 4.47: Pearson correlation plots of normalized protein ratios from proteome and phosphoproteome analysis across biological replicates in MCF7, HeLa, MDA-MB-231, CAKI-2, and HEK 293 +K8/K18 cells. Interphase, mitosis, and cytokinesis dimethyl mass tags were indicated as L: Light, M: Medium, and H: Heavy, respectively.

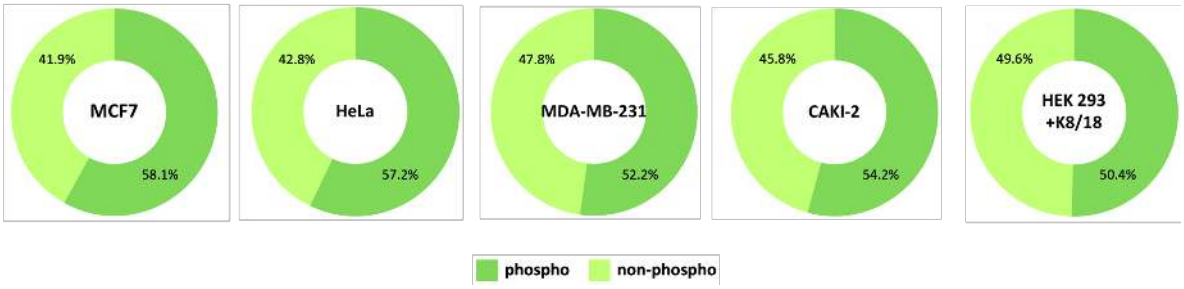

Figure 4.48: Phosphopeptide enrichment ratios in MCF7, HeLa, MDA-MB-231, CAKI-2, and HEK 293 +K8/K18 cells.

Focusing on keratin 8 from the global analysis, phosphorylation profiles in MCF7, HeLa, MDA-MB-231, CAKI-2, and HEK 293 +K8/K18 cells were analyzed. Based on the normalized M/L and H/L ratios, the phosphorylation sites specific to mitosis and cytokinesis were mapped (Figure 4.49).

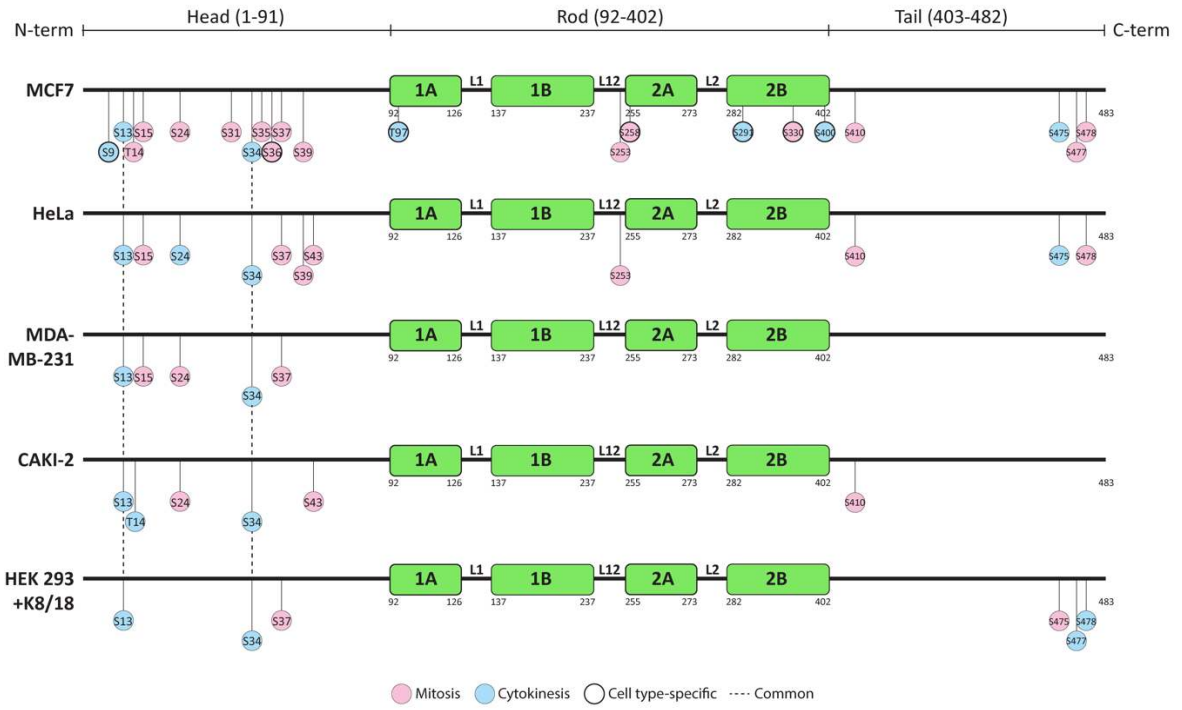

Figure 4.49: Quantitative DDA analysis of cell cycle-dependent phosphorylation sites on keratin 8 in MCF7, HeLa, MDA-MB-231, CAKI-2, and HEK 293 +K8/K18 cells. Mitosis- and cytokinesis-specific sites were colored in pink and blue, respectively. Cell type-specific sites were encircled with bold lines, and common sites were connected using dashed lines.

With the highest expression of the protein in MCF7 cells, 21 cell cycle-dependent phosphorylation sites were mapped. This was followed by HeLa cells with 11, CAKI-2 and HEK 293 +K8/K18 cells with 6, and MDA-MB-231 cells with 5 phosphorylation sites. Within those, S13 and S34 were quantified as commonly phosphorylated sites specific to cytokinesis in all cells. Some phosphorylation sites were cell-type specific, such as S9, S36, T97, S258, S291, S330, and S400 phosphorylation sites in MCF7 cells. Comparing the breast cancer cell lines, MDA-MB-231 cells showed the same 5 phosphorylation sites of MCF7 cells specific to mitosis or cytokinesis.

The results showed that the number of phosphorylation sites decreased with lower expression of keratin 8. To investigate if the phosphorylation level of keratin 8 was expression level-dependent, the DIA method was applied for a comprehensive and unbiased analysis.

4.2.3 DIA Analysis of Cell Cycle-Dependent Keratin 8 Phosphorylation

A comprehensive phosphoproteome analysis was performed in MCF7, HeLa, MDA-MB-231, and CAKI-2 cells. For this purpose, cells were arrested at interphase, mitosis, and cytokinesis, and isolated proteins were digested into peptides. In the label-free approach, 5 µg of peptides from each sample was separated, pooled, concentrated, and subjected to LC-MS/MS for the global proteome analysis. The remaining samples were fractionated into six for further phosphopeptide enrichment and enriched fractions were pooled, concentrated, and subjected to LC-MS/MS for the global phosphoproteome analysis (Figure 4.50). DIA was performed by fragmenting all precursor ions within defined m/z windows. Raw data files from two biological replicates, each with three technical replicates, were processed using PD (Appendix G, Appendix H, Appendix I) and Spectronaut.

With the label-free DIA analysis, approximately 4,000 proteins and 25,000 phosphopeptides were identified and indicated a pronounced difference. When compared with the quantitative DDA analysis, an additional 1,000 proteins and over three times the number of phosphopeptides were detected with DIA. Focusing on keratin 8 from the global analysis, phosphorylation sites identified in MCF7, HeLa, MDA-MB-231, and CAKI-2 cells during the cell cycle were mapped (Figure 4.51).

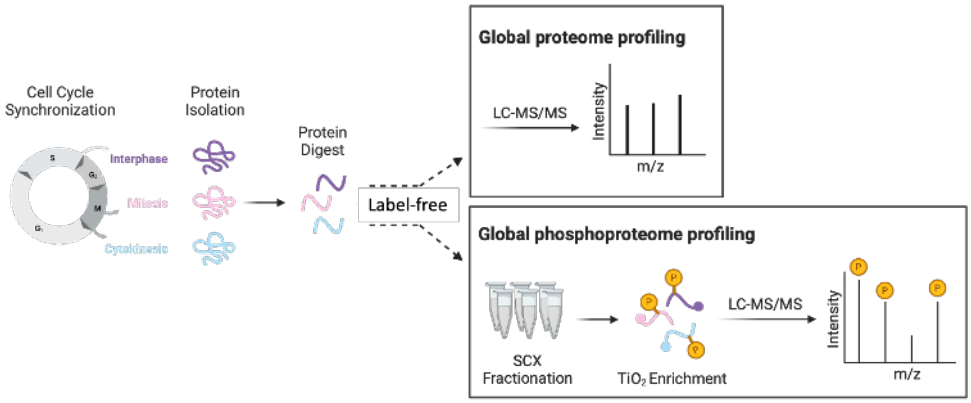

Figure 4.50: Experimental workflow of cell cycle-dependent and label-free proteome and phosphoproteome profiling.

DIA analysis identified additional phosphorylation sites of keratin 8 in MCF7, HeLa, MDA-MB-231, CAKI-2, and HEK 293 +K8/K18 cells. Identified phosphorylation sites suggested that the phosphorylation levels of the protein were not expression level-dependent.

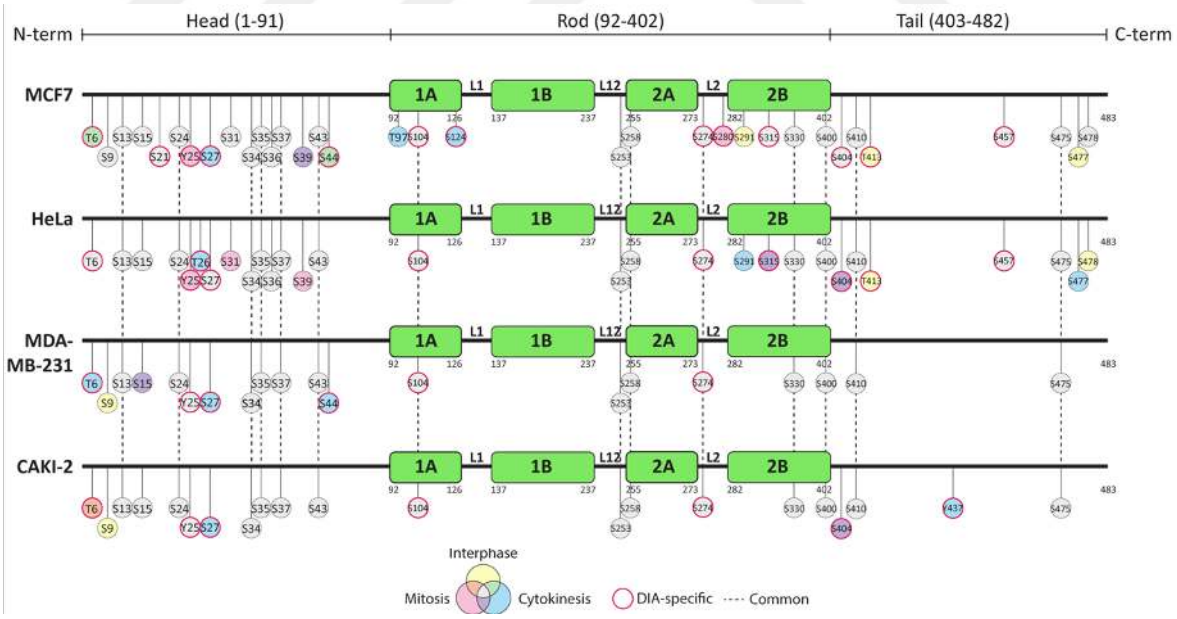

Figure 4.51: Label-free DIA analysis of cell cycle-dependent phosphorylation sites on keratin 8 in MCF7, HeLa, MDA-MB-231, CAKI-2, and HEK 293 +K8/K18 cells. Sites identified only in interphase, mitosis, and cytokinesis were colored yellow, pink, and blue, respectively. DIA-specific sites were encircled with pink lines, and common sites were connected using dashed lines.

4.2.4 Targeted Detection of Keratin 8 S34 Phosphorylation During Cytokinesis

To search for a promising cell division marker across different cells, S34 phosphorylation on keratin 8 was further validated. Initially, the phosphorylation was characterized using PRM in MCF7 cells. A DDA analysis was performed to build an inclusion list with m/z values of keratin 8 S34 phosphopeptides. Subsequently, PRM was performed with MCF7 cells synchronized to cytokinesis (Figure 4.52). Mitotic MCF7 cells were used as the control.

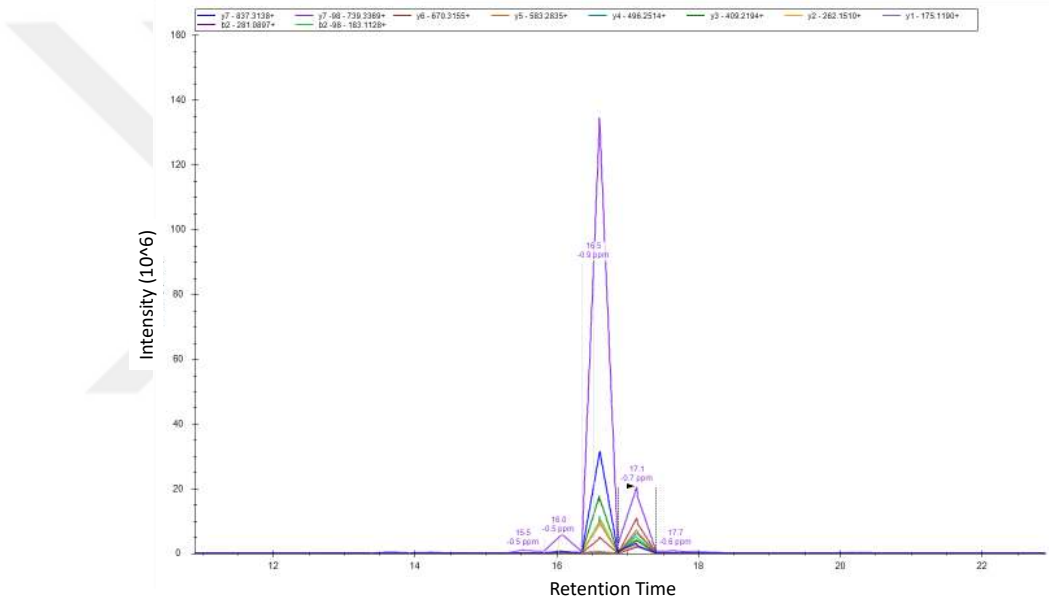

Figure 4.52: PRM peaks of K8 S34 phosphopeptides in MCF7 cells at cytokinesis. Peaks represent the fragment ion intensities plotted against the retention time.

PRM revealed keratin 8 S34 phosphorylation in MCF7 cells during cytokinesis. To further support the findings, a custom antibody for phospho-keratin 8 Serine 34 (p-K8 (S34)) was produced. The phosphorylation was imaged during cell division in HeLa cells (Figure 4.53a). Results showed that the phosphorylation starts in mitosis and reaches the highest levels at the midbody. To confirm the phosphorylation of ectopically expressed keratin 8, HEK 293 +K8/18 cells were stained with p-K8 (S34), and the phosphorylation was imaged during cell division (Figure 4.53b). Results showed that phosphorylation of keratin 8 on S34 marks cell division across cell types. This indicated that phosphorylation at S34 on keratin 8 is a promising marker for cell division.

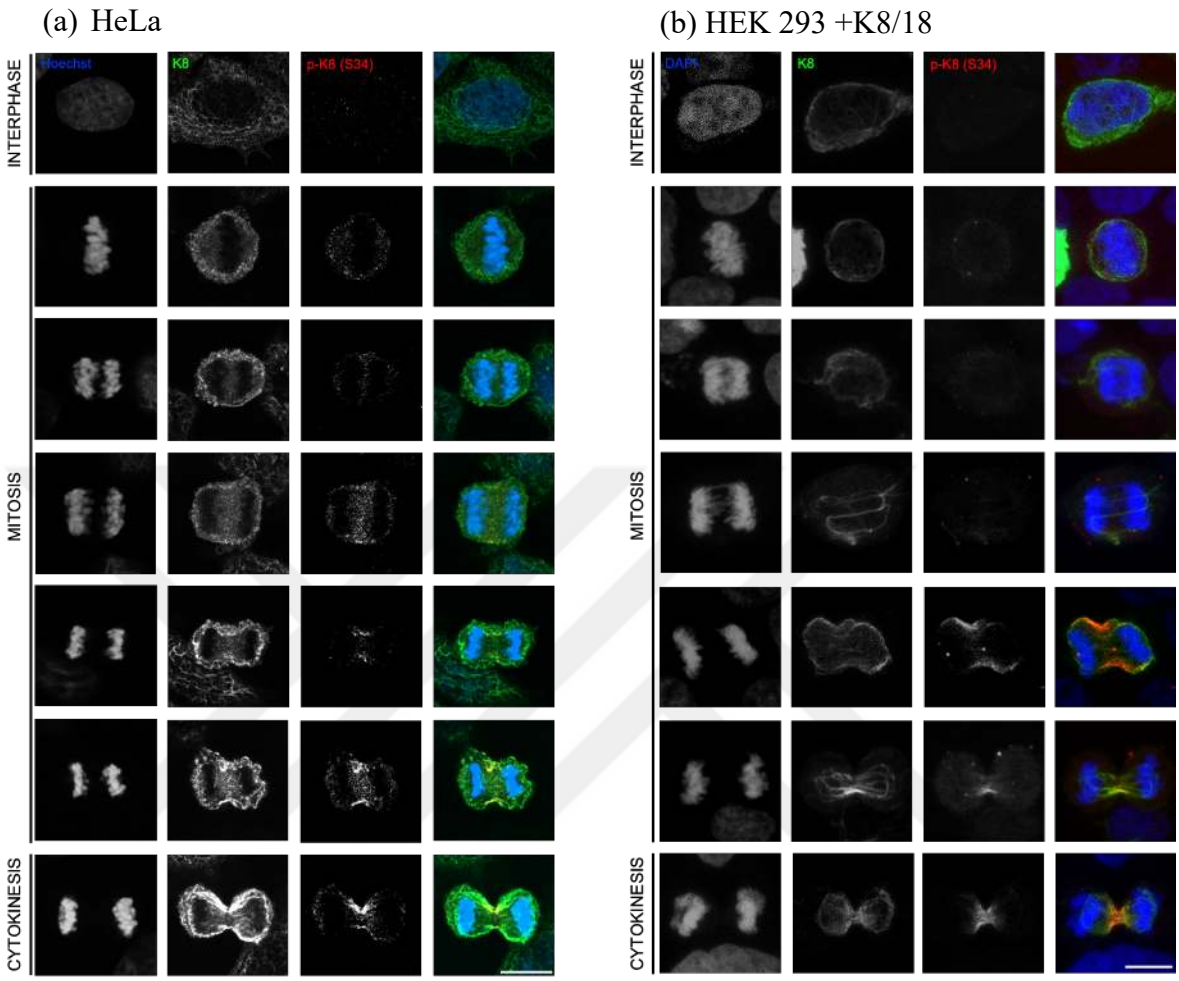

Figure 4.53: Confocal microscopy imaging of Hoechst/DAPI (blue), K8 (green), and p-K8(S34) (red) in (a) HeLa and (b) HEK 293 +K8/18 cells. Scale bar = 10 µm.

To understand the biological relevance of the S34 phosphorylation on keratin 8, occupancy analysis was performed. From the quantitative DDA analysis, the peptide list of the proteome and the phosphorylation site list of the phosphoproteome analysis were used to calculate the relative occupancy of S34 phosphorylation on keratin 8 in MCF7, HeLa, MDA-MB-231, CAKI-2, and HEK 293 +K8/K18 cells at cytokinesis. For this purpose, a scaled occupancy analysis was performed. To calculate the scaling factor, the normalized H/L ratio of keratin 8 from the phosphoproteome data was divided by the respective value from the proteome data. The scaling factor was applied to the peptide intensities in the proteome data, aligning the scales between datasets. Subsequently, occupancy was calculated for cytokinesis by dividing phosphopeptide values by non-phosphopeptides (Figure 4.54).

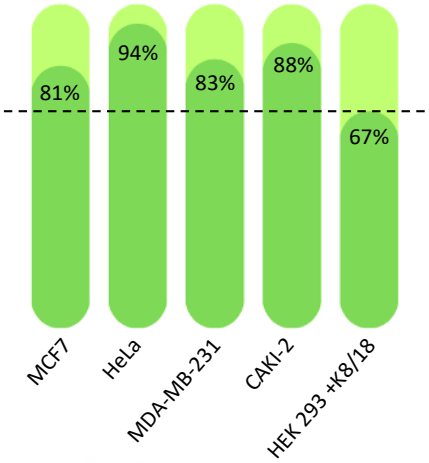

Figure 4.54: Relative occupancy of K8 S34 phosphorylation in MCF7, HeLa, MDA-MB-231, CAKI-2, and HEK 293 +K8/K18 cells at cytokinesis.

Results showed that the relative occupancy of S34 phosphorylation on keratin 8 was lower in HEK 293 +K8/18 cells. Following, to further investigate the division dynamics in HEK 293 +K8/18 cells, time-lapse imaging was performed (Figure 4.55). Live cell imaging showed that the accumulation of keratin 8 at the midbody caused the multinucleation of the cells. Considering the lower occupancy of phosphorylation and the lack of knowledge of the K8/18 filament structure in HEK 293 +K8/18 cells, it was suggested that the phosphorylation of keratin 8 may be limited with low accessibility of the protein and not sufficient enough for the solubility of the filaments.

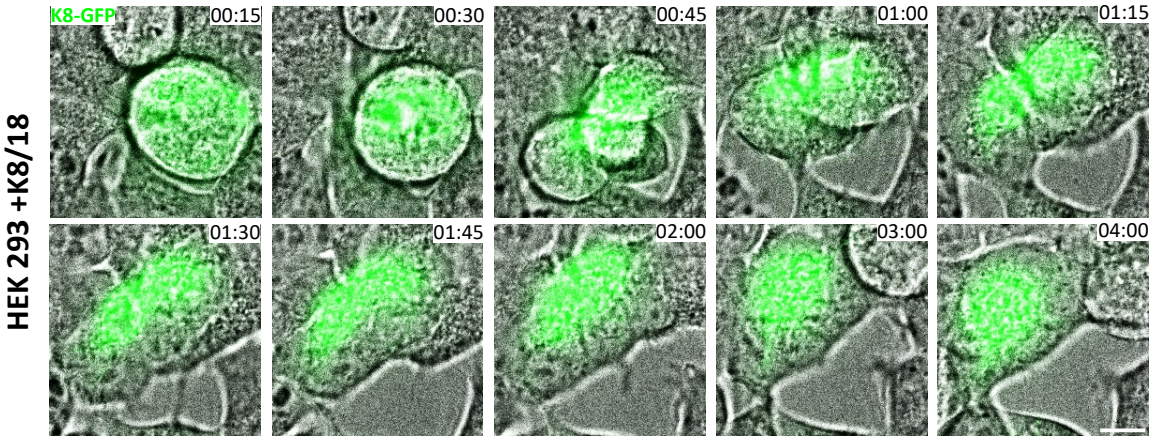

Figure 4.55: Live cell imaging of K8-GFP (green) in HEK 293 +K8/18 cells. Bright-field images representing the cell morphology. Scale bar = 10 µm.

To show the dynamics of keratin 8 without keratin 18 expression and to support that multinucleation was not a side effect of ectopic protein expression, HEK 293 was transfected with K8-GFP, and time-lapse imaging was performed (Figure 4.56). As expected, no filament formation was observed. Keratin 8 aggregated in the cells and in most cases, cells underwent bursting after rounding up for several hours.

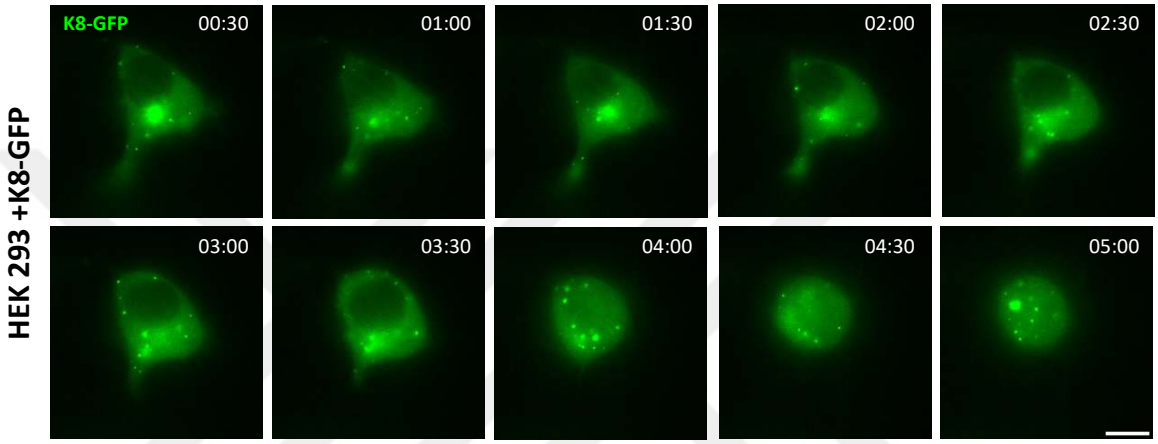

Figure 4.56: Live cell imaging of K8-GFP (green) transfected HEK 293 cells. Scale bar = 10 µm.

For the quantification of the multinucleation rate in HEK 293 +K8/18 cells, N-cadherin and DAPI staining were performed to visualize the cell boundaries and the nuclei (Figure 4.57a). To avoid a potential bias associated with an increased multinucleation in transduced cells, HEK 293 cells were freshly thawed, transfected with K8-GFP and K18, and directly fixed for multinucleation analysis. HEK 293 cells transfected with K8(S34-35D)-GFP and K18 were used to mimic the phosphorylation at S34 and S35 residues. HEK 293 cells transfected with GFP were used as the control. It was shown that K8/18 filament formation was causing a significantly high multinucleation rate in HEK 293 cells, which was significantly reduced in phosphomimetic mutants (Figure 4.57b). This highlighted the role of S34 phosphorylation in regulating cytokinesis.

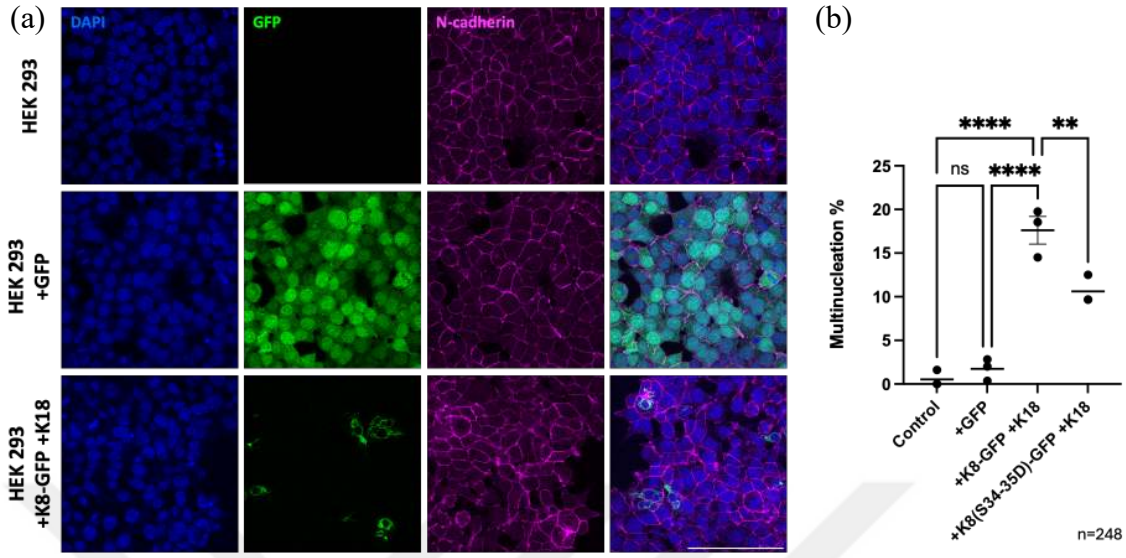

Figure 4.57: Multinucleation in HEK 293 +K8/18 cells: (a) Representative confocal microscopy images of DAPI (blue), GFP (green), and N-cadherin (magenta) in control, and GFP or K8-GFP and K18 transfected HEK 293 cells. Scale bar = 100 µm. (b) Quantification of multinucleation rate in HEK 293 (n = 248), HEK 293 +GFP (n = 248), HEK 293 +K8-GFP +K18 (n = 248), and HEK 293 +K8(S34-35D)-GFP +K18 (n = 248) cells. Data represents mean ± SEM. **** $p < 0.0001$. ns: not significant. One-way ANOVA.

Chapter 5

DISCUSSION

This study revealed numerous interactors of keratin 8 and indicated the importance of keratin 8 in cell cycle regulation and division. It was shown that the strong interactors of keratin 8, such as KNL1 and BUBR1, were involved in more specialized and dynamic roles at the M phase. During mitosis, the absence of keratin 8 disrupted the interactions of microtubule-binding proteins, including an outer kinetochore protein complex NDC80. By facilitating robust kinetochore-microtubule attachment, which is crucial for accurate chromosome segregation during mitosis, NDC80 was detected as a keratin 8-dependent microtubule interactor. The quantitative analysis of NDC80 indicated a reduced intensity on the metaphase plate in K8 KO cells compared to the control. Interestingly, the reintroduction of keratin 8 tagged with GFP in K8 KO cells restored the NDC80 levels, suggesting a rescue effect. These findings indicated the importance of keratin 8 in the proper functioning and localization of kinetochore proteins. As a model, our study proposed that keratin 8 functions as a scaffold and a regulatory protein at the outer kinetochore by binding to BUBR1 and KNL1 alongside microtubules. This interaction promotes kinetochore localization of NDC80 and supports proper kinetochore assembly. Furthermore, imaging of BUB1, an essential protein for spindle assembly checkpoint function, demonstrated that the checkpoint can still be activated in K8 KO cells despite the absence of keratin 8. This indicated that other compensatory mechanisms might be in place to ensure the proper functioning of the spindle assembly checkpoint in the absence of keratin 8.

Various advanced microscopy techniques were combined with immunofluorescence staining or labeling of live cells to further characterize K8 KO phenotypes in HeLa cells. Characterizing K8 KO cells revealed significant alterations in the cytoskeletal network, particularly impacting microtubule dynamics and actin localization on centrosomes. In the absence of keratin 8, a decrease in chromosomal density and defective spindle positioning

underscored the role of keratin 8 in maintaining microtubule stability. In K8 KO cells, the defects in chromosome alignment and segregation described in [36] supported the hypothesis that intermediate filaments scaffold and stabilize the kinetochore components, ensuring proper kinetochore function and chromosome segregation. Additionally, the actin localization on centrosomes during metaphase highlighted the involvement of keratin 8 in cytoskeletal reorganization and structural support during cell division. These findings can be contextualized within the broader understanding of keratin and actin filament interactions. Previous in vitro work focusing on the K8/18 pair provides specific insights into how keratin and actin work together to enhance the mechanical properties of cellular networks. In this study, it was shown that actin diminishes in keratin-dominant networks [38]. In our study, significant upregulation of the interaction between PLEC, a cytoskeletal linker protein, and TPM3, an actin-binding protein, with microtubules in the absence of keratin 8 highlighted the critical role of keratin 8 in regulating the actin dynamics. These findings emphasized the importance of the crosstalk between the keratin and actin cytoskeletal networks. Furthermore, several key actin-regulatory proteins, including IQGAP1, FLNB, MYO1C, MYO1E, and MISP, were identified as keratin 8 interactors. Notably, the interaction with MISP suggested a role for keratin 8 in spindle positioning, further emphasizing its involvement in actin cytoskeletal organization and cellular dynamics. However, there is a need for further investigation into the dynamic interplay between these filaments, highlighting their collaborative role in maintaining cytoskeletal network integrity.

As a possible side effect of K8 KO in HeLa cells, chromosome and microtubule integrities were observed to be defective. Their intensities were observed to be reduced in K8 KO compared to the control cells, suggesting a potential impact of the knockout gene on chromosomal characteristics or cytoskeletal dynamics. To understand how the absence of keratin 8 leads to the observed phenotypic changes, an orthogonal approach was taken for rapid and targeted protein degradation. The approach called the dTAG system, was employed together with an endogenous protein tagging CRISPR-Cas12a-assisted PCR technique. By utilizing the dTAG system, it was aimed to achieve precise temporal control over keratin 8 levels to further explore the roles and interactions of keratin 8 and its associated proteins in these cellular processes.

Focusing on intermediate filament reorganization, this study revealed the regulatory phosphorylation pattern of keratin 8 during cell division. To validate the detection of phosphorylation sites, DDA and DIA were compared, highlighting key differences in data completeness, sensitivity, and reproducibility between these two distinct acquisition methods. In principle, while DDA selects precursor ions for fragmentation, allowing for deeper but less comprehensive coverage, DIA fragments all ions, providing higher reproducibility and broader proteome coverage. During experimental optimization, a label-free DDA approach identified many phosphorylation sites in MCF7 cells. However, this number was significantly reduced in CAKI-2 cells, in which keratin 8 expression was decreased. This finding supported that DDA is effective for detecting phosphorylation sites in high-abundance proteins, whereas DIA is particularly advantageous for identifying phosphorylation sites in low-abundance proteins. In summary, the label-free DIA approach enabled the detection of phosphorylation sites that were undetectable by quantitative DDA in cells with low keratin 8 expression, thereby improving our ability to investigate the relationship between protein expression levels and phosphorylation dynamics. However, despite its advantages, DIA presented challenges in data processing due to the complexity of overlapping fragment spectra, which requires advanced computational tools and extensive data analysis for accurate quantification and interpretation.

The phosphorylation sites detected in this study were consistent with the data retrieved from PhosphoSitePlus (accessed January 2025). In addition to the data available in the literature, cell cycle-dependent keratin 8 phosphorylation was reported. It was shown that the phosphorylation profile of keratin 8 dynamically changes during cell division and varies between different cell lines independent of the expression levels. Additionally, the mutation effects predicted from sequence covariation were assessed using EVmutation (accessed January 2025). The majority of the keratin 8 phosphorylation sites exhibited strongly negative scores for both phosphomimetic (S/T/Y to D) and non-phosphorylatable mutations (S/T/Y to A), suggesting that these alterations are likely deleterious to protein function. The pronounced negative values indicated that these residues are evolutionarily conserved and may play essential roles in maintaining the structural integrity and functional regulation of keratin 8. These findings underscore the potential biological significance of keratin 8

phosphorylation, as their mutation may disrupt critical protein interactions or destabilize the keratin network.

Intercellular comparisons revealed that certain cell cycle-specific phosphorylation sites on keratin 8 are conserved across multiple cell lines. Targeting a specific phosphorylation site, our study indicated that S34 phosphorylation on keratin 8 is essential for the fitness and proper division of keratin-expressing cells. With the ectopic K8/18 expression and filament formation in HEK 293 cells, it was shown that the phosphorylation of keratin 8 may be defective depending on the filament structure and can cause multinucleation of the cells when insufficient. It was found that S34 phosphorylation on keratin 8 influences solubility through cytokinesis, highlighting its conformational significance and suggesting a key regulatory role in protein stability and function. Consequently, this phosphorylation site may facilitate the interactions between the soluble form of keratin 8 and other proteins, potentially affecting dynamic binding events within the cell. For S34 phosphorylation on keratin 8, potential roles in protein solubility, protein-protein interactions, structural stability, and subcellular localization were proposed.

The phosphorylation of keratin 8 was predominantly found to be upregulated during cytokinesis. In our study, it was shown that the interaction between keratin 8 and CDK1, a key regulatory kinase of mitotic progression that phosphorylates keratin 8 [39], was found to increase during cytokinesis, further supporting the idea that keratin 8 phosphorylation is enhanced during this process. Consistent with this, it was shown in [36] that keratin 8 promotes the translocation of Aurora B to the midzone during cytokinesis, enhancing its phosphorylation and facilitating filament disassembly, which allows the cleavage furrow to penetrate the keratin network. In our study, PLK1, another key regulatory kinase of the M phase, and AURKB were identified as weak keratin 8 interactors with low interaction scores. Specifically, the SAINT probability scores for PLK1 were 0.5 in interphase, 0.36 in mitosis, and 0.59 in cytokinesis, while for AURKB, the scores were 0.48 in interphase, 0.25 in mitosis, and 0.49 in cytokinesis. Notably, their interaction with keratin 8 increased during cytokinesis, supporting the hypothesis that keratin 8 may contribute to mitotic exit and cytokinetic progression by acting as a scaffold for key regulatory kinases while simultaneously being regulated by them in dynamic cellular regions. Together, these findings

suggested that keratin 8 phosphorylation plays a crucial role during the cell cycle by dynamically regulating keratin filament organization and facilitating successful division.

In previous studies, keratin 8, a type II IF protein traditionally classified as cytoplasmic, has been detected in the nucleus despite lacking a recognizable nuclear localization signal (NLS) [40]. The phosphorylation sites identified in this study are candidate post-translational modifications (PTMs) that may facilitate the solubilization of keratin 8, potentially enabling its recognition by Importin and/or accessory proteins for nuclear targeting [41]. However, further investigation is required to elucidate the precise role of these modifications in nuclear localization, as well as their potential implications for chromosomal integrity and broader cellular functions. A key question that remains is the structural form that keratins adopt within the nucleus. It was shown that mutated intermediate filament proteins, such as tailless human K8/K18, can assemble into conventional 10 nm filaments in addition to punctate structures inside the nucleus, suggesting that polymerization may occur under specific conditions [41]. These findings highlight the possibility that keratin conformation and assembly dynamics within the nucleus may differ significantly from those in the cytoplasm. Understanding these mechanisms in greater detail will be crucial for defining the functional significance of nuclear keratins and their broader impact on cellular homeostasis.

With the gain of knowledge in cell cycle-dependent keratin 8 phosphorylation, the results shed light on many other studies. The interactome and phosphoproteome analysis of keratin 8 in different epithelial and carcinoma cells will help us examine the cell-adaptive division mechanisms and the plasticity of cancer cells, which may open the door to anti-mitotic drugs specific to cancer origin and the potential development of phospho-antibodies to be used as immunohistochemical markers in pathological diagnosis. Findings support pathological tumor diagnosis and help targeted cancer therapy in the future. Additionally, revealing the cell type-specific division mechanisms in different cell lines provides valuable information for cancer research and cell biology.

Overall, keratin 8 was suggested as a scaffolding protein in cellular reorganization during cell division. This study provided proteomic resources with comprehensive affinity purification and sedimentation data, helping to better understand the mechanisms of cell division and cancer progression. Findings on the keratin 8 phosphorylation during cell

division highlighted the site-specific regulation of keratin 8 phosphorylation in cancer progression and cell division. Our study demonstrates the functioning of keratin 8 during mitosis and its regulatory phosphorylation during the cell cycle are required for a successful division in keratin 8 expressing cells.

BIBLIOGRAPHY

[1] B. Alberts, A. Johnson, J. Lewis, M. Raff, K. Roberts, and P. Walter, *Molecular Biology of the Cell*, 6th ed. New York: Garland Science, 2015.

[2] M. Hara and T. Fukagawa, "Dynamics of kinetochore structure and its regulations during mitotic progression," *Cell Mol Life Sci*, vol. 77, no. 15, pp. 2981–2995, 2020, doi: 10.1007/s00018-020-03472-4.

[3] R. Moll, M. Divo, and L. Langbein, "The human keratins: biology and pathology," *Histochem Cell Biol*, vol. 129, no. 6, pp. 705–733, 2008, doi: 10.1007/s00418-008-0435-6.

[4] A. S. Oriolo, F. A. Wald, V. P. Ramsauer, and P. J. I. Salas, "Intermediate filaments: A role in epithelial polarity," Jun. 10, 2007, *Academic Press Inc.* doi: 10.1016/j.yexcr.2007.02.030.

[5] K. M. Ridge *et al.*, "Keratin 8 phosphorylation by protein kinase C delta regulates shear stress-mediated disassembly of keratin intermediate filaments in alveolar epithelial cells," *J Biol Chem*, vol. 280, no. 34, pp. 30400–30405, 2005, doi: 10.1074/jbc.M504239200.

[6] H. J. Kim, W. J. Choi, and C. H. Lee, "Phosphorylation and Reorganization of Keratin Networks: Implications for Carcinogenesis and Epithelial Mesenchymal Transition," *Biomol Ther (Seoul)*, vol. 23, no. 4, pp. 301–312, 2015, doi: 10.4062/biomolther.2015.032.

[7] J. G. Carlton, H. Jones, and U. S. Eggert, "Membrane and organelle dynamics during cell division," *Nat Rev Mol Cell Biol*, vol. 21, no. 3, pp. 151–166, 2020, doi: 10.1038/s41580-019-0208-1.

[8] A. Banerjee, N. Adames, J. Peccoud, and J. J. Tyson, "A stochastic model for error correction of kinetochore-microtubule attachments in budding yeast," *PLoS One*, vol. 15, no. 8, p. e0236293, 2020, doi: 10.1371/journal.pone.0236293.

[9] P. Lara-Gonzalez, F. G. Westhorpe, and S. S. Taylor, "The spindle assembly checkpoint," *Curr Biol*, vol. 22, no. 22, pp. R966-80, 2012, doi: 10.1016/j.cub.2012.10.006.

[10] E. A. Foley and T. M. Kapoor, "Microtubule attachment and spindle assembly checkpoint signalling at the kinetochore," *Nat Rev Mol Cell Biol*, vol. 14, no. 1, pp. 25–37, 2013, doi: 10.1038/nrm3494.

[11] M. Kalantzaki, E. Kitamura, T. Zhang, A. Mino, B. Novak, and T. U. Tanaka, "Kinetochore-microtubule error correction is driven by differentially regulated interaction modes," *Nat Cell Biol*, vol. 17, no. 4, pp. 421–433, 2015, doi: 10.1038/ncb3128.

[12] E. A. Foley, M. Maldonado, and T. M. Kapoor, "Formation of stable attachments between kinetochores and microtubules depends on the B56-PP2A phosphatase," *Nat Cell Biol*, vol. 13, no. 10, pp. 1265–1271, 2011, doi: 10.1038/ncb2327.

[13] N. London, S. Ceto, J. A. Ranish, and S. Biggins, “Phosphoregulation of Spc105 by Mps1 and PP1 regulates Bub1 localization to kinetochores,” *Curr Biol*, vol. 22, no. 10, pp. 900–906, 2012, doi: 10.1016/j.cub.2012.03.052.

[14] S. Sarkar *et al.*, “Mitotic checkpoint defects: en route to cancer and drug resistance,” *Chromosome Res*, vol. 29, no. 2, pp. 131–144, 2021, doi: 10.1007/s10577-020-09646-x.

[15] I. M. Cheeseman and A. Desai, “Molecular architecture of the kinetochore-microtubule interface,” *Nat Rev Mol Cell Biol*, vol. 9, no. 1, pp. 33–46, 2008, doi: 10.1038/nrm2310.

[16] E. A. Scarborough, T. N. Davis, and C. L. Asbury, “Tight bending of the Ndc80 complex provides intrinsic regulation of its binding to microtubules,” *Elife*, vol. 8, 2019, doi: 10.7554/eLife.44489.

[17] N. B. Ustinov, A. V Korshunova, and N. B. Gudimchuk, “Protein Complex NDC80: Properties, Functions, and Possible Role in Pathophysiology of Cell Division,” *Biochemistry (Mosc)*, vol. 85, no. 4, pp. 448–462, 2020, doi: 10.1134/S0006297920040057.

[18] F. Huber, A. Boire, M. P. Lopez, and G. H. Koenderink, “Cytoskeletal crosstalk: when three different personalities team up,” *Curr Opin Cell Biol*, vol. 32, pp. 39–47, 2015, doi: 10.1016/j.ceb.2014.10.005.

[19] H. Lodish, *Molecular Cell Biology*, 6th ed. New York: Macmillan, 2008.

[20] V. Prahlad, M. Yoon, R. D. Moir, R. D. Vale, R. D. Goldman, and ‡ Howard, “Rapid Movements of Vimentin on Microtubule Tracks: Kinesin-dependent Assembly of Intermediate Filament Networks,” 1998. [Online]. Available: http://www.jcb.org

[21] D. L. Gard, “Confocal Microscopy and 3-D Reconstruction of the Cytoskeleton of Xenopus Oocytes,” 1999.

[22] M. Liovic, M. M. Mogensen, A. R. Prescott, and E. B. Lane, “Observation of keratin particles showing fast bidirectional movement colocalized with microtubules,” Apr. 15, 2003. doi: 10.1242/jcs.00363.

[23] R. Windoffer, M. Beil, T. M. Magin, and R. E. Leube, “Cytoskeleton in motion: The dynamics of keratin intermediate filaments in epithelia,” *Journal of Cell Biology*, vol. 194, no. 5, pp. 669–678, Sep. 2011, doi: 10.1083/jcb.201008095.

[24] N. T. Snider and M. B. Omary, “Post-translational modifications of intermediate filament proteins: mechanisms and functions,” *Nat Rev Mol Cell Biol*, vol. 15, no. 3, pp. 163–177, 2014, doi: 10.1038/nrm3753.

[25] Y. Nishimura, K. Kasahara, and M. Inagaki, “Intermediate filaments and IF-associated proteins: from cell architecture to cell proliferation,” *Proc Jpn Acad Ser B Phys Biol Sci*, vol. 95, no. 8, pp. 479–493, 2019, doi: 10.2183/pjab.95.034.

[26] V. Karantza, “Keratins in health and cancer: more than mere epithelial cell markers,” *Oncogene*, vol. 30, no. 2, pp. 127–138, 2011, doi: 10.1038/onc.2010.456.

[27] A. M. Fortier, E. Asselin, and M. Cadrin, “Keratin 8 and 18 loss in epithelial cancer cells increases collective cell migration and cisplatin sensitivity through claudin1 up-regulation,” *J Biol Chem*, vol. 288, no. 16, pp. 11555–11571, 2013, doi: 10.1074/jbc.M112.428920.

[28] D. M. Toivola, N. O. Ku, E. Z. Resurreccion, D. R. Nelson, T. L. Wright, and M. B. Omary, “Keratin 8 and 18 hyperphosphorylation is a marker of progression of human liver disease,” *Hepatology*, vol. 40, no. 2, pp. 459–466, 2004, doi: 10.1002/hep.20277.

[29] M. B. Omary, N. O. Ku, J. Liao, and D. Price, "Keratin modifications and solubility properties in epithelial cells and in vitro," *Subcell Biochem*, vol. 31, pp. 105–140, 1998.

[30] B. Srikanth, M. M. Vaidya, and R. D. Kalraiya, "O-GlcNAcylation determines the solubility, filament organization, and stability of keratins 8 and 18," *J Biol Chem*, vol. 285, no. 44, pp. 34062–34071, 2010, doi: 10.1074/jbc.M109.098996.

[31] D. G. Gibson, L. Young, R. Y. Chuang, J. C. Venter, C. A. Hutchison, and H. O. Smith, "Enzymatic assembly of DNA molecules up to several hundred kilobases," *Nat Methods*, vol. 6, no. 5, pp. 343–345, 2009, doi: 10.1038/nmeth.1318.

[32] J. Fueller *et al.*, "CRISPR-Cas12a-assisted PCR tagging of mammalian genes," *Journal of Cell Biology*, vol. 219, no. 6, Jun. 2020, doi: 10.1083/JCB.201910210.

[33] B. Nabet *et al.*, "The dTAG system for immediate and target-specific protein degradation," *Nat Chem Biol*, vol. 14, no. 5, pp. 431–441, May 2018, doi: 10.1038/s41589-018-0021-8.

[34] P. J. Boersema, R. Raijmakers, S. Lemeer, S. Mohammed, and A. J. R. Heck, "Multiplex peptide stable isotope dimethyl labeling for quantitative proteomics," *Nat Protoc*, vol. 4, no. 4, pp. 484–494, 2009, doi: 10.1038/nprot.2009.21.

[35] H. Zhou *et al.*, "Robust phosphoproteome enrichment using monodisperse microsphere-based immobilized titanium (IV) ion affinity chromatography," *Nat Protoc*, vol. 8, no. 3, pp. 461–480, Feb. 2013, doi: 10.1038/nprot.2013.010.

[36] B. Harmanda *et al.*, "Aurora B Kinase Dependent Phosphorylation of Keratin 8 is required for Cytokinesis in Mammalian Cells of Epithelial Origin," *bioRxiv*, p. 2023.01.22.525045, Jan. 2023, doi: 10.1101/2023.01.22.525045.

[37] W. C. Earnshaw, "Discovering centromere proteins: From cold white hands to the A, B, C of CENPs," Jun. 23, 2015, *Nature Publishing Group*. doi: 10.1038/nrm4001.

[38] I. Elbalasy, P. Mollenkopf, C. Tutmarc, H. Herrmann, and J. Schnauß, "Keratins determine network stress responsiveness in reconstituted actin-keratin filament systems," *Soft Matter*, vol. 17, no. 14, pp. 3954–3962, Apr. 2021, doi: 10.1039/d0sm02261f.

[39] G. Massacci, L. Perfetto, and F. Sacco, "The Cyclin-dependent kinase 1: more than a cell cycle regulator," *Br J Cancer*, vol. 129, no. 11, pp. 1707–1716, Nov. 2023, doi: 10.1038/s41416-023-02468-8.

[40] M. Kumeta, Y. Hirai, S. H. Yoshimura, T. Horigome, and K. Takeyasu, "Antibody-based analysis reveals 'filamentous vs. non-filamentous' and 'cytoplasmic vs. nuclear' crosstalk of cytoskeletal proteins," *Exp Cell Res*, vol. 319, no. 20, pp. 3226–3237, 2013, doi: https://doi.org/10.1016/j.yexcr.2013.07.021.

[41] R. P. Hobbs, J. T. Jacob, and P. A. Coulombe, "Keratins Are Going Nuclear," Aug. 08, 2016, *Cell Press*. doi: 10.1016/j.devcel.2016.07.022.

VITA

Ceyda Seren Ceyhan was born in Ankara, Türkiye on January 20, 1995. She graduated from Ümitköy Anatolian High School in 2013 and received her B.Sc. degree in Molecular Biology, Genetics, and Bioengineering with a minor degree in Chemistry from Sabancı University, İstanbul, Türkiye in 2018. She has done her Ph.D. study in the Cell Biology and Proteomics group under the supervision of Prof. Dr. Nurhan Özlü Sıcakkan and worked as a teaching and research assistant at Koç University from February 2019 to February 2024. Her research was supported by the EPIC-XS consortium in 2022, and she received the 2214-A International Research Fellowship from TÜBİTAK in 2023. She studied in the Organelle Dynamics During Mitosis group under the supervision of Dr. Anne-Lore Schlaitz from February 2024 to January 2025 and received her Ph.D. degree in Molecular Biology and Genetics with a dissertation titled “Regulation of Keratin 8 During Cancer Cell Division” in February 2025.

APPENDIX

Appendix A: Instrument specifications of BD FACSymphony A1 flow cytometer.

Laser	Position	Filter	Mirror	Antibody Reagents	Fluorescent Proteins	Nucleic Acid Stains
Violet 405	405-A	BP/780/60	LP/750	BV750, BV786		
	405-B	BP/710/50	LP/690	BV711		
	405-C	BP/670/30	LP/655	BV650		
	405-D	BP/610/20	LP/595	BV605		
	405-E	BP/525/50	LP/505	BV480, V500, BV510	AmCyan, GFP, T-Sapphire	
	405-F	BP/431/28		BV421, V450, PacificBlue	BFP, CFP	Hoechst, DAPI, SytoxBlue
Blue 488	488-A		595			
	488-B	BP/710/50	LP/690	BB700, PerCP, PerCP-Cy5.5		7-AAD
	488-C	BP/530/30	LP/505	BB515, FITC, AF488	GFP, NeonGreen, YFP	SytoxGreen, TOTO-1, TO-PRO-1
	488-D		595			
	488-E/SSC	BP/488/10		n.a.	n.a.	n.a.
	488-F/SP SSC	BP/488/10		n.a.	n.a.	n.a.
	FSC			n.a.	n.a.	n.a.
YellowGreen 561	561-A	BP/780/60	LP/750	PE-Cy7		
	561-B	BP/710/50	LP/690	PE-Cy5.5		7-AAD
	561-C	BP/670/30	LP/655	PE-Cy5		
	561-D	BP/610/20	LP/595	PE-CF594, PE-TexasRed, PI	mCherry, mRuby	PI
	561-E	BP/586/15	LP/580	RealYellow586, PE	tdTomato, dsRed, RFP	SytoxOrange
Red 637	637-A	BP/780/60	LP/750	APC-Cy7, APC-H7		
	637-B	BP/710/50	LP/690	AF700, APC-R700, Red718		
	637-C	BP/670/30	LP/655	APC, AF647		SytoxRed, TOTO-3, TO-PRO-3

Sample Flow Rate: low (12 µl/min), medium (35 µl/min), high (60 µl/min)
Sample Acquisition Rate: max. 25,000 events/s
Particle Size Resolution: 90 nm (Small Particle Detector)
High Throughput Sampler

Appendix B: FACS analysis results for negative control (-), asynchronous (A), interphase (I), mitosis (M), and cytokinesis (C) samples from MCF7 (1), HeLa (2), MDA-MB-231 (3), CAKI-2 (4), HEK 293 +K8/K18 (5), HeLa GFP (6), HeLa K8-GFP (7), HeLa control (8), HeLa K8 KO (9), HeLa K8 KO +K8-GFP (10) cells.

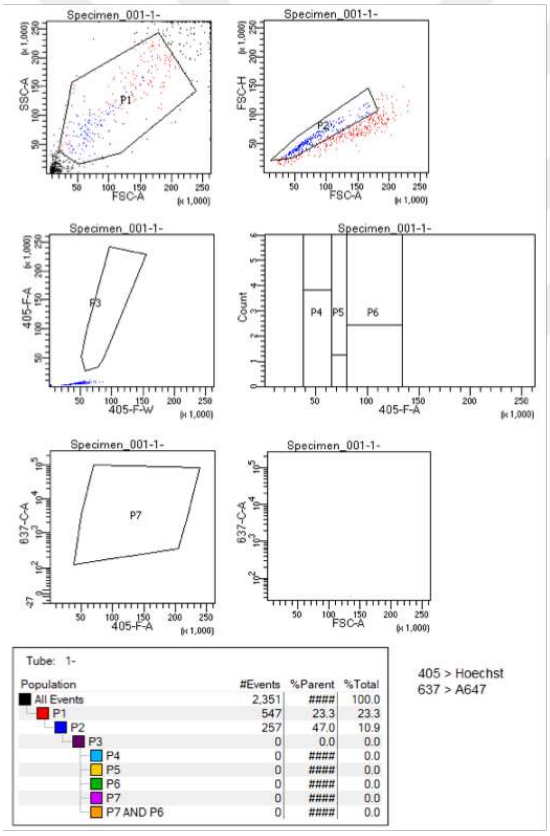

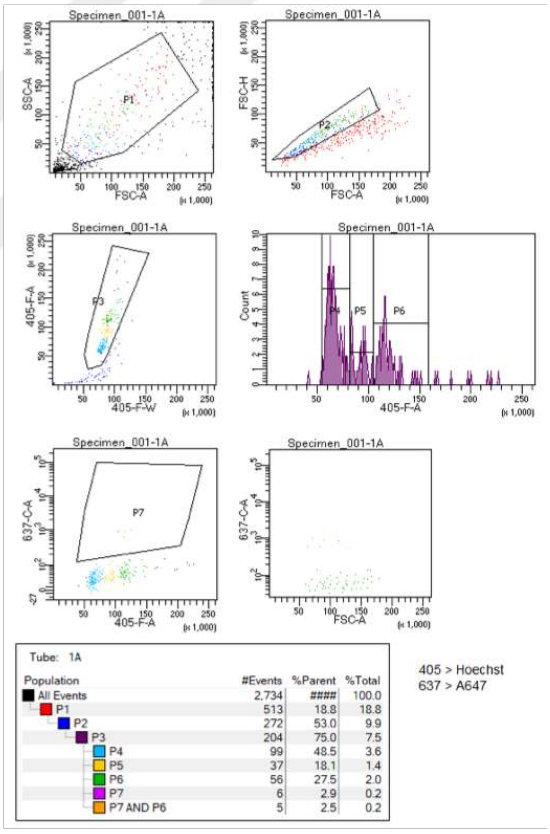

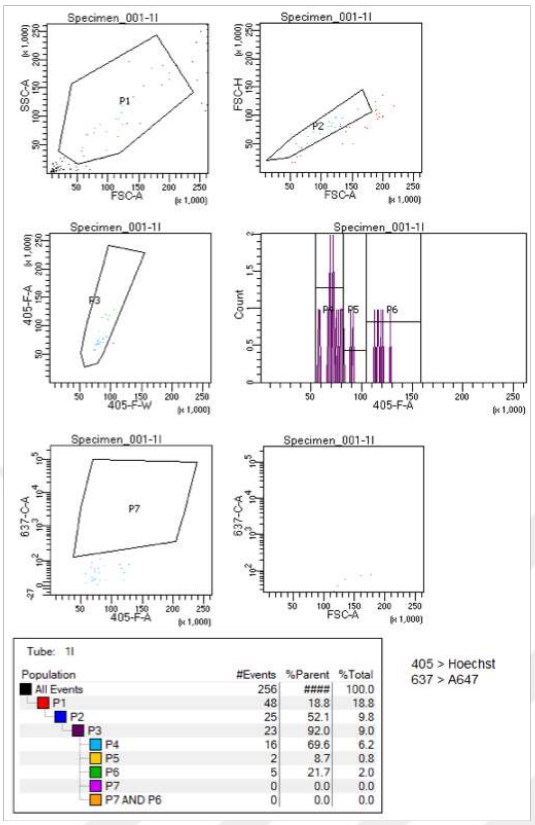

Tube: 1I

Population	#Events	%Parent	%Total
All Events	256	####	100.0
P1	48	18.8	18.8
P2	25	52.1	9.8
P3	23	92.0	9.0
P4	16	69.6	6.2
P5	2	8.7	0.8
P6	5	21.7	2.0
P7	0	0.0	0.0
P7 AND P6	0	0.0	0.0

405 > Hoechst
637 > A647

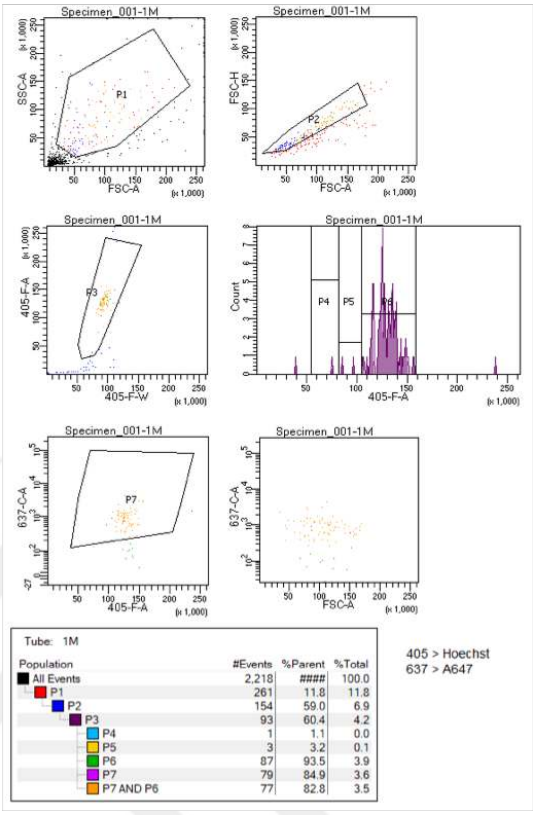

Tube: 1M

Population	#Events	%Parent	%Total
All Events	2,218	####	100.0
P1	261	11.8	11.8
P2	154	59.0	6.9
P3	93	60.4	4.2
P4	1	1.1	0.0
P5	3	3.2	0.1
P6	87	93.5	3.9
P7	79	84.9	3.6
P7 AND P6	77	82.8	3.5

405 > Hoechst
637 > A647

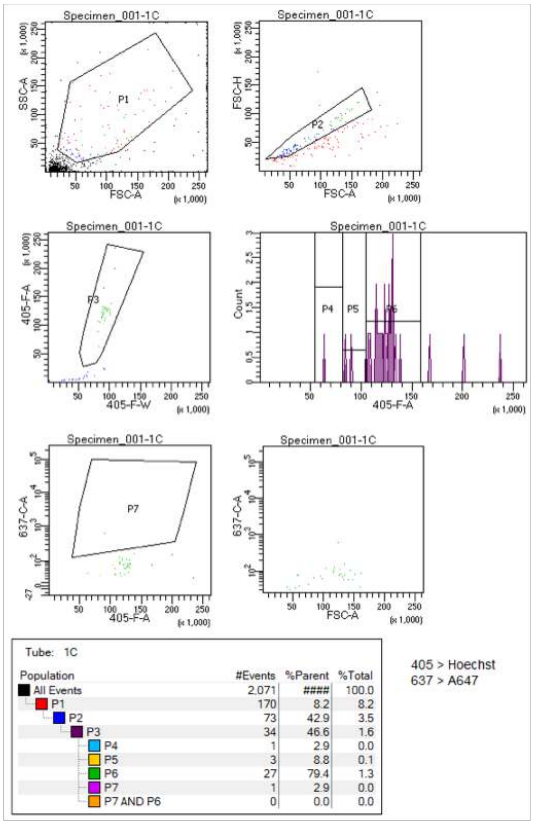

Tube: 1C

Population	#Events	%Parent	%Total
All Events	2,071	####	100.0
P1	170	8.2	8.2
P2	73	42.9	3.5
P3	34	46.6	1.6
P4	1	2.9	0.0
P5	3	8.8	0.1
P6	27	79.4	1.3
P7	1	2.9	0.0
P7 AND P6	0	0.0	0.0

405 > Hoechst
637 > A647

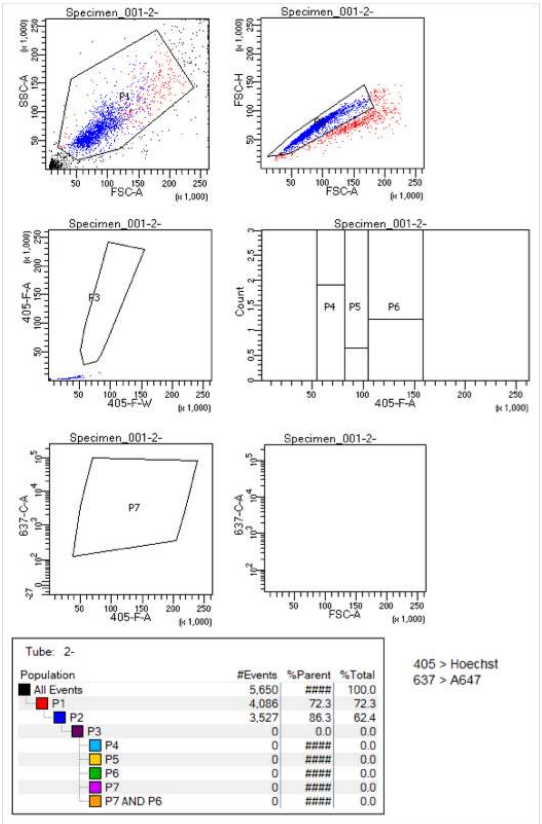

Tube: 2-

Population	#Events	%Parent	%Total
All Events	5,650	####	100.0
P1	4,086	72.3	72.3
P2	3,527	86.3	62.4
P3	0	0.0	0.0
P4	0	####	0.0
P5	0	####	0.0
P6	0	####	0.0
P7	0	####	0.0
P7 AND P6	0	####	0.0

405 > Hoechst
637 > A647

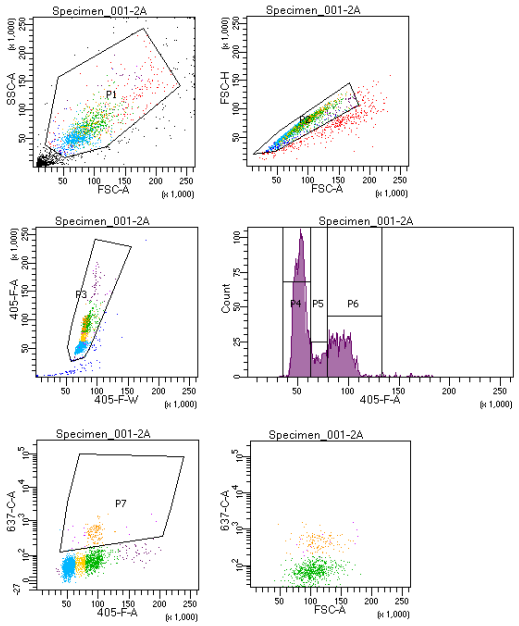

Tube: 2A

Population	#Events	%Parent	%Total
All Events	5,145	####	100.0
P1	2,846	55.3	55.3
P2	2,478	87.1	48.2
P3	2,353	95.0	45.7
P4	1,335	56.7	25.9
P5	241	10.2	4.7
P6	722	30.7	14.0
P7	142	6.0	2.8
P7 AND P6	127	5.4	2.5

405 > Hoechst
637 > A647

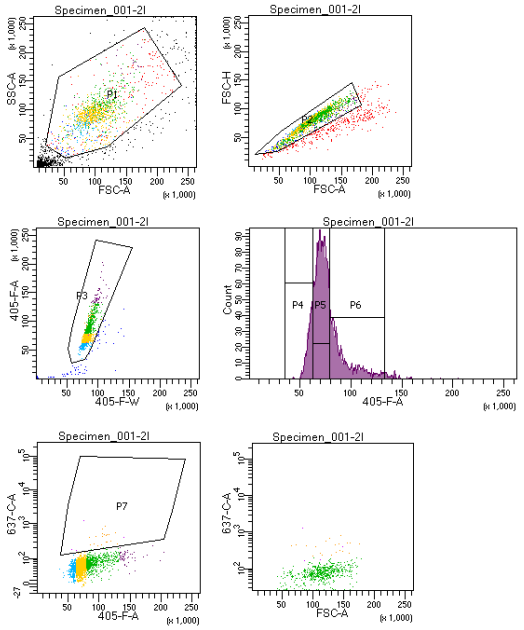

Tube: 2I

Population	#Events	%Parent	%Total
All Events	5,088	####	100.0
P1	2,617	51.4	51.4
P2	2,254	86.1	44.3
P3	2,172	96.4	42.7
P4	335	15.4	6.6
P5	1,233	56.8	24.2
P6	555	25.6	10.9
P7	24	1.1	0.5
P7 AND P6	20	0.9	0.4

405 > Hoechst
637 > A647

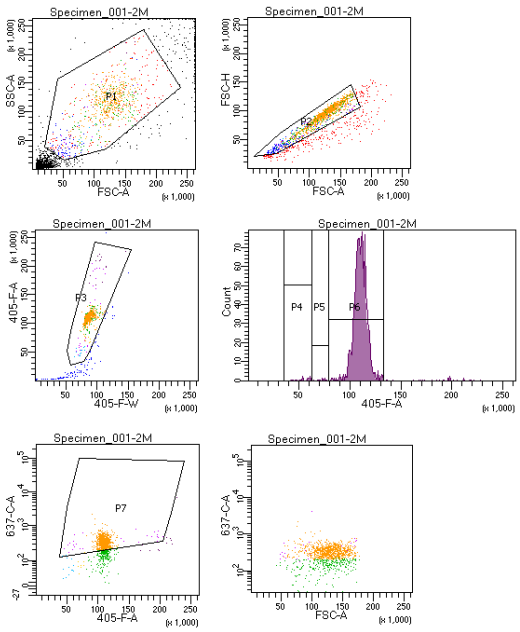

Tube: 2M

Population	#Events	%Parent	%Total
All Events	5,679	####	100.0
P1	1,602	28.2	28.2
P2	1,287	80.3	22.7
P3	1,136	88.3	20.0
P4	23	2.0	0.4
P5	12	1.1	0.2
P6	1,073	94.5	18.9
P7	834	73.4	14.7
P7 AND P6	807	71.0	14.2

405 > Hoechst
637 > A647

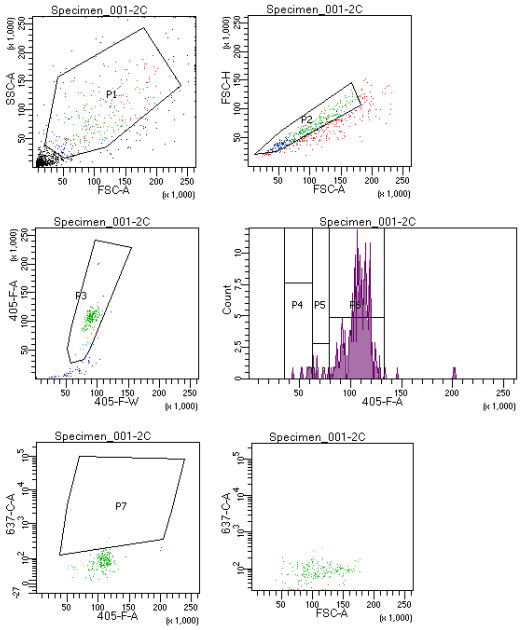

Tube: 2C

Population	#Events	%Parent	%Total
All Events	2,813	####	100.0
P1	522	18.6	18.6
P2	286	54.8	10.2
P3	202	70.6	7.2
P4	9	4.5	0.3
P5	6	3.0	0.2
P6	184	91.1	6.5
P7	5	2.5	0.2
P7 AND P6	4	2.0	0.1

405 > Hoechst
637 > A647

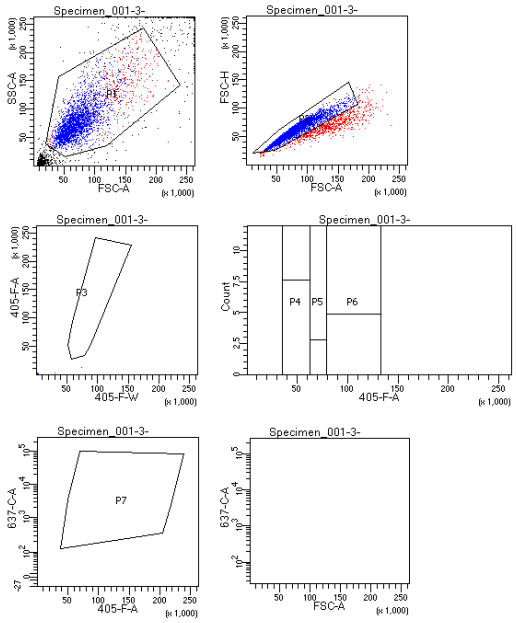

Tube: 3-

Population	#Events	%Parent	%Total
All Events	7,878	####	100.0
P1	5,808	73.7	73.7
P2	5,018	86.4	63.7
P3	0	0.0	0.0
P4	0	####	0.0
P5	0	####	0.0
P6	0	####	0.0
P7	0	####	0.0
P7 AND P6	0	####	0.0

405 > Hoechst
637 > A647

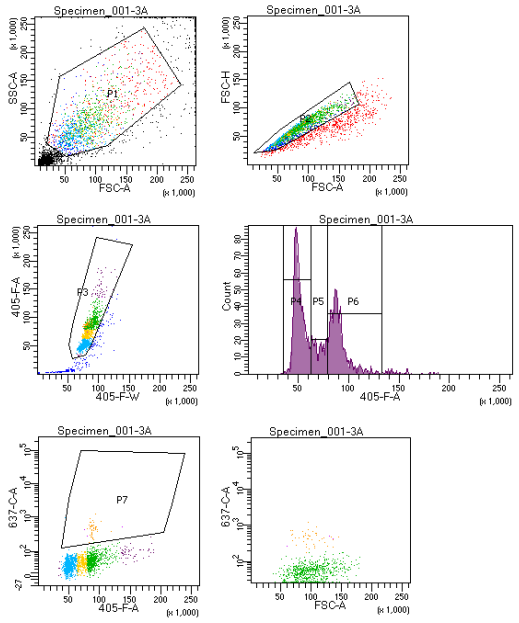

Tube: 3A

Population	#Events	%Parent	%Total
All Events	8,302	####	100.0
P1	2,864	34.5	34.5
P2	2,170	75.8	26.1
P3	1,874	86.4	22.6
P4	862	46.0	10.4
P5	272	14.5	3.3
P6	684	36.5	8.2
P7	46	2.5	0.6
P7 AND P6	43	2.3	0.5

405 > Hoechst
637 > A647

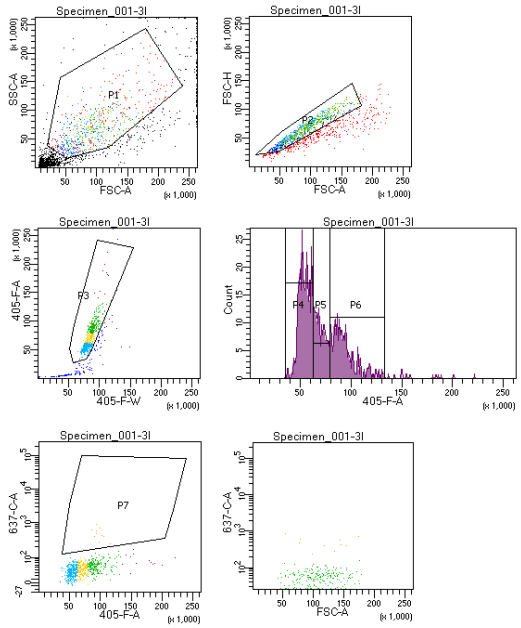

Tube: 3I

Population	#Events	%Parent	%Total
All Events	5,074	####	100.0
P1	1,231	24.3	24.3
P2	844	68.6	16.6
P3	669	79.3	13.2
P4	310	46.3	6.1
P5	151	22.6	3.0
P6	194	29.0	3.8
P7	10	1.5	0.2
P7 AND P6	10	1.5	0.2

405 > Hoechst
637 > A647

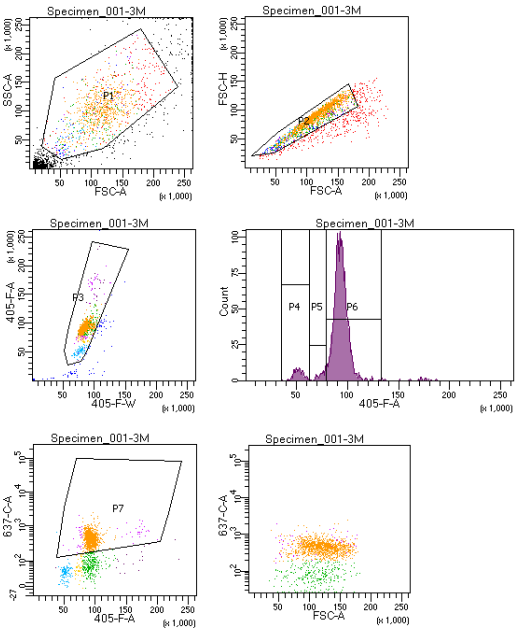

Tube: 3M

Population	#Events	%Parent	%Total
All Events	5,000	####	100.0
P1	2,114	42.3	42.3
P2	1,724	81.6	34.5
P3	1,634	94.8	32.7
P4	110	6.7	2.2
P5	71	4.3	1.4
P6	1,407	86.1	28.1
P7	1,186	72.6	23.7
P7 AND P6	1,135	69.5	22.7

405 > Hoechst
637 > A647

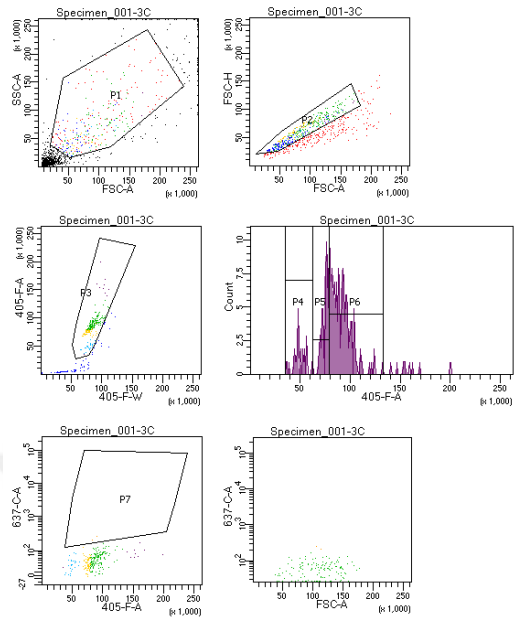

Tube: 3C

Population	#Events	%Parent	%Total
All Events	3,241	####	100.0
P1	601	18.5	18.5
P2	346	57.6	10.7
P3	238	68.8	7.3
P4	26	10.9	0.8
P5	62	26.1	1.9
P6	140	58.8	4.3
P7	2	0.8	0.1
P7 AND P6	2	0.8	0.1

405 > Hoechst
637 > A647

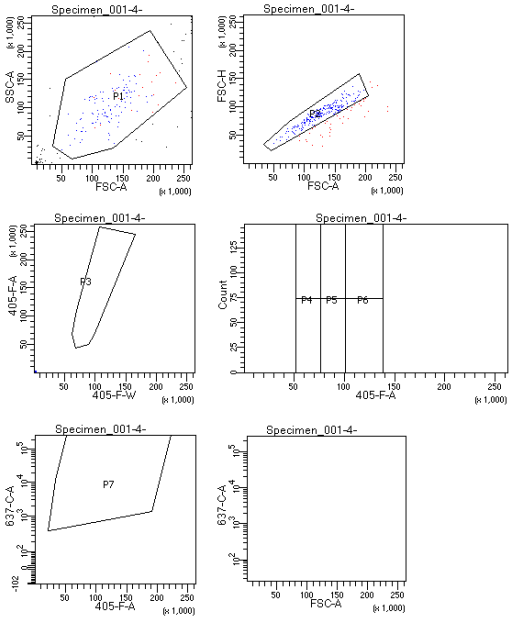

Tube: 4-

Population	#Events	%Parent	%Total
All Events	364	####	100.0
P1	259	71.2	71.2
P2	212	81.9	58.2
P3	0	0.0	0.0
P4	0	####	0.0
P5	0	####	0.0
P6	0	####	0.0
P7	0	####	0.0
P7 AND P6	0	####	0.0

405 > Hoechst
637 > A647

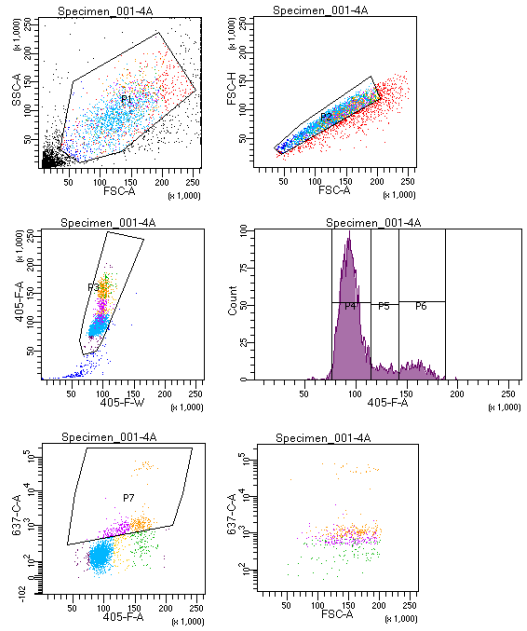

Tube: 4A

Population	#Events	%Parent	%Total
All Events	10,000	####	100.0
P1	3,513	35.1	35.1
P2	2,712	77.2	27.1
P3	2,523	93.0	25.2
P4	1,950	77.3	19.5
P5	207	8.2	2.1
P6	316	12.5	3.2
P7	390	15.5	3.9
P7 AND P6	196	7.8	2.0

405 > Hoechst
637 > A647

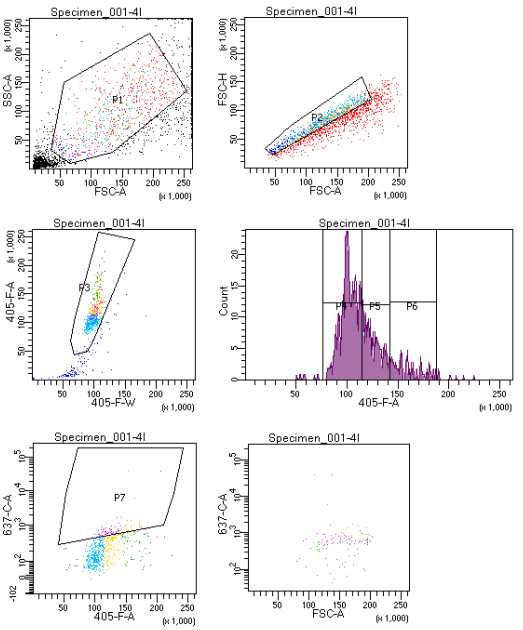

Tube: 4I

Population	#Events	%Parent	%Total
All Events	7,565	####	100.0
P1	1,640	21.7	21.7
P2	752	45.9	9.9
P3	625	83.1	8.3
P4	370	59.2	4.9
P5	165	26.4	2.2
P6	75	12.0	1.0
P7	73	11.7	1.0
P7 AND P6	24	3.8	0.3

405 > Hoechst
637 > A647

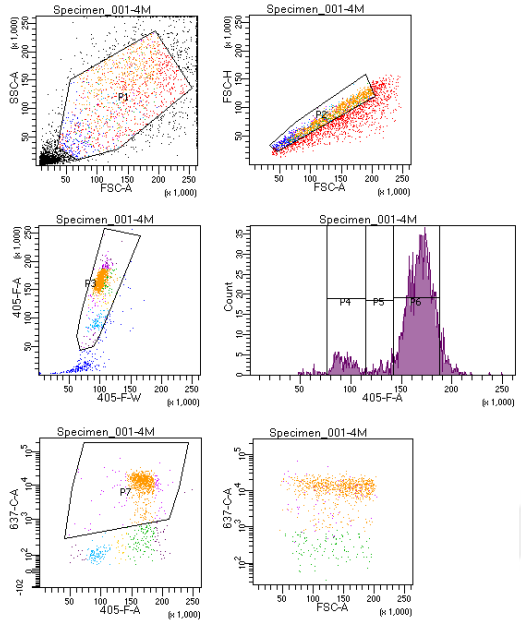

Tube: 4M

Population	#Events	%Parent	%Total
All Events	10,000	####	100.0
P1	2,580	25.8	25.8
P2	1,420	55.0	14.2
P3	1,149	80.9	11.5
P4	108	9.4	1.1
P5	46	4.0	0.5
P6	906	78.9	9.1
P7	875	76.2	8.8
P7 AND P6	796	69.3	8.0

405 > Hoechst
637 > A647

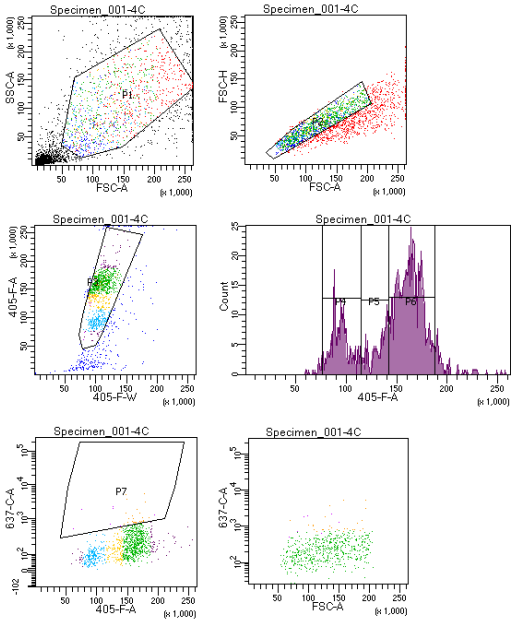

Tube: 4C

Population	#Events	%Parent	%Total
All Events	10,000	####	100.0
P1	2,139	21.4	21.4
P2	1,278	59.7	12.8
P3	986	77.2	9.9
P4	202	20.5	2.0
P5	130	13.2	1.3
P6	587	59.5	5.9
P7	33	3.3	0.3
P7 AND P6	26	2.6	0.3

405 > Hoechst
637 > A647

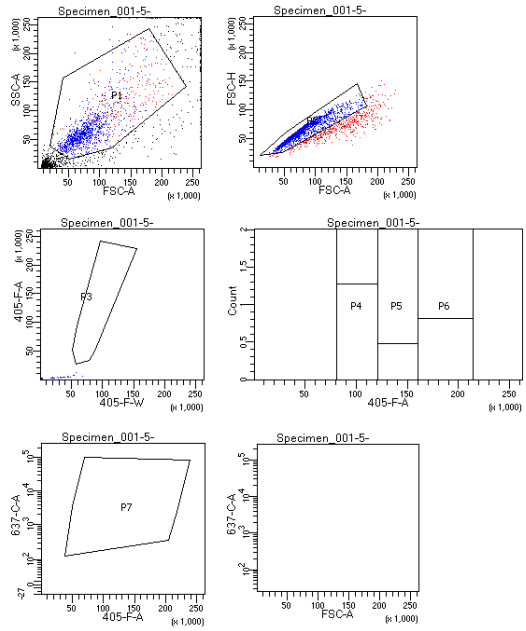

Tube: 5-

Population	#Events	%Parent	%Total
All Events	5,000	####	100.0
P1	2,333	46.7	46.7
P2	1,808	77.5	36.2
P3	0	0.0	0.0
P4	0	####	0.0
P5	0	####	0.0
P6	0	####	0.0
P7	0	####	0.0
P7 AND P6	0	####	0.0

405 > Hoechst
637 > A647

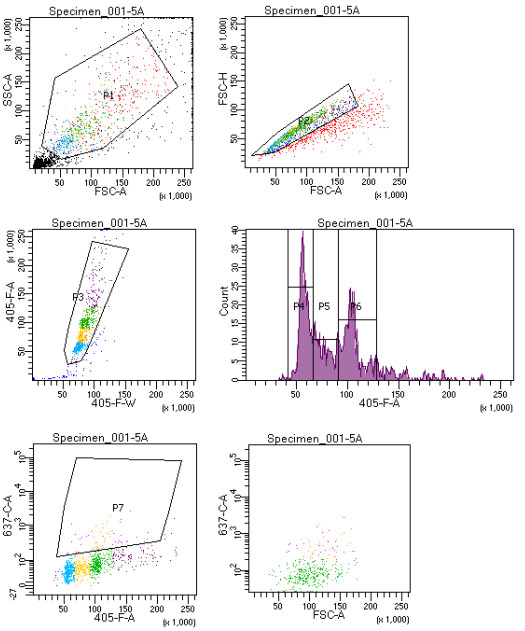

Tube: 5A

Population	#Events	%Parent	%Total
All Events	5,000	####	100.0
P1	1,628	32.6	32.6
P2	1,164	71.5	23.3
P3	1,033	88.7	20.7
P4	363	35.1	7.3
P5	211	20.4	4.2
P6	338	32.7	6.8
P7	59	5.7	1.2
P7 AND P6	31	3.0	0.6

405 > Hoechst
637 > A647

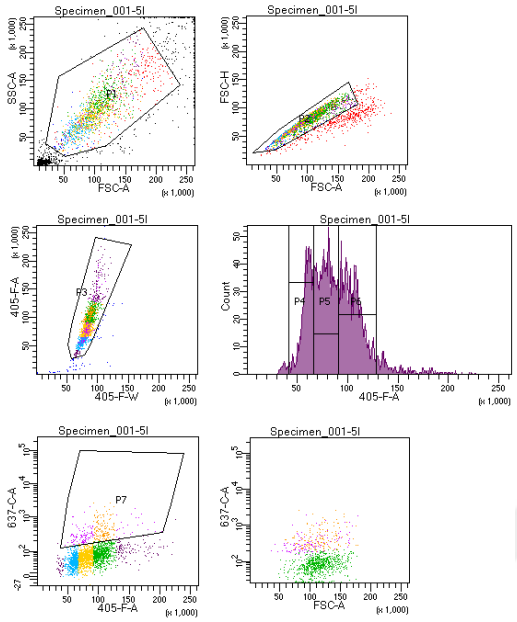

Tube: 5I

Population	#Events	%Parent	%Total
All Events	5,000	####	100.0
P1	2,960	59.2	59.2
P2	2,533	85.6	50.7
P3	2,465	97.3	49.3
P4	553	22.4	11.1
P5	883	35.8	17.7
P6	850	34.5	17.0
P7	268	10.9	5.4
P7 AND P6	147	6.0	2.9

405 > Hoechst
637 > A647

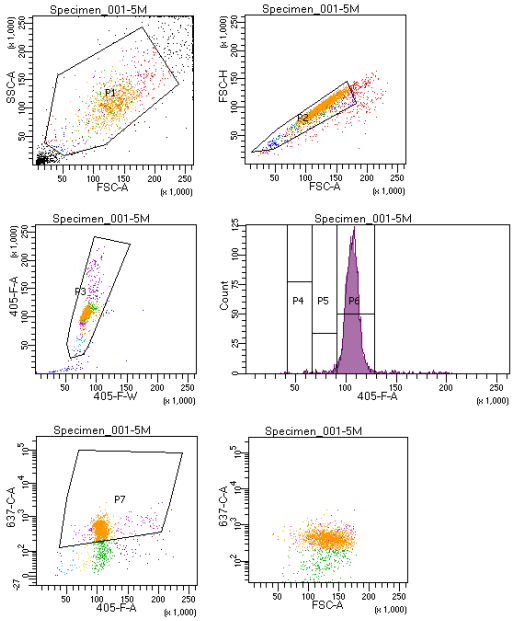

Tube: 5M

Population	#Events	%Parent	%Total
All Events	5,000	####	100.0
P1	2,301	46.0	46.0
P2	1,993	86.6	39.9
P3	1,920	96.3	38.4
P4	28	1.5	0.6
P5	64	3.3	1.3
P6	1,706	88.9	34.1
P7	1,552	80.8	31.0
P7 AND P6	1,451	75.6	29.0

405 > Hoechst
637 > A647

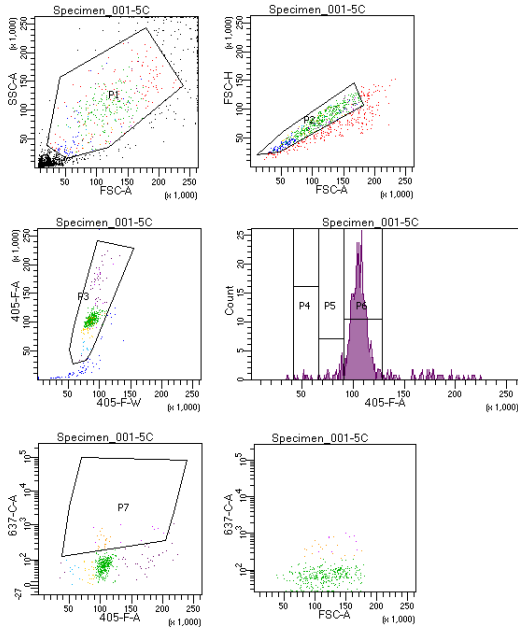

Tube: 5C

Population	#Events	%Parent	%Total
All Events	5,000	####	100.0
P1	786	15.7	15.7
P2	519	66.0	10.4
P3	423	81.5	8.5
P4	9	2.1	0.2
P5	24	5.7	0.5
P6	343	81.1	6.9
P7	27	6.4	0.5
P7 AND P6	18	4.3	0.4

405 > Hoechst
637 > A647

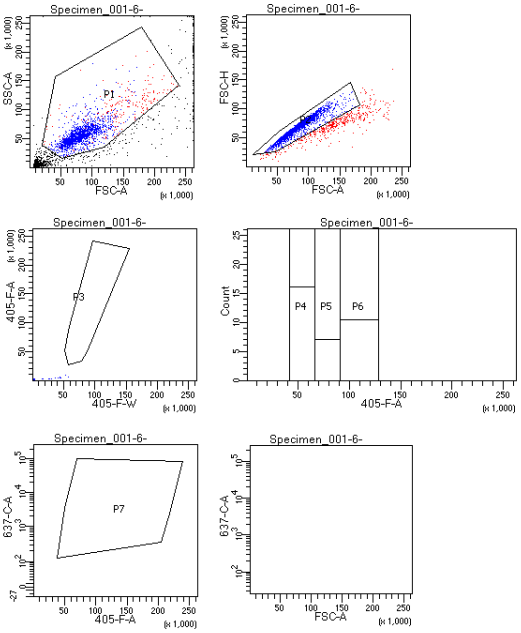

Tube: 6-

Population	#Events	%Parent	%Total
All Events	5,000	####	100.0
P1	3,368	67.4	67.4
P2	2,937	87.2	58.7
P3	0	0.0	0.0
P4	0	####	0.0
P5	0	####	0.0
P6	0	####	0.0
P7	0	####	0.0
P7 AND P6	0	####	0.0

405 > Hoechst
637 > A647

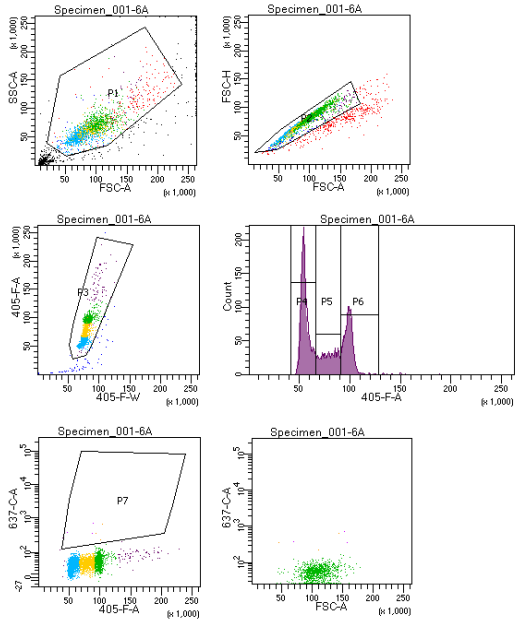

Tube: 6A

Population	#Events	%Parent	%Total
All Events	5,000	####	100.0
P1	3,807	76.1	76.1
P2	3,438	90.3	68.8
P3	3,366	97.9	67.3
P4	1,613	47.9	32.3
P5	738	21.9	14.8
P6	944	28.0	18.9
P7	6	0.2	0.1
P7 AND P6	3	0.1	0.1

405 > Hoechst
637 > A647

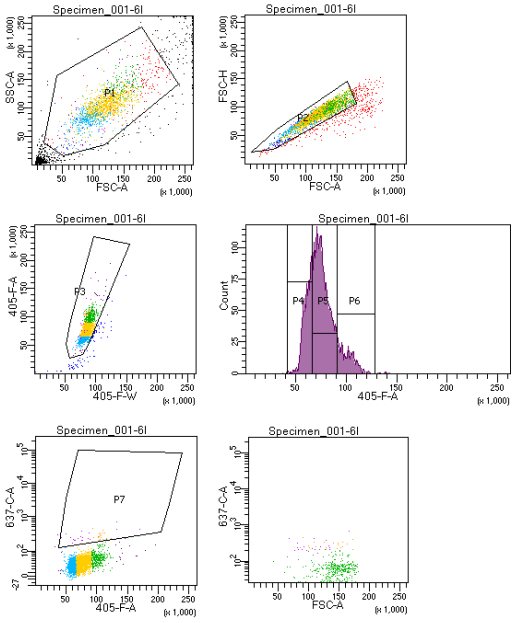

Tube: 6I

Population	#Events	%Parent	%Total
All Events	5,000	####	100.0
P1	3,390	67.8	67.8
P2	3,042	89.7	60.8
P3	2,954	97.1	59.1
P4	837	28.3	16.7
P5	1,738	58.8	34.8
P6	353	11.9	7.1
P7	38	1.3	0.8
P7 AND P6	19	0.6	0.4

405 > Hoechst
637 > A647

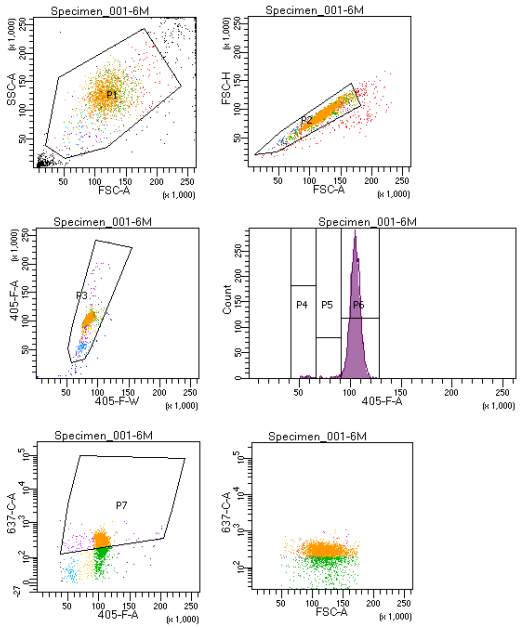

Tube: 6M

Population	#Events	%Parent	%Total
All Events	5,000	####	100.0
P1	3,633	72.7	72.7
P2	3,421	94.2	68.4
P3	3,378	98.7	67.6
P4	92	2.7	1.8
P5	102	3.0	2.0
P6	3,143	93.0	62.9
P7	2,400	71.0	48.0
P7 AND P6	2,335	69.1	46.7

405 > Hoechst
637 > A647

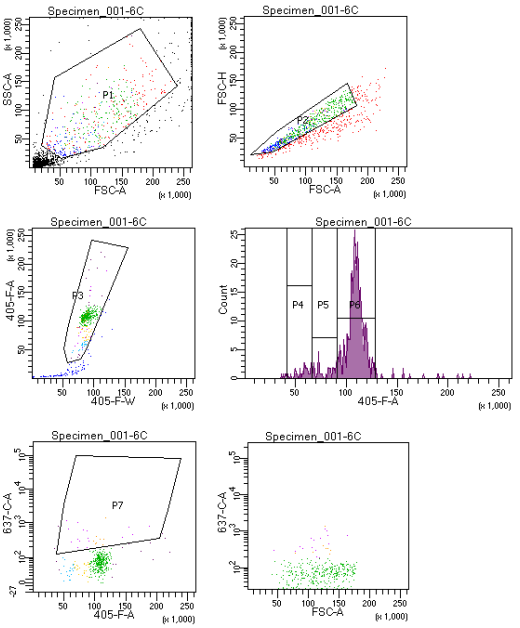

Tube: 6C

Population	#Events	%Parent	%Total
All Events	5,000	####	100.0
P1	871	17.4	17.4
P2	552	63.4	11.0
P3	399	72.3	8.0
P4	25	6.3	0.5
P5	35	8.8	0.7
P6	320	80.2	6.4
P7	24	6.0	0.5
P7 AND P6	8	2.0	0.2

405 > Hoechst
637 > A647

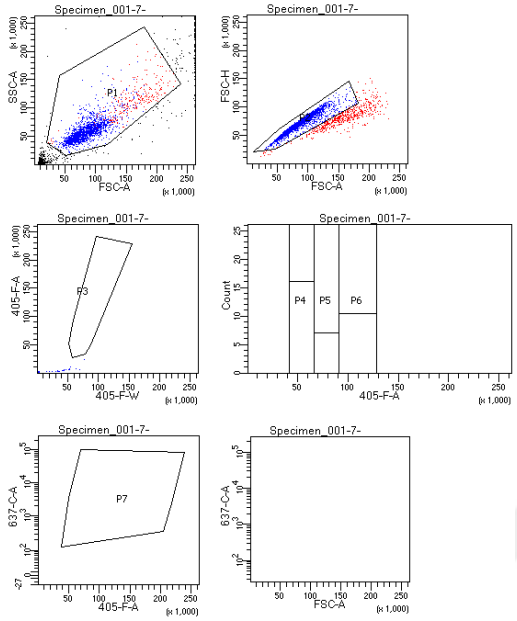

Tube: 7-

Population	#Events	%Parent	%Total
All Events	5,000	####	100.0
P1	3,944	78.9	78.9
P2	3,401	86.2	68.0
P3	0	0.0	0.0
P4	0	####	0.0
P5	0	####	0.0
P6	0	####	0.0
P7	0	####	0.0
P7 AND P6	0	####	0.0

405 > Hoechst
637 > A647

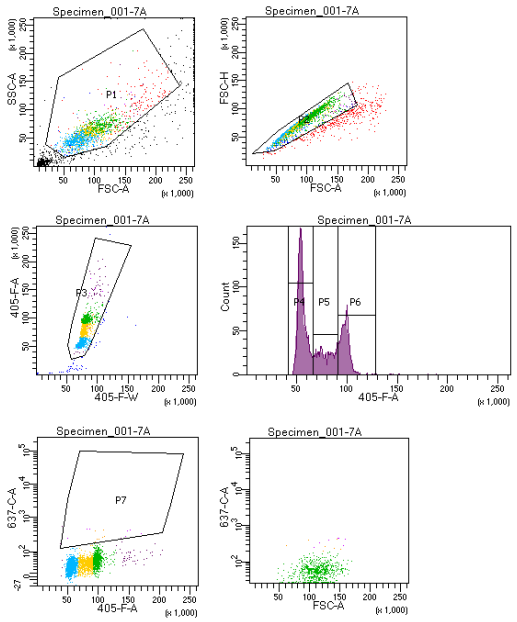

Tube: 7A

Population	#Events	%Parent	%Total
All Events	5,000	####	100.0
P1	3,114	62.3	62.3
P2	2,757	88.5	55.1
P3	2,690	97.6	53.8
P4	1,366	50.8	27.3
P5	612	22.8	12.2
P6	662	24.6	13.2
P7	14	0.5	0.3
P7 AND P6	7	0.3	0.1

405 > Hoechst
637 > A647

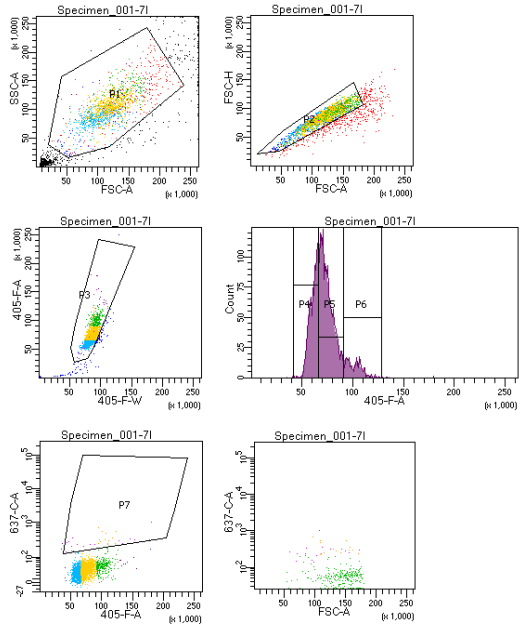

Tube: 7I

Population	#Events	%Parent	%Total
All Events	5,000	####	100.0
P1	3,337	66.7	66.7
P2	2,864	85.8	57.3
P3	2,736	95.5	54.7
P4	989	36.1	19.8
P5	1,457	53.3	29.1
P6	268	9.8	5.4
P7	30	1.1	0.6
P7 AND P6	13	0.5	0.3

405 > Hoechst
637 > A647

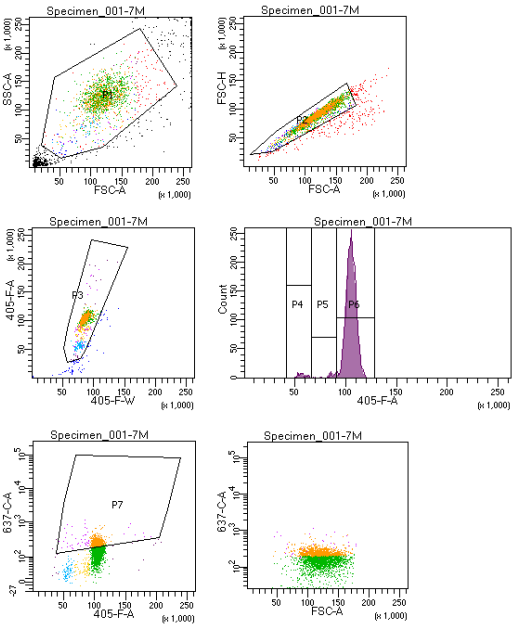

Tube: 7M

Population	#Events	%Parent	%Total
All Events	5,000	####	100.0
P1	3,389	67.8	67.8
P2	3,117	92.0	62.3
P3	3,043	97.6	60.9
P4	101	3.3	2.0
P5	107	3.5	2.1
P6	2,809	92.3	56.2
P7	1,034	34.0	20.7
P7 AND P6	984	32.3	19.7

405 > Hoechst
637 > A647

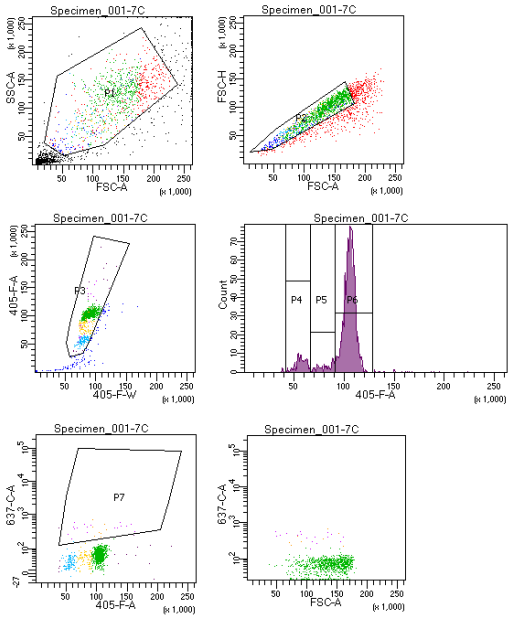

Tube: 7C

Population	#Events	%Parent	%Total
All Events	5,000	####	100.0
P1	1,912	38.2	38.2
P2	1,281	67.0	25.6
P3	1,142	89.1	22.8
P4	115	10.1	2.3
P5	87	7.6	1.7
P6	918	80.4	18.4
P7	25	2.2	0.5
P7 AND P6	8	0.7	0.2

405 > Hoechst
637 > A647

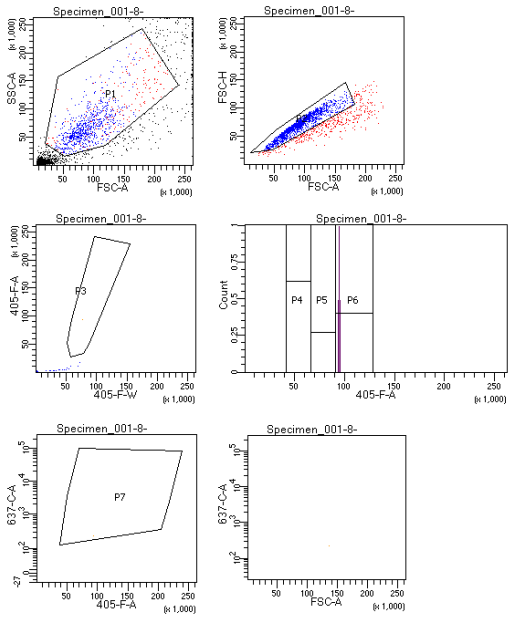

Tube: 8-

Population	#Events	%Parent	%Total
All Events	5,000	####	100.0
P1	1,800	36.0	36.0
P2	1,420	78.9	28.4
P3	1	0.1	0.0
P4	0	0.0	0.0
P5	0	0.0	0.0
P6	1	100.0	0.0
P7	1	100.0	0.0
P7 AND P6	1	100.0	0.0

405 > Hoechst
637 > A647

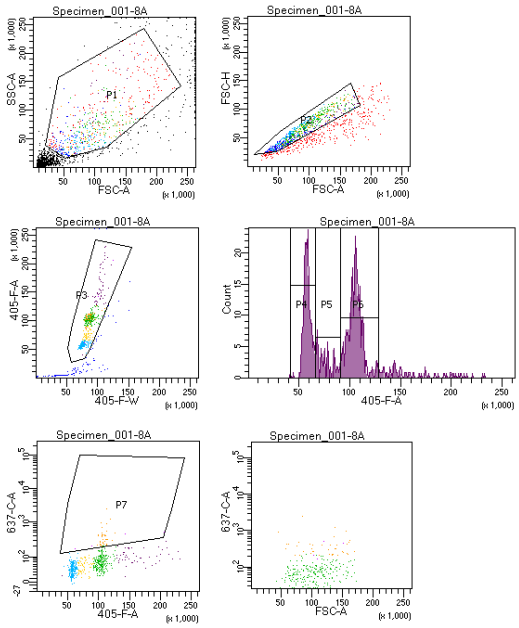

Tube: 8A

Population	#Events	%Parent	%Total
All Events	5,000	####	100.0
P1	1,075	21.5	21.5
P2	699	65.0	14.0
P3	532	76.1	10.6
P4	170	32.0	3.4
P5	59	11.1	1.2
P6	251	47.2	5.0
P7	43	8.1	0.9
P7 AND P6	39	7.3	0.8

405 > Hoechst
637 > A647

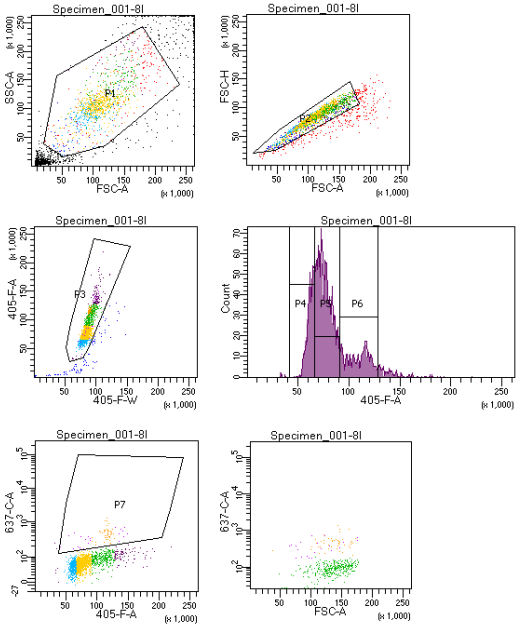

Tube: 8I

Population	#Events	%Parent	%Total
All Events	5,000	####	100.0
P1	2,279	45.6	45.6
P2	1,985	87.1	39.7
P3	1,888	95.1	37.8
P4	440	23.3	8.8
P5	997	52.8	19.9
P6	352	18.6	7.0
P7	67	3.5	1.3
P7 AND P6	46	2.4	0.9

405 > Hoechst
637 > A647

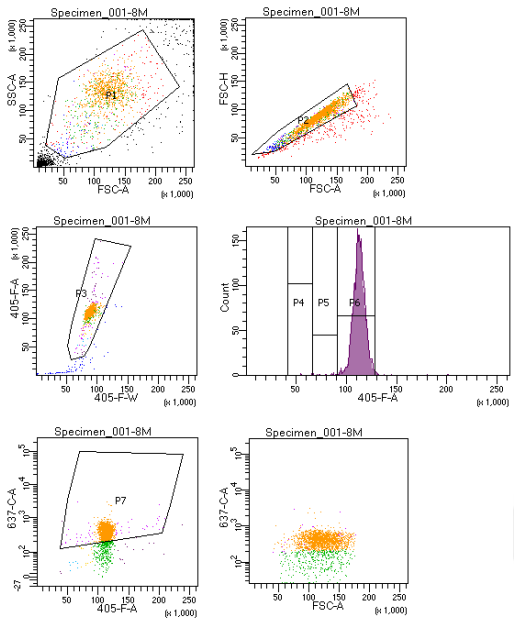

Tube: 8M

Population	#Events	%Parent	%Total
All Events	5,000	####	100.0
P1	2,532	50.6	50.6
P2	2,235	88.3	44.7
P3	2,150	96.2	43.0
P4	17	0.8	0.3
P5	30	1.4	0.6
P6	2,053	95.5	41.1
P7	1,748	81.3	35.0
P7 AND P6	1,695	78.8	33.9

405 > Hoechst
637 > A647

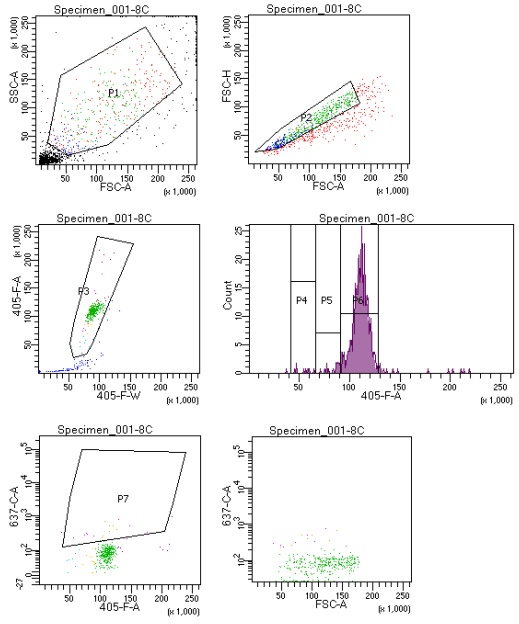

Tube: 8C

Population	#Events	%Parent	%Total
All Events	5,000	####	100.0
P1	812	16.2	16.2
P2	490	60.3	9.8
P3	363	74.1	7.3
P4	8	2.2	0.2
P5	16	4.4	0.3
P6	325	89.5	6.5
P7	15	4.1	0.3
P7 AND P6	7	1.9	0.1

405 > Hoechst
637 > A647

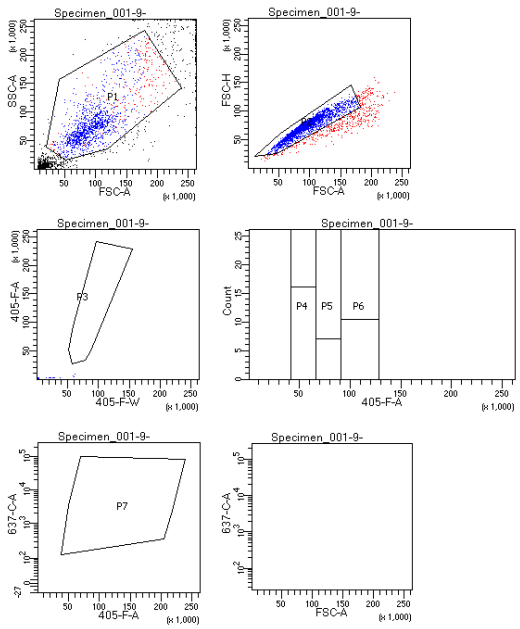

Tube: 9-

Population	#Events	%Parent	%Total
All Events	5,000	####	100.0
P1	2,758	55.2	55.2
P2	2,303	83.5	46.1
P3	0	0.0	0.0
P4	0	####	0.0
P5	0	####	0.0
P6	0	####	0.0
P7	0	####	0.0
P7 AND P6	0	####	0.0

405 > Hoechst
637 > A647

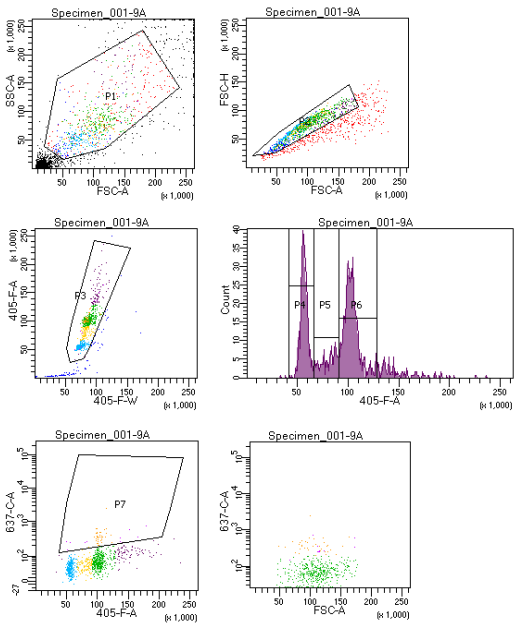

Tube: 9A

Population	#Events	%Parent	%Total
All Events	5,000	####	100.0
P1	1,464	29.3	29.3
P2	1,050	71.7	21.0
P3	924	88.0	18.5
P4	288	31.2	5.8
P5	120	13.0	2.4
P6	426	46.1	8.5
P7	46	5.0	0.9
P7 AND P6	36	3.9	0.7

405 > Hoechst
637 > A647

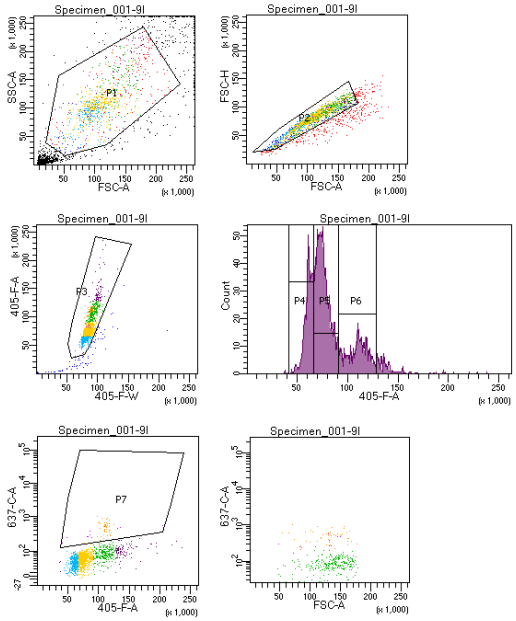

Tube: 9I

Population	#Events	%Parent	%Total
All Events	5,000	####	100.0
P1	1,986	39.7	39.7
P2	1,641	82.6	32.8
P3	1,550	94.5	31.0
P4	404	26.1	8.1
P5	746	48.1	14.9
P6	309	19.9	6.2
P7	60	3.9	1.2
P7 AND P6	49	3.2	1.0

405 > Hoechst
637 > A647

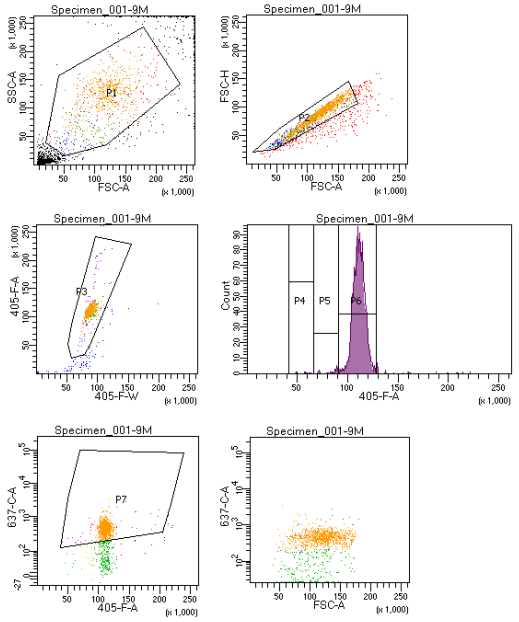

Tube: 9M

Population	#Events	%Parent	%Total
All Events	5,000	####	100.0
P1	1,709	34.2	34.2
P2	1,410	82.5	28.2
P3	1,301	92.3	26.0
P4	12	0.9	0.2
P5	33	2.5	0.7
P6	1,223	94.0	24.5
P7	1,033	79.4	20.7
P7 AND P6	999	76.8	20.0

405 > Hoechst
637 > A647

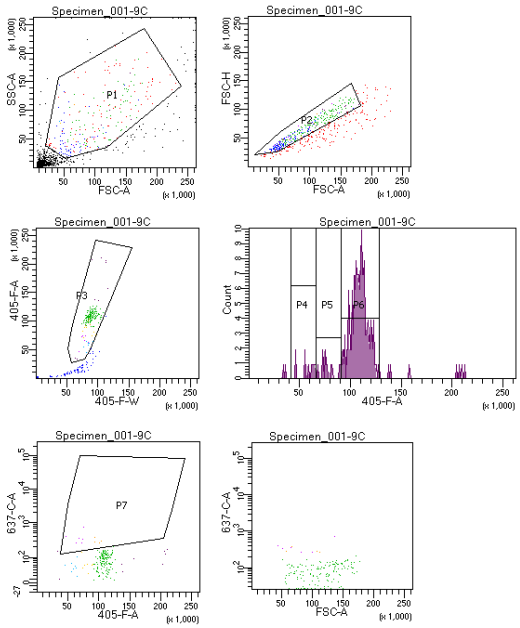

Tube: 9C

Population	#Events	%Parent	%Total
All Events	3,016	####	100.0
P1	468	15.5	15.5
P2	281	60.0	9.3
P3	173	61.6	5.7
P4	10	5.8	0.3
P5	11	6.4	0.4
P6	143	82.7	4.7
P7	10	5.8	0.3
P7 AND P6	4	2.3	0.1

405 > Hoechst
637 > A647

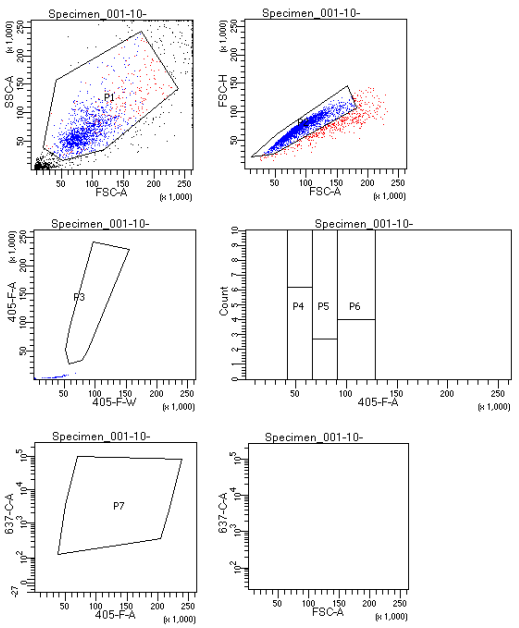

Tube: 10-

Population	#Events	%Parent	%Total
All Events	5,000	####	100.0
P1	2,908	58.2	58.2
P2	2,487	85.5	49.7
P3	0	0.0	0.0
P4	0	####	0.0
P5	0	####	0.0
P6	0	####	0.0
P7	0	####	0.0
P7 AND P6	0	####	0.0

405 > Hoechst
637 > A647

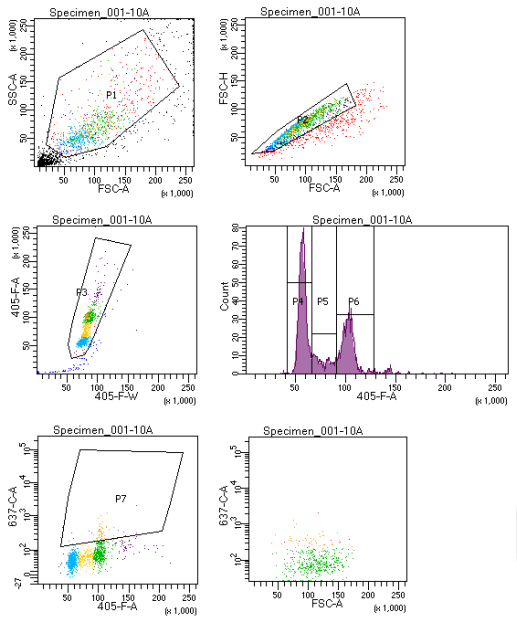

Tube: 10A

Population	#Events	%Parent	%Total
All Events	5,000	####	100.0
P1	1,869	37.4	37.4
P2	1,458	78.0	29.2
P3	1,347	92.4	26.9
P4	656	48.7	13.1
P5	182	13.5	3.6
P6	447	33.2	8.9
P7	60	4.5	1.2
P7 AND P6	51	3.8	1.0

405 > Hoechst
637 > A647

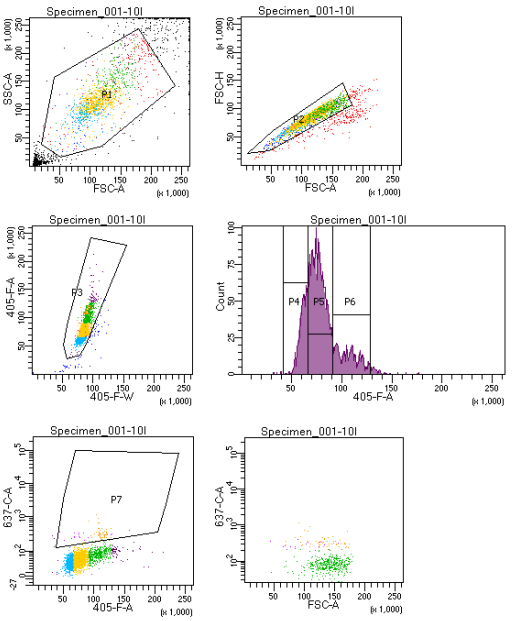

Tube: 10I

Population	#Events	%Parent	%Total
All Events	5,000	####	100.0
P1	3,019	60.4	60.4
P2	2,719	90.1	54.4
P3	2,643	97.2	52.9
P4	585	22.1	11.7
P5	1,522	57.6	30.4
P6	471	17.8	9.4
P7	68	2.6	1.4
P7 AND P6	52	2.0	1.0

405 > Hoechst
637 > A647

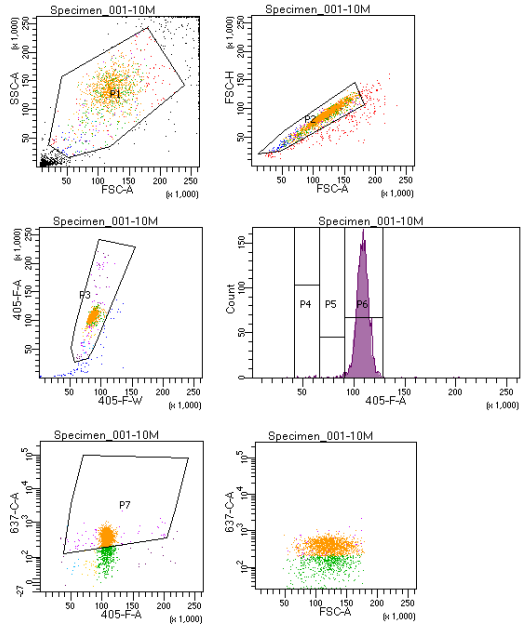

Tube: 10M

Population	#Events	%Parent	%Total
All Events	5,000	####	100.0
P1	2,561	51.2	51.2
P2	2,313	90.3	46.3
P3	2,230	96.4	44.6
P4	23	1.0	0.5
P5	47	2.1	0.9
P6	2,116	94.9	42.3
P7	1,605	72.0	32.1
P7 AND P6	1,551	69.6	31.0

405 > Hoechst
637 > A647

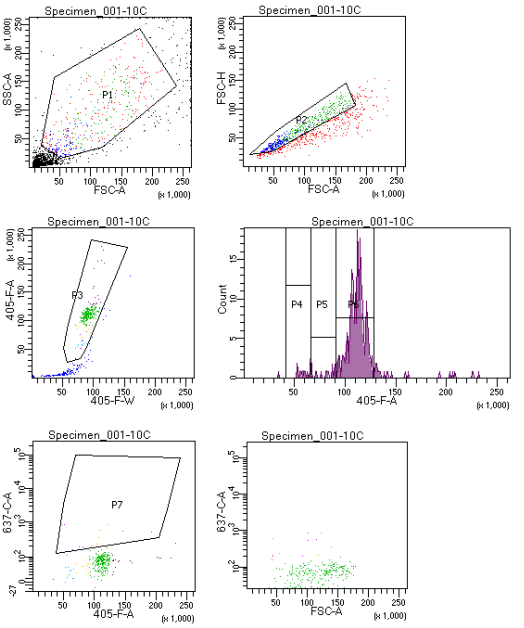

Tube: 10C

Population	#Events	%Parent	%Total
All Events	5,000	####	100.0
P1	853	17.1	17.1
P2	472	55.3	9.4
P3	277	58.7	5.5
P4	13	4.7	0.3
P5	11	4.0	0.2
P6	233	84.1	4.7
P7	12	4.3	0.2
P7 AND P6	6	2.2	0.1

405 > Hoechst
637 > A647

Appendix C: Ezrin-RFP plasmid map and sequence.

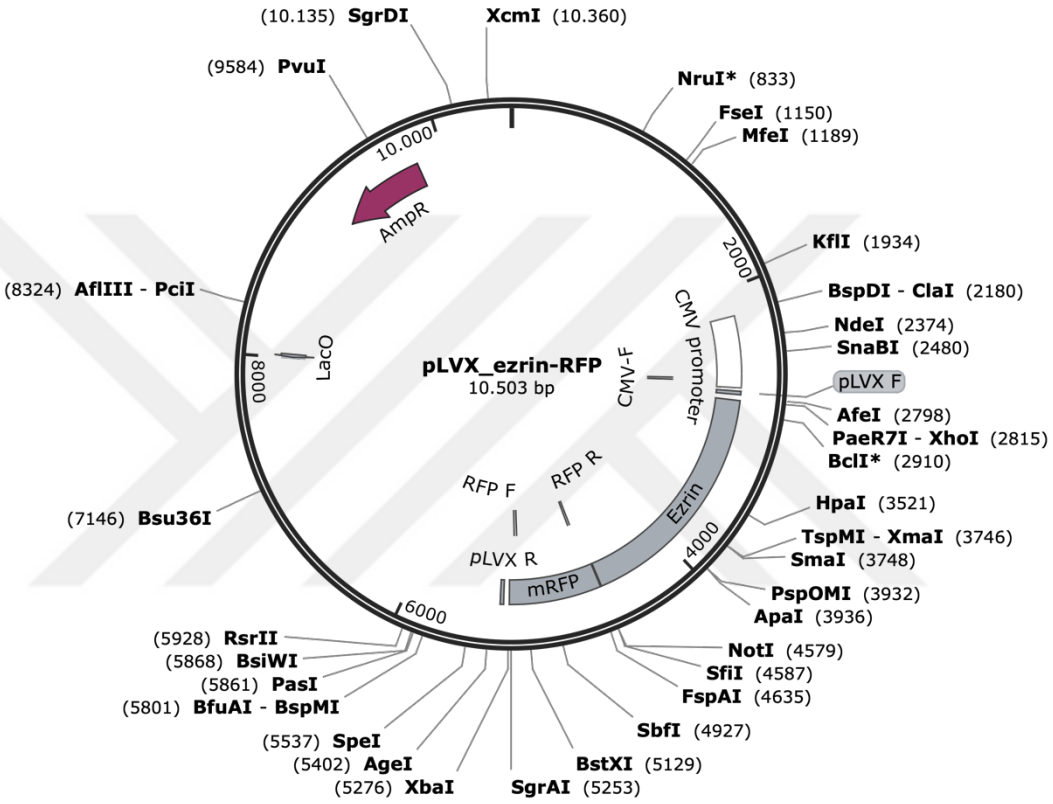


```
>pLVX_ezrin-RFP
TGGAAGGGCTAATTCACTCCCAAAGAAGACAAGATATCCTTGATCTGTGGATCTACCACACACAAGGCTACTT
CCCTGATTAGCAGAACTACACACCAGGGCCAGGGGTCAGATATCCACTGACCTTTGGATGGTGCTACAAGCTA
GTACCAGTTGAGCCAGATAAGGTAGAAGAGGCCAATAAAGGAGAGAACACCAGCTTGTTACACCCTGTGAGCC
TGCATGGGATGGATGACCCGGAGAGAGAAGTGTTAGAGTGGAGGTTTGACAGCCGCCTAGCATTTCATCACGT
GGCCCGAGAGCTGCATCCGGAGTACTTCAAGAACTGCTGATATCGAGCTTGCTACAAGGGACTTTCCGCTGGG
GACTTTCCAGGGAGGCGTGGCCTGGGCGGGACTGGGGAGTGGCGAGCCCTCAGATCCTGCATATAAGCAGCTG
CTTTTTGCCTGTACTGGGTCTCTCTGGTTAGACCAGATCTGAGCCTGGGAGCTCTCTGGCTAACTAGGGAACC
CACTGCTTAAGCCTCAATAAAGCTTGCCTTGAGTGCTTCAAGTAGTGTGTGCCCGTCTGTTGTGTGACTCTGG
TAACTAGAGATCCCTCAGACCCTTTTAGTCAGTGTGGAAAATCTCTAGCAGTGGCGCCCGAACAGGGACTTGA
AAGCGAAAGGGAAACCAGAGGAGCTCTCTCGACGCAGGACTCGGCTTGCTGAAGCGCGCACGGCAAGAGGCGA
GGGGCGGCGACTGGTGAGTACGCCAAAAATTTTGACTAGCGGAGGCTAGAAGGAGAGAGATGGGTGCGAGAGC
GTCAGTATTAAGCGGGGGAGAATTAGATCGCGATGGGAAAAAATTCGGTTAAGGCCAGGGGGAAAGAAAAAAT
ATAAATTAAAACATATAGTATGGGCAAGCAGGGAGCTAGAACGATTCGCAGTTAATCCTGGCCTGTTAGAAAC
ATCAGAAGGCTGTAGACAAATACTGGGACAGCTACAACCATCCCTTCAGACAGGATCAGAAGAACTTAGATCA
TTATATAATACAGTAGCAACCCTCTATTGTGTGCATCAAAGGATAGAGATAAAAGACACCAAGGAAGCTTTAG
ACAAGATAGAGGAAGAGCAAAACAAAAGTAAGACCACCGCACAGCAAGCGGCCGGCCGCTGATCTTCAGACCT
GGAGGAGGAGATATGAGGGACAATTGGAGAAGTGAATTATATAAATATAAAGTAGTAAAAATTGAACCATTAG
GAGTAGCACCCACCAAGGCAAAGAGAAGAGTGGTGCAGAGAGAAAAAAGAGCAGTGGGAATAGGAGCTTTGTT
CCTTGGGTTCTTGGGAGCAGCAGGAAGCACTATGGGCGCAGCGTCAATGACGCTGACGGTACAGGCCAGACAA
```

TTATTGTCTGGTATAGTGCAGCAGCAGAACAATTTGCTGAGGGCTATTGAGGCGCAACAGCATCTGTTGCAAC
TCACAGTCTGGGGCATCAAGCAGCTCCAGGCAAGAATCCTGGCTGTGGAAAGATACCTAAAGGATCAACAGCT
CCTGGGGATTTGGGGTTGCTCTGGAAAACTCATTTGCACCACTGCTGTGCCTTGGAATGCTAGTTGGAGTAAT
AAATCTCTGGAACAGATTTGGAATCACACGACCTGGATGGAGTGGGACAGAGAAATTAACAATTACACAAGCT
TAATACACTCCTTAATTGAAGAATCGCAAAACCAGCAAGAAAAGAATGAACAAGAATTATTGGAATTAGATAA
ATGGGCAAGTTTGTGGAATTGGTTTAACATAACAAATTGGCTGTGGTATATAAAATTATTCATAATGATAGTA
GGAGGCTTGGTAGGTTTAAGAATAGTTTTTGCTGTACTTTCTATAGTGAATAGAGTTAGGCAGGGATATTCAC
CATTATCGTTTCAGACCCACCTCCCAACCCCGAGGGGACCCGACAGGCCCGAAGGAATAGAAGAAGAAGGTGG
AGAGAGAGACAGAGACAGATCCATTCGATTAGTGAACGGATCTCGACGGTATCGCCTTTAAAAGAAAAGGGGG
GATTGGGGGGTACAGTGCAGGGGAAAGAATAGTAGACATAATAGCAACAGACATACAAACTAAAGAACTACAA
AAACAAATTACAAAAATTCAAAATTTTCGGGTTTATTACAGGGACAGCAGAGATCCAGTTTATCGATAAGCTT
GGGAGTTCCGCGTTACATAACTTACGGTAAATGGCCCGCCTGGCTGACCGCCCAACGACCCCCGCCCATTGAC
GTCAATAATGACGTATGTTCCCATAGTAACGCCAATAGGGACTTTCCATTGACGTCAATGGGTGGAGTATTTA
CGGTAAACTGCCCACTTGGCAGTACATCAAGTGTATCATATGCCAAGTACGCCCCCTATTGACGTCAATGACG
GTAAATGGCCCGCCTGGCATTATGCCCAGTACATGACCTTATGGGACTTTCCTACTTGGCAGTACATCTACGT
ATTAGTCATCGCTATTACCATGGTGATGCGGTTTTGGCAGTACATCAATGGGCGTGGATAGCGGTTTGACTCA
CGGGGATTTCCAAGTCTCCACCCCATTGACGTCAATGGGAGTTTGTTTTGGCACCAAAATCAACGGGACTTTC
CAAAATGTCGTAACAACTCCGCCCCATTGACGCAAATGGGCGGTAGGCGTGTACGGTGGGAGGTCTATATAAG
CAGAGCTCGTTTAGTGAACCGTCAGATCGCCTGGAGACGCCATCCACGCTGTTTTGACCTCCATAGAAGACAC
CGACTCTACTAGAGGATCGCTAGCGCTACCGGACTCAGATCTCGAGATGCCGAAACCAATCAATGTCCGAGTT
ACCACCATGGATGCAGAGCTGGAGTTTGCAATCCAGCCAAATACAACTGGAAAACAGCTTTTTGATCAGGTGG
TAAAGACTATCGGCCTCCGGGAAGTGTGGTACTTTGGCCTCCACTATGTGGATAATAAAGGATTTCCTACCTG
GCTGAAGCTGGATAAGAAGGTGTCTGCCCAGGAGGTCAGGAAGGAGAATCCCCTCCAGTTCAAGTTCCGGGCC
AAGTTCTACCCTGAAGATGTGGCTGAGGAGCTCATCCAGGACATCACCCAGAAACTTTTCTTCCTCCAAGTGA
AGGAAGGAATCCTTAGCGATGAGATCTACTGCCCCCCTGAGACTGCCGTGCTCTTGGGGTCCTACGCTGTGCA
GGCCAAGTTTGGGGACTACAACAAAGAAGTGCACAAGTCTGGGTACCTCAGCTCTGAGCGGCTGATCCCTCAA
AGAGTGATGGACCAGCACAAACTTACCAGGGACCAGTGGGAGGACCGGATCCAGGTGTGGCATGCGGAACACC
GTGGGATGCTCAAAGATAATGCTATGTTGGAATACCTGAAGATTGCTCAGGACCTGGAAATGTATGGAATCAA
CTATTTCGAGATAAAAAACAAGAAAGGAACAGACCTTTGGCTTGGAGTTGATGCCCTTGGACTGAATATTTAT
GAGAAAGATGATAAGTTAACCCCAAAGATTGGCTTTCCTTGGAGTGAAATCAGGAACATCTCTTTCAATGACA
AAAAGTTTGTCATTAAACCCATCGACAAGAAGGCACCTGACTTTGTGTTTTATGCCCCACGTCTGAGAATCAA
CAAGCGGATCCTGCAGCTCTGCATGGGCAACCATGAGTTGTATATGCGCCGCAGGAAGCCTGACACCATCGAG
GTGCAGCAGATGAAGGCCCAGGCCCGGGAGGAGAAGCATCAGAAGCAGCTGGAGCGGCAACAGCTGGAAACAG
AGAAGAAAAGGAGAGAAACCGTGGAGAGAGAGAAAGAGCAGATGATGCGCGAGAAGGAGGAGTTGATGCTGCG
GCTGCAGGACTATGAGGAGAAGACAAAGAAGGCAGAGAGAGAGCTCTCGGAGCAGATTCAGAGGGCCCTGCAG
CTGGAGGAGGAGAGGAAGCGGGCACAGGAGGAGGCCGAGCGCCTAGAGGCTGACCGTATGGCTGCACTGCGGG
CTAAGGAGGAGCTGGAGAGACAGGCGGTGGATCAGATAAAGAGCCAGGAGCAGCTGGCTGCGGAGCTTGCAGA
ATACACTGCCAAGATTGCCCTCCTGGAAGAGGCGCGGAGGCGCAAGGAGGATGAAGTTGAAGAGTGGCAGCAC
AGGGCCAAAGAAGCCCAGGATGACCTGGTGAAGACCAAGGAGGAGCTGCACCTGGTGATGACAGCACCCCCGC
CCCCACCACCCCCCGTGTACGAGCCGGTGAGCTACCATGTCCAGGAGAGCTTGCAGGATGAGGGCGCAGAGCC
CACGGGCTACAGCGCGGAGCTGTCTAGTGAGGGCATCCGGGATGACCGCAATGAGGAGAAGCGCATCACTGAG
GCAGAGAAGAACGAGCGTGTGCAGCGGCAGCTGCTGACGCTGAGCAGCGAGCTGTCCCAGGCCCGAGATGAGA
ATAAGAGGACCCACAATGACATCATCCACAACGAGAACATGAGGCAAGGCCGGGACAAGTACAAGACGCTGCG
GCAGATCCGGCAGGGCAACACCAAGCAGCGCATCGACGAGTTCGAGGCCCTGCGGCCGCCATGGCCTCCTCCG
AGGACGTCATCAAGGAGTTCATGCGCTTCAAGGTGCGCATGGAGGGCTCCGTGAACGGCCACGAGTTCGAGAT
CGAGGGCGAGGGCGAGGGCCGCCCCTACGAGGGCACCCAGACCGCCAAGCTGAAGGTGACCAAGGGCGGCCCC
CTGCCCTTCGCCTGGGACATCCTGTCCCCTCAGTTCCAGTACGGCTCCAAGGCCTACGTGAAGCACCCCGCCG
ACATCCCCGACTACTTGAAGCTGTCCTTCCCCGAGGGCTTCAAGTGGGAGCGCGTGATGAACTTCGAGGACGG
CGGCGTGGTGACCGTGACCCAGGACTCCTCCCTGCAGGACGGCGAGTTCATCTACAAGGTGAAGCTGCGCGGC
ACCAACTTCCCCTCCGACGGCCCCGTAATGCAGAAGAAGACCATGGGCTGGGAGGCCTCCACCGAGCGGATGT
ACCCCGAGGACGGCGCCCTGAAGGGCGAGATCAAGATGAGGCTGAAGCTGAAGGACGGCGGCCACTACGACGC
CGAGGTCAAGACCACCTACATGGCCAAGAAGCCCGTGCAGCTGCCCGGCGCCTACAAGACCGACATCAAGCTG
GACATCACCTCCCACAACGAGGACTACACCATCGTGGAACAGTACGAGCGCGCCGAGGGCCGCCACTCCACCG
GCGCCTAAGATCCCGCGACTCTAGATAATTCTACCGGGTAGGGGAGGCGCTTTTCCCAAGGCAGTCTGGAGCA
TGCGCTTTAGCAGCCCCGCTGGGCACTTGGCGCTACACAAGTGGCCTCTGGCCTCGCACACATTCCACATCCA
CCGGTAGGCGCCAACCGGCTCCGTTCTTTGGTGGCCCCTTCGCGCCACCTTCTACTCCTCCCCTAGTCAGGAA
GTTCCCCCCCGCCCCGCAGCTCGCGTCGTGCAGGACGTGACAAATGGAAGTAGCACGTCTCACTAGTCTCGTG

CAGATGGACAGCACCGCTGAGCAATGGAAGCGGGTAGGCCTTTGGGGCAGCGGCCAATAGCAGCTTTGCTCCT
TCGCTTTCTGGGCTCAGAGGCTGGGAAGGGGTGGGTCCGGGGGCGGGCTCAGGGGCGGGCTCAGGGGCGGGGC
GGGCGCCCGAAGGTCCTCCGGAGGCCCGGCATTCTGCACGCTTCAAAAGCGCACGTCTGCCGCGCTGTTCTCC
TCTTCCTCATCTCCGGGCCTTTCGACCTGCAGCCCAAGCTTACCATGACCGAGTACAAGCCCACGGTGCGCCT
CGCCACCCGCGACGACGTCCCCAGGGCCGTACGCACCCTCGCCGCCGCGTTCGCCGACTACCCCGCCACGCGC
CACACCGTCGATCCGGACCGCCACATCGAGCGGGTCACCGAGCTGCAAGAACTCTTCCTCACGCGCGTCGGGC
TCGACATCGGCAAGGTGTGGGTCGCGGACGACGGCGCCGCGGTGGCGGTCTGGACCACGCCGGAGAGCGTCGA
AGCGGGGGCGGTGTTCGCCGAGATCGGCCCGCGCATGGCCGAGTTGAGCGGTTCCCGGCTGGCCGCGCAGCAA
CAGATGGAAGGCCTCCTGGCGCCGCACCGGCCCAAGGAGCCCGCGTGGTTCCTGGCCACCGTCGGCGTCTCGC
CCGACCACCAGGGCAAGGGTCTGGGCAGCGCCGTCGTGCTCCCCGGAGTGGAGGCGGCCGAGCGCGCCGGGGT
GCCCGCCTTCCTGGAGACCTCCGCGCCCCGCAACCTCCCCTTCTACGAGCGGCTCGGCTTCACCGTCACCGCC
GACGTCGAGGTGCCCGAAGGACCGCGCACCTGGTGCATGACCCGCAAGCCCGGTGCCTGACCGCGTCTGGAAC
AATCAACCTCTGGATTACAAAATTTGTGAAAGATTGACTGGTATTCTTAACTATGTTGCTCCTTTTACGCTAT
GTGGATACGCTGCTTTAATGCCTTTGTATCATGCTATTGCTTCCCGTATGGCTTTCATTTTCTCCTCCTTGTA
TAAATCCTGGTTGCTGTCTCTTTATGAGGAGTTGTGGCCCGTTGTCAGGCAACGTGGCGTGGTGTGCACTGTG
TTTGCTGACGCAACCCCCACTGGTTGGGGCATTGCCACCACCTGTCAGCTCCTTTCCGGGACTTTCGCTTTCC
CCCTCCCTATTGCCACGGCGGAACTCATCGCCGCCTGCCTTGCCCGCTGCTGGACAGGGGCTCGGCTGTTGGG
CACTGACAATTCCGTGGTGTTGTCGGGGAAGCTGACGTCCTTTCCATGGCTGCTCGCCTGTGTTGCCACCTGG
ATTCTGCGCGGGACGTCCTTCTGCTACGTCCCTTCGGCCCTCAATCCAGCGGACCTTCCTTCCCGCGGCCTGC
TGCCGGCTCTGCGGCCTCTTCCGCGTCTTCGCCTTCGCCCTCAGACGAGTCGGATCTCCCTTTGGGCCGCCTC
CCCGCCTGGAATTAATTCTGCAGTCGAGACCTAGAAAAACATGGAGCAATCACAAGTAGCAATACAGCAGCTA
CCAATGCTGATTGTGCCTGGCTAGAAGCACAAGAGGAGGAGGAGGTGGGTTTTTCCAGTCACACCTCAGGTAC
CTTTAAGACCAATGACTTACAAGGCAGCTGTAGATCTTAGCCACTTTTTAAAAGAAAAGAGGGGACTGGAAGG
GCTAATTCACTCCCAACGAAGACAAGATATCCTTGATCTGTGGATCTACCACACACAAGGCTACTTCCCTGAT
TAGCAGAACTACACACCAGGGCCAGGGGTCAGATATCCACTGACCTTTGGATGGTGCTACAAGCTAGTACCAG
TTGAGCCAGATAAGGTAGAAGAGGCCAATAAAGGAGAGAACACCAGCTTGTTACACCCTGTGAGCCTGCATGG
GATGGATGACCCGGAGAGAGAAGTGTTAGAGTGGAGGTTTGACAGCCGCCTAGCATTTCATCACGTGGCCCGA
GAGCTGCATCCGGAGTACTTCAAGAACTGCTGATATCGAGCTTGCTACAAGGGACTTTCCGCTGGGGACTTTC
CAGGGAGGCGTGGCCTGGGCGGGACTGGGGAGTGGCGAGCCCTCAGATCCTGCATATAAGCAGCTGCTTTTTG
CCTGTACTGGGTCTCTCTGGTTAGACCAGATCTGAGCCTGGGAGCTCTCTGGCTAACTAGGGAACCCACTGCT
TAAGCCTCAATAAAGCTTGCCTTGAGTGCTTCAAGTAGTGTGTGCCCGTCTGTTGTGTGACTCTGGTAACTAG
AGATCCCTCAGACCCTTTTAGTCAGTGTGGAAAATCTCTAGCAGTAGTAGTTCATGTCATCTTATTATTCAGT
ATTTATAACTTGCAAAGAAATGAATATCAGAGAGTGAGAGGCCTTGACATTGCTAGCGTTTTACCGTCGACCT
CTAGCTAGAGCTTGGCGTAATCATGGTCATAGCTGTTTCCTGTGTGAAATTGTTATCCGCTCACAATTCCACA
CAACATACGAGCCGGAAGCATAAAGTGTAAAGCCTGGGGTGCCTAATGAGTGAGCTAACTCACATTAATTGCG
TTGCGCTCACTGCCCGCTTTCCAGTCGGGAAACCTGTCGTGCCAGCTGCATTAATGAATCGGCCAACGCGCGG
GGAGAGGCGGTTTGCGTATTGGGCGCTCTTCCGCTTCCTCGCTCACTGACTCGCTGCGCTCGGTCGTTCGGCT
GCGGCGAGCGGTATCAGCTCACTCAAAGGCGGTAATACGGTTATCCACAGAATCAGGGGATAACGCAGGAAAG
AACATGTGAGCAAAAGGCCAGCAAAAGGCCAGGAACCGTAAAAAGGCCGCGTTGCTGGCGTTTTTCCATAGGC
TCCGCCCCCCTGACGAGCATCACAAAAATCGACGCTCAAGTCAGAGGTGGCGAAACCCGACAGGACTATAAAG
ATACCAGGCGTTTCCCCCTGGAAGCTCCCTCGTGCGCTCTCCTGTTCCGACCCTGCCGCTTACCGGATACCTG
TCCGCCTTTCTCCCTTCGGGAAGCGTGGCGCTTTCTCATAGCTCACGCTGTAGGTATCTCAGTTCGGTGTAGG
TCGTTCGCTCCAAGCTGGGCTGTGTGCACGAACCCCCCGTTCAGCCCGACCGCTGCGCCTTATCCGGTAACTA
TCGTCTTGAGTCCAACCCGGTAAGACACGACTTATCGCCACTGGCAGCAGCCACTGGTAACAGGATTAGCAGA
GCGAGGTATGTAGGCGGTGCTACAGAGTTCTTGAAGTGGTGGCCTAACTACGGCTACACTAGAAGAACAGTAT
TTGGTATCTGCGCTCTGCTGAAGCCAGTTACCTTCGGAAAAAGAGTTGGTAGCTCTTGATCCGGCAAACAAAC
CACCGCTGGTAGCGGTTTTTTTGTTTGCAAGCAGCAGATTACGCGCAGAAAAAAAGGATCTCAAGAAGATCCT
TTGATCTTTTCTACGGGGTCTGACGCTCAGTGGAACGAAAACTCACGTTAAGGGATTTTGGTCATGAGATTAT
CAAAAAGGATCTTCACCTAGATCCTTTTAAATTAAAAATGAAGTTTTAAATCAATCTAAAGTATATATGAGTA
AACTTGGTCTGACAGTTACCAATGCTTAATCAGTGAGGCACCTATCTCAGCGATCTGTCTATTTCGTTCATCC
ATAGTTGCCTGACTCCCCGTCGTGTAGATAACTACGATACGGGAGGGCTTACCATCTGGCCCCAGTGCTGCAA
TGATACCGCGAGACCCACGCTCACCGGCTCCAGATTTATCAGCAATAAACCAGCCAGCCGGAAGGGCCGAGCG
CAGAAGTGGTCCTGCAACTTTATCCGCCTCCATCCAGTCTATTAATTGTTGCCGGGAAGCTAGAGTAAGTAGT
TCGCCAGTTAATAGTTTGCGCAACGTTGTTGCCATTGCTACAGGCATCGTGGTGTCACGCTCGTCGTTTGGTA
TGGCTTCATTCAGCTCCGGTTCCCAACGATCAAGGCGAGTTACATGATCCCCCATGTTGTGCAAAAAAGCGGT
TAGCTCCTTCGGTCCTCCGATCGTTGTCAGAAGTAAGTTGGCCGCAGTGTTATCACTCATGGTTATGGCAGCA
CTGCATAATTCTCTTACTGTCATGCCATCCGTAAGATGCTTTTCTGTGACTGGTGAGTACTCAACCAAGTCAT

TCTGAGAATAGTGTATGCGGCGACCGAGTTGCTCTTGCCCGGCGTCAATACGGGATAATACCGCGCCACATAG
CAGAACTTTAAAAGTGCTCATCATTGGAAAACGTTCTTCGGGGCGAAAACTCTCAAGGATCTTACCGCTGTTG
AGATCCAGTTCGATGTAACCCACTCGTGCACCCAACTGATCTTCAGCATCTTTTACTTTCACCAGCGTTTCTG
GGTGAGCAAAAACAGGAAGGCAAAATGCCGCAAAAAAGGGAATAAGGGCGACACGGAAATGTTGAATACTCAT
ACTCTTCCTTTTTCAATATTATTGAAGCATTTATCAGGGTTATTGTCTCATGAGCGGATACATATTTGAATGT
ATTTAGAAAAATAAACAAATAGGGGTTCCGCGCACATTTCCCCGAAAAGTGCCACCTGACGTCGACGGATCGG
GAGATCAACTTGTTTATTGCAGCTTATAATGGTTACAAATAAAGCAATAGCATCACAAATTTCACAAATAAAG
CATTTTTTTCACTGCATTCTAGTTGTGGTTTGTCCAAACTCATCAATGTATCTTATCATGTCTGGATCAACTG
GATAACTCAAGCTAACCAAAATCATCCCAAACTTCCCACCCCATACCCTATTACCACTGCCAATTACCTAGTG
GTTTCATTTACTCTAAACCTGTGATTCCTCTGAATTATTTTCATTTTAAAGAAATTGTATTTGTTAAATATGT
ACTACAAACTTAGTAGTTTTTAAAGAAATTGTATTTGTTAAATATGTACTACAAACTTAGTAGT

Appendix D: pLVX_keratin18-RFP plasmid map and sequence.

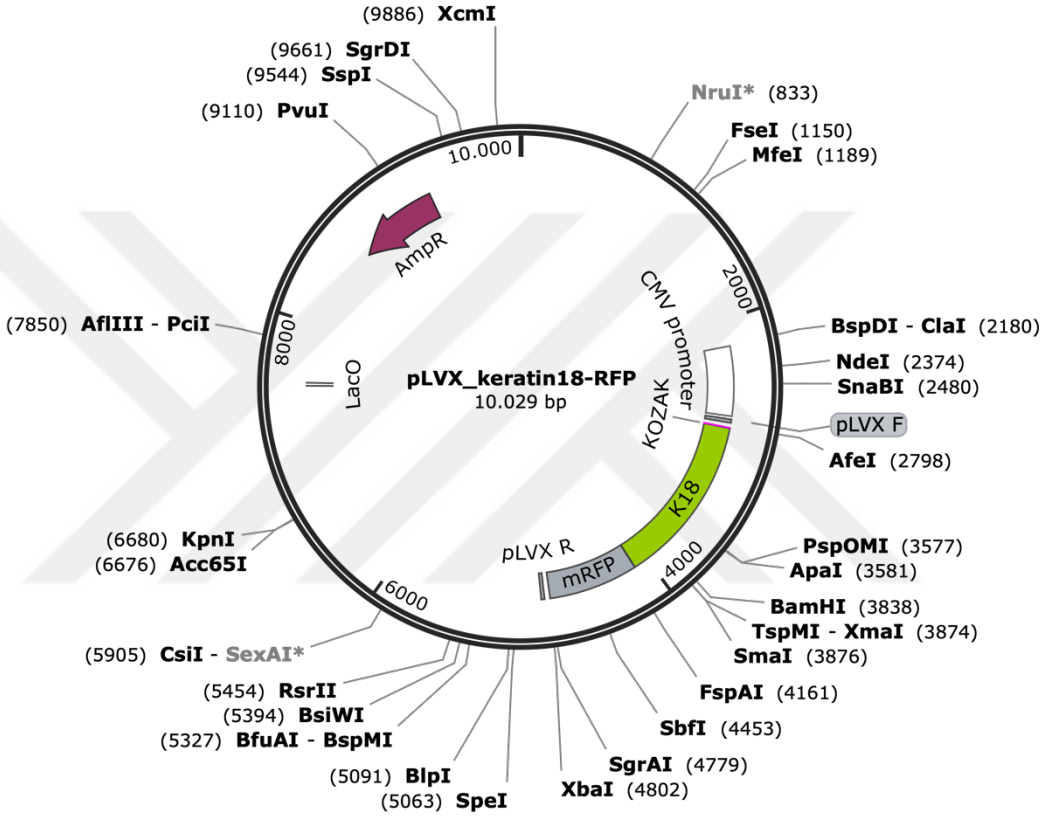


```
>pLVX_keratin18-RFP
TGGAAGGGCTAATTCACTCCCAAAGAAGACAAGATATCCTTGATCTGTGGATCTACCACACACAAGGCTACTT
CCCTGATTAGCAGAACTACACACCAGGGCCAGGGGTCAGATATCCACTGACCTTTGGATGGTGCTACAAGCTA
GTACCAGTTGAGCCAGATAAGGTAGAAGAGGCCAATAAAGGAGAGAACACCAGCTTGTTACACCCTGTGAGCC
TGCATGGGATGGATGACCCGGAGAGAGAAGTGTTAGAGTGGAGGTTTGACAGCCGCCTAGCATTTCATCACGT
GGCCCGAGAGCTGCATCCGGAGTACTTCAAGAACTGCTGATATCGAGCTTGCTACAAGGGACTTTCCGCTGGG
GACTTTCCAGGGAGGCGTGGCCTGGGCGGGACTGGGGAGTGGCGAGCCCTCAGATCCTGCATATAAGCAGCTG
CTTTTTGCCTGTACTGGGTCTCTCTGGTTAGACCAGATCTGAGCCTGGGAGCTCTCTGGCTAACTAGGGAACC
CACTGCTTAAGCCTCAATAAAGCTTGCCTTGAGTGCTTCAAGTAGTGTGTGCCCGTCTGTTGTGTGACTCTGG
TAACTAGAGATCCCTCAGACCCTTTTAGTCAGTGTGGAAAATCTCTAGCAGTGGCGCCCGAACAGGGACTTGA
AAGCGAAAGGGAAACCAGAGGAGCTCTCTCGACGCAGGACTCGGCTTGCTGAAGCGCGCACGGCAAGAGGCGA
GGGGCGGCGACTGGTGAGTACGCCAAAAATTTTGACTAGCGGAGGCTAGAAGGAGAGAGATGGGTGCGAGAGC
GTCAGTATTAAGCGGGGGAGAATTAGATCGCGATGGGAAAAAATTCGGTTAAGGCCAGGGGGAAAGAAAAAAT
ATAAATTAAAACATATAGTATGGGCAAGCAGGGAGCTAGAACGATTCGCAGTTAATCCTGGCCTGTTAGAAAC
ATCAGAAGGCTGTAGACAAATACTGGGACAGCTACAACCATCCCTTCAGACAGGATCAGAAGAACTTAGATCA
TTATATAATACAGTAGCAACCCTCTATTGTGTGCATCAAAGGATAGAGATAAAAGACACCAAGGAAGCTTTAG
ACAAGATAGAGGAAGAGCAAAACAAAAGTAAGACCACCGCACAGCAAGCGGCCGGCCGCTGATCTTCAGACCT
GGAGGAGGAGATATGAGGGACAATTGGAGAAGTGAATTATATAAATATAAAGTAGTAAAAATTGAACCATTAG
GAGTAGCACCCACCAAGGCAAAGAGAAGAGTGGTGCAGAGAGAAAAAAGAGCAGTGGGAATAGGAGCTTTGTT
CCTTGGGTTCTTGGGAGCAGCAGGAAGCACTATGGGCGCAGCGTCAATGACGCTGACGGTACAGGCCAGACAA
```

TTATTGTCTGGTATAGTGCAGCAGCAGAACAATTTGCTGAGGGCTATTGAGGCGCAACAGCATCTGTTGCAAC
TCACAGTCTGGGGCATCAAGCAGCTCCAGGCAAGAATCCTGGCTGTGGAAAGATACCTAAAGGATCAACAGCT
CCTGGGGATTTGGGGTTGCTCTGGAAAACTCATTTGCACCACTGCTGTGCCTTGGAATGCTAGTTGGAGTAAT
AAATCTCTGGAACAGATTTGGAATCACACGACCTGGATGGAGTGGGACAGAGAAATTAACAATTACACAAGCT
TAATACACTCCTTAATTGAAGAATCGCAAAACCAGCAAGAAAAGAATGAACAAGAATTATTGGAATTAGATAA
ATGGGCAAGTTTGTGGAATTGGTTTAACATAACAAATTGGCTGTGGTATATAAAATTATTCATAATGATAGTA
GGAGGCTTGGTAGGTTTAAGAATAGTTTTTGCTGTACTTTCTATAGTGAATAGAGTTAGGCAGGGATATTCAC
CATTATCGTTTCAGACCCACCTCCCAACCCCGAGGGGACCCGACAGGCCCGAAGGAATAGAAGAAGAAGGTGG
AGAGAGAGACAGAGACAGATCCATTCGATTAGTGAACGGATCTCGACGGTATCGCCTTTAAAAGAAAAGGGGG
GATTGGGGGGTACAGTGCAGGGGAAAGAATAGTAGACATAATAGCAACAGACATACAAACTAAAGAACTACAA
AAACAAATTACAAAAATTCAAAATTTTCGGGTTTATTACAGGGACAGCAGAGATCCAGTTTATCGATAAGCTT
GGGAGTTCCGCGTTACATAACTTACGGTAAATGGCCCGCCTGGCTGACCGCCCAACGACCCCCGCCCATTGAC
GTCAATAATGACGTATGTTCCCATAGTAACGCCAATAGGGACTTTCCATTGACGTCAATGGGTGGAGTATTTA
CGGTAAACTGCCCACTTGGCAGTACATCAAGTGTATCATATGCCAAGTACGCCCCCTATTGACGTCAATGACG
GTAAATGGCCCGCCTGGCATTATGCCCAGTACATGACCTTATGGGACTTTCCTACTTGGCAGTACATCTACGT
ATTAGTCATCGCTATTACCATGGTGATGCGGTTTTGGCAGTACATCAATGGGCGTGGATAGCGGTTTGACTCA
CGGGGATTTCCAAGTCTCCACCCCATTGACGTCAATGGGAGTTTGTTTTGGCACCAAAATCAACGGGACTTTC
CAAAATGTCGTAACAACTCCGCCCCATTGACGCAAATGGGCGGTAGGCGTGTACGGTGGGAGGTCTATATAAG
CAGAGCTCGTTTAGTGAACCGTCAGATCGCCTGGAGACGCCATCCACGCTGTTTTGACCTCCATAGAAGACAC
CGACTCTACTAGAGGATCGCTAGCGCTACCGGACTCAGATCCACCATGAGCTTCACCACTCGCTCCACCTTCT
CCACCAACTACCGGTCCCTGGGCTCTGTCCAGGCGCCCAGCTACGGCGCCCGGCCGGTCAGCAGCGCGGCCAG
CGTCTATGCAGGCGCTGGGGGCTCTGGTTCCCGGATCTCCGTGTCCCGCTCCACCAGCTTCAGGGGCGGCATG
GGGTCCGGGGGCCTGGCCACCGGGATAGCCGGGGGTCTGGCAGGAATGGGAGGCATCCAGAACGAGAAGGAGA
CCATGCAAAGCCTGAACGACCGCCTGGCCTCTTACCTGGACAGAGTGAGGAGCCTGGAGACCGAGAACCGGAG
GCTGGAGAGCAAAATCCGGGAGCACTTGGAGAAGAAGGGACCCCAGGTCAGAGACTGGAGCCATTACTTCAAG
ATCATCGAGGACCTGAGGGCTCAGATCTTCGCAAATACTGTGGACAATGCCCGCATCGTTCTGCAGATTGACA
ATGCCCGTCTTGCTGCTGATGACTTTAGAGTCAAGTATGAGACAGAGCTGGCCATGCGCCAGTCTGTGGAGAA
CGACATCCATGGGCTCCGCAAGGTCATTGATGACACCAATATCACACGACTGCAGCTGGAGACAGAGATCGAG
GCTCTCAAGGAGGAGCTGCTCTTCATGAAGAAGAACCACGAAGAGGAAGTAAAAGGCCTACAAGCCCAGATTG
CCAGCTCTGGGTTGACCGTGGAGGTAGATGCCCCCAAATCTCAGGACCTCGCCAAGATCATGGCAGACATCCG
GGCCCAATATGACGAGCTGGCTCGGAAGAACCGAGAGGAGCTAGACAAGTACTGGTCTCAGCAGATTGAGGAG
AGCACCACAGTGGTCACCACACAGTCTGCTGAGGTTGGAGCTGCTGAGACGACGCTCACAGAGCTGAGACGTA
CAGTCCAGTCCTTGGAGATCGACCTGGACTCCATGAGAAATCTGAAGGCCAGCTTGGAGAACAGCCTGAGGGA
GGTGGAGGCCCGCTACGCCCTACAGATGGAGCAGCTCAACGGGATCCTGCTGCACCTTGAGTCAGAGCTGGCA
CAGACCCGGGCAGAGGGACAGCGCCAGGCCCAGGAGTATGAGGCCCTGCTGAACATCAAGGTCAAGCTGGAGG
CTGAGATCGCCACCTACCGCCGCCTGCTGGAAGATGGCGAGGACTTTAATCTTGGTGATGCCTTGGACAGCAG
CAACTCCATGCAAACCATCCAAAAGACCACCACCCGCCGGATAGTGGATGGCAAAGTGGTGTCTGAGACCAAT
GACACCAAAGTTCTGAGGCATGCCATGGCCTCCTCCGAGGACGTCATCAAGGAGTTCATGCGCTTCAAGGTGC
GCATGGAGGGCTCCGTGAACGGCCACGAGTTCGAGATCGAGGGCGAGGGCGAGGGCCGCCCCTACGAGGGCAC
CCAGACCGCCAAGCTGAAGGTGACCAAGGGCGGCCCCCTGCCCTTCGCCTGGGACATCCTGTCCCCTCAGTTC
CAGTACGGCTCCAAGGCCTACGTGAAGCACCCCGCCGACATCCCCGACTACTTGAAGCTGTCCTTCCCCGAGG
GCTTCAAGTGGGAGCGCGTGATGAACTTCGAGGACGGCGGCGTGGTGACCGTGACCCAGGACTCCTCCCTGCA
GGACGGCGAGTTCATCTACAAGGTGAAGCTGCGCGGCACCAACTTCCCCTCCGACGGCCCCGTAATGCAGAAG
AAGACCATGGGCTGGGAGGCCTCCACCGAGCGGATGTACCCCGAGGACGGCGCCCTGAAGGGCGAGATCAAGA
TGAGGCTGAAGCTGAAGGACGGCGGCCACTACGACGCCGAGGTCAAGACCACCTACATGGCCAAGAAGCCCGT
GCAGCTGCCCGGCGCCTACAAGACCGACATCAAGCTGGACATCACCTCCCACAACGAGGACTACACCATCGTG
GAACAGTACGAGCGCGCCGAGGGCCGCCACTCCACCGGCGCCTAAGATCCCGCGACTCTAGATAATTCTACCG
GGTAGGGGAGGCGCTTTTCCCAAGGCAGTCTGGAGCATGCGCTTTAGCAGCCCCGCTGGGCACTTGGCGCTAC
ACAAGTGGCCTCTGGCCTCGCACACATTCCACATCCACCGGTAGGCGCCAACCGGCTCCGTTCTTTGGTGGCC
CCTTCGCGCCACCTTCTACTCCTCCCCTAGTCAGGAAGTTCCCCCCCGCCCCGCAGCTCGCGTCGTGCAGGAC
GTGACAAATGGAAGTAGCACGTCTCACTAGTCTCGTGCAGATGGACAGCACCGCTGAGCAATGGAAGCGGGTA
GGCCTTTGGGGCAGCGGCCAATAGCAGCTTTGCTCCTTCGCTTTCTGGGCTCAGAGGCTGGGAAGGGGTGGGT
CCGGGGGCGGGCTCAGGGGCGGGCTCAGGGGCGGGGCGGGCGCCCGAAGGTCCTCCGGAGGCCCGGCATTCTG
CACGCTTCAAAAGCGCACGTCTGCCGCGCTGTTCTCCTCTTCCTCATCTCCGGGCCTTTCGACCTGCAGCCCA
AGCTTACCATGACCGAGTACAAGCCCACGGTGCGCCTCGCCACCCGCGACGACGTCCCCAGGGCCGTACGCAC
CCTCGCCGCCGCGTTCGCCGACTACCCCGCCACGCGCCACACCGTCGATCCGGACCGCCACATCGAGCGGGTC
ACCGAGCTGCAAGAACTCTTCCTCACGCGCGTCGGGCTCGACATCGGCAAGGTGTGGGTCGCGGACGACGGCG

CCGCGGTGGCGGTCTGGACCACGCCGGAGAGCGTCGAAGCGGGGGCGGTGTTCGCCGAGATCGGCCCGCGCAT
GGCCGAGTTGAGCGGTTCCCGGCTGGCCGCGCAGCAACAGATGGAAGGCCTCCTGGCGCCGCACCGGCCCAAG
GAGCCCGCGTGGTTCCTGGCCACCGTCGGCGTCTCGCCCGACCACCAGGGCAAGGGTCTGGGCAGCGCCGTCG
TGCTCCCCGGAGTGGAGGCGGCCGAGCGCGCCGGGGTGCCCGCCTTCCTGGAGACCTCCGCGCCCCGCAACCT
CCCCTTCTACGAGCGGCTCGGCTTCACCGTCACCGCCGACGTCGAGGTGCCCGAAGGACCGCGCACCTGGTGC
ATGACCCGCAAGCCCGGTGCCTGACCGCGTCTGGAACAATCAACCTCTGGATTACAAAATTTGTGAAAGATTG
ACTGGTATTCTTAACTATGTTGCTCCTTTTACGCTATGTGGATACGCTGCTTTAATGCCTTTGTATCATGCTA
TTGCTTCCCGTATGGCTTTCATTTTCTCCTCCTTGTATAAATCCTGGTTGCTGTCTCTTTATGAGGAGTTGTG
GCCCGTTGTCAGGCAACGTGGCGTGGTGTGCACTGTGTTTGCTGACGCAACCCCCACTGGTTGGGGCATTGCC
ACCACCTGTCAGCTCCTTTCCGGGACTTTCGCTTTCCCCCTCCCTATTGCCACGGCGGAACTCATCGCCGCCT
GCCTTGCCCGCTGCTGGACAGGGGCTCGGCTGTTGGGCACTGACAATTCCGTGGTGTTGTCGGGGAAGCTGAC
GTCCTTTCCATGGCTGCTCGCCTGTGTTGCCACCTGGATTCTGCGCGGGACGTCCTTCTGCTACGTCCCTTCG
GCCCTCAATCCAGCGGACCTTCCTTCCCGCGGCCTGCTGCCGGCTCTGCGGCCTCTTCCGCGTCTTCGCCTTC
GCCCTCAGACGAGTCGGATCTCCCTTTGGGCCGCCTCCCCGCCTGGAATTAATTCTGCAGTCGAGACCTAGAA
AAACATGGAGCAATCACAAGTAGCAATACAGCAGCTACCAATGCTGATTGTGCCTGGCTAGAAGCACAAGAGG
AGGAGGAGGTGGGTTTTTCCAGTCACACCTCAGGTACCTTTAAGACCAATGACTTACAAGGCAGCTGTAGATC
TTAGCCACTTTTTAAAAGAAAAGAGGGGACTGGAAGGGCTAATTCACTCCCAACGAAGACAAGATATCCTTGA
TCTGTGGATCTACCACACACAAGGCTACTTCCCTGATTAGCAGAACTACACACCAGGGCCAGGGGTCAGATAT
CCACTGACCTTTGGATGGTGCTACAAGCTAGTACCAGTTGAGCCAGATAAGGTAGAAGAGGCCAATAAAGGAG
AGAACACCAGCTTGTTACACCCTGTGAGCCTGCATGGGATGGATGACCCGGAGAGAGAAGTGTTAGAGTGGAG
GTTTGACAGCCGCCTAGCATTTCATCACGTGGCCCGAGAGCTGCATCCGGAGTACTTCAAGAACTGCTGATAT
CGAGCTTGCTACAAGGGACTTTCCGCTGGGGACTTTCCAGGGAGGCGTGGCCTGGGCGGGACTGGGGAGTGGC
GAGCCCTCAGATCCTGCATATAAGCAGCTGCTTTTTGCCTGTACTGGGTCTCTCTGGTTAGACCAGATCTGAG
CCTGGGAGCTCTCTGGCTAACTAGGGAACCCACTGCTTAAGCCTCAATAAAGCTTGCCTTGAGTGCTTCAAGT
AGTGTGTGCCCGTCTGTTGTGTGACTCTGGTAACTAGAGATCCCTCAGACCCTTTTAGTCAGTGTGGAAAATC
TCTAGCAGTAGTAGTTCATGTCATCTTATTATTCAGTATTTATAACTTGCAAAGAAATGAATATCAGAGAGTG
AGAGGCCTTGACATTGCTAGCGTTTTACCGTCGACCTCTAGCTAGAGCTTGGCGTAATCATGGTCATAGCTGT
TTCCTGTGTGAAATTGTTATCCGCTCACAATTCCACACAACATACGAGCCGGAAGCATAAAGTGTAAAGCCTG
GGGTGCCTAATGAGTGAGCTAACTCACATTAATTGCGTTGCGCTCACTGCCCGCTTTCCAGTCGGGAAACCTG
TCGTGCCAGCTGCATTAATGAATCGGCCAACGCGCGGGGAGAGGCGGTTTGCGTATTGGGCGCTCTTCCGCTT
CCTCGCTCACTGACTCGCTGCGCTCGGTCGTTCGGCTGCGGCGAGCGGTATCAGCTCACTCAAAGGCGGTAAT
ACGGTTATCCACAGAATCAGGGGATAACGCAGGAAAGAACATGTGAGCAAAAGGCCAGCAAAAGGCCAGGAAC
CGTAAAAAGGCCGCGTTGCTGGCGTTTTTCCATAGGCTCCGCCCCCCTGACGAGCATCACAAAAATCGACGCT
CAAGTCAGAGGTGGCGAAACCCGACAGGACTATAAAGATACCAGGCGTTTCCCCCTGGAAGCTCCCTCGTGCG
CTCTCCTGTTCCGACCCTGCCGCTTACCGGATACCTGTCCGCCTTTCTCCCTTCGGGAAGCGTGGCGCTTTCT
CATAGCTCACGCTGTAGGTATCTCAGTTCGGTGTAGGTCGTTCGCTCCAAGCTGGGCTGTGTGCACGAACCCC
CCGTTCAGCCCGACCGCTGCGCCTTATCCGGTAACTATCGTCTTGAGTCCAACCCGGTAAGACACGACTTATC
GCCACTGGCAGCAGCCACTGGTAACAGGATTAGCAGAGCGAGGTATGTAGGCGGTGCTACAGAGTTCTTGAAG
TGGTGGCCTAACTACGGCTACACTAGAAGAACAGTATTTGGTATCTGCGCTCTGCTGAAGCCAGTTACCTTCG
GAAAAAGAGTTGGTAGCTCTTGATCCGGCAAACAAACCACCGCTGGTAGCGGTTTTTTTGTTTGCAAGCAGCA
GATTACGCGCAGAAAAAAAGGATCTCAAGAAGATCCTTTGATCTTTTCTACGGGGTCTGACGCTCAGTGGAAC
GAAAACTCACGTTAAGGGATTTTGGTCATGAGATTATCAAAAAGGATCTTCACCTAGATCCTTTTAAATTAAA
AATGAAGTTTTAAATCAATCTAAAGTATATATGAGTAAACTTGGTCTGACAGTTACCAATGCTTAATCAGTGA
GGCACCTATCTCAGCGATCTGTCTATTTCGTTCATCCATAGTTGCCTGACTCCCCGTCGTGTAGATAACTACG
ATACGGGAGGGCTTACCATCTGGCCCCAGTGCTGCAATGATACCGCGAGACCCACGCTCACCGGCTCCAGATT
TATCAGCAATAAACCAGCCAGCCGGAAGGGCCGAGCGCAGAAGTGGTCCTGCAACTTTATCCGCCTCCATCCA
GTCTATTAATTGTTGCCGGGAAGCTAGAGTAAGTAGTTCGCCAGTTAATAGTTTGCGCAACGTTGTTGCCATT
GCTACAGGCATCGTGGTGTCACGCTCGTCGTTTGGTATGGCTTCATTCAGCTCCGGTTCCCAACGATCAAGGC
GAGTTACATGATCCCCCATGTTGTGCAAAAAAGCGGTTAGCTCCTTCGGTCCTCCGATCGTTGTCAGAAGTAA
GTTGGCCGCAGTGTTATCACTCATGGTTATGGCAGCACTGCATAATTCTCTTACTGTCATGCCATCCGTAAGA
TGCTTTTCTGTGACTGGTGAGTACTCAACCAAGTCATTCTGAGAATAGTGTATGCGGCGACCGAGTTGCTCTT
GCCCGGCGTCAATACGGGATAATACCGCGCCACATAGCAGAACTTTAAAAGTGCTCATCATTGGAAAACGTTC
TTCGGGGCGAAAACTCTCAAGGATCTTACCGCTGTTGAGATCCAGTTCGATGTAACCCACTCGTGCACCCAAC
TGATCTTCAGCATCTTTTACTTTCACCAGCGTTTCTGGGTGAGCAAAAACAGGAAGGCAAAATGCCGCAAAAA
AGGGAATAAGGGCGACACGGAAATGTTGAATACTCATACTCTTCCTTTTTCAATATTATTGAAGCATTTATCA
GGGTTATTGTCTCATGAGCGGATACATATTTGAATGTATTTAGAAAAATAAACAAATAGGGGTTCCGCGCACA
TTTCCCCGAAAAGTGCCACCTGACGTCGACGGATCGGGAGATCAACTTGTTTATTGCAGCTTATAATGGTTAC

AAATAAAGCAATAGCATCACAAATTTCACAAATAAAGCATTTTTTTCACTGCATTCTAGTTGTGGTTTGTCCA
AACTCATCAATGTATCTTATCATGTCTGGATCAACTGGATAACTCAAGCTAACCAAAATCATCCCAAACTTCC
CACCCCATACCCTATTACCACTGCCAATTACCTAGTGGTTTCATTTACTCTAAACCTGTGATTCCTCTGAATT
ATTTTCATTTTAAAGAAATTGTATTTGTTAAATATGTACTACAAACTTAGTAGTTTTTAAAGAAATTGTATTT
GTTAAATATGTACTACAAACTTAGTAGT

Appendix E: pMacTag-2A-AS02N_dTAG HA T2A NeoR plasmid map and sequence.

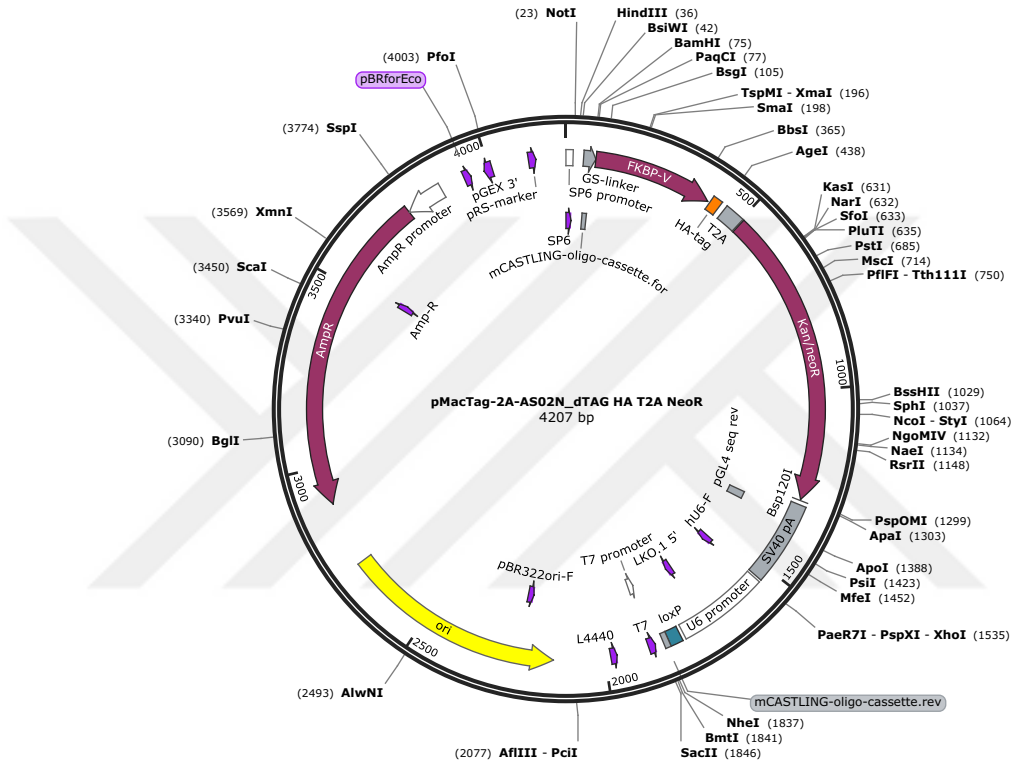


```
>pMacTag-2A-AS02N_dTAG HA T2A NEOR
ATTTAGGTGACACTATAGAACGCGGCCGCCAGCTGAAGCTTCGTACGTCAGGTGGAGGAGGTAGTGGCGGAGG
CGGATCCGGAGTGCAGGTGGAAACCATCTCCCCAGGAGACGGGCGCACCTTCCCCAAGCGCGGCCAGACCTGC
GTGGTGCACTACACCGGGATGCTTGAAGATGGAAAGAAAGTTGATTCCTCCCGGGACAGAAACAAGCCCTTTA
AGTTTATGCTAGGCAAGCAGGAGGTGATCCGAGGCTGGGAAGAAGGGGTTGCCCAGATGAGTGTGGGTCAGAG
AGCCAAACTGACTATATCTCCAGATTATGCCTATGGTGCCACTGGGCACCCAGGCATCATCCCACCACATGCC
ACTCTCGTCTTCGATGTGGAGCTTCTAAAACTGGAAGGCGGCTACCCATACGATGTTCCAGATTACGCTGGTA
CCGGTTCCGGAGAGGGCAGAGGAAGTCTGCTAACATGCGGTGACGTCGAGGAGAATCCTGGCCCAATGATTGA
ACAAGATGGATTGCACGCAGGTTCTCCGGCCGCTTGGGTGGAGAGGCTATTCGGCTATGACTGGGCACAACAG
ACAATCGGCTGCTCTGATGCCGCCGTGTTCCGGCTGTCAGCGCAGGGGCGCCCGGTTCTTTTTGTCAAGACCG
ACCTGTCCGGTGCCCTGAATGAACTGCAGGACGAGGCAGCGCGGCTATCGTGGCTGGCCACGACGGGCGTTCC
TTGCGCAGCTGTGCTCGACGTTGTCACTGAAGCGGGAAGGGACTGGCTGCTATTGGGCGAAGTGCCGGGGCAG
GATCTCCTGTCATCTCACCTTGCTCCTGCCGAGAAAGTATCCATCATGGCTGATGCAATGCGGCGGCTGCATA
CGCTTGATCCGGCTACCTGCCCATTCGACCACCAAGCGAAACATCGCATCGAGCGAGCACGTACTCGGATGGA
AGCCGGTCTTGTCGATCAGGATGATCTGGACGAAGAGCATCAGGGGCTCGCGCCAGCCGAACTGTTCGCCAGG
CTCAAGGCGCGCATGCCCGACGGCGAGGATCTCGTCGTGACCCATGGCGATGCCTGCTTGCCGAATATCATGG
TGGAAAATGGCCGCTTTTCTGGATTCATCGACTGTGGCCGGCTGGGTGTGGCGGACCGCTATCAGGACATAGC
GTTGGCTACCCGTGATATTGCTGAAGAGCTTGGCGGCGAATGGGCTGACCGCTTCCTCGTGCTTTACGGTATC
GCCGCTCCCGATTCGCAGCGCATCGCCTTCTATCGCCTTCTTGACGAGTTCTTCTGAGGGCCCGCTTCGAGCA
GACATGATAAGATACATTGATGAGTTTGGACAAACCACAACTAGAATGCAGTGAAAAAAATGCTTTATTTGTG
AAATTTGTGATGCTATTGCTTTATTTGTAACCATTATAAGCTGCAATAAACAAGTTAACAACAACAATTGCAT
```

TCATTTTATGTTTCAGGTTCAGGGGGAGGTGTGGGAGGTTTTTTAAAGCAAGTAAAACCTCTACAAATGTGGT
ACTCGAGGAGGGCCTATTTCCCATGATTCCTTCATATTTGCATATACGATACAAGGCTGTTAGAGAGATAATT
GGAATTAATTTGACTGTAAACACAAAGATATTAGTACAAAATACGTGACGTAGAAAGTAATAATTTCTTGGGT
AGTTTGCAGTTTTAAAATTATGTTTTAAAATGGACTATCATATGCTTACCGTAACTTGAAAGTATTTCGATTT
CTTGGCTTTATATATCTTGTGGAAAGGACGAAACACCGATAACTTCGTATAGCATACATTATACGAAGTTATG
GTACCGATGCAGCTAGCCCGCGGATCTGCCGGTCTCCCTATAGTGAGTCGTATTAATTTCGATAAGCCAGGTT
AACCTGCATTAATGAATCGGCCAACGCGCGGGGAGAGGCGGTTTGCGTATTGGGCGCTCTTCCGCTTCCTCGC
TCACTGACTCGCTGCGCTCGGTCGTTCGGCTGCGGCGAGCGGTATCAGCTCACTCAAAGGCGGTAATACGGTT
ATCCACAGAATCAGGGGATAACGCAGGAAAGAACATGTGAGCAAAAGGCCAGCAAAAGGCCAGGAACCGTAAA
AAGGCCGCGTTGCTGGCGTTTTTCCATAGGCTCCGCCCCCCTGACGAGCATCACAAAAATCGACGCTCAAGTC
AGAGGTGGCGAAACCCGACAGGACTATAAAGATACCAGGCGTTTCCCCCTGGAAGCTCCCTCGTGCGCTCTCC
TGTTCCGACCCTGCCGCTTACCGGATACCTGTCCGCCTTTCTCCCTTCGGGAAGCGTGGCGCTTTCTCATAGC
TCACGCTGTAGGTATCTCAGTTCGGTGTAGGTCGTTCGCTCCAAGCTGGGCTGTGTGCACGAACCCCCCGTTC
AGCCCGACCGCTGCGCCTTATCCGGTAACTATCGTCTTGAGTCCAACCCGGTAAGACACGACTTATCGCCACT
GGCAGCAGCCACTGGTAACAGGATTAGCAGAGCGAGGTATGTAGGCGGTGCTACAGAGTTCTTGAAGTGGTGG
CCTAACTACGGCTACACTAGAAGAACAGTATTTGGTATCTGCGCTCTGCTGAAGCCAGTTACCTTCGGAAAAA
GAGTTGGTAGCTCTTGATCCGGCAAACAAACCACCGCTGGTAGCGGTGGTTTTTTTGTTTGCAAGCAGCAGAT
TACGCGCAGAAAAAAAGGATCTCAAGAAGATCCTTTGATCTTTTCTACGGGGTCTGACGCTCAGTGGAACGAA
AACTCACGTTAAGGGATTTTGGTCATGAGATTATCAAAAAGGATCTTCACCTAGATCCTTTTAAATTAAAAAT
GAAGTTTTAAATCAATCTAAAGTATATATGAGTAAACTTGGTCTGACAGTTACCAATGCTTAATCAGTGAGGC
ACCTATCTCAGCGATCTGTCTATTTCGTTCATCCATAGTTGCCTGACTCCCCGTCGTGTAGATAACTACGATA
CGGGAGGGCTTACCATCTGGCCCCAGTGCTGCAATGATACCGCGAGACCCACGCTCACCGGCTCCAGATTTAT
CAGCAATAAACCAGCCAGCCGGAAGGGCCGAGCGCAGAAGTGGTCCTGCAACTTTATCCGCCTCCATCCAGTC
TATTAATTGTTGCCGGGAAGCTAGAGTAAGTAGTTCGCCAGTTAATAGTTTGCGCAACGTTGTTGCCATTGCT
ACAGGCATCGTGGTGTCACGCTCGTCGTTTGGTATGGCTTCATTCAGCTCCGGTTCCCAACGATCAAGGCGAG
TTACATGATCCCCCATGTTGTGCAAAAAAGCGGTTAGCTCCTTCGGTCCTCCGATCGTTGTCAGAAGTAAGTT
GGCCGCAGTGTTATCACTCATGGTTATGGCAGCACTGCATAATTCTCTTACTGTCATGCCATCCGTAAGATGC
TTTTCTGTGACTGGTGAGTACTCAACCAAGTCATTCTGAGAATAGTGTATGCGGCGACCGAGTTGCTCTTGCC
CGGCGTCAATACGGGATAATACCGCGCCACATAGCAGAACTTTAAAAGTGCTCATCATTGGAAAACGTTCTTC
GGGGCGAAAACTCTCAAGGATCTTACCGCTGTTGAGATCCAGTTCGATGTAACCCACTCGTGCACCCAACTGA
TCTTCAGCATCTTTTACTTTCACCAGCGTTTCTGGGTGAGCAAAAACAGGAAGGCAAAATGCCGCAAAAAAGG
GAATAAGGGCGACACGGAAATGTTGAATACTCATACTCTTCCTTTTTCAATATTATTGAAGCATTTATCAGGG
TTATTGTCTCATGAGCGGATACATATTTGAATGTATTTAGAAAAATAAACAAATAGGGGTTCCGCGCACATTT
CCCCGAAAAGTGCCACCTGACGTCTAAGAAACCATTATTATCATGACATTAACCTATAAAAATAGGCGTATCA
CGAGGCCCTTTCGTCTCGCGCGTTTCGGTGATGACGGTGAAAACCTCTGACACATGCAGCTCCCGGAGACGGT
CACAGCTTGTCTGTAAGCGGATGCCGGGAGCAGACAAGCCCGTCAGGGCGCGTCAGCGGGTGTTGGCGGGTGT
CGGGGCTGGCTTAACTATGCGGCATCAGAGCAGATTGTACTGAGAGTGCACCATATGGACATATTGTCGTTAG
AACGCGGCTACAATTAATACATAACCTTATGTATCATACACATACG

Appendix F: Keratin 8 interaction partners including clusters and singletons.

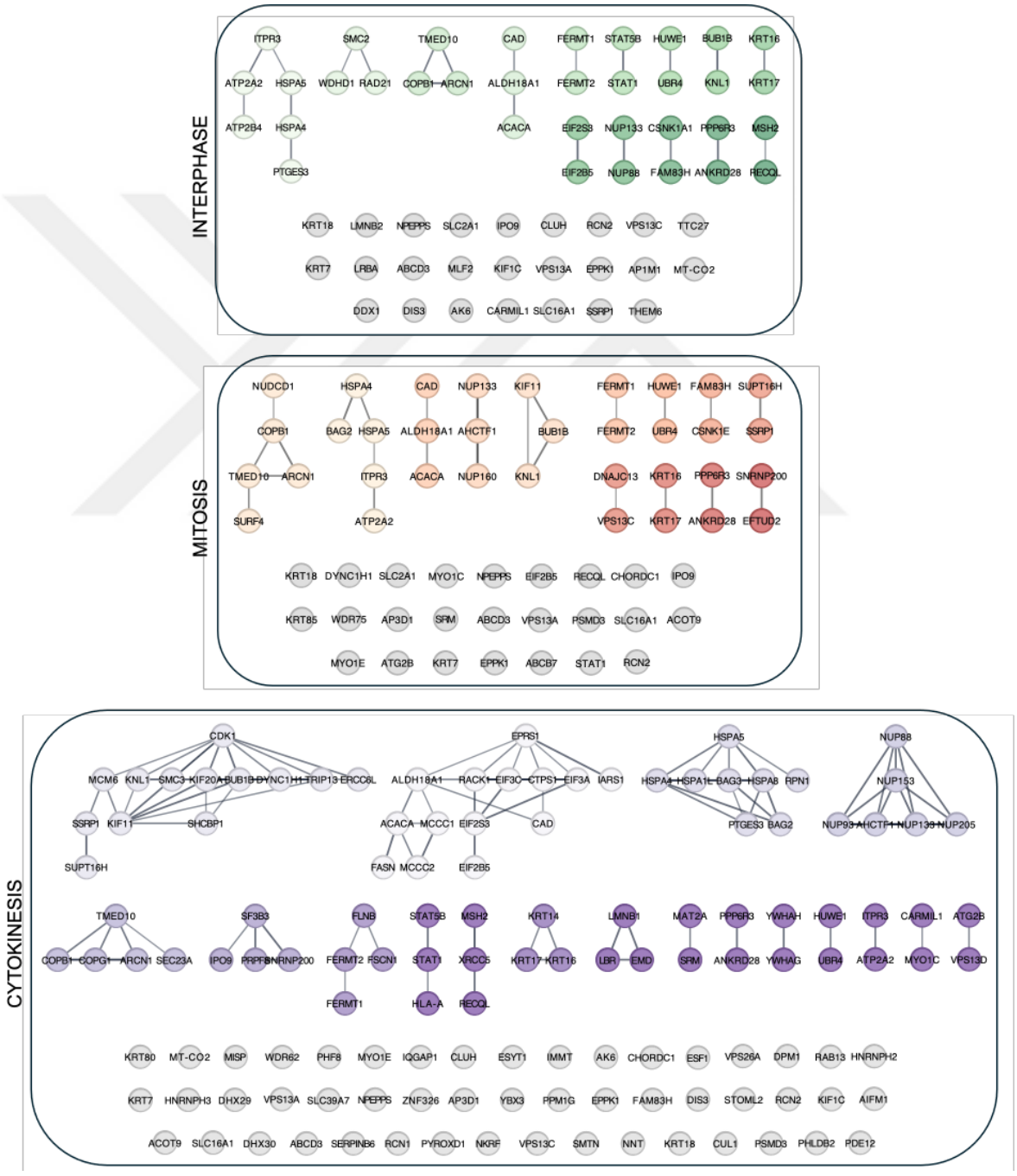

Appendix G: PD results of DIA library generation. Peptide (a-c) and protein (d-g) identifications were analyzed and filtered based on thresholds of ≥3 PSMs or ≥2 peptides.

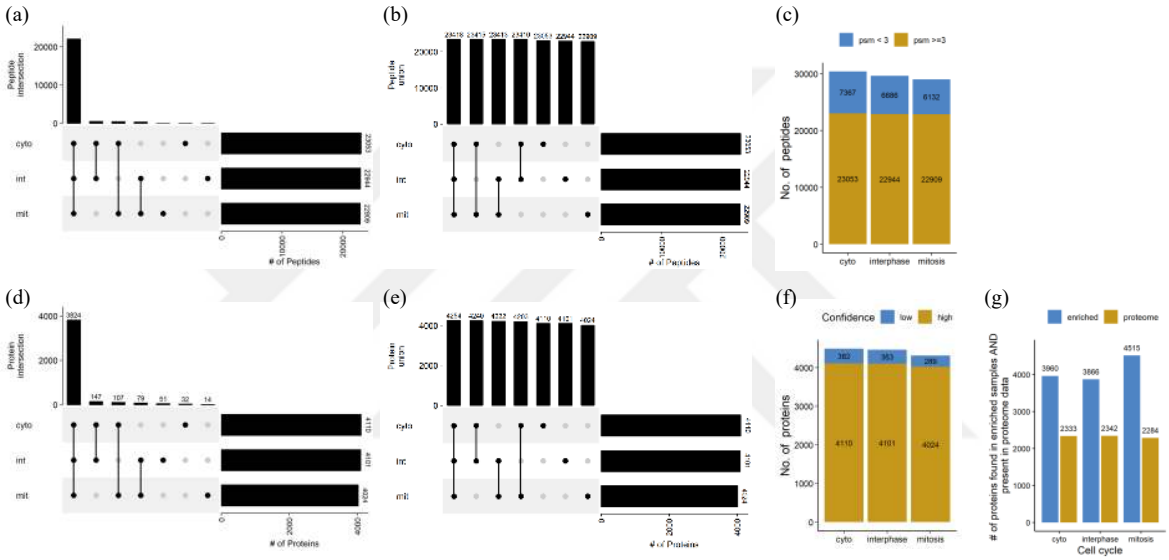

Appendix H: PD results of DDA analysis for DIA library generation.

(a) Overlap of p-peptides, p-class 1 only

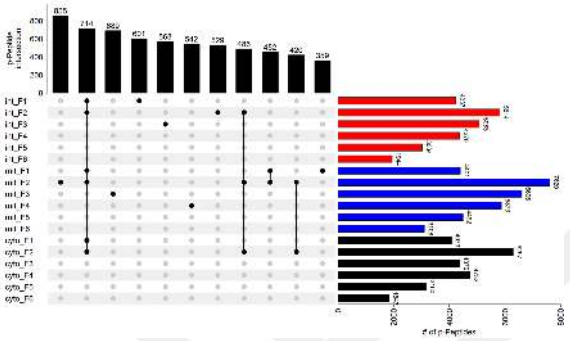

(b) Overlap of p-peptides across stage, p-class 1 only

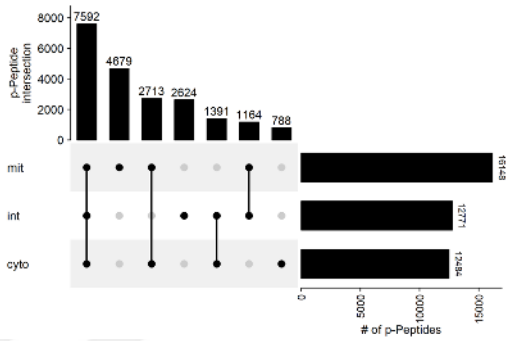

(c) Cumulative # of peptides per fraction

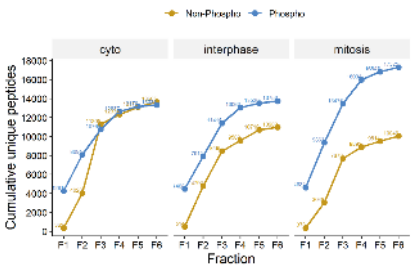

(d) # of peptides per fraction

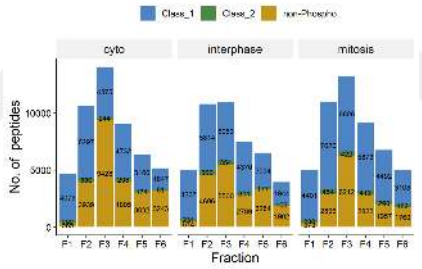

(e) # of peptides

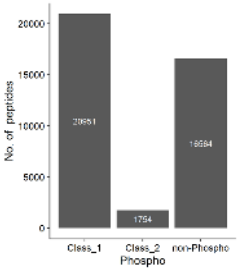

(f) Overlap of p-proteins

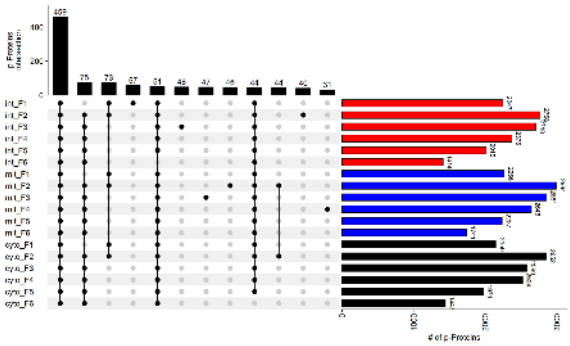

(g) Overlap of p-proteins across stage

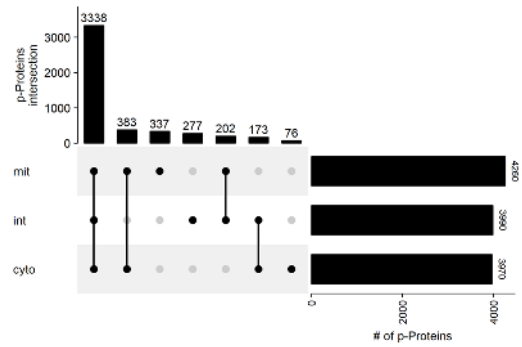

(h) Cumulative # of peptides per fraction

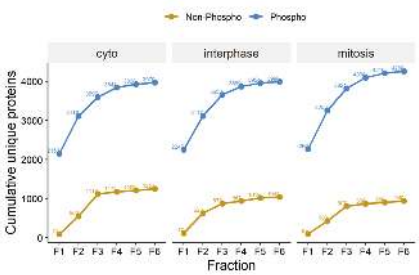

(i) # of peptides per fraction

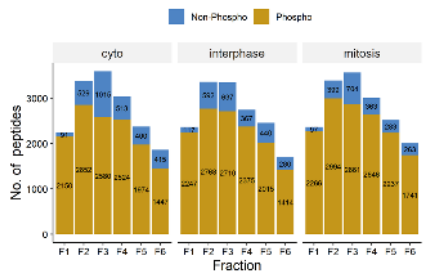

(j) # of peptides

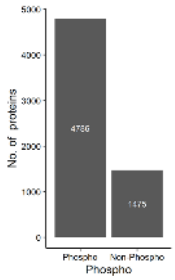

Appendix I: PD results of DIA analysis for library generation.

(a) Overlap of p-peptides, p-class 1 only

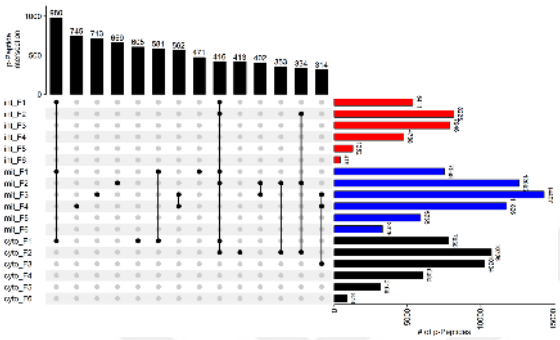

(b) Overlap of p-peptides across stage, p-class 1 only

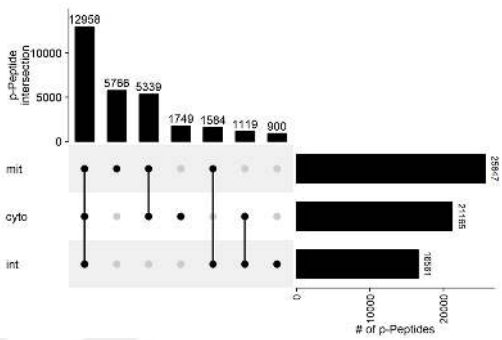

(c) Cumulative # of peptides per fraction

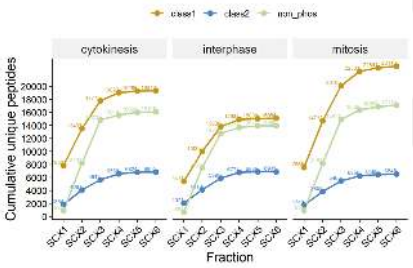

(d) # of peptides per fraction

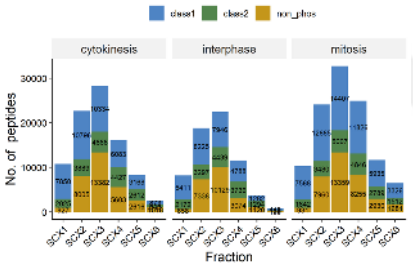

(e) # of peptides

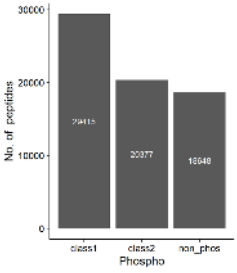

(f) Overlap of p-proteins

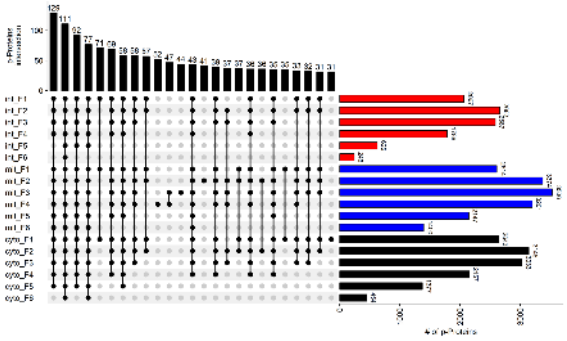

(g) Overlap of p-proteins across stage

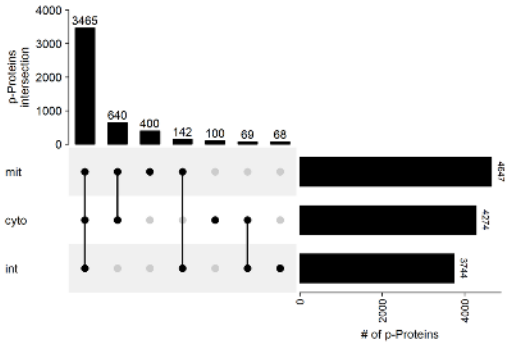

(h) Cumulative # of peptides per fraction

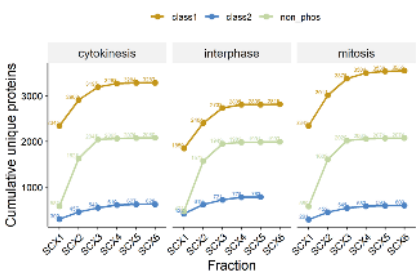

(i) # of peptides per fraction

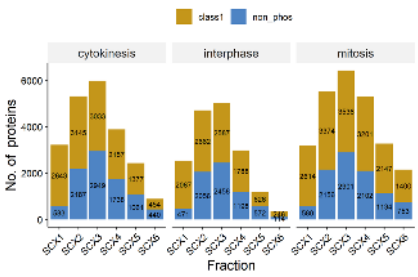

(j) # of peptides